IONOSPHERIC MODELLING FOR HIGH PRECISION GPS REAL TIME KINEMATIC SURVEYING OVER LONG DISTANCES

YUNG-LUNG TSOU

Thesis submitted for the Degree of
Doctor of Philosophy
of the University of London

Department of Geomatic Engineering, University College London
Gower Street, London, WC1E 6BT, United Kingdom

June 2000

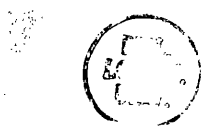

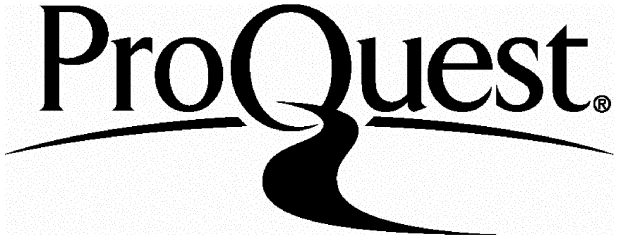

ABSTRACT

Over the past decade real time kinematic (RTK) GPS has evolved into an important practical tool for a wide range of positioning applications. For short baselines the current accuracy is limited only by multipathing problems but as the distance increases so other errors begin to decorrelate. In particular errors due to the ionosphere play an increasingly important role and typically RTK cannot be used beyond about 10km. Many practical applications require RTK to operate over longer distances and this thesis is concerned with the ionospheric modelling necessary for this to be possible.

At present global and regional ionosphere maps (broadcast on web) based on global ionosphere models (GIM) and regional ionosphere models (RIM) are available for worldwide DGPS (WWDGPS) and wide area DGPS (WDGPS). Because of the limited accuracy of these models, a local ionosphere model (LIM) has been developed to see whether it would be possible to enhance the performance of RTK GPS.

Several LIMs based on different mapping functions, and using data from one station only, have been constructed. These have been used to predict the double difference ionospheric corrections for a pair of stations and compared with the "true" corrections based on the data actually collected at the two stations (and knowing the exact coordinates of the two stations). In this way the accuracy of the different LIMs has been compared. These (LIM-based) corrections have also been used to correct raw GPS phase data before use in RTK software in order to see whether or not integer ambiguity determination can be improved - especially over distances greater than those currently used in practical RTK GPS. It has been found that significant improvements can result from the use of these corrections over distances of up to 20km when using clean GPS data in relatively benign multipathing.

TABLE OF CONTENTS

LIST OF FIGURES

LIST OF TABLES

LIST OF ABBREVIATIONS

A/S	Anti-Spoofing
AFM	Ambiguity Function Method
AFT	Ambiguity Function Technique
AFV	Ambiguity Function Value
C/A-Code	Coarse Acquisition/Clear Access GPS signal
cm	centimeters
DD	Double Differenced
DGPS	Differential GPS
FAAR	Fully Automatic Ambiguity Function
FARA	Fast Ambiguity Function Approach
FARA	Fast Ambiguity Search Filter
FOC	Fully Operating Capability
F-test	Fisher Test
GASP	GPS Ambiguity Searching Program
GFA	Geometry Free Approach
GIM	Global Ionospheric Model
GIPSY	GPS Inferred Positioning System
GLONASS	GLObal Navigation Satellite System
GPS	Global Positioning System
Hz	Hertz
HOW	Hand Over Word
IGS	the International GPS Service
IPP	Ionospheric Pierce Point
JPL	Jet Propulsion Laboratory
KART	Kinematic Application Real Time
km	kilometers
LADGPS	Local Area DGPS
LAMBDA	Least squares AMBiguity Decorrelation Adjustment
LCA	Linear Combination Approach
LIM(s)	Local Ionospheric Model(s)/Modelling
LRK	Long Range Kinematic
LSA	Least Squares Adjustment

mbar	millibar
mm	milliters
NGS	US's Navigation Geodetic Survey
ns	nanoseconds
NXF	Newcastle data eXchange Format
OASIS	Orbit Analysis and Simulation Software
P-code	Precise/Protected code
PDOP	Positional Dilution of Precision
PGA	Permanent GPS Arrays
ppm	parts per million
PPS	Precise Positioning Service
PRARE	Precise Range And Range-rate Equipment
PRN	PseudoRandom Noise
RIM	Regional Ionospheric Model
RINTONXF	RINEX to NXF Conversion Program
RMS/rms	root mean square
RTK GPS	Real Time Kinematic GPS
RTK	Real Time Kinematic
RT-SKI	Real Time Static and KInematic
RTZ	Real Time Z-tracking
S/A	Select Availability
SD	Single Differenced
SEAS	Single Epoch Approximate Solution
Sec	seconds
SNR	Signals to Noise Ratio
SPS	Standard GPS services
SV	Space Vehicle
SVN	Space Vehicle launch Number
TEC	Total Electron Content
TECU/tecu	TEC Unit
TIDs	the Travelling Ionospheric Disturbances
TLM	Telemetry Word
U.S. DoD	United State Department of Defense
UD	UnDifferenced

UTC	Universal Time Coordiated
VLBI	Very Long Baseline Interferometry
VTEC	Vertical TEC
WAAS	Wide Area Augmentation Service
WADGPS	Wide Area DGPS
WGS84	Weighted Geodetic System 1984
WWDGPS	Worldwide DGPS

ACKNOWLEDGEMENT

First of all, I would like to express my special thanks to my supervisor Professor Paul Cross for his excellent guidance and constant discussion, continuous support and encouragement throughout the research. My sincere appreciation cannot express without the words for his kindness to arrange the visiting of Taiwan for reading and correcting this thesis.

Equally, expressed are many thanks to Dr. Simon Corbett and Dr. Yahia Mohamed Hasan Al-Haifi for their support and experience at early stage of this research, to Mr. Joel Borne and Dr. Paul Cruddace for their useful advice, discussion, and lots of aids during the difficult time of the research, and to those who helped me during the period of my studying.

Finally, I am thankful for the economic support of my government and the paper work assistance of my colleagues. In particular, I am greatly indebted to my family for my less caring, and the concentration on my studying must accompany their lots of patience and suffering during the research period.

CHAPTER ONE
INTRODUCTION

1.1 RESEARCH BACKGROUND

During the last two decades, many activities have been undertaken to increase the capability of GPS (Global Positioning System) techniques. To date, however, although phase-based precise RTK (Real Time Kinematic) GPS can deliver a positioning accuracy at the centimetre level, it can only do so over short distances. Also for some techniques, the biggest challenge is to resolve the problem of initialisation or re-initialisation, which can be totally unacceptable for some RTK applications over long distances. Hence, in recent years, the linked challenges within RTK GPS have centred on

- shortening the time of the initialisation or re- initialisation process, and
- extending the use of current RTK technique over long distances

In its strict sense, RTK positioning is achievable only when using GPS data received at the single epoch – although in practice the term is used to describe instantaneous positioning with already determined integer ambiguities. Among current techniques, the single epoch AFT (Ambiguity Function Technique), with its ability to provide instantaneous positions on the basis of a single epoch GPS dual frequency data, can be considered to be the optimal RTK strategy because it is free of the problem of initialisation or re-initialisation. After a significant amount of research over short baselines, currently this technique can achieve centimetre level positioning accuracy in a multipath benign environment. It is still, however, limited to short distances (roving station within about 10km of the base station). Basically, the ambiguity resolution strategy is the key element of this technique and the effects of measurement errors can directly impact on its effectiveness. Over short baselines, these errors are limited to only the multipathing, but as the baseline distance increases other errors (mainly atmospheric) begin to decorrelate, resolution of ambiguities becomes difficult and even if successful the positioning accuracy can be degraded. In particular, errors due to the ionosphere play an increasingly important role, and typically this technique cannot be used beyond about 10km in times of increased ionospheric activity. Besides, as the

level of solar activity increases (a maximum in the eleven-year cycle is expected to occur around 2000) this distance may further decrease.

In recent years, the provision of an infrastructure to deliver precise real time positioning services via the establishment of national PGA (Permanent GPS Arrays), has widely been discussed in many countries. The accomplishment of this scheme will require the establishment of a high density of reference stations since, as has been explained, current RTK techniques can only operate over short distances. Therefore, of great current concern is the technical problem of modelling or otherwise reducing errors, to keep the cost of establishing, operating and maintaining reference stations as low as possible (by reducing their density). For the foreseeable future we are therefore likely to require RTK to operate over longer distances than it can do presently. Of course for some applications (e.g. those offshore) such a requirement will always exist.

1.2 RESEARCH MOTIVATION AND OBJECTIVES

In this thesis, the attempt to extend the use of single epoch AFT over longer distances by ionospheric modelling is aimed at resolving two related current problems of RTK GPS simultaneously. For single epoch AFT operations with a self-contained tropospheric model, the modelling of ionospheric delays is crucial for its range to be extended. For general phase-based ionospheric modelling derived from GPS networks such as LIM, RIM and GIM (Local, regional and Global Ionospheric Modelling), the main drawback of current methods is the necessity for pre-processing data to obtain the ambiguities or hardware biases. A refined modelling of the ionosphere based on a single reference (base) station without any pre-processing of the ambiguities or hardware biases, is proposed and evaluated in this thesis. The main task is to see whether it would be possible to use the method to enhance the performance of RTK GPS over long distances.

In general, the research work presented in this thesis can be divided into seven sections. These are listed in the following along with their specific objectives.

1. GPS relative positioning over long baselines
   - The achievements, requirements, and the bottlenecks of current RTK GPS

- The processing strategies of current techniques
- The optimal processing strategies of current RTK GPS

2. Single epoch AFT over long distances
   - The achievements, the advantages, and the problems of the current AFT
   - The error effects on the AFT performance
   - The performance and evaluation of the AFT

3. The propagation errors and current ionospheric models
   - The nature of the propagation errors
   - The ionospheric impacts on GPS
   - The key problems of current ionospheric models
   - The concept of ionospheric modelling
   - The evaluation of current ionospheric models

4. The behaviour of ionospheric delays and tropospheric delays over long distances
   - The approaches based on two known stations
   - The behaviour of ionospheric delays and tropospheric delays
   - The actual size of the effects of ionosphere and troposphere
   - The evaluation of the tropospheric model

5. Local ionospheric modelling
   - The refinement of current ionospheric models
   - The generation of ionospheric models
   - The performance of ionospheric models
   - The evaluation of ionospheric models
   - The RTK applications of ionospheric models

6. Ionospheric prediction
   - The prediction of ionospheric corrections
   - The performance of ionospheric modelling and predictions
   - The verification of double differenced ionospheric estimations

7. The single epoch AFT with ionospheric corrections

- The performance of the AFT after the ionospheric correction
- The evaluation of the AFT with the ionospheric corrections
- The error analysis and improvements of the AFT with the ionospheric model

1.3 RESEARCH METHODOLOGY

From the overview of current GPS positioning irrespective of the technology or the mode of operation, the single epoch AFT has been found to be the optimal current technique that satisfies the current requirements of RTK GPS. For the investigations into AFT positioning over long distances, the basic parameters of this research, following the previous research over short baselines (< 10km), have been set as follows.

1. The experiments are focused on baselines of length from about 10km to 30km.
2. Dual frequency observations of pseudorange and carrier phase are collected at both the base and the rover stations for a period of time of at least an hour.
3. Using a self-contained tropospheric model, the AFT positioning computations are carried out epoch by epoch in a post-processing mode (using the GASP software) for each time series of observations.

Investigations have been carried out in the following major stages.

1. Overview and analysis of GPS relative positioning over long baselines,
2. Initial investigations of AFT performance over long baselines (> 10km),
3. Analysis of propagation errors and current ionospheric models,
4. Investigations on the behaviour of ionospheric and tropospheric delays,
5. Generation of local ionospheric models for testing,
6. Ionospheric prediction based on the ionospheric models generated,
7. Performance of the AFT with ionospheric corrections.

In order to achieve the goal of increasing the capability of current RTK techniques for long distances, the technical and operational problems of RTK GPS are of great concern. At each stage of the investigations, the exploration of problems, the analysis of error effects, the proposing of the optimal processing strategy and the evaluation of

investigation results, are essential to achieve the objects of this research. The following are some key elements of the research that relate to this general point.

- Instead of using commercial GPS positioning software, the precise GPS software, GIPSY II is used to compute the rover position for each baseline trial in a static mode using at least an hour of data. This precise solution, achievable at the millimetre level of positioning accuracy, can be considered as criterion suitable to evaluate the centimetre level results of AFT positioning.

- The investigations on the behaviour of ionospheric and tropospheric errors are carried out with linear combinations of observations based on two known stations. The generation of the ionospheric model is, however, based on a single reference (base) station. It is in this sense that it is called a local ionospheric model.

- For the ionospheric modelling, the pre-processing for cycle slip detection and repair is necessary to ensure that the data sets used in the processing are 100% "clean" (i.e. no cycle slips). TurboEdit, currently considered to be the most reliable software for cycle slip detection and repair, is adopted in this research to carry out this task.

- In order to evaluate the quality of the ionospheric modelling and prediction, two verification steps have been undertaken. These are based on comparisons of the estimations of single path and double differenced values with those obtained from the approaches based on two known stations.

- The evaluation of the tropospheric model implemented in GASP is carried out via comparisons of the results obtained from the linear combination approach with those using the ionosphere-free combination.

1.4 APPLICATIONS

As has been stated the overall objective of this research is to contribute to the resolution of the two bottlenecks of current RTK GPS simultaneously. If successful it will have important impacts on the operation of RTK GPS because it will no longer be restricted

to such short distances and it will no longer be necessary to wait for a period of time before the ambiguities are fixed if the reception of GPS signals is interrupted. It will open up new RTK GPS applications such as in offshore surveys and those on land and sea, and in space, which require operation over longer distances. In particular, national PGA (Permanent GPS Arrays, Ir. Kees de Jong, 1999) are being widely established for the precise real time positioning services in many European countries, e.g. UK, Japan, and America. Most current techniques are available only for operations over short range, and the prerequisite for this to be possible is the establishment of a high density of reference stations. However, this is very expensive and it is anticipated that this situation can be improved by the success of this research.

Moreover, the upcoming ionospheric impacts on GPS at Solar Max can cause severe "loss-of-lock" of the operating receivers from several cases reported (G. Bishop et. al., 1996). The task of monitoring the variation of ionosphere becomes more important for GPS operation and atmospheric research (E. Engler et. al., 1995, L. Wanninger et. al., 1995a, 1995b and 1995c, A. J. Mannucci et. al. 1995, F. Darin et.al., 1997). For current ionospheric models based on reference stations or network, the time required to update the ionospheric grid and transmit the corrections to users will tag the actual ionospheric changes (P. H. Doherty et. al., 1997). With considerations of the spatial and time variation of the ionosphere, a modelling of the ionosphere based on a single reference station, proposed in this thesis, might be adequate for these tasks.

1.5 THESIS LAYOUT

This thesis has been divided into eight chapters and three appendices including this introductory chapter and the last chapter of conclusions and suggestions. The major seven stages of investigations are arranged in Chapter Two to Chapter Six. The work has generated a large number of figures containing the investigation results. Those relating to the investigations into the behaviour of ionosphere and troposphere (Chapter 5), the single path and double differenced ionospheric estimations and comparisons (Chapter 6 and Chapter 7), and the AFT positioning performance without/with ionospheric corrections (Chapter 3 and Chapter 7) are respectively included in Appendix A, B, and C.

Chapter Two introduces the Global Positioning System in general terms, along with current strategies of RTK GPS, and the applications of long baseline GPS. Basically, all of the discussion and analysis is from the viewpoint of long baseline GPS and is hence concerned with the objects of the first stage of the investigation.

Chapter Three introduces current single epoch AFT concepts including the basic theory, the factors affecting performance, current achievements and limitations, the single epoch AFT over long baselines with emphasis on the experiments conducted during this research, processing strategies, and the positioning quality. The objects of this stage of the investigation are focused on introducing the key methodology used for GPS processing in this research.

Chapter Four considers ionospheric delays and their modelling with emphasis on the propagation errors in the atmosphere, ionospheric effects on GPS, the concept of ionospheric modelling, the analysis of current ionospheric models, the verification of ionospheric modelling, and its applications to GPS.

Chapter Five concentrates on the investigations on the behaviour of atmospheric delays (consisting of the ionospheric and tropospheric delays) over long distances. Two approaches using linear combination of observations (ionospheric combination, widelane combination, and ionosphere-free combination) are carried out based on two known stations for obtaining the apparent true values of ionospheric and tropospheric delays. The necessary steps of pre-processing for cycle slip detection and repair, and the evaluation of the current tropospheric model in GASP are also included.

Chapter Six and Chapter Seven contain the main tasks of this research, which follow on from the previous initial investigations and analysis. A well-considered and practical modelling of ionosphere based on a single reference station can thus be proposed in Chapter Six. This chapter includes the generation of local ionospheric model with emphasis on the applied observables. It also deals with the spatial and time variations of ionosphere, the construction of (vertical) ionospheric profiles, the modes of this modelling for testing, and the performance, evaluation and RTK applications of the models. Chapter Seven is focused on the use of the models generated for the prediction of ionospheric corrections and the AFT positioning after applying the ionospheric

corrections. The former consists of the procedures and performances of ionospheric prediction and the verification of the ionospheric estimations. Subsequently, the computation, the performance, the evaluation, and the error analysis of single epoch AFT with ionospheric corrections is discussed. Finally, the comparisons are carried out and conclusions made.

The final chapter summarises the conclusions drawn from all stages of the investigations of this research and indicates possible directions for further research work for RTK GPS over long distances.

CHAPTER TWO

GPS POSITIONING OVER LONG BASELINES

2.1 INTRODUCTION

Since the introduction of the *Global Positioning System* (GPS), many different techniques have become available for high precision GPS. Moreover, the system has been found to be useful for a wide area of applications on land, sea, and in space, and has become an increasingly important component of many practical and scientific tasks. However, despite these many developments, real time kinematic (RTK) GPS is still limited to short range applications (typically less than 15km for the latest real time kinematic products). Currently many applications, especially those offshore and those for which the density (and hence the cost of installation and maintenance) of operating reference stations are important, require RTK to operate over longer distances. Therefore, the extension of the use of current kinematic techniques to longer baselines has become an important current research subject in GPS, and the increasing importance of this subject can be seen, for example, from the requirements of national precise RTK service schemes. These are now being established in many parts of the world and for most of these far too many base stations would be required if the distances to the mobiles had to be restricted to less than say 15km.

For precise GPS in RTK mode, successful ambiguity resolution is usually the key problem with current techniques, and the effect of measurement errors is the inherent problem of resolving them. Over short baselines, ambiguity resolution is limited only by the multipathing problem, but as the baseline distance increases the other errors begin to decorrelate. In particular, the effect of ionospheric delays is generally considered to be the main problem of fixing ambiguities. In recent years, refining kinematic techniques and converting them from a post-processing to a real time activity has occupied much development and research time. Meanwhile, in order to obtain corrections for the relevant errors for the enhancement of current techniques, much research into ionospheric modelling has been carried out, based largely on Differential GPS (DGPS) reference stations or networks, but the accuracy of current models is still limited. Currently two ways are considered to increase the capability of RTK GPS, one is to add the other data sources such as GLONASS (Danaher et. al., 1993, Christle et. al., 1996, Vollath et. al., 1998, and Pratt et. al., 1998), and the other is to reduce the effect of

measurement errors. In fact, not only the technical problems but also the economic and practical problems have to be taken into account for future RTK GPS services.

This chapter, which focuses on the need to obtain an optimal strategy for future RTK GPS for long distance applications, is divided into four main sections. In section 2.2, the main problems of GPS positioning over long baselines are reviewed by presenting the Global Positioning System from a viewpoint of parameter analysis, and hence covering the basic strategy of GPS relative positioning. In section 2.3, some of the current strategies of GPS kinematic positioning are described along with the refinement of current kinematic techniques and their achievements. In section 2.4, a review of the applications of long baseline positioning reveals why this subject is so important and the key practical problems. Finally, an optimal strategy for RTK GPS for long baseline positioning is presented.

2.2 GLOBAL POSITIONING SYSTEM

Since the early 1960s, *the Global Positioning System* (GPS), a space-based satellite radionavigation positioning system covering large areas over the globe, has been deployed and operated by the U.S. Department of Defence (US DoD) - providing both *the Standard Positioning Service* (SPS) and *the Precise Positioning Service* (PPS). For this purpose, with a design of nominally 24 GPS satellites distributed in 6 orbital planes, at least 4 satellites are in view at anytime and anywhere and are available for positioning with the pseudorange measurements from the satellites to ground stations. In principle, the positioning concept is quite simple, but many different techniques have evolved over recent years. In this section, the development of GPS positioning from the basic concept of single point positioning to the problem of long baseline positioning is described by the eight subsections, mainly based on discussions of the parameter analysis and from a viewpoint of GPS positioning over long baselines.

2.2.1 BASIC CONCEPT OF GPS POSITIONING

As shown in figure 2.1 below, the basic concept of GPS positioning is simply based on trilateration and the application of fundamental three-dimensional geometry. In equation (2.1), with given satellite positions (discussed in section 2.2.3), theoretically

three measurements (pseudoranges to 3 satellites, discussed in section 2.2.1) are sufficient to solve the equations for three parameters (i.e. station co-ordinates). This results in positioning in a geodetic co-ordinate system (e.g. WGS84) - leading to perfect positions if there were no measurement errors. With consideration of the major measurement errors (discussed in section 2.2.2), the pseudorange measurements can be simply expressed as a range function in terms of satellite co-ordinates, station co-ordinates, and the parameter of measurement errors in space as below.

$$P_j^k(t_j) = [\,(x_j - x^k)^2 + (y_j - y^k)^2 + (z_j - z^k)^2\,]^{-1/2} + c\,dt_j^k(t_j) \quad \text{.....(2.1)}$$

Where

$P_j^k(t_j)$, is the pseudorange measurement from station j to satellite k (=1,n),

x_j, y_j, z_j are the co-ordinates of the ground stations which are unknown parameters,

x^k, y^k, z^k are the co-ordinates of the satellites which are known parameters obtained from the orbital message in the navigation file,

$c\,dt_j^k(t_j)$ is the effect of measurement errors, c is the speed of light in vacuum, and

n is the number of satellites ($n \geq 4$).

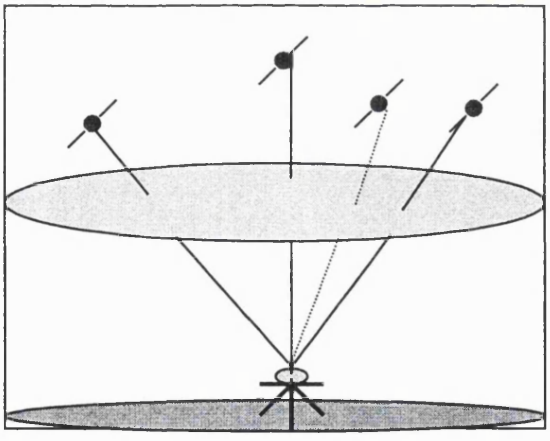

Figure 2.1 Basic concept of GPS positioning

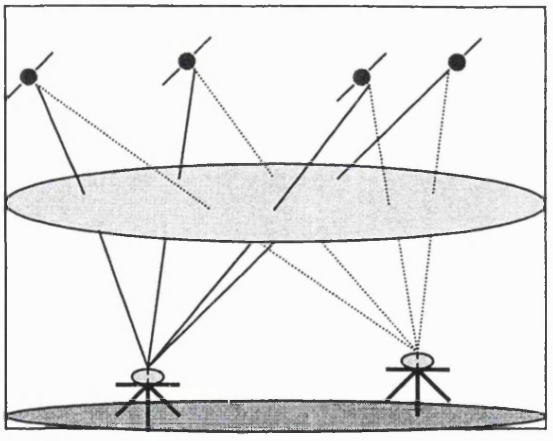

Figure 2.2 GPS relative positioning

In fact, there are many sources of measurement errors such as the timing errors in the receiver and satellite clock, hardware biases, and propagation delays, which can affect the accuracy of the positioning. For example, a one μsec delay of a clock will cause a 300m difference to the distance. Therefore GPS positioning needs the measurement from a fourth satellite with the basic three measurements to estimate three co-ordinate

parameters and the parameter of the timing error simultaneously. In real time positioning, an accuracy of the navigation solution (using the navigation message) of about 5 to 20m can typically be achieved if the P-code is used. It is less accurate (about 100m) if the C/A-code is used (Leick, 1995). If more than 4 satellites are available, then least squares adjustment is applied. However the accuracy of GPS positioning using the code data is still limited because of the effect of measurement errors. In many applications, the pseudoranges (C/A-code and/or P-code) are suitable only for a low accuracy - for instance for an approximate position to aid another method.

In high accuracy GPS positioning another type of data, the carrier phase, is normally used. This data is far more precise than the code data, but it is biased with the initial ambiguity, which is an unknown integer constant (a function of the total number of wavelengths to the satellite at initialisation and the initial phase counter setting of the tracking register). For GPS using the phase, this extra ambiguity parameter in the observation equations is usually resolved before computing position, but this can be a difficult task due to measurement errors such the clock errors, hardware biases, propagation delays, and the phase multipath.

The *absolute positioning* and *relative positioning* modes are shown in figure 2.1 and 2.2 and what follows refers to relative positioning - which is normally carried out in high precision surveying. Also positioning can be either static (unknown receiver is stationary) or dynamic (unknown receiver is moving). These are the basic modes of GPS positioning using the code and/or the phase. The static mode is supposed to gain redundant observations after a time period of observation (initially at least over one hour, now from say 2 minutes to 15 minutes for rapid static surveying) at one or more stations. By using these observations, the effect of measurement errors can be reduced by methods such as data smoothing (e.g. a Kalman filter). Longer sessions of observations are usually necessary for very long baseline positioning (Herring, 1986, 1990, and 1992, Blewitt, 1989, and Ma et. al., 1990). However static positioning is only suitable for some special applications such as basic control surveying. The relative mode is capable of eliminating the effect of the clock errors and hardware biases, and reducing the atmospheric effects, simply after the double differencing process based on two stations: one known (called reference or base) station and the other unknown (called rover or mobile) station. This is the simplest form of *Differential GPS*. Currently for precise kinematic GPS, only the relative positioning mode is possible but

its disadvantage is that it needs at least two receivers. Based on this positioning concept, a baseline (the distance from the rover station to the base station) positioning is therefore defined. For short baselines (i.e. few kilometers), the positioning accuracy or the ambiguity resolution is limited only by multipathing problems but as the distance increases so other errors begin to decorrelate (discussed in section 2.2.3). Therefore, for precise GPS, the problem of positioning over long distance baselines is focused on fixing ambiguities by reducing the effect of measurement errors, mainly by modelling them.

2.2.2 GPS SEGMENTS AND FUNCTIONS

GPS can be considered to consist of three main segments: space segment, control segment, and user segment. *The space segment* is the satellite constellation used for the generation and transmission of two modulated frequency signals and a navigation message file. *The control segment*, consisting a master station and several monitor stations around the world, is set up for monitoring the satellite transmissions continuously, predicting the satellite ephemeris, calibrating the satellite clocks, and updating the navigation message periodically. *The user segment*, including hardware (receiver) for the generating, tracking and locking and timing of signals to measure the pseudoranges and phases from the satellite to the receiver, and software for data processing and positioning, refers to the GPS users on land and sea or in space. Basically it is sufficient for GPS to be supported by these three segments but sometimes a fourth is considered: the *ground segment*. The ground segment, including civilian tracking networks which provides the user segment with reference control, precise ephemeris, and real time services, can be used to support a higher accuracy of positioning, especially over long baselines.

Therefore, measurements are undertaken by the user segment, and the satellite co-ordinates can be obtained from the orbital data in the navigation message file transmitted from the space segment, or based on the precise ephemeris from the ground segment. Some other information, such as clock estimation and coefficients of ionospheric and tropospheric models, are also supplied by these two segments, but however their limited accuracy means that they cannot be used for precise positioning.

2.2.3 GPS MEASUREMENTS

Basically the principle of a GPS receiver is that of a time measurement system. All receivers are able to generate codes, track and lock on to the satellite-emitted signals, and use the correlators to measure the time shift of the signals coming from the satellites with respect to the receiver-generated signals. Thus the travel time of GPS signals can be obtained and the pseudorange measurement between satellite k and receiver j, $P_j^k(t_j)$ is expressed to be the scaled difference of the nominal time (Leick, 1995) such that

$$P_j^k(t_j) = (t_j - t^k) c \quad \text{.....(2.2)}$$

where c denotes the speed of light.

Two carrier signals, L_1 (154×10.23Mhz = 1575.42Mhz; wave length = 19.0cm) and L_2 , (120×10.23Mhz = 1227.60Mhz; wave length = 24.4cm) are generated and broadcast based on the fundamental frequency (10.23Mhz) of the signal from GPS satellites. With digital modulation methods, P1 code (and/or C/A code), L_1 carrier phase can be found on the L_1 channel, and P2 code , L_2 carrier phase can be found on the L_2 channel. Hence two fundamental observables, code and carrier phase, are available for single or dual frequency GPS users. The code observable is measured by the code-tracking loop within the receiver, which shifts the internal replica of the pseudorandom noise (PRN) code in time, until maximum correlation occurs. The phase observable is the difference between the received satellite carrier phase and the phase of the internal receiver oscillator. P code is more precise than C/A code, but currently all high precision GPS techniques rely on the phase.

However the dual frequency code and phase observables can be affected by many sources of errors summarized as shown in Table 2.1. *Anti-Spoofing* (A/S) and *Selective Availability* (S/A) are two types of denial of positioning accuracy to civilian users. The former can be thought of as encryption of the P code and the latter can be thought of as intentional errors imposed on the GPS signal. For modern geodetic receivers, P code can still be locked onto even if A/S is switched on, albeit with increased noise. Hence A/S does not pose a significant problem, other than a small increase in noise, to the precise user since precise GPS techniques rely on the phase observables. There are two types of S/A: epsilon and dither. Both are designed to degrade deliberately the accuracy of GPS positioning. Epsilon is implemented by adding errors in the broadcast satellite orbits and dither entails falsification of the satellite clock. Since use of the precise ephemeris is recommended for very high positioning applications over long

ranges and since double differencing removes clock errors, it is possible to completely negate the effect of S/A for some applications (Blewitt, 1997). It anyway has only very limited effects on any kind of relative surveying application.

Table 2.1 Types of errors in GPS observables

TYPE / ERROR	CODE			PHASE	
	C/A	P1	P2	L1	L2
Anti-Spoofing	—	y	y	—	—
Select-Availability	y	y	y	y	y
Satellite orbit	y	y	y	y	y
Integer ambiguity	n	n	n	y	y
Cycle slip	n	n	n	y	y
Receiver clock	y	y	y	y	y
Satellite clock	y	y	y	y	y
Satellite hardware	y	y	y	y	y
Receiver hardware	y	y	y	y	y
Ionospheric delay	+	+	+	–	–
Tropospheric delay	+	+	+	+	+
Multipath	L	L	L	S	S
Measurement noise	L	P	P	H	H
Error: y exists, n does not exist Error size: L-large, S-small, P-precise, H-high precision Error sign: + positive, – negative					

For the phase, an arbitrary counter setting of the track register at the start of observations (phase lock) and the unknown distance at that time leads to an unknown integer number of cycles, called *the initial integer ambiguity*. Consequently this can become a key problem of a high precision positioning. During the operation of GPS, this integer setting will restart if the receiver loses lock, e.g. due to obstructions (masking) or interference to signal transmission. This integer discontinuity in phase data is called a "*cycle slip*". The rest of the errors are included in both types of observables. The multipath and the measurement noise on the code are much larger than those on the phase. The ionospheric delay on code and phase is characterised by having the opposite sign, but being of the same size. For clock errors and tropospheric delay,

there is no difference between code and phase. The clock errors can be the largest source of the remaining errors. But by using relative positioning, the clock errors and the hardware biases can be eliminated. Also the propagation errors, including the ionospheric and tropospheric delays, can be reduced. For short baseline relative positioning, only the multipathing problem needs to be considered. However for long baseline relative positioning, the combined effect of other errors such as ionospheric and tropospheric delays cannot be ignored, and can lead to problems in resolving ambiguities in current precise GPS techniques.

The observation equations of code and phase can be expressed in units of meters as follows.

$$P^k_{j,1}(t) = \rho^k_j(t) - c\,dt^k_j + T^k_j(t) + I^k_{j,1,p}(t) + B^k_{j,1,p}(t) + M^k_{j,1,p}(t) + \varepsilon_{1,p} \quad \text{.....(2.3a)}$$

$$P^k_{j,2}(t) = \rho^k_j(t) - c\,dt^k_j + T^k_j(t) + \frac{f_1^2}{f_2^2} I^k_{j,1,p}(t) + B^k_{j,2,p}(t) + M^k_{j,2,p}(t) + \varepsilon_{2,p} \quad \text{.....(2.3b)}$$

$$\Phi^k_{j,1}(t) = \rho^k_j(t) - c\,dt^k_j + T^k_j(t) + \frac{c}{f_1} N^k_{j,1}(1) - I^k_{j,1,p}(t) + B^k_{j,1,\Phi}(t) + M^k_{j,1,\Phi}(t) + \varepsilon_{1,\Phi} \quad \text{.....(2.4a)}$$

$$\Phi^k_{j,2}(t) = \rho^k_j(t) - c\,dt^k_j + T^k_j(t) + \frac{c}{f_2} N^k_{j,2}(1) - \frac{f_1^2}{f_2^2} I^k_{j,1,p}(t) + B^k_{j,2,\Phi}(t) + M^k_{j,2,\Phi}(t) + \varepsilon_{2,\Phi} \quad \text{..(2.4b)}$$

where

$P^k_{j,1}(t)$, $P^k_{j,2}(t)$ are the L_1 and L_2 code observations in units of meters,

$\Phi^k_{j,1}(t)$, $\Phi^k_{j,2}(t)$ are the L_1 and L_2 carrier phase observations in units of meters, relating to the observables in cycles expressed as $\varphi^k_{j,1}(t) = \Phi^k_{j,1}(t)/\lambda_1$ and $\varphi^k_{j,2}(t) = \Phi^k_{j,2}(t)/\lambda_2$, where $\lambda_1 = c/f_1$ ($\approx$ 19cm) and $\lambda_2 = c/f_2$ ($\approx$ 24.4cm) are the wavelengths of the dual frequency signals, and c is the speed of light in vacuum,

$\rho^k_j(t)$ is the true range between the satellite and the antenna,
$= [\,(x_j - x^k)^2 + (y_j - y^k)^2 + (z_j - z^k)^2\,]^{-1/2}$,

dt^k_j is the combined clock error of receiver and satellite,

$T^k_j(t)$ is the propagation error of troposphere,

$N^k_{j,1}(1)$, $N^k_{j,2}(1)$ are the initial integer ambiguity of L_1 and L_2 carrier phase,

$I^k_{j,1,p}(t)$, $I^k_{j,1,\Phi}(t)$ are the ionospheric propagation errors on L_1 code and phase, and

$$I^k_{j,2,p}(t) = \frac{f_1^2}{f_2^2} I^k_{j,1,p}(t),\ I^k_{j,1,\Phi}(t) = -I^k_{j,1,p}(t),\ I^k_{j,2,\Phi}(t) = -I^k_{j,2,p}(t),$$

$B^k_{j,1,p}(t)$, $B^k_{j,2,p}(t)$ are the combined effect of receiver and satellite hardware delays on L_1 and L_2 code,

$B^k_{j,1,\Phi}(t)$, $B^k_{j,2,\Phi}(t)$ are the combined effect of receiver and satellite hardware delays on L_1 and L_2 phase,

$M^k_{j,1,p}(t)$, $M^k_{j,2,p}(t)$ are the mutlipathing errors on L_1 and L_2 code,

$M^k_{j,1,\Phi}(t)$, $M^k_{j,2,\Phi}(t)$ are the mutlipathing errors on L_1 and L_2 phase,

$\varepsilon_{1,p}$, $\varepsilon_{2,p}$ are the measurement noises on L_1 and L_2 code,

$\varepsilon_{1,\Phi}$, $\varepsilon_{2,\Phi}$ are the measurement noises on L_1 and L_2 phase.

To simplify equation (2.3a), (2.3b), (2.4a) and (2.4b) above by combining the common parameters for further analysis, the corresponding equation (in meters) can be rewritten as

$P1 = R + r_1 I + B_1 + M_1 + e_1$ .....(2.5a)

$P2 = R + r_2 I + B_2 + M_2 + e_2$ .....(2.5b)

$L1 = R + \lambda_1 N_1 - r_1 I + B_1 + m_1 + e_1$ .....(2.6a)

$L2 = R + \lambda_2 N_2 - r_2 I + B_2 + m_2 + e_2$ .....(2.6b)

where

R is a combination of the true range ρ, clock errors dt, and the tropospheric delay T, ($= \rho + dt + T$),

$r_1 I$, $r_2 I$ are the L_1 and L_2 frequency ionospheric delays, $r_1 = 1.5457$, $r_2 = 2.5457$ (see section 4.3.1),

N_1, N_2 are the L_1 and L_2 frequency ambiguities,

λ_1, λ_2 are the wavelengths of L_1 and L_2 frequency signals,

B, *B* denote the code and phase hardware biases,

M, m denote the code and phase multipath errors,

e, *e* denote the code and phase measurement noises.

2.2.4 SATELLITE ORBITS

In the basic concept of GPS positioning, the satellite co-ordinates are considered as known parameters. In GPS either the broadcast ephemeris from the GPS navigation file provided by the control segment or a precise ephemeris (usually accessed through the Internet) provided by the ground segment, can be used to obtain the satellite co-ordinates.

The GPS navigation message file consists of 25 frames of data. Each frame consists of 5 subframes and each subframe begins with the telemetry word (TLM) and the handover word (HOW). The information in each subframe is listed as follows.

Frame 1: clock corrections

Frame 2 and 3: ephemeris parameters

Frame 4: special message, eight polynomial coefficients of ionospheric broadcast model, time conversion data of GPS to UTC, the almanac for satellites with SVN number 25 and higher

Frame 5: the almanac for satellites 1 through 24.

The almanac contains the data necessary to compute the approximate positions of satellites for general prediction purposes. The accuracy of satellite positions from the broadcast ephemeris is about 5m, which is equivalent to a baseline error of about 0.25 ppm and is sufficient for relative positioning over distances smaller than 20 km (Al-Haifi, 1995).

The precise orbits are based on well-defined tracking networks established by the ground segment (e.g. IGS, NGS) and broadcast on the Internet for use on a post-processing basis. The accuracy of the precise ephemeris is typically about a few parts in 10^{-9}. Therefore, to reduce the effect of orbit errors over long distances, this precise ephemeris is useful for the long baseline research described in this thesis.

2.2.5 PARAMETER ESTIMATION

As described in the previous two subsections, both code and phase observations, along with the satellite orbits and other ephemeris data, are provided by GPS receivers for the positioning computations. Usually the user cannot directly access this binary information because the format of the recorded data is unknown. For many applications (and for most research), it is therefore necessary to rely on the tools supplied by GPS manufacturers to convert the GPS data from the company's own data format to an

international GPS data exchange format (RINEX, Gurtner, 1994). Normally three types of files: the observation file and the navigation file, and the meteorology file are provided. Another format for GPS data exchange, known as the Newcastle Exchange Format (NXF) has been devised to include not only the standard observables but also a number of parameters. The conversion of RINEX to NXF has been implemented by the RINTONXF software (Corbett, 1995). For NXF, only a single file including the observables, some parameters and the satellite co-ordinates is created.

Based on equation (2.6a) and (2.6b), the double differencing form of observation equation for phase can be written as

1. Over short baselines

$$\Delta\nabla L1 = \Delta\nabla\rho + \Delta\nabla(\lambda_1 N_1) + \Delta\nabla m_1 + \Delta\nabla e_1 \quad \text{.....(2.7a)}$$

$$\Delta\nabla L2 = \Delta\nabla\rho + \Delta\nabla(\lambda_2 N_2) + \Delta\nabla m_2 + \Delta\nabla e_2 \quad \text{.....(2.7b)}$$

2. Over long baselines

$$\Delta\nabla L1 = \Delta\nabla\rho + \Delta\nabla(\lambda_1 N_1) + \Delta\nabla T - \Delta\nabla(r_1 I) + \Delta\nabla m_1 + \Delta\nabla e_1 \quad \text{.....(2.8a)}$$

$$\Delta\nabla L2 = \Delta\nabla\rho + \Delta\nabla(\lambda_2 N_2) + \Delta\nabla T - \Delta\nabla(r_2 I) + \Delta\nabla m_2 + \Delta\nabla e_2 \quad \text{.....(2.8b)}$$

where $\Delta\nabla$ is the double differencing operator. The range ρ is a function of station co-ordinates, x_j, y_j, ,z_j, and satellite co-ordinates, x^k, y^k, z^k, as follows

$$\rho = [\,(x_j - x^k)^2 + (y_j - y^k)^2 + (z_j - z^k)^2\,]^{-1/2} \quad \text{.....(2.9)}$$

After linearisation, the observation equations can be expressed as a matrix form.

$L_i = A_{ij} X_j$, $i = 1,m, j = 1,n$ .....(2.10a)

If $m = n$, then $X_j = A_{ij}^{-1} L_i$ .....(2.10b)

If $m > n$, then $X_j = (A_{ji}^T A_{ij})^{-1} (A_{ji}^T L_i)$ .....(2.10c)

where

L_i is the matrix of the observations, and m is the number of observation,

A_{ij} is the coefficient matrix of observation equations,

X_j is the matrix of parameters to be estimated, and n is the number of parameters.

The derivation of these equations is simply based on basic theory of Least Squares Adjustment (Mikhail, 1981). Usually the code solution can be used as an approximation for positioning using the phase. If the ambiguities N_1 or N_2 can be fixed previously, then the "best" solution can be obtained after the process of Least Squares

Adjustment. For most kinematic techniques, the key point is not the parameter estimation but the ambiguity resolution, and its success has to rely on minimising the effect of measurement errors. For long distance positioning, ambiguity resolution is affected by the increasing effect of errors decorrelating with the baseline distance, and hence the final solution of Least Squares Adjustment can be affected by not only the fixed ambiguities (if wrong) but also the effect of these errors. Therefore, an accurate modelling of these errors is useful for resolving ambiguities by reducing these effects, and then high precision positioning can be expected, especially for long distance applications.

2.2.6 DIFFERENCING STRATEGIES

Undoubtedly the accuracy of GPS positioning is limited, mainly due to the errors listed in Table 2.1. The purpose of adopting the differencing strategy is to eliminate or reduce the effect of these errors (e.g. the clock errors). There are several forms of the differencing process, so called single differencing, double differencing, triple differencing, and delta range. All are based on the undifferenced form as in equations (2.3) and (2.4), or (2.5) and (2.6). The differencing process can clearly only make sense when it involves two quantities (e.g. data of two stations, two satellites, or two observing epochs). Mathematically, the differencing process is called single differencing by taking differences only once, double differencing by taking differences twice, and triple differencing by taking differences three times. Delta range is a single differencing process based on the data of two observing epochs. For phase data, the observation equations of these differencing observables (also suitable for code data) can respectively be written as follows:

1. Single differencing

$$\Phi_{AB}^{k}(t)=\Phi_{A}^{k}(t)-\Phi_{B}^{k}(t) \quad \text{.....(2.14a)}$$

$$\Phi_{A}^{k\,l}(t)=\Phi_{A}^{k}(t)-\Phi_{A}^{l}(t) \quad \text{.....(2.14b)}$$

2. Double differencing

$$\Phi_{AB}^{k\,l}(t)=[\Phi_{A}^{k}(t)-\Phi_{B}^{k}(t)]-[\Phi_{A}^{l}(t)-\Phi_{B}^{l}(t)] \quad \text{.....(2.15)}$$

3. Triple differencing

$$\Phi_{AB}^{k\,l}(t_{12})=\Phi_{AB}^{k\,l}(t_{2})-\Phi_{AB}^{k\,l}(t_{1}) \quad \text{.....(2.16)}$$

4. Delta range

$$\Phi_{A}^{k}(t_{2},t_{1})=\Phi_{A}^{k}(t_{2})-\Phi_{A}^{k}(t_{1}) \quad \text{.....(2.17)}$$

The between-station single differencing as equation (2.14a) eliminates the common errors from satellite k, which include satellite clock errors and hardware biases, and reduces orbital errors and atmospheric delays. The between-satellite single differencing as in equation (2.14b) can eliminate the common errors from receiver A, which include receiver clock errors and hardware biases, and reduces atmospheric delays. With the basic parameters of station co-ordinates, all parameters of the satellite (or receiver) clock, the troposphere, the ionosphere, and the multipath still remain in the observation equation, and the effect of these errors can decrease the positioning accuracy if using single differencing observables.

After double differencing as equation (2.15), the clock errors and hardware biases are all cancelled, and the orbital errors and the atmospheric delays are reduced. Remaining are the basic co-ordinates, the troposphere, the ionosphere, and the ambiguity for the phase, and the multipath for the code and the phase. Over short distances, for phase, the combined effects of the troposphere, the ionosphere, and the small phase multipath can be neglected, resolving the ambiguities can therefore become the key issue of GPS techniques adopting the double differencing strategy. However as the baseline length extends, the combined effects can no longer be ignored and these errors can hence be the inherent problems of resolving ambiguities for long baseline positioning. For phase users, usually the code solution, affected by the code multipath, is used for obtaining the approximate co-ordinates. Up to now, double differencing is adopted by most current GPS techniques.

Actually if there are no cycle slips in the phase data, the cancellation of ambiguities can be the great advantage of using triple differencing based on double differencing and two epoch differencing. Theoretically the more times the differencing, the less the geometric strength. Parameter estimation using Least Squares Adjustment, can then result in a divergence of the solution due to even a small error. Usually triple differencing is often used for cycle slip detection and repair (introduced in chapter 5). This strategy has been utilised by the KART and LRK techniques (introduced in section 2.3.2) and the achievement of centimeter positioning accuracy over 40 km baselines has been reported (Barboux, 1994, Gounon and Erceau, 1998).

Delta range is a single differencing process based on data from two epoch differencing. This observable depends on the change of the receiver and satellite clock errors between two epochs. The hardware biases can be deleted because the observing interval time between two epochs is short (usually the hardware biases are assumed constant on a time scale of weeks to months, see Wilson and Mannucci, 1993). The orbital errors and the atmospheric delays can greatly be reduced. For the phase, the ambiguities are eliminated providing there is no cycle slip between two epochs. This can be the greatest advantage of using the delta range observable. Therefore this observable can be used for point positioning, but the clock errors and the poor geometric strength then become a critical concern.

The benefits of the various differencing strategies can be summarised as follows.

- After the single differencing process, the common errors of the receiver are cancelled based on two satellites (the first), the common errors of satellites are deleted based on two stations (the second), and the errors of ambiguity and hardware biases are eliminated based on two observing epochs (the third). The first and third single differencing observables can be used for point positioning, and the second one demanding the data of two stations is not as often used as the double differencing observable.
- Double differencing is the popular way for achieving relative positioning because the clock errors and hardware biases are no longer taken into consideration, but some problems are still of concern in this the method, especially that of resolving ambiguities, and the effect of atmospheric delays and multipath. The problem of resolving ambiguities in the relative positioning can be solved simply by using triple differencing, but the low geometric strength of the triple differencing observable (even the double differencing one) cannot be ignored because the parameter estimation can be too sensitive to these remaining errors.
- For GPS relative positioning over short baselines, the effect of the atmosphere is almost eliminated because of the almost equivalent path of signal transmitted from the same satellite to two close receivers, but the effect of multipath, depending on the environment of observing sites, may be even larger after differencing. For long distance baseline positioning, the equivalent condition of similar signal path can no longer exist, and the effect of propagation delays, depending on the baseline distance and variation of atmosphere, cannot be ignored.

- If using the differencing between two observing epochs (e.g. triple differencing and delta range), the constant biases in the observables such as ambiguities and hardware biases can be eliminated, but the low geometric strength can be a problem for positioning. However, positioning with a low geometric strength cannot result in a high accuracy level, unless the effect of measurement errors can be reduced by an accurate modelling or the strength can be increased (e.g. by a long observation session).

2.2.7 LINEAR COMBINATIONS OF GPS OBSERVABLES

A dual frequency receiver can track and lock the L_1 ad L_2 frequency signals broadcast by the satellites. Initially the second signal was supposed to be used for self-calibration of the ionospheric delay of the signal through a linear combination with the first signal. After certain linear combinations of code or phase observables as expressed in (2.3) and (2.4), some parameters can be eliminated correspondingly. Therefore, certain linear combinations of observables can be used for GPS positioning, and modelling of measurement errors. The general form of a linear combination of GPS observables can simply be written as

$$L = \mu_1 A + \mu_2 B \quad \text{.....(2.18)}$$

where

L is the GPS combination observable,

A is the L_1 frequency phase (or code) observable,

B is the L_2 frequency phase (or code) observable,

μ_1, μ_2 are arbitrary constants.

Based on equation (2.18), *the ionosphere free combination* L3, *the ionospheric combination* L4 (often called *the geometry free observable*), and *the widelane combination* L5 can be obtained from a linear combination of dual frequency observables L1 and L2.

Substituting $\mu_1 = r_2$, $\mu_2 = -r_1$, A = L1, and B = L2, then

$$L3 = r_2 L1 - r_1 L2 \quad \text{.....(2.19)}$$

If $\mu_1 = 1$, $\mu_2 = -1$, A = L1, and B = L2, then

$$L4 = L1 - L2 \quad \text{.....(2.20)}$$

If given $\mu_1 = r_1/\lambda_1$, $\mu_2 = -r_2/\lambda_2$, A = L1, and B = L2, then

$$L5 = (r_1/\lambda_1)L1 - (r_2/\lambda_2)L2 \quad \text{.....(2.21)}$$

The observation equation of L3, L4, and L5 can be written as

$$L3 = R + (r_2\lambda_1 N_1 - r_1\lambda_2 N_2) + (r_2 B_1 - r_1 B_2) + (r_2 m_1 - r_1 m_2) + (r_2 e_1 - r_1 e_2) \quad \text{.....(2.22)}$$

$$L4 = (\lambda_1 N_1 - \lambda_2 N_2) - I + (B_1 - B_2) + (m_1 - m_2) + (e_1 - e_2) \quad \text{.....(2.23)}$$

$$L5 = (1/\lambda_1 - 1/\lambda_2) R + (N_1 - N_2) - (r_1/\lambda_1 - r_2/\lambda_2) I + [(1/\lambda_1) B_1 - (1/\lambda_2) B_2)] + [(1/\lambda_1) m_1 - (1/\lambda_2) m_2)] + [(1/\lambda_1) e_1 - (1/\lambda_2) e_2)] \quad \text{.....(2.24)}$$

In fact, as well as the basic L1 and L2 observables, the ionosphere free combination observable L3 and the widelane combination observable L5 are often used for positioning, and L4 is often used for ionospheric modelling. For GPS, these observables can be more useful if applied together with the differencing processes. Based on GPS phase observables (including the basic dual frequency observables and the three combination observables), the comparisons in terms of the ambiguity (integer or float), the remaining parameters (including undifferenced and differenced modes), the noise level, and the applications, has been made as in Table 2.2. The contents of this table are summarised below, assuming there are no cycle slips and the hardware biases are constant within a period of a few hours.

- The initial idea of using the L3 observable was to eliminate the effect of ionosphere, which can be its greatest advantage. However the noise level in the L3 observable is about three times as large as that in the L1 observable, and the combined ambiguity is no longer an integer. Both are the disadvantages of using this observable. Unfortunately this observable is not suitable for GPS techniques that utilise the integer nature of the initial ambiguities (e.g. the Ambiguity Function Method). For GPS positioning and the investigation of tropospheric delay, this observable can be useful, but compared to the L1or L2 observable, its larger noise can result in lower positioning accuracy - especially over short distances.
- The greatest advantage of using the widelane observable L5 is that the combined ambiguity is still an integer. Usually this observable can be used for cycle slip detection and repair because the combined ambiguity is still an integer (introduced in chapter 5). For relative positioning, the noise level of this observable is about seven times that of L1 and this can be the limitation of the positioning accuracy

eventually. Also the effect of both tropospheric and ionospheric delays has to be taken into consideration over long distance positioning.

- The ionospheric combination observable L4, the so called geometry free combination observable, is often used for ionospheric modelling, hardware bias modelling, and cycle slip detection and repair, since the parameters of range, clock, and troposphere are cancelled. For ionospheric modelling using the single differenced L4 and double differenced L4, the former, including the ambiguity, the hardware biases, and the multipath, is based on one reference station, and the latter, consisting of the ambiguity and the multipath, is based on at least two reference stations.

Table 2.2 Comparison of GPS phase observables

OBS / ITEM		L1	L2	L3	L4	L5
Parameter	ud	All	All	—	—	—
	sd	All	All	All,-5	4,5,6,7	All
	dd	All,-2,-6	All,-2,-6	1,3,4,7	4,5,7	All,-2,-6
	td	1,3,4,7	1,3,4,7	1,3,7	5,7	1,3,4,7
	dg	All,-4,-6	All,-4,-6	all,-4,-5,-6	5,7	All,-4,-6
Ambiguity		Integer	Integer	Float	Float	Integer
Noise level		σ	σ	~2.98σ	~1.4σ	~6.67σ
Application		P,C	P,C	P,Mt	C,Mi,Mh	P,C

(1)Parameter 1.range 2.clock 3.troposphere 4.ambiguity
5.ionosphere 6.hardware biases 7.multipath; "-" deleted
.....ud–undifferenced, sd–single differenced,
dd–double differenced, td–triple differenced,
dg–delta range
(2)Ambiguity: Float, Integer.
(3)Noise level: L1 $-\sigma_1$, L2 $-\sigma_2$, $\sigma_2 \cong \sigma_1$, assuming$\sigma=\sigma_1=\sigma_2$
(4)Application: P–positioning, C–cycle slip detection and repair
Mt–tropospheric modelling, Mi–ionospheric modelling
Mh–modelling of hardware biases (instrument biases)
Presumption: 1. There are no cycle slips
2. The hardware biases are constant in few hour period.

- The triple differenced L4 observables (based on the data from two stations and two observing epochs) and delta ranges L4 observables (based on the data at one station and two epochs), only consist of two parameters: ionosphere and multipath.

Compared to the other observables, the delta range L4 observable seems to be an optimal observable for ionospheric modelling (introduced in chapter 7). The reason is that this observable only consists of the ionosphere and the multipath for phase data and is not affected by the other errors, as is the case with the other observables described here. Also it can be used on a one station basis. All that is necessary to be taken into consideration is the variation of the ionosphere with time and space, and the effect of phase multipath. The phase multipath has been investigated using the signal to noise ratio method in recent years (e.g. Axelrad, 1994, and Barnes, 1999). A more accurate ionospheric modelling can hence be expected in the future.

2.2.8 BASIC GPS RELATIVE POSITIONING STRATEGIES

As described in section 2.2.1, GPS positioning using the static or relative mode is capable of reducing the effect of measurement errors. For achieving precise GPS, both methods can be used separately or together, so called static positioning, static relative positioning, or relative positioning. All are suitable for single or dual frequency users, and for code and/or phase users. Usually GPS positioning using dual frequency phase data is preferred for achieving the highest accuracy positioning. Based on the strategy of static, relative, or both, many techniques have therefore been developed for static or kinematic GPS applications. However positioning using the static mode is suitable only for some applications such as the static survey, whereas relative positioning can be used for kinematic applications such as navigation.

In a *static relative positioning*, a long observation session and post-processing including pre-processing for cycle slip detection and repair are necessary for high precision positioning to be possible. Over short baselines, the problem of GPS positioning is focused on the code multipath if using code measurements, and ambiguity resolution if using phase measurements. As the baseline length increases, the propagation errors and the orbital errors (less important if using the precise ephemeris) can no longer be ignored and the combined effect may cause a serious problem in resolving ambiguities. The benefit of using the static mode is that a time series of data can be utilized. Over short baselines, the ambiguities are resolved more easily using the linear combination observables. Over long baselines, a sequential least squares adjustment, the sequential bias fixing method, and the sequential bias optimising method can be used to resolve ambiguities (Blewitt, 1989).

Kinematic relative positioning, differs from static positioning in that the roving receiver is allowed to move continuously, the processing algorithm should be capable of working in real time, and an initilization procedure (for ambiguity determination) is usually necessary. Kinematic GPS surveys are possible with the code, the phase, or both, the more accurate positions being derived from the phase observables. For real-time kinematic GPS, the resolution of ambiguities is essential during the initialization at the beginning of the operation. Once the ambiguities are fixed, they can be used for the subsequent mission. Many kinematic techniques, with both static and "on the fly" initialization have been developed for kinematic positioning as follows.

- Static initilization

  For kinematic GPS with static initilization, many techniques have been developed as follows.

  1. Conventional static initial approach: a classical static mode, two known station occupation method, and the antenna swapping technique (Hofmann-Wellenhof and Remondi, 1988).
  2. Pseudo-kinematic (reoccupation) mode: a modified classical static mode (Remondi, 1990), two visits method (Ashkenazi & Summerfield, 1989).
  3. Stop-and-go (semi-kinematic) mode.

  The common problems of these techniques are the long occupation and practical limitation since the initialization constants N are only valid with a premise of no cycle slips after moving. This is unacceptable for some applications such as hydrographic survey and airborne applications because re-initialisation is not possible if cycle slips occur during the operation.

- On The Fly (OTF) initilization

  Kinematic GPS without static initilization (so called "On The Fly" initilization) usually requires five satellites to fix the initial integer ambiguities while moving. This is carried out using one or more of various ambiguity search techniques, which include:

  1. The least squares ambiguity search technique (Hatch, 1989,1990),
  2. The Ambiguity Function Method (Counselman and Gourevitch, 1981; Remondi, 1984,1990; Mader, 1986; Cross et. al., 1993; Corbett, 1994),
  3. The ambiguity covariance method (Frei and Beutler, 1990; Euler and Landau, 1992).

The basic procedure of all techniques involves generating a search volume from the initial solution, qualifying possible candidates for the ambiguities, and determining the correct position by a statistical test. Many efforts, such as reducing the size of search volume, increasing the computation efficiency and increasing reliability and quality of positioning have been made (Lachapelle, 1992, Erickson, 1992, Hansen, 1994, Al-Haifi 1996, Han, 1995, Teunissen et. al., 1994, Chen 1994a and 1994b,). However the need for continuous phase lock on the satellites is a basic requirement for a productive implementation of these search techniques.

2.3 CURRENT STRATEGIES FOR KINEMATIC RELATIVE GPS

To date, kinematic techniques with either static initialization or OTF initialization are applicable only for short baselines if centimeter level positioning is to be achieved. Practically there are many limitations (e.g. cycle slip problems) and long occupation times during the static initialization are required for some applications. In order to decrease the time (or number of epochs) needed for initialization during kinematic GPS, and to extend its use to longer distances more research will be needed onto the following.

1.DGPS: high accuracy DGPS, with the corrections based on networks of reference stations, for better quality approximate positions,
2.RTK: refining the OTF method and enhancing its real time capability, and
3.Single-epoch AFT: increasing the reliability of ambiguity resolution and hence the flexibility of the method.

2.3.1 DIFFERENTIAL GPS (DGPS)

Differential GPS applies corrections to the observed code and/or phase measurements to enhance the performance of current GPS techniques. Depending on the observables, *conventional DGPS* using (raw or smoothed) code data and *precise DGPS* using phase data can be distinguished. *Extended DGPS* based on networks of reference stations, depending on the coverage area of reference stations of the network, can be divided into three subsets. Local Area DGPS (LADGPS), based on single reference station or a

local network (i.e. at least three reference stations), is confined to small areas. Wide Area DGPS (WADGPS), based on more than three reference stations, can extend to a continental range. Worldwide DGPS (WWDGPS), based on global networks of permanent stations (e.g. IGS stations or even private reference stations), can extend to a global range. Differential positioning also allows for real time positioning. Its achievable accuracy depends on the accuracy of current models for corrections. For conventional DGPS, the differential corrections have focused on dealing with errors due to the ephemeris, clock, atmosphere (ionosphere and troposphere), and S/A. For precise DGPS, two main error sources (i.e. ephemeris and atmosphere) are of most concern. Although corrections can be obtained from the navigation message file or from results of modelling, they are still not suitable for precise DGPS.

In recent years, many ionospheric models (including global, regional, and local models) have been developed, and hourly vertical total electron content (TEC) maps are available on the Internet. The results of comparisons of ionospheric models have indicated an accuracy of 5-10 TECU (introduced in Chapter Four). Many models (e.g. Langley, 1992, Coster et. al., 1996, Collins and Langley, 1998) have been tested for tropospheric corrections, most based on the Sasstamoinen model. In Collins's model, the value of a zenith delay error is almost $\pm$20cm, which can lead to a potential 2m bias in height. Many studies of DGPS of the use of corrections, particularly wide area DGPS, have been carried out (Kee et. al., 1992, Ashkenazi et. al., 1992, Klobuchar, 1993, Catchpole et. al., 1993, Johnston, 1993, Chavin, 1996). In general, sub-meter accuracy is achievable with conventional DGPS using phase smoothed code ranges and obtaining correction data from one reference station only. Precise DGPS is suitable for applications demanding accuracies in the sub-decimeter range. However, the accuracy decreases with increasing distance from the base station (WARSAW University of Technology, 1998). Also, for network DGPS, disadvantages such as the cost of installation and maintenance of reference stations, more complex hardware and software, and data communication, lead to many practical operational problems. The result is that the capability of current kinematic techniques is still limited to short baseline positioning. For the establishment of reference operating stations, the density of reference stations must be high. Therefore the development of a high precision kinematic technique for long distances continues to be necessary.

2.3.2 REAL TIME KINEMATIC (RTK) GPS

Real Time Kinematic (RTK) GPS with two receivers and a radio-link between the receivers has led to the OTF kinematic techniques being extended from a post-processing to a real time mode. Their ability to increase the capability of RTK GPS can be characterised as follows.

- Shortening the initilisation time (or reducing the number of epochs),
- improving the reliability of ambiguity resolution over long baselines and in difficult environments, and
- reducing latency.

Currently the operation of GPS RTK (e.g. Ashtech's RTZ, Leica's RT-SKI, and Trimble's GPS Total Station) is based on dual frequency uninterrupted phase data (continuously collected at least about several tens of seconds depending on the configuration of available satellites). With using these initially collected data, at least four (but ideally five) common satellites observed at the base and rover stations are necessary for resolving ambiguities. After the ambiguities are fixed, they can be used for the rest of the data, but only if phase lock on not less than four common satellites is maintained. If not, re-initialisation is necessary. In general, centimetre level accuracy, 10-15 km operating ranges and initialisation time of about 2 minutes can be achieved by most of current RTK techniques. However, as has been previously emphasised the limitation of short range applications is still a problem of RTK GPS.

Triple differencing positioning - the KART (Kinematic Application Real Time) or LRK (Long Range Kinematic) - is a technique for Real Time Kinematic GPS (Gounon et. al., 1998). In the processing principle of both techniques, first, an initialisation process generates an approximate position. Then a computation through recurrent calculation of the approximate position can gradually converge on the basis of a combination of code and/or phase triple-differences, and finally the true solution at the centimetre level of positioning accuracy can be achieved after a number of iterations. However, to obtain the approximate position a reliable OTF, or Rapid Static initialisation process, is necessary for both techniques. KART works with single frequency data and needs an initialisation time of few minutes on average, which is four times slower than that required by the LRK working with dual frequency data. The coverage of the former is

limited to 10 km to 15 km whereas it is claimed that of the latter can extend up to 40 km (Barboux, 1994, Gounon and Erceau, 1998).

2.3.3 A SINGLE-EPOCH AFT

Single epoch positioning—the Single-Epoch Ambiguity Function Technique (AFT, details see next chapter) has been developed to resolve ambiguities and thus the positioning with a single epoch of dual frequency data (Cross, 1993, Corbett, 1994, Al-Haifi, 1996, and Al-Haifi et. al., 1998) in a static or kinematic mode. This method has been found to be quite successful in centimeter level positioning accuracy over short baselines (< 10km), provided there are at least 5 satellites, relatively small multipath, and ionospheric effects are reduced to a negligible level after double differencing. This technique is immune to corruption from cycle slips and provides instantaneous positioning which are the greatest advantages of using the measurements from only a single epoch (Pratt et. al., 1998). However, highly accurate, reliable, and practical ionospheric modelling is necessary before this technique can be extended to long baselines.

2.4 APPLICATIONS OF LONG BASELINE GPS

In general, GPS applications can be classified into navigation and survey and can be further divided into global, regional, and local uses. Depending on the required positioning accuracy, either the Standard Positioning Service (SPS), or the Precise Positioning Service (PPS) can be used. Currently, for static positioning over long baselines (few hundred kilometers), an accuracy of almost 1 part in 10^9 can be achieved. Therefore, in survey applications, high precision GPS is available for global uses. For initialization kinematic applications, RTK GPS on the market is still limited to short range applications (e.g. baseline < 14 km, correct 99.93%, < 30 sec, Leica System 500, 1999). For some applications, the LRK, with centimetric level accuracy and a range of up to 40 km is available for local use.

In addition, high precision GPS services, are expected to be available with the establishment of permanent national reference stations for many developed countries in the near future. Based on current GPS techniques, the density of reference stations might have to be very high for RTK work. Especially in recent years national GPS

networks combined with private reference stations have been established for future DGPS and RTK GPS services in many countries. For example, the national GPS network in Great Britain consists of about 900 GPS ground marks (covering the country at a typical station separation of 20-30 km in its original form). The active data based on 25-30 operating reference stations will become available to users by the end of 1999, and a national real time precise positioning service in sub-decimeter positioning accuracy is expected within the next five years (Ordnance survey, 1999). Station spacing is, however, too high for a complete national coverage of RTK GPS with its current operational limitations.

2.5 SUMMARY

RTK GPS has been improved recently, but it still needs a few tens of seconds initialisation and is limited to short baselines. For a real time kinematic survey based on the OTF techniques, the point is not to gain computation speed but to accomplish the initialization (reliably) in fewer epochs (Remondi, 1992b). Currently the accuracy of DGPS with these corrections generated based on the reference station and network, decreases as the baseline distance increases. However reducing the effect of measurement errors can increase the reliability of ambiguity resolution and the accuracy of positioning. The LRK has shown that triple differencing positioning (even with low geometric strength) is still able to achieve the positioning at centimetre accuracy level up to 40 km. In the strict sense of real time kinematic GPS, instantaneous positioning is only possible with a technique that uses single epoch measurements. The advantage of single epoch positioning is that it is immune to corruption from cycle slips, but at this moment, the single-epoch AFT (introduced in Chapter 3) is only applicable for short baselines.

For network DGPS, the measurements from each station are sent to a master station for the computation of vertical ionospheric delays, and then the corrections are broadcast to users. If changes in the ionosphere occur too quickly, the time required to update the ionospheric grid and the transmission of the corrections to users will lag the actual ionospheric changes (Doherty and Gendron, 1997). Hence this cannot fully satisfy all of the real time requirements of kinematic GPS users.

In a scheme for the establishment of national reference operating stations for future RTK GPS services, the following factors need to be considered.

- cost, especially of: station installation and maintenance,
- density, i.e. distance between reference stations, and
- methodology, i.e. the capability, reliability, and accuracy of current techniques, and data communication.

If the RTK technique can fully operate over 20-30 km baselines, the number of station set-up can reduce 4 times, with comparison of current RTK capability of about 15 km baselines.

Based on the comparison of the properties of GPS observables, either single differenced or double differenced L4 phases are necessary to resolve the ambiguities or hardware biases prior to ionospheric modelling. In practice, the preprocessing of ambiguities or hardware biases is time consuming, and the speed of updating the correction data cannot reflect the actual variation of the ionosphere with time, and hence satisfy the real time requirements of many GPS applications.

Therefore, after considering the practical and technical requirements of RTK GPS, the following conclusions can be drawn.

- The optimal strategy of RTK GPS should be based on single epoch positioning.
- A more accurate modelling of GPS errors is necessary to extend the use of current techniques for longer distances.
- Modelling these errors, using single reference station would be more practical than using networks.
- For the ionosphere, use of the delta range L4 would appear to be the most hopeful strategy to achieve high accuracy modelling.

Therefore high precision instantaneous positioning for long range applications can be possible if the single-epoch AFT can be adapted to operate over long baselines. To do this accurate ionospheric modelling must play a significant role. Ionospheric modelling might be accomplished by just using one reference station with the past hour's (or few hours') dual frequency data at a reference station. Then the generated ionospheric

profile can be used for predicting the instant ionospheric corrections at the rover. Finally, the single-epoch AFT with these corrections might then work for long baseline positioning. However because of the occurrence of cycle-slips, which are unavoidable during data collection, reliable software for cycle slip detection and repair is necessary for ionospheric modelling, and the optimal candidate observable for this is the delta range $L4$.

CHAPTER THREE

SINGLE EPOCH AMBIGUITY FUNCTION TECHNIQUE OVER LONG BASELINES

3.1 INTRODUCTION

As discussed in the previous chapter, a large amount of research has focused on the refinement of processing strategies for OTF ambiguity resolution so as to enhance the positioning performance and achieve a goal of high precision real time kinematic (RTK) GPS. To date, an initialization process of about a few tens of seconds and a continuous phase lock on satellites are required for most of current RTK techniques during the operation of GPS positioning. In particular the process of re-initialisation is necessary if the signals are interrupted during an RTK survey and this is not acceptable for some GPS applications such as offshore survey. Moreover, most of these techniques are still currently limited to short range applications. Consequently due to these limitations, the shortening of the initialisation time, and the extension of the use of these techniques to long distances and to difficult environments is of great importance to the development of RTK GPS and remains as a major challenge.

Fortunately, an algorithm called the single epoch Ambiguity Function Technique (AFT), exploited for example by P.A.Cross, 1993, is a searching technique to resolve the ambiguities and thus the position with the independent single epoch dual frequency GPS data based on the ambiguity function method (AFM) and a statistical test. This technique, without any process of initialisation, has the great advantage of providing instantaneous positioning, which is a benefit beyond the capability of other current RTK techniques. After two stages of research, the capability of this technique has been greatly improved, and currently the accuracy of positioning at the centimeter level can be achieved for short baseline applications as long as the level of noise in the phase data from five or more satellites is small. Nevertheless, this technique is still limited to short distance applications. In order to extend the use of this technique for the RTK GPS applications over long baselines, further investigations are necessary and these form the key foundation of this research.

This chapter is presented in five sections. The first describes the problems of current RTK GPS techniques and the importance of this research on the single epoch AFT to future RTK GPS. Through the review of previous research on the single epoch technique over short baselines in next three sections, the actual problems of this technique can be examined from a viewpoint of long distance applications. The subsequent section investigates the performance of this technique over different baselines of long distances, including the description of the experiments carried out, the criteria of the performance evaluation, and the analysis of final results. Based on the theoretic and practical analysis in the previous sections, the exploitation and possible solutions to the actual problems of single epoch AFT over long baselines are summarized in the final section.

3.2 THE SINGLE EPOCH AMBIGUITY FUNCTION TECHNIQUE

With the single epoch (instantly received) dual frequency GPS data at the base (known) and rover (unknown) station, an algorithm called the single epoch ambiguity function technique (AFT) has been developed to resolve the ambiguities and hence determine the position of unknown station for the applications of a high precision static and kinematic surveying (Cross 1991, 1991, and Cross al. et., 1993). The basic theories of this technique are based on the AFM and an associated statistical test. During the first stage of the development of this technique, it was implemented within the so-called the GPS Ambiguity Search Program (GASP), and the computation time was optimized for searching the correct integer ambiguity and mobile position among a reduced number of test points in a search volume (Corbett, 1994, and Corbett al. et., 1995a, 1995b, and 1995c). During the second stage, the ability of this technique for searching the correct ambiguity candidate and position has been greatly improved with the modified procedure of initial solution generation for the rover station, the flexible searching algorithm, and a weighting approach (Al-Haifa, 1996).

Both of these two stages have focussed on the accomplishment and the performance improvement of the technique over short baselines. In comparison of the results with those of commercial techniques, it has been found that positioning can be achieved at the sub-centimeter level for all of the observing time (100 percent success) provided that

the effect of noise level in the phase data from five or more satellites is less than 1 cm (Al-Haifi et. al., 1998). The single epoch AFT is now available for a high precision RTK GPS positioning, but nevertheless it is still limited to short distance applications. This technique is carried out basically with the procedures described in the following subsections.

3.2.1 GENERATION OF THE INITIAL SOLUTION

The first step of this technique is to obtain the approximate coordinates of the rover station and the associated variance/covariance information. This initial solution is used to determine the center of the search volume (introduced in the next subsection) and as an initial value in the parameter estimation in the Least Squares Adjustment (LSA). In GASP, this approximate solution is generated based on the built-in single epoch code solution algorithms and is called the Single Epoch Approximate Solution (SEAS) procedure (for details see Al-Haifi, 1996). Basically, based on the code observations from 4 satellites with the best geometry, this procedure has been implemented for obtaining the best solution (details see Al-Haifi, 1996).

However, for obtaining successful OTF ambiguity resolution, a good approximate solution has to be provided to initialize the searching process, denoted in Al-Haifi's research. In the case of long distance baselines, this solution can be affected by the increasing effect of errors due to the atmospheric delays, but compared to the effect of code-multipath, this differential effect is considered much smaller. Since the procedure of SEAS is based on the dual frequency GPS code data in a double differencing mode, to reduce the larger effect of the code multipath is more important than to reduce the effect of the ionospheric delays at the stage of initial solution generation. In practice, it is very difficult to model the effect of multipath in real time kinematic applications (Al-Haifi, 1998).

3.2.2 CONSTRUCTION OF A SEARCH VOLUME

To construct a search volume, the initial solution of the approximate rover position obtained based on the SEAS is used as a centre and expanded with a search size for

generating the trial positions, one of which is hopefully the correct one. To accomplish this procedure in the single epoch AFT algorithm, the following steps are carried out.

1. Considering all available satellites at the base and rover stations, 4 common satellites with best PDOP (i.e. minimum value) based on the possible combinations of 4 satellites are first used.
2. On the basis of these four satellites, the double differenced L1 phase data, with the highest satellite being chosen as the reference, is used to estimate the initial ambiguities using the provided approximate coordinates of rover station and the known coordinates of the base station. These estimated ambiguities are then rounded to the nearest integers.
3. These rounded ambiguities are considered as the integer solutions of initial ambiguities at the approximation position. These initial integer ambiguities with an option range of a search size from 1 cycle to 8 cycles are sequentially added to each corresponding ambiguity parameter of the second time least squares computation to obtain the test positions. For example, there are 343 (=7×7×7) double differencing ambiguities with their corresponding positions for a search volume of a search size of 3 cycles.

The process of this procedure may sound as if the computation load is significant at this stage. Actually, the computation is very quick indeed because the normal matrix and its inverse only needs to be calculated once (Cross et. al., 1993). Due to the increasing effect of observation errors over long distance baselines, a larger search size than usually used may be necessary to ensure the inclusion of the correct position of rover station. Therefore, the number of test positions tested in the next step of candidate qualification for the case of long baselines may be larger than that for short ones, leading to longer processing time.

3.2.3 QUALIFICATION OF TRIAL POSITIONS WITH AMBIGUITY FUNCTION METHOD

The basic concept of single epoch AFT to qualify the trial position in a search volume is based on the ambiguity function method (AFM). This method was first introduced by Counselman and Gourevitch, 1981. Subsequently many researches such as (Remondi, 1984 and 1990), (Mader, 1992), (Cross et. Al., 1993), (Corbett, 1994), (Al-Haifi, 1996)

and (Han, 1995) have been made to enhance this method for a high precision GPS relative positioning. The concept of AFM is that the true position of the rover is the one whose ambiguity function value is nearly equal to unity. Once the search volume has been constructed, several candidate positions will be identified from the trial positions including hopefully the true one by using the ambiguity function method (AFM) with a predefined threshold. Hence the two sub-steps included in this procedure are the computation of the ambiguity function value (AFV) at the trial positions and the determination of the threshold, are carried out in order to obtain the candidate positions as follows.

The computation of the AFV at the trial positions is shown in the following equations. After subtracting the phase observable with the range $\rho_i(t)$ calculated with the coordinates of the trial positions and the tropospheric delays based on the Saastamoinen model in a double difference mode (as equation 3.1a in unit of cycles), what is left in the observable is only the real-value ambiguity. This includes the integer portion and the combined errors, which can be neglected for the short baselines. This computed observation (the real-value ambiguity scaled by 2π), after taking the trigonometric cosine function (as equation 3.1b), is called the *ambiguity function value* AFV, and it should nearly equal unity if the trial position is located at the correct position.

$$AFV(x_i, y_i, z_i) = cos\ \{2\pi\ [\nabla\Delta\ \Phi_i(t) - f/c\ (\nabla\Delta\ \rho_i\ (t) + \nabla\Delta\ T_i(t))]\} \quad \text{.....(3.1a)}$$

$$= cos\ (2\pi\ [\nabla\Delta\ N + \nabla\Delta\ \varepsilon_i\ (t)\ ]\ ) \quad \text{.....(3.1b)}$$

$$= cos\ \{2\pi\ [\nabla\Delta\Psi_i(t)]\ \} \quad \text{.....(3.1.c)}$$

$$\rho_i(t) = [\ (x_i - x_s)^2 + (y_i - y_s)^2 + (z_i - z_s)^2\ ]^{-1/2} \quad \text{.....(3.1.d)}$$

where

$AFV(x_i, y_i, z_i)$ is the ambiguity function value of the trial positions, x_i, y_i, z_i ,

$\Phi(t)$ is the carrier phase measurement at the single epoch time t.

f is the GPS operating L_1 or L_2 frequency,

$\nabla\Delta$ is the double differencing operator,

N is the integer ambiguity,

$\nabla\Delta\ \varepsilon\ (t)$ are the estimation errors of the range based on the coordinates of trial positions and satellite, the estimation errors of tropospheric modelling, the ionospheric delays, and the phase multipath in a double difference

mode.

x_i, y_i, z_i are the coordinates of trial positions,

x_s, y_s, z_s are the coordinates of the satellites.

Currently in GASP, a combination of the L_1 and L_2 phase data has been used for obtaining the ambiguity function value on each test position, i, as expressed in the following equation.

$$AFV_i=\Sigma_{j=1,M-1}\Sigma_{k=1,L}\{cos\ [2\pi\ (\nabla\Delta L_1)_i\ ]+ cos\ [2\pi\ (S\cdot\nabla\Delta\ L_2)]_i\ ]\}\ /\ [2L(M-1)] \quad \text{.....(3.2)}$$

where

L is the number of reference receivers,

M is the number of satellites,

S is the weighting factor on L2.

By using an acceptance/rejection criterion called the *threshold*, these trial positions are then tested to isolate the correct candidate position on the basis of its corresponding ambiguity function value. If the trial position's ambiguity function value is within the threshold region, then this position is considered as a candidate position and passed to the next step. After this procedure, only a fixed percentage of the positions still qualify, including the correct one. However, this threshold has to be specified by the user (an option in GASP), and using the experience of previous research, 10% or 5% is usually used depending on the size of errors remaining in the observations. For long distance applications, the magnitude of ambiguity function value is associated not only with the effect of multipath, but also the increasing atmospheric errors remaining in the differenced observations. If the ambiguity function value at the true position is not within the threshold due to the effect of the remaining errors, then the true position is excluded from the group of candidates, leading to a failure of the procedure.

3.2.4 THE ESTIMATOR AND STATISTICAL TEST

After the application of the previous procedures, the correct position should be one of the selected candidate positions. In order to identify the correct position from these candidate solutions, a further identification procedure from a statistical point of view is carried out using the Fisher Test (F-Test) on the unit variance. The parameter estimation of least squares adjustment (introduced in the next subsection) is performed by using the L_1 and L_2 phase data, based on the population of each candidate position. The set of

adjustment weighted residuals is then computed for each candidate point and the corresponding solution unit variance which is considered as a sample estimator of the related candidate population. Based on the solutions of unit variance of these candidate positions, the one with the smallest variance is statistically considered the most likely solution of the correct position. For a statistical test with the F-test, the minimum variance $\hat{\sigma}^2_{0(\min)}$ will be validated against the other candidate variances $\hat{\sigma}^2_{0(i)}$ with this estimator F_s as follows.

$$F_s = \frac{\hat{\sigma}^2_{0(\min)}}{\hat{\sigma}^2_{0(i)}} \quad \text{.....(3.3.a)}$$

$$\hat{\sigma}^2_{0(i)} = \frac{\sum (V^T WV)}{n-3} \quad \text{.....(3.3.b)}$$

where $\hat{\sigma}^2_{0(i)}$ is the unit variance of the candidate positions from the least squares adjustment.

With this estimator, the test is then carried out as follows.

The null hypothesis is set up as:

$$H_0 : \hat{\sigma}^2_{0(\min)} = \hat{\sigma}^2_{0(i)} \quad \text{.....(3.4.a)}$$

and the hypothesis is tested against an alternative hypothesis:

$$H_A : \hat{\sigma}^2_{0(\min)} < \hat{\sigma}^2_{0(i)} \quad \text{.....(3.4.b)}$$

,and hence the test is

$$F_s = \frac{\hat{\sigma}^2_{0(\min)}}{\hat{\sigma}^2_{0(i)}} < F_{v,v,1-\alpha} \quad \text{.....(3.4.c)}$$

Where $F_{v,v,1-\alpha}$ is the critical percentile from the F distribution table with the v (= n-3) degrees of freedom, the α (usually set to 5%, the confidence interval is 95%) significant level, and n is the number of the observation equations. If the null hypothesis is rejected, it can be concluded that the positions corresponding to the minimum variance fix the data significantly better than any other and it can be accepted as the correct solution. On the contrary, if the null hypothesis is accepted it can be concluded that this position cannot be differentiated from the others and it cannot be known whether or not it is correct. However, in the case of long distance baselines, a wrong decision of this test can be made due to the increasing effect of errors, leading to the possible acceptance of a wrong position.

3.2.5 PARAMETER ESTIMATION AND THE APPLIED MODELS

For RTK GPS, the observation equations of single epoch AFT can be expressed as follows.

$$\nabla\Delta\Phi(t) = f/c\,(\nabla\Delta\rho\,(t) + \nabla\Delta T(t)) + \nabla\Delta N + \nabla\Delta\varepsilon(t) \quad \text{.....(3.5)}$$

After they have been linearized, the observation equations can be written as a form of matrix as follows.

$$V = A\,X + L \quad \text{.....(3.6)}$$

where

V is a matrix of residuals,

A is a coefficient matrix of observation equations,

X is a matrix of parameters which include x, y, z coordinate of rover station,

L is a matrix of constant part ($= f/c\,\nabla\Delta T_i(t) + \nabla\Delta N - \nabla\Delta\Phi(t)$).

$T_i(t)$ is the tropospheric correction computed using Saastamoinen model (Saastamoinen, 1973) with standard atmosphere parameters (temperature:18 degree, pressure: 1013.25 mbar, humidity: 50 mbar).

The details of least square adjustment are not supposed to be introduced in this thesis. Interested readers can see many textbooks (Mikhail, 1981, Cross, 1983).

The position corresponding to the correct set of integer ambiguities identified following successful application of the F-test is now accepted. Also accepted are the associated set of residuals, variance-covariance matrix, and unit variance.

3.3 FACTORS AFFECTING THE PERFORMANCE OF SINGLE EPOCH AFT

As shown in Table 2.1, there are many sources of error during the transmission of radio signals from a satellite to a receiver. The amount by which the accuracy of any particular current GPS positioning technique is affected by any of these errors depends on the processing strategy adopted. Therefore, in order to optimize positioning accuracy, different GPS positioning techniques may have different ways to reduce or eliminate the effect of these errors. The ways in which the single-epoch AFT deals (reduces or eliminates) with these errors can be summarized as follows.

1. The single-epoch AFT is insensitive to cycle slips.
2. The effects of clock errors (including the S/A dithering effect) and hardware biases are eliminated after double differencing.
3. The effect of errors in the satellite coordinates can be reduced to an irrelevant level if applying the precise ephemeris (no effect of S/A epsilon on the precise ephemeris), although they are any way likely to be insignificant over the ranges for which the method is applied.
4. The effect of tropospheric delays is reduced after applying the Saastamoinen model. However, the accuracy of this model still needs to be fully evaluated and remains a significant error source that reduces the distances over which the method can be successfully used. There are some evidences (Collins and Langley, 1998) that this model could be successfully used to obtain the zenith delays of the troposphere if a more sophisticated mapping function is used.

For most applications, the main effective error limitation on the performance of single epoch AFT result from multipath errors and the ionospheric delays, providing the use of the Saastamoinen model does not lead to a problem. Multipath is generally considered to be the main problem over short baselines, and the ionospheric delay is assumed to be the main problem over longer baselines. As discussed in the previous section, if these errors remain in the observations they may have a significant effect on the performance of the procedure at each step of single epoch AFT.

In summary, the following factors have the most significant effect on the performance of single epoch AFT.

- the surveying environment, area, time, and season (e.g. severe multipathing effects in urban areas and severe ionospheric effects in the equatorial anomaly region and during the solar maximum periods),
- the configuration, the elevation angle, and the number of satellites,
- the choice of threshold value during the application of the method.

3.4 ACHIEVEMENTS AND LIMITATIONS OF SINGLE EPOCH AFT OVER SHORT BASELINES

During the second stage of the development of the single-epoch AFT over short baselines significant improvements were achieved (Al-Haifi, 1996). Generally, using only a single epoch of dual frequency GPS data collected at the base station and the rover station from the signals from at least 5 satellites in a benign environment, the single epoch AFT can correctly resolve the ambiguities and achieve instantaneous positioning at a level of a single centimeter or better over a baseline of less than about 10km length.

In summary, the investigations on the performance of single epoch AFT over short baselines has found the following

- The procedure can produce the correct position all of the time and for 95% of the time, from 7 satellite dual frequency data observed over short baselines (< 1km) and over a 8.5km baseline, respectively. The lower percentage over the longer distance could be due to the effect of un-modelled distance related biases (e.g. atmospheric effects) or due to multipathing effects.
- Over even longer baselines the method continues to show a good performance with 7 satellites, but as the number of satellites decreases, the success rate diminishes.
- Severe multipathing effects are the limiting factors for single epoch AFT over short baselines (and even over a baseline of 11.5m length), particularly those from low elevation satellites (below 25° elevation angles). They may lead to a total failure of the AFT in resolving the correct ambiguities.

The results of the investigations on the performance of single epoch AFT with biased data (i.e. simulation observations obtained by adding arbitrary errors) have indicated the following.

- The double difference tropospheric residuals between the base and the unknown receiver are not negligible over height differences of more than 100m, even over less than 5km baseline lengths. This has been revealed by a linear drift of up to 3cm and an offset of between 7cm and 14cm in the resulting horizontal position components and height. Applying tropospheric corrections based on a standard model over such height differences largely removes the effects.

- The performance of the ambiguity function over short baselines (between 300 m and 1500 km) with data contaminated by generated random errors coupled with system noise and bias residuals have shown that the effect of the added errors on the performance of the AFT is largely proportional to the number of the satellites involved, rather than distance separation between the base and the unknown receiver. The tolerable noise size from 5 satellites has been shown to be within 1cm. This size increases with 7 satellites to reach almost 3cm.

Apparently, the limitation of using the single-epoch AFT for GPS positioning over short baselines is mainly due to the multipath problem. Currently, this problem is still a research topic. As far as the tropospheric model (Saastamoinen model) applied in this technique is concerned, it has been shown to work well over baselines of 300m and 1500m. Nevertheless, the results indicate that even adding only small errors can cause a poor performance of the AFT. In other words, even in a mild multipathing environment, a poor performance of this technique over short baselines may occur if the other errors such as tropospheric and ionospheric delays increase.

Overall, significant progress has been made in the development of the AFT as an operational method over short baselines and the associated research has provided very valuable conclusions on which to base further research, especially over long baselines (Corbett, 1995, Al-Haifi, 1996).

3.5 SINGLE-EPOCH AFT OVER LONG BASELINES

In order to develop further the single-epoch AFT so that it can be used over longer distances it is first necessary to examine its existing performance. The main purpose of this section is therefore to obtain a picture of the AFT performance as the length of baselines increase. Various trials over different lengths of baseline (> 10km) have been carried out with data collected (in a static mode) using modern GPS dual frequency receivers at both the base and rover station. The processing strategies follow the procedure described in the previous section (without modification), i.e. a kinematic experiment has been simulated by processing each epoch independently. The coordinates of the rover station have been calculated by the highly reliable and accurate

GPS software—GIPSY (JPL, 1992, and Gregorius, 1996) in a static post-processing with tropospheric and ionospheric corrections and with antenna center offset corrections made. These coordinates are considered as the true values for checking the results of the AFT.

3.5.1 EXPERIMENTS

As shown in Table 3.1 below, the experiments have focused on five data sets of GPS baselines from about 10km to 30km length between the base station and the rover station using about an hour dual frequency data with 30 second interval. The experiment area was located in a middle latitude region. Four sets of data were collected with Ashtech Z12 receivers and one set of data was collected with the latest product of Leica, the real time System 500. Two types of phase observations (L1 and L2) and code observations (C1 and/or P1, and P2) were recorded for all of the experiments in this research.

Table 3.1 Experiment trials

Baselines		Observing time	Length (km)	Receiver	Data types	Latitude (degree)	Height Diff. (m)
Base	Rover						
PSMS	SEMA	25/09/98 12:30:00-13:29:30	12.8	Ashtech z12	c1,p1,p2,L1,L2	40.35	323.70
CG54	KRPI	13/07/98 09:16:00-11:54:30	15	Ashtech z12	c1,p1,p2,L1,L2	37.90	222.52
INED	SHEN	19/08/99 11:11:00-12:10:30	21	Leica sys.500	c1,p2,L1,L2	51.71	-11.33
PSMS	PLAT	25/09/98 12:30:00-13:29:30	25	Ashtech z12	c1,p1,p2,L1,L2	40.64	269.92
PSMS	SOHO	25/09/98 12:30:00-13:29:30	33	Ashtech z12	c1,p1,p2,L1,L2	40.79	202.71

3.5.2 THE CRITERION USED TO EVALUATE THE PERFORMACE OF AFT

Comparison with the true position of the rover station is the most popular way to evaluate the final result when developing a new GPS technique. Basically there are two ways to obtain the true position of rover station. One is from previously known coordinates (eg when testing at stations that are part of a previously observed network) and the other is based on another reliable and high precision GPS software package. The GPS-Inferred Positioning System (GIPSY) is a GPS software package for precise

positioning over distance of metres to thousand of kilometres. In general, static positioning with GIPSY can be achieved with a baseline accuracy of 2 mm plus 2×10^{-9} of the length of the baseline (GIPSY II, Blewitt and Lichten, 1992) Other figures have also been found, e.g. 3 mm horizontal and 7 mm vertical precision in absolute station coordinates (GIPSY II, Heflin, 1996).

In GIPSY, many features, such as wet and dry tropospheric modelling, stochastic estimation of clock biases, have been used for obtaining a high precision positioning (see GIPSY II, 199). As a result, coordinates calculated from GIPSY are without doubt sufficiently reliable and accurate to be used for evaluating the results of the single epoch ambiguity technique. This point is important to this investigation of the AFT performance (or other further investigations) since the difference of results between the two techniques can be at centimeter, or even millimeter level, and it is important to be sure that the 'truth system' can be fully relied upon. If there were no higher accuracy positioning results from some techniques or methods, this investigation may lead to wrong conclusions. Therefore, before commencing the investigation of AFT over long baselines, the accurate coordinates of the rover station are obtained from the static positioning result of GIPSY with the same data sets and these are assumed to be the true values of the coordinates of the rover station. Comparison with these is the fundamental criterion used in this investigation.

In the GIPSY processing, precise products used are:

1. JPL final precise orbit (accurate to 5-8cm) files
2. JPL final satellite clock information files
3. JPL polar motion and earth rotation files
4. JPL satellite shadow event files
5. JPL daily transformation files from local system to ITRF97.

Daily coordinate estimates for each station are at the <1cm level (2d) and <2cm level for the height (both 95%). The final combined coordinates are <5mm in 2d (95%) and <1cm (95%) in height.

3.5.3 PROCESSING STRATEGIES

As described in section 3.3, the performance of single epoch AFT can be affected not only by observation errors but also by other factors. The former consists largely of the multipathing and atmospheric effects. The latter could include the initial approximate coordinates of rover station, the accuracy of the base station coordinates, the configuration, the elevation mask, the number and geometry of the satellites in the constellation, the accuracy of the satellite coordinates, and the accuracy of the applied models for other errors such as for tropospheric refraction. The combined effect of these factors makes it very difficult to distinguish the actual source and size of effective errors in different situations and survey environments when investigating the single epoch AFT over long baselines. Therefore, the isolation of error sources is important to further investigation and modelling of errors so as to enhance the final performance of this technique for long distances. This problem can be solved either by reducing the effect of other factors or by using the combined observables. For example, the adoption of precise ephemeris can be utilized for reducing the orbital errors, the higher elevation satellites can be chosen for reducing the effect of multipath, and the ionospheric combination or ionosphere-free combination based on the dual frequency observables are useful for investigating the tropospheric and ionospheric delays respectively (see section 2.2). Basically, multipath is the main error source of the AFT over short baselines, but as the baseline distance increases, the atmospheric error start to decorrelate because there is no longer complete geometrical equivalence of the signal path through the atmosphere between the satellite to the base and to the rover. Hence the effect of this error cannot be considered irrelevant and ignored.

However, for an initial investigation on the AFT performance over long baselines in this chapter, the processing strategies adopted are as follows.

1. Satellite coordinates are computed from the IGS precise ephemeris obtained over the Internet
2. The approximate coordinates of the rover station at each epoch are based on the code observations relating to that particular epoch.
3. Before processing the AFT software, all of the data from satellites below 20° elevation angle are deleted to reduce multipath and atmospheric effects.
4. As applied in the cases of short baseline investigations, the Saastamoinen model is still used for reducing the tropospheric effect.

5. The threshold of 90 % is set up to ensure the inclusion of the true positions.
6. The evaluation of final result of AFT over long baselines is based on the comparison with the result calculated using GYPSY II.

3.5.4 PERFORMANCE OF SINGLE EPOCH AFT AND ERROR ANALYSIS

Based on the strategies described in previous section, the trials in table 3.1 have been processed with GASP. After this processing, the performance of AFT over the baselines from 12.8 km to 33 km have been shown in the form of x, y, and z coordinates (in the WGS84 Cartesian coordinate system) and baseline length in Figure C.1 to Figure C.5 respectively. These figures are shown in Appendix C. The true values obtained based on processing with GIPSY, for all experiment baselines, are also shown in the same format as described above in each corresponding figure in order to enable an evaluation of the estimation results of the AFT.

In these figures, GASP results are denoted with a solid line while the true value is denoted with a dotted line. There are two types of solid line in the figure. The curved ones show the individual GASP results and the straight ones show the average of GASP estimation for the period of observation. The reason to take an average process of GASP estimation is that the effect of multipath has shown a characteristic of sinusoid for a period of observing time and the average of this effect is assumed near zero. Because of this characteristic of multipath, it seems that at least an hour of observing time is needed to reflect the effect of double differencing multipath in the RMS of the estimated baseline length. The effect of double differencing ionospheric delays (including the error of tropospheric imperfect modelling) should be reflected in the difference of the average of the estimated baseline length and known (from GIPSY) baseline length. For further analysis of the error effect, the RMS and average baseline length are also calculated only for epochs at which it can be certain that all of integers have been correctly fixed (i.e. excluding the unfixed epoch data, which would bias the estimation). The criteria: 2cm for baselines <13km and 5cm for baselines >13km), have been used for evaluating the positioning results and for the comparison of the positioning results with/without the ionospheric corrections (later discussed in Chapter 7). In order to see the differences after applying the ionospheric model (generated in Chapter 6), a smaller criterion is recommended for those lines since the differential effects that we are dealing with is

only at the few centimetre level over this range. Use of identical criteria would not allow the improvement to be seen for all lengths of baseline.

The statistics of success rate (epochs) of positioning for all trials are summarized in Table 3.2.

Table 3.2 Percentage of success epochs of AFT over different baselines

BASELINES		LENGTH (km)	X	Y	Z	Baseline length
BASE	ROVER					
PSMS	SEMA	12.8	80%	28%	71%	17%
CG54	KRPI	14.9	2%	39%	53%	17%
INED	SHEN	21	57%	82%	51%	60%
PSMS	PLAT	25	44%	58%	65%	19%
PSMS	SOHO	33	30%	45%	22%	33%
Criteria: difference between the estimated x, y, z, and baseline length, and the true x, y, z, and baseline length: < 2 cm (baseline length < 13 km), < 5 cm (baseline length > 13 km).						

The analysis of AFT performance over different baselines is summarized as follows.

1. The performance of AFT has shown that the percentage of successful ambiguity fixing is quite low as the baseline distance extends to more than10 km.
2. The difference between the GASP estimation and the true value of the baseline length indicates that the combined effect of all errors on the performance of AFT includes a constant drift (mainly atmospheric variations with time) and an error with a characteristic of sinusoid variation (due to multipath).
3. From the 12.8 km baseline trial in Figure C.1.d, the effect of double differencing multipath is about 0.94 cm (RMS of estimated baseline length) and the effect of double differencing ionospheric delays (including the error of tropospheric imperfect modelling) is about 2.92 cm (true baseline length: 12795.4915 m, average of estimated baseline length: 12795.4623 m). Similarly, in the case of the 21 km baseline between base station INED and rover station SHEN, the effect of double differencing multipath is about 2.06 cm (RMS of estimated baseline length) and the

effect of double differencing ionospheric delays (including the error of tropospheric imperfect modelling) is about 3.72 cm (true baseline length: 21950.3682 m, average of estimated baseline length: 21950.3311 m). Therefore, between these two trials, even an extra effect of multipath about 1.12 cm plus the extra ionospheric effect about 0.8cm can cause much worse performance of AFT over a 21 km baseline, compared to that over 12.8km. In other words, this indicates that the tolerable error size of AFT is quite narrow (e.g. about 2 cm in this specific case). For other trials of 15km, 25km, and 33km baselines, the biased statistics of RMS and average may lead to a wrong analysis and conclusion, because the number of successfully fixed epochs is not sufficient. However, Figure C.2, C.4, and C.5 have shown that the combined error effect on the performances of these cases of 15 km, 25 km, and 33km baselines is too large for the AFT to fix the correct ambiguities and obtain high precision positioning.

4. From the percentage success rate of ambiguity resolution in table 3.2, it is apparent that there is no definite relationship between the success rate of ambiguity resolution and the baseline length. In particular for the case of the 21km baseline, the performance of 60% success rate shows a better result than the performance of 17% success rate in the case of 15km baseline. The actual source of errors affecting the positioning performance cannot be identified in these cases since the combined effect consists of both the multipathing and atmospheric effects.

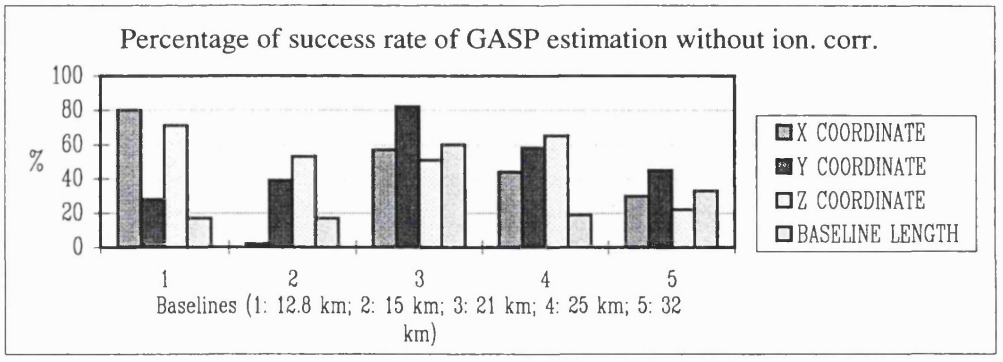

Figure 3.1 Percentage of success rate of GASP estimation

3.6 SUMMARY

The following points can be summarized based on theoretical analysis and practical investigations for the single epoch AFT over long baselines.

- The limitation of initialisation or re-initialisation during the RTK operation with using current RTK techniques is no longer considered as a problem if adopting a processing strategy such as that used in this technique, where each single epoch of dual frequency GPS data is independently processed.
- The ambiguity resolution and the positioning accuracy are limited mainly by multipathing problems in a case of short baseline applications but as the length of a baseline increases so other errors begin to decorrelate.
- According to the investigation of the AFT over short baselines with biased data by Al-Haifi (Al-Haifi, 1996), and the investigation of AFT over long baselines in this chapter, it can be concluded that the tolerable error size of the AFT is quite narrow. Although a function of many variables, it appears to be less than about two centimeters in most cases.
- As the length of the baseline extends to more than 10km, the ionospheric delays (perhaps also including the error of imperfect tropospheric modelling) may become the dominant error effect on the performance of AFT, but the multipath still plays an important role. In other words, poor positioning results from the AFT can be still be obtained in situations where the ionosphere is benign but there is a severe multipathing effect. Equally even relatively mild ionospheric effects combined with mild multipathing errors can lead to a poor performance of the method.
- In general, the multipath on phase can be from few millimeters to few centimeters. Theoretically, the maximum multipath is less than 5cm, but the double differencing multipath could be four times this size. Up to now, the investigation of the multipathing effect on phase is a subject of research still. However, it is a fact that the performance of AFT either over short baselines or over long baselines is affected by multipath and multipath research is still an important issue.
- It seems that the ionospheric effect increases as the length of the baseline increases however the increasing rate of ionospheric error over the baseline from about 10km to about 20km is slow. Over baseline of more than about 25km, a total failure of the AFT can be caused due to the increasing effect of ionospheric delays.

Overall it can be concluded that, although many error sources combine to complicate the problem of the application of the single epoch AFT over long distances, the atmosphere plays a dominant role. Therefore, in order to extend the use of AFT over long baselines, it is crucial to reduce the effect of ionospheric and tropospheric errors, and in order to do this it is necessary to construct appropriate models. This, along with the evaluation of some existing models, is the main topic of the rest of this thesis..

CHAPTER FOUR

IONOSPHERIC DELAY AND MODELLING

4.1 INTRODUCTION

The ionospheric delay has been considered as the key problem of high precision DGPS and RTK GPS over longer baselines for many years. Over short baselines (< 10km) the single epoch Ambiguity Function Technique (AFT) has been found to be quite successful in centimeter level positioning accuracy, provided there are at least 5 satellites, insignificant multipath, and ionospheric effects being reduced or neglected after double differencing (Corbett, 1994, Al-Haifi 1996). As the length of baseline increases, however this technique becomes unstable and unreliable, and its success rate decreases as described in Chapter 3. In order to find out the real problems so as to extend the use of this technique over longer baselines, the study of the ionospheric delay and modelling is necessary.

In this chapter a study of ionospheric delay and modelling is discussed in answer to eight main questions as follows.

- What is the main problem? Why an ionospheric model is necessary? (Section 4.1)
- What is happening in the atmosphere (the ionosphere)? (Section 4.2)
- Can the ionosphere have important impacts on GPS? (Section 4.3)
- What is necessary and how is ionospheric modelling carried out? (Section 4.4.1)
- What are the current ionospheric models and their differences? (Section 4.4.2)
- How can the ionospheric modelling be verified? (Section 4.5)
- What is the application of the ionospheric modelling for GPS? (Section 4.6)
- What is the best way to solve the problem? (Section 4.7)

Note that there is no attempt to refine the existing tropospheric model in this research but the troposphere however still needs to be discussed because it is likely that any estimation errors caused by the tropospheric model may affect the verification of ionospheric modelling.

4.2 GPS PROPAGATION MEDIA—THE ATMOSPHERE

When travelling in the atmosphere GPS signals are affected by the content of the various atmospheric regions. On the basis of common physical properties and appearances such as temperature, composition, state of mixing, and ionization, the earth's atmosphere can be briefly divided into lower and upper atmosphere (Leick, 1995). The lower atmosphere, up to 1000km height, includes the troposphere, tropopause, stratosphere, stratopause, mesosphere, and mesopause. Most of the mass of the atmosphere is located up to a height of around 50km in the troposphere and tropopause. The combined effect of the troposphere, tropopause, and the stratosphere (up to about 40km) on GPS signals is labelled tropospheric refraction. The refraction of higher layers is too small to have a measurable effect.

In the nomenclature of ionization, two distinct regions, labelled the ionosphere and the magnetosphere, need to be considered. The former, covering the region from about 50km up to 1500km above the earth, is a dispersive medium at radio frequencies, and is characterised by the presence of free (negatively charged) electrons. The particle motion of the latter located at the height of outermost region (higher than 1500 km) is controlled by the geomagnetic field. During the transmission of GPS signals, signal disturbances can be caused due to the effects of ionosphere and the troposphere. They are introduced respectively in the following two subsections.

4.2.1 THE IONOSPHERE

In the dispersive region of the atmosphere the number of free electrons is a key parameter to determine the state of ionosphere. Usually the electron density is measured by counting the number of electrons in a vertical column with a cross sectional area of one square meter called the *total electron content* (TEC) in unit of el/m^2, and it is used as a refractive index of the ionosphere. One unit of TEC contains 10^{16} electrons per square meter column.

The variation of TEC with location and time is dependent on the amount of ultraviolet radiation from the sun and the relative position of the sun. In the nighttime (on the dark side of the earth) it shows stable characteristics because of the recombination of negatively charged electrons and positively charged atoms. On the contrary, as long as

the solar activity during the daytime is strong enough to split molecules (neutral), the number of free electrons starts become greater. An irregular but rapid variation by means of diffraction in amplitude and phase called *scintillation* can be created by significant amount of electrons, and radio signals can occasionally experience short-term fading. Moreover as the level of solar activity increases (the maximum in the current eleven year cycle 23 is expected to occur around 2000) severe scintillation may cause many severe problems such as communication interruption, and a GPS receiver's loss of signal lock. For the phenomena of ionospheric rapid changes, which have characteristic of the order of 10 minutes, travelling ionospheric disturbances (TIDs) are believed to be caused in part by severe weather fronts and volcanic eruptions (Klobuchar, 1991, Bishop, 1996, Warrant, 1997, and Conway, 1998). However, more details about the ionospheric effects on GPS measurements and operation, the modelling of the ionosphere and analysis of current models will be discussed in the following sections.

4.2.2 THE TROPOSPHERE

In the non-dispersive region of the atmosphere the effect on GPS code and phase measurements is the same because refraction in a neutral medium is not dispersive for the radio signals below 30 GHz frequency. This effect due to the neutral nature of troposphere characterized as the group delays has an opposite sign comparing to the ionospheric effect's on phase, and the same amount irrespective on L_1 or L_2 signals (see GPS observation equations in (2.3) and (2.4)). The total tropospheric refraction, T, accumulated along the path of the GPS signals, can be expressed as follows.

$$T_V = T_{dry} + T_{wet} \quad \text{.....(4.1.a)}$$

$$T = M(\theta)\,(T_{dry} + T_{wet}) \quad \text{.....(4.1.b)}$$

where

T_V is the total tropospheric refraction accumulated along the vertical path of the GPS signals

T_{dry} is the dry part, which is proportional to the total density of the parcels in the air,

T_{wet} is the wet part, mainly determined by the density of the water vapor contained in the air parcels.

$M(\theta)$ is the mapping function, which is a constant scalar between the conversion of the vertical vector and the slant vector of the tropospheric delays.

Usually the effect of tropospheric propagation can be expressed as a function of temperature, pressure, and relative humidity, and may have a measured apparent range of 2.4m in zenith direction and may reach to about 9.3m for a zenith angle of 75°. The reduction of this effect is essential for one to achieve high precision GPS applications (Langley, 1992 and Brunner et. al., 1993). Brunner also indicates that unfortunately the tropospheric delays cannot be modelled directly by using the GPS dual frequency data themselves. For an accurate modelling of troposphere, it requires a survey with the equipment such as radiosonde (instrumented weather balloon for measuring the pressure, temperature, and humidity) and water vapor radiometry (WVR for measuring the water vapor delay), which are very expensive tasks and certainly not in routine GPS survey work. The empirical tropospheric models such as the Hopfield model and the Saastamoinen model (the following equation) is often adopted to calculate tropospheric corrections for improving the performance of GPS techniques (Hopfield, 1963 and Hofmann-Wellenhof et. al., 1994, Saastamoinen, 1973).

$$T = (0.002277 / \cos z) [\, p + (1255 / C + 0.05)\, e - B \tan^2 z \,] + \delta R \quad \text{.....(4.2)}$$

where

z is the zenith distance (= 90° - elevation angle) of the satellite in Degrees,

p is the atmospheric pressure in mbar,

C is the temperature in Kelvin,

e is the partial pressure of water vapor in mbar,

B and δR are the corrections for refined Saastamoinen model.

With simple models, the zenith delay can be predicted very easily to the accuracy of better than 20 centimeters. For low accurate GPS applications, it may not be of concern, but the tropospheric effects may however be a severe accuracy limitation for high precision GPS positioning. Recently, many efforts have involved studying water vapor effects (Bar-Sever, 1996, Nam, 1996, Coster et. al., 1996) and improving the modelling with refined mapping functions (Bar-Sever and Kroger, 1996, Gendt, 1996a and 1996b, Collins and Langley, 1998). However, one of the difficulties in the modelling can be the error due to the rapid and local variations of humidity distribution, which may have a

10% range of the delays (Leick, 1995). In this research there is no attempt to develop new tropospheric models. What is of concern is whether or not the errors of the tropospheric model in GPS techniques would affect the evaluation of ionospheric modelling since the combined effect on the AFT positioning accuracy has involved the ionospheric and the tropospheric model's. For evaluating a novel ionospheric modelling, this problem cannot be neglected and will be discussed in section 4.5 this chapter and chapter 6.

4.3 IONOSPHERIC EFFECTS ON GPS

Undoubtedly ionospheric effects on very short baseline GPS can be neglected after the differential process. However it is known that the ionosphere is a problem for longer baselines. But how long is long? In fact the ionosphere can sometimes cause severe problems even over quite short baselines. A related problem is what will happen during the coming solar maximum cycle? Hence the study of ionospheric effects on GPS is necessary not only for the ionospheric modelling over longer baselines but also for the exploration of these general problems.

4.3.1 IONOSPHERIC EFFECTS ON CODE AND PHASE MEASUREMENTS

Usually the measurement errors caused by either the code ionospheric refraction or the phase ionospheric refraction are called *ionospheric delays.* However the propagation characteristics of GPS signals for code and for phase along the path of the ionosphere are different, and can be characterised as the delay of the P1 (or C/A) and P2 code (called *group delays*) and the advance of the L1 and L2 carrier phase (called *phase advances*) mainly because the phase velocity based on binary phase modulation is larger than vacuum speed and the group (code) velocity based on the modulation or the energy is smaller than vacuum speed by the same amount but opposite sign (see measurement expressions (2.4a) and (2.4b)). The integral effect of the ionosphere on GPS code and phase observables (S_C and S_P), is related to the velocity which depends on the frequency and the number of free electrons (referred to as the electron density) along the path and can be respectively formulated as follows (Tsedillina et. al., 1994, Stewart, 1997).

$$S_C = \int_{path} N_g \, ds \qquad (4.3.a)$$

$= \int_{path} [1 + 40.3\ N / f^2]\ ds$ .....(4.3.b)

$= S + 40.3\ TEC / f^2$ .....(4.3.c)

$S_p = \int_{path} N_p\ ds$ .....(4.4.a)

$= \int_{path} [1 - 40.3\ N / f^2]\ ds$ .....(4.4.b)

$= S - 40.3\ TEC / f^2$ .....(4.4.c)

where S is the true range, TEC is the total electron content integrated along the signal path, N is the electron density in el/m^2, and f is the operating frequency in hertz.

The corresponding ionospheric time delay or time advance of the ionospheric delay follows as

$TECns = 40.3\ TEC / (c\ f^2)$ .....(4.4.d)

where TECns is the ionospheric time delay in unit of nanoseconds (ns).

The conversion between the TEC in el/m^2 and the L_1 and L_2 frequency ionospheric delay in metres, I_1 and I_2 in (2.1) and (2.2) can be written as the following expressions.

$I_1 = 40.3\ TEC / f_1^2$ .....(4.5.a)

$= \Upsilon_1\ I$ .....(4.5.b)

$I_2 = 40.3\ TEC / f_2^2$ .....(4.6.a)

$= \Upsilon_2\ I$ .....(4.6.b)

where $f_1 = 1575.42$ MHz and $f_2 = 1227.60$ MHz,

$\Upsilon_1 = f_2^2 / (f_1^2 - f_2^2) \cong 1.5457$ and $\Upsilon_2 = f_1^2 / (f_1^2 - f_2^2) \cong 2.5457$,

$I = [(f_1^2 - f_2^2) / (f_1^2\ f_2^2)]\ (40.3\ TEC)$ in units of meters.

The conversion of the ionospheric delay I between meters and TECU or nanosecond can be written as

$TEC = I\ [(f_1^2\ f_2^2) / (f_1^2 - f_2^2)] / 40.3$ in unit of TECU .....(4.7)

$TEC = I\ (1/c)\ 10^9$ in unit of ns (nanosecond) .....(4.8)

Where c is the light speed, and 1 TECU = 10^{16} el/m^2.

Therefore the ionospheric delay in meters can be converted into TECU and ns as

0.9 m = 3 ns = 8.5676789 TECU

Ionospheric effects on GPS measurements depend on the signal characteristic and frequency, and the total number of electrons along the path. The total number of electrons per square meter (or say the electron density) vary with location and time, and the ionospheric delay is proportional to the inverse of the frequency squared. From many investigation results on the ionospheric behaviour (Klobuchar, 1986 and 1991,

Knight et. al., 1996 and 1998, and Doherty et. al., 1997), it can however be summarized as follows.

- The ionospheric effects introduced into the GPS observations can vary from less than 1 meter to more than 100 meters. In particular, as the satellites remain at a low elevation mask, the ionospheric delays cannot be ignored. At nighttime, the ionosphere has shown a static characteristic of less effect.
- The ionosphere changes with time of day, season, location of the survey, viewing direction (azimuth), solar activity, and the magnetic state.
- The higher the frequency, the smaller the ionospheric effect.

4.3.2 IMPACTS OF THE IONOSPHERE ON GPS OPERATIONS

As described previously the ionospheric effects vary with time and location, but during GPS operations would these effects cause problems even over short baselines? If yes, when? or where? Many studies on this have been made. (Klobuchar, 1991, Aarons, 1994, Clynch, 1994, Bishop, 1996, Skone and Cannon, 1997-8, Skone, 1998, Pullen et. al., 1998, Stewart et. al., 1998, and Conway, 1998). These results can be summarised as follows.

- Severe scintillation may occur for several hours after sunset during the solar maximum periods.
- Seasonal variation follows the Sun's 27-day rotational period and the roughly 11-year cycle of solar activity.
- Scintillation may fade the signal low and long enough and even cause loss of signal lock.
- The worst source of scintillation is the equatorial anomaly region -- approximately 15° north and 15° south of the magnetic equator. Ascension island in the Atlantic, Diego Garcia in the Indian Ocean, Hong Kong, and Taiwan in the Pacific are some of stations that fall directly under the anomaly region.
- The other potentially active regions are at Auroral and polar cap latitude.
- Intense magnetic storms may occur even during periods of low solar flux. When severe magnetic storms occur, the ionospheric effect may last up to one or two days and the auroral effect can move down into the mid-latitudes.

- Depending on the model used, the grid modelling accuracy can vary from couples of tens of centimeters to meters.

Overall the ionospheric effect changes with the time of the day, season, location of the receiver, viewing direction, solar activity, the state of the earth's magnetic field and severe scintillation can occur during the solar maximum or strong magnetic storm periods and cause severe problems such as loss of signal lock. Therefore monitoring and broadcasting the ionosphere by an accurate, reliable, and practical ionospheric model is necessary for many GPS operations possibly even over short baselines. Particularly, the monitoring of the occurrence of ionospheric irregularities for a wide and even global area can hence be implemented with the ionospheric model through the establishment of PGA (Wanninger, 1992 and 1995, Engler et. al., 1995, Mannucci et. al., 1995, Darin et. al., 1997).

4.4 IONOSPHERIC MODELLING

The ionospheric effects on GPS cannot be ignored even over short baselines in some scenario. Either to enhance the performance of GPS techniques over longer baselines or to monitor the change of the ionosphere the measurement of the ionosphere is possible for an ionospheric modelling based on GPS observables. Usually the observations for ionospheric modelling are based on the linear combinations of GPS observables, which can lead to various strategies of ionospheric modelling because the remaining biases or errors are different in the various combined observations. Modelling the ionosphere is usually called *ionospheric modelling* (or *deterministic modelling*) from the viewpoint of geometry mathematics, and called *stochastic modelling* from the viewpoint of statistics. These will be described in the following sections respectively.

4.4.1 DETERMINISTIC MODELLING

As expressed in Equations (4.3) and (4.4), the integral effect of ionosphere on GPS measurements is dependent on the frequency and the electron density (total electron contents) along the path from the satellite to the receiver. The integrated ionosphere (the slant ionosphere) along the signal path can be measured using the data of the single or dual frequency receivers and expressed as a function of the vertical delay (called *vertical*

TEC) and non-scaled quantity (called *mapping function*) based on the geometry of the spherical shell (called *single ionospheric layer*) by mapping the slant delays onto the vertical direction. This way to model the ionosphere is usually called *deterministic modelling*.

To accomplish this modelling many factors in terms of the applied observations, data preprocessing, the concept of single ionospheric layer, mapping function, vertical TEC, parameter estimation and even finally the verification of the modelling are all important. However the construction of the ionosphere by two parameters, the mapping function and the vertical TEC, can be the key points of the ionospheric modelling. To summarize, the following is a review and analysis of current models that can be used to achieve a higher accuracy in ionospheric modelling.

4.4.1.1 OBSERVATIONS

Pseudoranges and carrier phases are two basic types of GPS observables introduced in chapter 2. Basically the former is noisier and the latter is favoured in high precision surveying. Data from L_1 and L_2 frequency based on code (C/A or P1, and P2) and phase (L1 and L2 in meters; $\Phi 1$ and $\Phi 2$ in cycles) are available for dual frequency users of which single frequency users only have P1 (or C/A), and L1 (due to the low costs of this kind of receiver). Through the combinations of these observables as described in chapter 2.2 the combined observations usually can be used for the modelling of specific errors such as multipath, troposphere, ionosphere, and instrument bias. For the ionospheric modelling based on P1 (or C/A), P2, L1, L2 observables, there are four types of observations often used in current models, and after the process of geometry free combination (so called ionospheric combination) the ionospheric observations are summarised as follows.

(1) P4 observation based on geometry free combination on code

$$P4 = P1 - P2 \quad (4.9a)$$

(2) P_L observation based on geometry free combination on L_1 frequency code and phase

$$P_L = P1 - L1 \quad (4.9b)$$

(3) L_C observation based on geometry free combination plus averaging process (so called levelling),

$$L_C = (L1 - L2) - C \quad (4.9c)$$

$$C = \sum_{i=1}^{n} (L4_i - P4_i) / n$$

where C is a constant, and n is the number of observing epochs.

(4) L4 observation based on geometry free combination on phase,

$L4 = L1 - L2$ .....(4.9d)

As shown in table 4.1 below, all ionospheric observations are free of ranges (so called geometry free), clock errors, and tropospheric delays. For high accurate ionospheric modelling, those observations containing the parameter of code multipath such as P4 and P_L are too noisy to be used. The P_L observation is only suitable for the single frequency modelling.

Table 4.1 Analysis of ionospheric observations

TYPE	REMAINING PARAMETER	DELETED PARAMETER
P1,P2	(1),(2),(3),(5),(6),(7)	
L1,L2	(1),(2),(3),(4),(5),(6),(8)	
P4	(5),(6),(7)	(1), (2),(3)
P_L	(4),(5),(6),(7),(8)	(1), (2),(3)
L_C	(5),(6),(9)	(1), (2),(3),(4)
L4	(4)(5),(6),(8)	(1), (2),(3)
(1)ranges (station coordinates and satellite coordinates) (2)clock errors (3)tropospheric delays (4)ambiguities (5)ionospheric delays (6)instrument biases (satellite and receiver) (7)code multipath (8)phase multipath (9)non-zeromean multipath		

The L_C observation, since the average process has been applied to reduce the effect of multipath (theoretically considered to be zero after the averaging process), is considered to be a good candidate even though it still contains the instrument biases and the so called non-zeromean which is a small bias. The L4 observation, consisting of these parameters: the ambiguities, the instrument bias, and the small phase multipath is however still popular mainly because this observation has only low noise (purely combined with dual frequency phase data). Hence the ambiguities and/or the instrument biases (or even the non-zeromean) have to be solved previously if using the L4 (or L_C) observation, such that, this preprocessing step is currently necessary for the modelling.

If the constant parameters (e.g. the ambiguities, the instrument biases, or even the non-zeromean) of ionospheric observations are not determined it will lead to reduced accuracy of the vertical TEC (Georgiadou and Kleusberg, 1988).

There are several ways to solve the problem of the constant biases of ionospheric observations. The instrument biases can be eliminated by adopting double differencing strategy, resolved by hardware precalibration and broadcast information, by using the corrections of the hardware bias estimation, even kept as a parameter of the final parameter estimation step. The solution of these parameter is based on the assumption that they are constant during periods of few hours (Chao et al, 1995, Wilson et al, 1993). However, the data from at least two reference stations is necessary for the first method, time consumption can be a problem of RTK GPS for the second method, and the accuracy of vertical TEC can be limited for the rest of the methods. Usually the ambiguities can be previously solved using GPS software or kept as a parameter (with the instrument biases) at the final parameter estimation stage of processing. The problem is that the ambiguities cannot be always resolved and thus the accuracy of the estimation can be reduced. Moreover both the phase multipath and the non-zeromean bias are always considered as being small and thus are neglected for most of current models using the L_C observation. Nevertheless the non-zeromean bias can be at decimeter level (Borne, 1999), and the study of the phase multipath has recently been made by the method of Signal-to-Noise Ratio (Borne, 1999, Axelrad et al, 1994). Currently the preprocessing of these constant parameters is necessary for a high accurate ionospheric modelling.

4.4.1.2 PREPROCESSING

Ionospheric modelling seems impossible by just using a single epoch data instead of a time period of data, and data preprocessing is necessary to detect and repair the phase cycle slips and code outliers (introduced in chapter 5) before using this data. If the data are not clean (i.e. if it still includes the cycle slips or outliers) the result of the modelling can lead to a very wrong impression of the ionospheric delays. Therefore reliable software for cycle slip detection and repair is important to the ionospheric modelling. In addition, depending on the application for the ionospheric observations, the

preprocessing of the constant biases has to be fulfilled (already discussed in section 4.4.1.2) before going to the next step of the ionospheric modelling. To summarise, it is currently necessary to perform not only cycle slip preprocessing but also constant bias preprocessing for ionospheric modelling.

4.4.1.3 SINGLE IONOSPHERIC LAYER

As described previously the ionospheric effects vary with space (location and viewing direction) and time. At present, it is assumed that the integrated ionosphere along the path from the satellite to the receiver can be represented by a spherical shell with infinitesimal thickness and the height of this shell is defined to be the mean ionospheric height which can be 300 km to 450 km above the mean sea level, Figure 4.1. This spherical shell is called *the single ionospheric layer* or called *the ionospheric density profile* (or *vertical TEC profile*), and the intersection of the signal path and the shell is called *the ionospheric pierce point* (or called IPP). The slant ionosphere is considered as a function of the electron density and its effective distance between the pierce point and the operating station. If mapping the slant ionosphere onto the vertical direction (the vertical plumb line) at the pierce point, then it can be expressed as

$$I = M(\theta)\, V(\varphi,\lambda) \qquad (4.10)$$

Where

I is the slant ionosphere,

$M(\theta)$ is a mapping function, θ can be the elevation angle or the zenith angle,

$V(\varphi,\lambda)$ is the vertical TEC at the pierce point , φ ,λ is the latitude and the longitude in a geodetic coordinate system.

Therefore based on this single ionospheric layer one can deal with the problem of the ionospheric variation with space by this equation.

Regarding the problem of ionospheric variation with time, some of the modelling has made the assumption that the ionosphere is constant for a short period, at least half an hour up to two or three hours. It has been impossible to model the ionosphere just using one or a few epochs of data. For longer sessions of more than few couples of hours, another way is to use the sun-earth reference coordinate system considered to be time independent after the conversion of two coordinate systems in some modelling. These

important factors of ionospheric modelling described above will be introduced in the next two subsections.

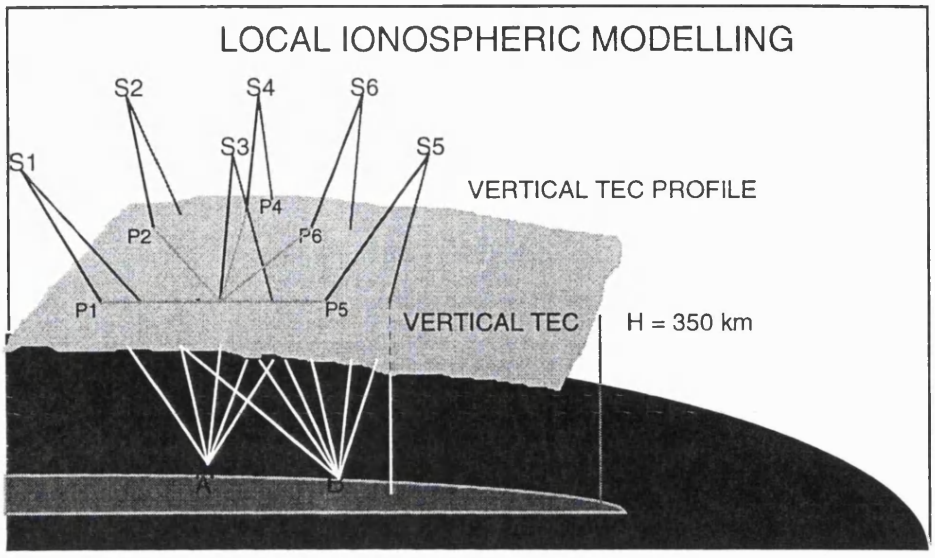

Figure 4.1 Local ionospheric modelling based on the single ionospheric layer

4.4.1.4 MAPPING FUNCTION

The mapping function, one of the two factors in the slant ionospheric expression, expresses the geometry relationship between the vertical TEC and the slant ionosphere. It can be seen in Figure 4.1 that the ratio of the vertical TEC and the slant ionosphere can be simply considered as a cosine function of zenith angle or a sine function of elevation angle based on the assumption of a sphere. In this case it is obvious that the lower the elevation angle, the greater the error due to the mapping function.

As expressed below these functions have been used as a mapping function in ionospheric modelling. (References see 4.11: Wild et. al., 1989, Georgiadou and Kleusberg, 1988, 4.12: Mamucci et. al., 1993, Schaer et. al., 1995 and 1996, Lanyi, 1988, Feltens et. al., 1996, 4.13: Klobuchar, 1987, 4.14: Schaer et. al., 1995, 4.15: Sardon et. al., 1994).

$M(z) = 1 / cos(z)$ .....(4.11)

$M(\theta) = \{1-[cos(\theta)/(1+h/R)]^2\}^{-1/2}$ .....(4.12)

$$M(\theta) = 1.0 + 16.0\,(0.53-\theta)^3 \quad (4.13)$$

$$M(\theta) = 1 / [R(R+h)^{-1} cos(\theta)] \quad (4.14)$$

$$M(\theta) = [(R^2\, sin^2(\theta)+2Rh_2+h_2)- (R^2\, sin^2(\theta)+2Rh_1+h_1)]/ (h_2 - h_1) \quad (4.15)$$

where

θ, z is the elevation angle and the zenith angle,

R is the radius of the earth,

h is the height of spherical shell, h_1, h_2 are the lower and the upper height of the ionosphere.

In ionospheric modelling, usually it is necessary to cut off data below a elevation angle of 20 degrees to avoid errors due to imperfect mapping functions (unless the perfect one can be found). Not only the vertical TEC but also the mapping function is an important factor in the ionospheric modelling.

4.4.1.5 VERTICAL TEC

Another factor of ionospheric modelling is the vertical TEC which is a two dimensional function of geodetic longitude . and latitude ϕ of the pierce points on that ionospheric profile, Figure 4.1. Usually it is considered that a vertical TEC of two or three hours can be modelled by a first, second, or higher order polynomial for each available satellite or all of the vertical TECs can be expressed by a spherical harmonic function. As shown below these equations have been used to express the vertical TECs, $V(\phi,\eta)$, in the ionospheric modelling.

1. Triangular interpolation model (Manucci et. al., 1993),

$$V(\phi,\lambda) = \sum_{I=Va,Vb,Vc} W(\phi,\lambda,i)\, V_i \quad (4.16)$$

where $V(\phi,\lambda)$ is the vertical TEC at the grid point p, $W(\phi,\lambda,i)$ is the weighting function based on a great circle arc from the vertex i to the point p, and V_a, V_b, V_c are the vertical TECs of the vertex i.

2. Spherical harmonic function (Schaer et. al., 1995 and 1996, and Chao et. al., 1995),

$$V(\phi,s) = \sum_{n=0}^{n_{MAX}} \sum_{m=0}^{n} P_{n\,m}(sin\ \phi)\, [a_{n\,m}\, cos\ (ms) + b_{n\,m}\, sin\ (ms)] \quad \text{with } t \in [t_i, t_{i+1}] \quad (4.17)$$

where

s (=λ-λ_0) is the sun-fixed longitude of the pierce point which corresponds to the local solar time, .is its geodetic longitude, and.$_0$ is the true (or mean) longitude of the sun,

$P_{n\,m}$ are the normalized associated Legendre polynomials of degree n and order m.

3. Gauss-Type Exponential (GE) functions (Feltens et. al., 1996),

$$VTEC = \Xi + G\, e^{-A} - e^{-B} - e^{-C} \quad \text{.....(4.18)}$$

$$A = a_1 x^1 + a_2 x^2 + a_3 x^3 + \cdots + a_{2n} x^{2n}$$

$$B = b_1 y^1 + b_2 y^2 + b_3 y^3 + \cdots + b_{2n} y^{2n}$$

$$C = c_1 x y + c_2 x^2 y + c_3 x y^2 + \cdots + c_{l-k+2} x^{k-l} y + \cdots + c_l x y^{k-l}$$

with k = minimum(2n,2m) , $l = k(k-l)/2$

where x is a function of local time, y is a function of latitude, Ξ is constant offset, and G is amplitude.

4. Polynomial (Geogiadou and Kleusberg, 1988, Lanyi, 1988, Sardon, 1994),

$$V(\phi,\eta) = C_1 + C_2\,\phi + C_3\lambda + C_4\,\phi^2 + C_5\,\phi\lambda + C_6\,\lambda^2 \quad \text{.....(4.19)}$$

where ϕ,$\lambda$are the latitude and longitude in a geodetic coordinate system or a sun-earth reference system (e.g. a reference latitude and longitude corresponds to the middle of the observing session in Lanyi's model).

5.Taylor expansion (Wild et. al., 1989),

$$E(\phi,S) = \sum_{i=0}^{n} \sum_{j=0}^{m} E_{ij}\,(\phi-\phi_0)^i\,(S-S_0)^j \quad \text{.....(4.20)}$$

where

E(ϕ,S) is the total electron content which is a function of latitude ϕ and of the hour angle S of the sun (local time),

n, m are the maximum degrees of the two-dimensional Tyalor series expansion in latitude ϕ and in the sun-fixed longitude S,

E_{ij} are the (unknown) coefficients of the Tyalor series, and $E_{00} = E(\phi_0,S_0)$,

ϕ_0,S_0 are the coordinates of the origin of the development. The origin in latitude ϕ_0 is the mean value of the latitude ϕ of all stations, the time origin t_0 is computed as the mean value of the lowest start time and of the highest ending time of all

observation files of one session, S_0 is then computed as the hour angle at time t_0 of "the mean station" of the session

Before applying the vertical TEC equations to the ionospheric modelling the longitude and the latitude of all pierce points have to be computed on the basis of the height of the ionospheric shell, the satellite and station coordinates. The height of the shell has to be spherical and 350 km is preferred in most models. The study of the effect of shell height on high precision ionospheric modelling using GPS (Komjathy and Langley, 1996) has shown that the height of single ionospheric layer on a small regional network can vary with geographic location, time of day, season, and solar activity. The effect can be up to 0.3 nanosecond in the differential delays.

The behaviour of the ionosphere appears to be time dependent as observed in the rotating terrestrial coordinate system. The effect is greater during the day time (appears to be more static during the nighttime). After fixing all observed directions to earth-sun axis, then it is assumed to be time independent in a reference frame (Lanyi, 1988). The sun-earth coordinate system's origin is in terms of local time, the mean of geodetic latitudes and/or longitudes of all stations has to be decided and computed, for example the origin ϕ_0,S_0 as expressed in Equation (4.19). The noon time or the mean value of the lowest start time and of the highest end time has ever used to determine the origin of this reference system. In Lanyi's model the reference latitude and longitude are simply calculated based on the middle of the observing session. It is assumed that this static ionosphere is time independent in this reference system after the transformation of two coordinate systems. (Wilson et al, 1993) denoted that the ionosphere is changing even in the sun-earth reference system over hours, hence the time span of the fit should be minimised in order to optimise the accuracy and temporal resolution of the vertical TEC. However the determination of either the height of the shell or the origin of the sun-earth reference system is still an open question. Both factors can affect the accuracy of the modelling

4.4.1.6 PARAMETER ESTIMATION STRATEGY

Depending on the use of the observations as shown in Table 4.1, the parameters of each observation can respectively be expressed and shown as follow. The parameter of the

ionosphere I is however split into two sub-parameters, $M(\theta)$ and $V(\phi,\eta)$ ($I = M(\theta)\ V(\phi,\eta)$, where $M(\theta)$ is the mapping function and $V(\phi,\eta)$ is the vertical TEC). These ionospheric observations can be constructed for a series time of data ($i = 1,n$) by these equations as follows.

$$P4_i = M(\theta_i)\ V(\phi_i, .\lambda_i) + B + E_i \quad \text{.....(4.21)}$$

$$P_{L\,i} = M(\theta_i)\ V(\phi_i, \lambda_{.i}) + C + E1_i + e_{1i} \quad \text{.....(4.22)}$$

$$L4_i = M(\theta_i)\ V(\phi_i, \lambda_{.i}) + N + B + e_i \quad \text{.....(4.23)}$$

$$L_{C\,i} = M(\theta_i)\ V(\phi_i, \lambda_{.i}) + B + E_{O\,i} \quad \text{.....(4.24)}$$

where $M(\theta_i)$ is the mapping function, θ can be elevation angle or zenith angle,

$V(\phi_i,\lambda_i)$ is the vertical TEC, ϕ,λ are latitude and longitude of the pierce points in a geographical coordinate system,

B is the instrument bias (receiver and satellite),

C is the constant part (the ambiguity and the instrument bias),

E_i is the code multipath, E1 is the L_1 frequency code multipath,

e_i is the phase multipath, e_1 is the L_1 frequency phase multipath,

N is the ambiguity (ionospheric combination),

$E_{O\,i}$ is the non-zeromean bias.

The instrument bias and the ambiguity (or say the constant part C) are expressed as a constant parameter. This is possible because the instrument bias is supposed to be independent of time for a few hour period and after the preprocessing of cycle slips, the data are all assumed to be clean. This means the ambiguity of each available satellite is constant (only one parameter in the observation equations). Different equations for the mapping function and the vertical TEC, (4.11-14) and (4.15-17), are used to construct the ionospheric parameter. All these observation equations however can be applied to all satellites and stations. Usually at least half an hour data is necessary to provide sufficient elevation angle change and least squares adjustment or Kalman filter can be applied to solve these observation equations. The details of least squares adjustment and Kalman filter are respectively introduced in (Mikhail, 1981, and Cross, 1983) and (Cross, 1986, 1987, and 1994, and Napier, 1991).

4.4.1.7 CURRENT IONOSPHERIC MODELS AND ANALYSIS

Many ionospheric models have been developed for the estimation of the ionosphere delays. An ionospheric estimation about 50 percent accuracy based on the broadcast model can be conveniently obtained from the coefficients of these polynomials in navigation message files (Klobuchar, 1987, Feess, 1987, and Leick, 1995). This model may be suitable for general GPS users but nevertheless does not satisfy with the need of high precision GPS users. A model based on P-code was tried by using Kalman filtering technique to smooth the P4 observations (Stewart, 1997 and Webster, 1993). The advantage of this modelling is that no ambiguity is involved but nevertheless the instrument biases have to be previously calibrated and the code multipath is too noisy to be exactly modelled. For a high precision ionospheric modelling the precise phase data is used optimally. These models (Lanyi, 1988, Georgiadou and Kleusberg, 1987, Wild et. al., 1989, Mannucci et. al., 1993, Sardon et. al., 1994a, Schaer et. al., 1995, Chao et. al., 1995, Schaer et. al., 1996, and Feltens et. al., 1996) are summarized and analyzed as below.

1. For these models using L4 observation, model (C), (E), and (F) keep the constant (ambiguity and instrument bias) as a parameter of the observation equations and Model (B) and (D) take double differencing strategy with pre-resolution of ambiguities to eliminate the constant. For these models using L_C observation, Model (G) and (H) keep the instrument bias as a parameter of the observation equations, and Model (A) and (I) use the preprocessing of hardware calibration (at least one station the biases have to be fixed for Model (A)).
2. All current models need to remove the cycle slips for a time series of data.
3 Data below the elevation angle of 20 degrees are not used in most of current models.
4 The most popular equation of the mapping function is shown as in (4.12).
5 The equations used to describe the vertical TEC can basically be divided into polynomials, Taylor expansion, spherical harmonic functions, and triangular interpolation.
6 The height of the shell adopted by most models is 350 km.
7 The sun-earth reference system is adopted by most models to deal with the problem of time variation of the ionosphere.
8 Basically the parameter estimation strategy of these models is the least squares adjustment or Kalman filtering technique.

Table 4.2 A summary of ionospheric models

Item \ Model	(A)	(B)	(C)	(D)	(E)	(F)	(G)	(H)	(I)
1.OBS	L_C	L4	L4	L4	L4	L4	L_C	L_C	L_C
2.DIFF	UD	DD	UD	DD	U/SD	UD	UD	UD	UD
3.PRE1-slip	Yes	Yes	Yes	yes	Yes	Yes	yes	Yes	yes
4.PRE2-bias	Yes	no	No	no	No	No	no	No	yes
5.PRE3-amb	No	Yes	No	yes	No	No	no	No	no
6.MAP	4.12	4.12	—	4.12	4.11	4.11	4.12	4.15	4.12
7.VTEC	4.16	4.17	4.17	4.17	4.20	4.19	4.19	4.19	4.18
8.SHELL	350	400	—	350	350	400	350	—	350
9.SOLAR	Yes	Yes	Yes	yes	Yes	No	yes	No	yes
a.ESTM	K-B	L-N	L-C	L-N	L-C	L-C	L-B	K-B	—
b.Cut-off	20	20	—	20	—	—	—	20	20
c.VERF	A-a	B-p	B-p	B-n	B-p	B-l	A-a	No	A-a
d.RMS (unit: cm)	5 tecu	17.6/ 6.2	82/ 37	85%/ 75%	1.2/ 1.0	0.07 ppm	3 ns	No	10 tecu
e.Area/Term	G	G/R	G	G	L	L	L	L	G

(A) JPL, A.J. Mannucci et. al., 1993 (B) Berne, S. Schaer et. al., 1995
(C) Stanford, Y.Chao et. al., 1995 (D) CODE, S. Schaer et. al., 1996
(E) Berne, U. Wild et. al., 1989 (F) Y. Georgiadou and A. Kleusberg, 1988
(G) G.E. Lanyi, 1988 (H) E.Sardon et. al., 1994a
(I) ESOC, J. Feltens et. al., 1996

1.OBS: ionospheric observations
2.DIFF: UD-undifferenced, SD-single differenced, DD-double differenced
3.PRE1-slip: preprocessing of cycle-slip detection and repair
4.PRE2-bias: precalibration of instrument biases
5.PRE3-amb: preresolution of ambiguities
6.MAP: the mapping function (equation no.)
7.VTEC: the vertical TEC (equation no.)
8.SHELL: the height of spherical shell (unit: km)
9.SOLAR: sun-earth reference system
a.ESTM: parameter estimation strategy ,
L-least squares adjustment, K-kalman filtering
B-with instrument parameters,N- with ambiguity parameters
C-with ambiguity and instrument parameters
b.Cut-off: elevation angle cutoff (unit: degree)
c.VERF: verification of the modelling,
A-differences with comparison of another method,
B-comparison without/with the model, (default: cm)
p-positioning accuracy a-absolute vertical TEC (0.9cm=3ns=8.5tecu),
n-ambiguity resolution(%), l-baseline length (ppm)
d.RMS accuracy of the result: t-TECU, s-nanosecond, p-ppm
e.Area G-global, R-regional, L-local
— no comments

9 The resultant comparison with other models such as Model (A), (G), and (I), or the result of the comparison with and without the model such as Model (B), (C), (D), (E), and (F) is the usual way to verify the modelling. The results of the modelling

can be the absolute vertical TEC (e.g. cm, ns, or TECU), the positioning accuracy (cm), the percentage of ambiguity resolution (%), and the ratio of the error and baseline length (ppm). By using the former verification method, the accuracy of vertical TEC of Model (A), (G), and (I) can be achieved at about 5 to 10 TECU (~ 52 cm to ~ 104 cm, see Feltens J. et. al., 1996). By using the latter verification method, the improvement of GPS positioning accuracy or ambiguity resolution has been made by Model (B) to (F). However the evaluation of these models seems impossible to be accomplished without using the same data set and under the same processing conditions.

4.4.2 STOCHASTIC MODELLING

If the ionospheric observation is interpreted as a stochastic variable, then it can be split into the deterministic trend E(X), and the stochastic part ($S + \varepsilon$) for a time series of ionospheric delays as

$$X_i = E(X_i) + S_i + \varepsilon_i \quad , i = 1,n \qquad (4.25)$$

where ε is the measurement noise.

The stochastic part has attempted to be modelled by an auto-regressive process model (Delikaraoglou, 1989). Based on the single ionospheric layer a refined way to study ionospheric correlation, using a correlation function in time and space, has been used to improve the deterministic model for the stochastic part. It has been found that more refined ways to compute correlation functions are necessary to prove the collocation process (Wild et. al., 1990). However this research is not concerned with the stochastic modelling of the ionosphere.

4.5 VERIFICATION OF IONOSPHERIC MODELLING

After ionospheric modelling, its verification is a necessary step for its subsequent applications. Up to date it is hard to obtain the true ionospheric delays or an accurate method to verify the result of the ionospheric modelling. However there are many current methods to verify the ionospheric modelling:

1. the result comparison with other space based techniques, such as GLONASS, PRARE, and TOPEX dual frequency radar altimeter,
2. comparisons between different models,

3. the performance of the GPS techniques without/with ionospheric corrections,
4. a refined approach with knowledge of the coordinates and the ambiguities.

Among these verification methods introduced by the next three subsections, usually the third method is the most popular way.

4.5.1 DIFFERENT SOURCES

Another similar positioning system to GPS is the Russian Global Navigation Satellite System (GLONASS) which transmits L_1 and L_2 spread-spectrum ranging signals, two different ones per satellites, (e.g. at 1614.9375 MHz and 1256.0625 MHz on channel 23 satellite). With GLONASS, similar L_1 and L_2 frequency P-code pseudorange and carrier phase measurements are available for the estimation of ionospheric delays (Danaher et. al., 1993, Riley and Daly, 1993; Beser and Balendra, 1994, Christle et. al., 1996, Vollath et. al., 1998). Since May 1995 a two-way microwave satellite tracking system called PRARE provides very precise 2-way range and range-rate measurements to ERS-2 which also can be used to estimate the ionospheric delays (Flechtner, 1998). The ionospheric measurements from the TOPEX dual frequency radar altimeter (TPXALT) can be applied to assess the accuracy of GPS-based ionospheric estimation since October 1992 (Mannucci et. al., 1995). With the results based on these systems verification of GPS derived ionospheric models is possible, but it is only available for certain researchers who have access to the data and facilities for processing.

Since June 1992, an inter-comparison activity of several center's ionospheric models has been conducted by the European Space Operations Centre (ESOC). These include ESOC JPL, EMR, CODE, DLR, and UNB solutions. The resultant comparison has shown a general agreement of 5 TECU and better, normally 3 TECU (Feltens et. al., 1996). Such comparisons are beyond the bounds of this research.

4.5.2 AMBIGUITY RESOLUTION AND POSITIONING ACCURACY

Once ionospheric corrections are calculated by the ionospheric model, the performance of GPS techniques with and without the ionospheric corrections can be assessed. This is performed, for example, by checking the ambiguity resolution or positioning accuracy. There are however still some error sources that effect these checking methodologies, for

example tropospheric modelling, coordinate, and phase multipath error, may cause the difficulty in the accurate verification of the modelling because these unresolved differential errors may be even larger than the differential ionospheric delays. Hence the performance of different GPS techniques with ionospheric corrections can only validate the efficiency of the ionospheric modelling but cannot verify its exactness unless other unresolved errors can be fixed and confirmed previously or the more accurate ionospheric delays can be calculated by some external methods.

4.5.3 A REFINED APPROACH

"If the coordinates are kept fixed on 'good' values (e.g. on a solution using the ionosphere free linear combination) and the ambiguities are left free, then the solution (wide lane linear combination) only contains the influence of the ionosphere. Therefore this solution is ideal to check the influence of the ionosphere." in (Wild et. al., 1990). For local ionospheric modelling it is possible to obtain the more accurate absolute double differencing ionospheric delays based on two reference stations. This approach can therefore provide a more accurate method to verify ionospheric modelling.

4.6 GPS APPLICATION OF THE IONOSPHERIC MODEL

Once, the ionospheric model has been generated based on the single ionospheric layer with a time period of the GPS single or dual frequency data collected at one or more reference stations, the vertical TEC of the pierce points on the ionospheric profile can be calculated by the ionospheric model (The vertical TEC of point p1 to p5 for one epoch above base station A on the vertical TEC profile in Figure 4.1). Depending on the sky coverage of the satellites, global network data is required to generate global ionospheric maps, regional network data to generate regional ionospheric maps and local network data to generate local ionospheric maps (based on the vertical TEC obtained from the ionospheric model). These maps (currently only hourly maps are available) can be used for the vertical TEC of any rover station (e.g. station B in Figure 4.1) surrounding the base (reference) station at any epoch of the observation duration by an interpolation approach (ionospheric prediction). The slant ionospheric corrections can therefore be simply calculated by the equation (4.9), based on the mapping function and the vertical TEC. The L_1 and L_2 frequency ionospheric corrections, the constant scale (Υ_1=1.5457

and Υ_2=2.5457) terms timing the slant ionospheric corrections can respectively be obtained from equation (4.4b) and (4.5b). However with these ionospheric corrections on both the base and the reference stations, enhancement of DGPS or RTK GPS performance over longer baselines can be expected.

For the GPS services, measurements are collected from each station of a GPS network for a period of time and sent to a master station or a analysis center for the computation of vertical ionospheric delays at each grid point on the ionospheric profile. These grid vertical TECs are transmitted to the satellite for broadcast to users. Single or dual frequency users are then able to use these vertical TECs to calculate the slant ionospheric corrections by an interpolation approach. In practice, the ionosphere is a highly variable and complex physical system that is difficult to predict, and the time required to update the ionospheric grid and transmit these data to users will retard the actual ionospheric changes if changes in the ionosphere occur too quickly (Doherty and Gendron, 1997). For RTK operation, a local ionospheric model, just using a single-reference station, satisfied the need for rapid data transmissions and increased accuracy.

4.7 SUMMARY

At present global and regional ionosphere maps (broadcast on the internet for example), based on global ionosphere models (GIM) and regional ionosphere models (RIM) are available for wide area DGPS (WADGPS) and worldwide DGPS (WWDGPS). Because of the limited accuracy of these models, a local ionosphere model (LIM) using local GPS networks has been developed to see whether it can enhance the performance of RTK GPS. To date local area DGPS (LADGPS) using a single-reference station has been attempted but the accuracy decreases with increased distance from the base station (WARSAW University, 1998). Nevertheless LADGPS may become mainstream DGPS method for GPS services in the future.

To improve the GPS current techniques for DGPS or RTK GPS over long distance baselines, a high accurate ionospheric model is expected for this to be possible. Based on the previous description of the ionospheric delays and modelling, the direction of future work for high accuracy ionospheric modelling can be summarised as follows.

- By using dual frequency phase data rather than code data with the pre-assumption that the instrument biases are constant over a few hour time period.
- Preprocessing for cycle slip detection and repair is necessary for all current models, therefore the software dealing with the problem of the cycle slips has to be very reliable and able to get a time series of data 100% "clean".
- Currently ionospheric modelling using either the L4 observations or the L_C observations is affected by the constant biases. The preprocessing of these constant biases is necessary, otherwise the accuracy of the vertical TEC is limited. However one of the problems of RTK is that the precalibration of instrument biases is time consuming and the ambiguity fixing is not always 100% successful. If taking the double differencing strategy to eliminate the effect of the instrument biases the data of at least two reference stations is necessary for the modelling then the problem of the ambiguity pre-resolution still remains. Obviously, this strategy is not suitable for the modelling just using the data from a single-reference station. Therefore, in order to enhance the accuracy of the ionospheric modelling, the ambiguities and the instrument biases have to be resolved.The non-zeromean also cannot be ignored if using the L_C observations. However by taking the difference between two epochs of ionospheric observations (L4 or L_C), the problem of the constant biases can be resolved without any preprocessing of hardware calibration and ambiguity fixing. Hence this can be an optimal strategy for high accurate ionospheric modelling because what is the temporal nature of the ionosphere which is easier to analyse. This strategy will be introduced in Chapter 7.
- Current equations for the mapping function and the vertical TEC may not be accurate enough to achieve high precision modelling. Therefore the construction of the ionosphere with the mapping function and the vertical TEC will be the key problems of the ionospheric modelling.
- As most current models set the height of spherical shell at 350 km, this figure is adopted in this research.
- Even though the sun-earth reference system is used to solve the problem of temporal changes in the ionosphere by most models, the definition of the origin of the reference system is not currently identical. As mentioned in (Wilson and Mannucci, 1993), the ionosphere is changing even in the sun-earth reference system over hours, therefore the time span of the fit should be minimised in order to

optimise the accuracy of the vertical TEC. For the long-term sessions, this problem may cause the limited accuracy of current models. For the short-term sessions this problem should be considered so as to obtain high accuracy ionospheric modelling.

- Although the positioning accuracy or the percentage of ambiguity resolution is the popular way to verify the ionospheric modelling, these can be affected by the other remaining errors like the tropospheric modelling errors. However it may be a good way to verify the ionospheric modelling if two steps are taken, a refined approach for the exactness of the modelling and the positioning accuracy (or the percentage of ambiguity resolution) for its efficiency when applying to DGPS or RTK GPS.

CHAPTER FIVE

INITIAL INVESTIGATIONS ON THE BEHAVIOUR OF ATMOSPHERIC DELAYS OVER LONG BASELINES

5.1 INTRODUCTION

Undoubtedly, single epoch AFT with the ability of instantaneous positioning is an optimal RTK technique, which is free of the initialisation or re-initialisation problem of RTK GPS with other current techniques. Due to the limitation of this technique to short distance applications, further research is required to resolve the latent problems over long baselines. As carried out in chapter three, the initial investigation on AFT performance over long baselines has found that the performance of the AFT is dependent on the size of the combined errors and the capability of the AFT method itself to handle them. The sizes of the errors for any particular application depend on the survey environment, area, and time, and consist of the multipath and the atmospheric effects. The tolerable error in the method is, however, small and is usually less than 2cm. In order to achieve high precision RTK GPS with this technique over long distances, it is necessary to reduce the effect of these errors. It is well known that multipath is very hard to model in RTK GPS applications so the modelling of atmospheric delays (including both ionospheric and tropospheric delays) is crucial. It has been shown in Chapter 4 that current ionospheric models are of limited accuracy and unsuitable for this purpose and the Saastamoinen tropospheric model used in the current version of GASP needs further investigation to evaluate its suitability.

In this chapter, an investigation of the behaviour of atmospheric delays over different lengths of baselines is carried out in order to estimate the actual tropospheric delays and the ionospheric delays in the atmosphere with the dual frequency GPS data collected at two known stations for a period of at least an hour. Data used in the experiments carried out in Chapter 3 is used for this purpose. This investigation is carried out with two approaches, the geometry free approach (GFA) and a linear combination approach (LCA). The first approach is able to investigate the behaviour of ionospheric single path delays and the second approach is capable of obtaining the true combined double differenced delays of the troposphere and ionosphere under the assumption of negligible multipathing effects on phase. This investigation is also important for the verification of

ionospheric and tropospheric modelling carried out as part of this research (later in this Chapter and in Chapter 6).

5.2 PROCESSING STRATEGY

The geometry free approach requires dual frequency code and phase data, and the linear combination approach only requires dual frequency phase data. Before starting the two approaches, a pre-processing stage of cycle slip detection and repair introduced in the following section is implemented through the use of the TurboEdit routine in GIPSY. This is necessary to ensure the quality of the data sets that will be used for the processing. Since the second approach is based on two known stations, the coordinates of base and rover stations have to be known or calculated previously. This has been implemented in section 3.2 through the use of GIPSY. Use of the precise orbits ensures that the effects of errors in satellite coordinates are irrelevant and thus the range between the satellite and the station is considered as a known parameter. The geometry free observable is anyway free of coordinate problems. The processing strategy and expected investigation outcomes with respect to tropospheric and ionospheric behaviour are summarized as shown in Table 5.1.

Table 5.1 Basic requirements and investigation outcomes of the geometry free approach and the linear combination approach

APPROACH	OBSERVABLE	Base/Rover coordinate	INVESTIGATION
Geometry free	P1,P2,L1,L2	Unknown/Unknown	(1)
Linear combination	L1,L2	Known/Known	(2),(3),(4)
Investigation outcomes: (1) Behaviour of single path ionospheric delays (2) Behaviour of double differencing ionospheric delays (3) Behaviour of double differencing tropospheric delays (4) Evaluation of Saastamoinen tropospheric model Preprocessing of cycle slip detection and repair: necessary for both approaches			

5.3 PREPROCESSING—CYCLE SLIP DETECTION AND REPAIR

Since a time series of data is required for this investigation, the problem of cycle slips has to be first resolved. As mentioned in (IESSG, 1996), the occurrence of cycle slips can be caused by the following factors:

1. the loss of lock between the receiver and the satellite signal,
2. obstructions to the satellite signal,
3. a low Signal to Noise Ratio (SNR),
4. interference from other radio signal sources
5. high ionospheric activity,
6. high antenna acceleration,
7. incorrect signal processing within the receiver software.

Any GPS technique that needs to utilize the phase data at more than one epoch will be sensitive to any cycle slips that may have occurred, and the preprocessing of the data is necessary to detect and repair any cycle slips before it can be used. Even if only one cycle slip remains in the data set, it can cause totally wrong results and conclusions about the ionosphere and the troposphere. As described in Chapter Four, this is the first step of all current ionospheric modelling from GPS phase data. However, in order to obtain a total clean (no cycle slips) data set, reliable software for cycle slip detection and repair is necessary.

Up to date, various routine and algorithms for cycle slip detection and repair have been developed. Probably the best known are

1. TurboEdit (Blewitt, 1990, Gregorius, 1996), and
2. PhaseEdit (Freymueller, 1997)

Also (Chu, 1993) lists the following methods: the Ohio State University Method, the dual frequency method, the Newcastle method, Kalman filtering, phase-range combinations, the polynomial approach, the additional parameter method, and the UNSW method.

TurboEdit has been used in this research for the following reasons.

1. It has been adopted by JPL and integrated in the high precision GIPSY software.
2. It claims a more than 99% success rate in the test of fifty GPS data sets tested by its authors.

Visual screening all of data sets used in research and edited with TurboEdit indicates that they are totally clean (see Figures A.16 to A.23 in Appendix A).

5.4 GEOMETRY FREE APPROACH

The main purpose of geometry free approach introduced in this section is to investigate the behaviour of single path ionospheric delays. This approach requires GPS dual frequency code and phase observations. Based on geometry free combination and an averaging process with dual frequency GPS data, the derived observable called the L_C observable (or L_C observation) consists of only two parameters of ionosphere and instrument bias in the observation if it is assumed that the average of multipath for a period time of data equals zero. The elimination of parameters for range, clock errors, tropospheric delays is the main advantage of using this observable. As a matter of fact, this derived observable in a undifferenced form is widely used for ionospheric modelling, for instance, JPL's and ESOC's global ionospheric model, and Lanyi's and Sardon's local ionospheric model (see Table 4.1). In this research, this observable is only used for an initial investigation of ionospheric behaviour over longer baselines.

The following subsections cover

- the basic geometry free procedure (on the assumption that cycle slips have been repaired), and
- the results and conclusions from applying the geometry free approach to the data collected for the trials described in the chapter Three.

5.4.1 THE GEOMETRY FREE APPROACH

The first step in the geometry free approach is to form the geometry free observable, the so-called the ionospheric combination observable, which is the difference between the L1 and L2 code and phase observables as below:

$P4i = P_{1,i} - P_{2,i}$, i = 1,n .....(5.1)

$L4i = L_{1,i} - L_{2,i}$, i = 1,n .....(5.2)

where

P_1, P_2 is the L1 and L2 frequency code observable in unit of metres,

L_1, L_2 is the L1 and L2 frequency carrier phase observable in unit of metres – obtained by multiplying the phase data (in units of cycles) by the appropriate wave length,

$P4_i$ is the ionospheric combination observable for code,

$L4_i$ is the ionospheric combination observable for phase,

n is the number of measurement epochs.

Once the geometry free observable for code and phase is formed. The range, receiver and satellite clock errors, and the tropospheric error are eliminated after the process of differencing. That is the main advantage of this approach and why the ionospheric combination observable is also called the geometry free observable. After the differencing, the ionospheric combination observable for code is dominated by the differential code multipath and the differential instrument biases (L1-L2), and the ionospheric combination observable for phase is dominated by the differential ambiguity. After pre-processing (cycle slip detection and repair described in the previous section) of GPS raw data, the differential ambiguity is considered being constant and the differential instrument biases are assumed constant, during 2 or 3 hours period of time. If the multipath noise follows a Gaussian zero-mean distribution (Mannucci, 1993), then a constant (consisting of ambiguities and instrument biases) can be obtained from a combination of P4 and L4 by an averaging process as follows:

$B4 = \sum [(P_{1,i} - P_{2,i}) - (L_{1,i} - L_{2,i})] / n$, i = 1,n .....(5.3)

where

B4 is a constant combined with ambiguity and instrument biases.

Because the carrier phase is much more precise than the code, the ionospheric combination observable for phase, L4, is taken into account to obtain the single path

ionospheric delay by a process, so called "leveling", which involves simply subtracting the constant ,B4, from L4 as follows:

$$I_i = L4_i - B4 \quad , i = 1,n \qquad (5.4)$$

where

I_i is the single path ionospheric delay.

Therefore, the single differenced ionospheric delay after single differencing and the double differenced ionospheric delay after double differencing can be obtained based on equation (5.4). However, because the multipath noise is usually not zero-mean (Mannucci, 1993, Barnes, 1999), a constant bias still remains in the ionospheric estimate when using the geometry free approach. For the single path ionospheric delay, the bias is a combination of receiver and satellite instrument biases, and this non-zero mean multipath. For the single differenced ionospheric delay, the receiver or satellite instrument biases are not included. Only the "non-zero mean" multipath remains in the double differenced ionospheric delay. All estimates are, however, affected by phase multipath but this is small and has an effective zero mean in this application. Even though the geometry free approach can only provide the trend of the ionospheric delays (because of the biases), it still is an effective method for an initial investigation of ionospheric behaviour. The geometry free approach is summarized as follows:

1. Formation of the geometry free observable on code and phase (equation 5.1 and 5.2),
2. The leveling process (equation 5.3),
3. The subtracting of a constant bias (equation 5.4),
4. Calculation of single path ionospheric delays (equation 5.4).

5.4.2 RESULTS AND CONCLUSIONS

The geometry free approach, as introduced in the previous section, has been used to investigate the behaviour of single path ionospheric delays over periods of at least one hour for a variety of different length baselines. The results, as shown in Appendix A.16 to A.23 are the single path ionospheric delays with the constant biases of hardware and non-zero mean. Although affected by the constant biases, the variation and rate of change of the ionosphere can be clearly seen. The following conclusions can be drawn.

1. Generally, the lower the elevation angle of the satellite the greater the rate of change of the ionospheric delays.
2. The ionospheric delays change very slowly if the satellite maintains the same elevation, irrespective of whether it is low or high. This can be seen for satellite 18 in Appendix A.16, A.17, A.22, and A.23, and satellite 16 and 25 in Appendix A.20 and A.21. Exceptionally there is no apparent change of ionospheric delay in the case of satellite 16 in Appendix A.21 where the elevation angle changes from 64.8 at the starting epoch to 84.3 at the ending epoch.
3. The maximum change in any one hourly period has been found to be about 3.5 m.
4. The largest variations are seen at the stations in Greece (PSMS, SEMA, PLAT and SOHO) - indicating a latitude dependence of the results. This can be seen from, for instance, Figure A.16, A18 and A.19.
5. Without knowledge of the biases remaining in the observations, the absolute ionospheric delays cannot be obtained by this approach. This is in contrast to the methodology of ionospheric modelling by JPL, which relies on a hardware calibration procedure.

5.5 LINEAR COMBINATION APPROACH (LCA)

As indicated in Chapter Three, the performance of the AFT over long distances can be affected not only by the ionospheric delays but also by the tropospheric delays. The accuracy of the Saastamoinen model applied in GASP over long distances is still not fully researched. With this linear combination approach presented in this chapter, the true double differencing ionospheric and tropospheric delays can be obtained if neglecting the small effects of phase multipath, and can also be used for evaluating the Saastamoinen model. The main requirement of this linear combination approach is that the ranges between the working stations (the base and rover stations) and all available satellites are known.

The following subsections cover

- The background to and steps involved in applying the linear combination approach (on the assumption that the data has already been cleaned of cycle slips),

- The results (and their analysis) of tests carried out using the same data sets as used to investigate the geometry free approach, and
- The evaluation of the tropospheric model (Saastamoinen) used in GASP.

5.5.1 THE LINEAR COMBINATION APPROACH

In order to obtain more accurate estimates of the ionospheric delay, three types of linear combination: the widelane, the ionosphere free, and the ionospheric are used along with known station and satellite coordinates. The formation of the widelane and ionosphere free combination are described in equation (5.5), (5.6) and (5.7), and (5.8) respectively as follows:

$P5i = P_{1,i} - P_{2,i}$, i = 1,n .....(5.5)

$L5i = L_{1,i} - L_{2,i}$, i = 1,n .....(5.6)

$P6i = \Upsilon_2 P_{1,i} - \Upsilon_1 P_{2,i}$, i = 1,n .....(5.7)

$L6i = \Upsilon_2 L_{1,i} - \Upsilon_1 L_{2,i}$, i = 1,n .....(5.8)

P_1, P_2 are the L1 and L2 frequency code observables in unit of cycles,

L_1, L_2 are the L1 and L2 frequency carrier phase observables in unit of cycles,

P5 is the widelane combination observable for code,

L5 is the widelane combination observable for phase,

Υ_1, Υ_2 are constants of about 1.5457 and 2.5457 respectively,

P6 is the ionosphere free combination observable for code,

L6 is the ionosphere free combination observable for phase,

n is the number of measurement epochs.

After these combination observables are formed, the double differencing process is adopted to eliminate of clock errors and instrument biases because it would be impossible to obtain the single path ionospheric delay or the single differencing ionospheric delay without any knowledge of these errors and biases. Simultaneously the double differencing tropospheric delay and the double differenced range are calculated using Saastamoinen model and the known coordinate of stations and satellites. They are then subtracted from this observable. At this stage the double differenced L1-L2 integer ambiguity, ionospheric delay, and phase multipath still remain, and the observable may also be affected by the small errors resulting from tropospheric estimation and imprecise coordinates of station and orbits. Because the ionospheric delay is very sensitive to these

errors, the precise ephemeris and station coordinates have to be taken into account to reduce the effect of these errors in this approach. However the advantage of using widelane combination observable is that the ambiguities are integer. If the combined effect of tropospheric estimation error, coordinate error, double differencing ionospheric delay, and double differenced L1-L2 phase multipath can be kept below 0.5cycle, then the widelane double differenced integer ambiguities can be determined. This widelane ambiguity together with the (real-valued) ionosphere free combination ambiguity can be used to evaluate both the L1 and L2 double differenced integer ambiguities. For a period of processing epochs, the correct integer ambiguities can be determined with using the ambiguity resolution of each satellite at the highest elevation angle where the corresponding error effect is smaller according to the previous investigations in section 5.4. This step is so important to ensure an errorless investigation on the atmospheric behaviour in this chapter. The "true" double differenced ionospheric delay can now be obtained by using the ionospheric combination observable. Also the "true" double differencing tropospheric delay can be obtained by using the ionosphere free combination. The linear combination approach is summarized as follows:

1. Formation of the linear combination observations (Equation 5.2, 5.6, and 5.8),
2. The process of "true" range on the basis of the station and satellite coordinates, and tropospheric corrections based on the Saastamoinen model,
3. The resolution of the simultaneous equations: the widelane ambiguity and the ionosphere free combination ambiguity (Equation 5.6 and 5.8),
4. Determination of the correct L1 and L2 double differencing integer ambiguities,
5. The subtracting of the L1 and L2 integer ambiguities from the ionospheric combination observation to obtain the double differenced ionospheric delays after double differencing (Equation 5.2),
6. The subtracting of the "true" range and the L1 and L2 integer ambiguities from the observation of ionosphere free combination to obtain the double differenced tropospheric delays after double differencing (Equation 5.8).

5.5.2 RESULTS AND ANALYSIS

In Appendix A, the figures of the results obtained from the linear combination approach based on two known stations demonstrates the ambiguity resolution, the ionospheric

delays, and the tropospheric delays in a form of double difference over the various long distance baselines. From the results of these trials, all of integer ambiguities on L1 and L2, shown in Figure A.11 to A.15, are exactly fixed at most of the processing epochs. Although there are some epochs unfixed (due to the effects of the remaining errors), the determination of correct integer ambiguities by the method described in the previous subsection seems valid that the ambiguities are fixed for the majority of epochs in a period of time. The "true" double differenced ionospheric and tropospheric delays are respectively shown in the Figure A.24 to A.28 and Figure A.29 to A.33. Note that since the process involves double differencing the phase data, the "true" ionospheric and tropospheric delays can only be obtained if the small effect of phase multipath is resolved or ignored. The remaining effect of phase multipath in the combined observable of ionospheric combination and ionosphere free combination causes the high frequency variation of the curves in these figures.

From the results shown in Figure A.24-28, the statistics including the maximum, the minimum, the average, and the RMS concerning the investigation of double differenced ionospheric errors for each on the various distances tested are summarized in Table 5.2. The RMS shown in Figure 5.1 represents the high frequency portion of the curves, which is used to investigate the effect of multipath on the double differenced ionospheric errors. The maximum of RMS of all pairs of available satellites for each trial, shown in Figure 5.2, is supposed to indicate the maximum effect of multipath at the area of working stations. The range of these errors, Rng (the maximum – the minimum), is to show the variation of double differenced ionospheric errors for each pair of satellites during the period of surveying. This is shown in Figure 5.3. These ranges for each trial are averaged to represent the local ionospheric variation after double differencing. The distance dependence of the double differenced ionospheric errors is therefore shown in Figure 5.4. After averaging, the Avg (the average of double differenced ionospheric errors) shown in Figure 5.5 is to demonstrate the "true" double differenced ionospheric errors where the maximum is to represent the maximum effect of double differenced ionospheric errors at the local area for each on various distance baselines. The distance dependence of double differenced ionospheric errors can be seen in Figure 5.6.

Table 5.2 Results of the investigation on the double differenced ionospheric errors based on the linear combination approach

Unit: cm

Ion / SVs		PSMS-SEMA (12.8km)	CG54-KRPI (15km)	INED-SHEN (21km)	PSMS-PLAT (25km)	PSMS-SOHO (33km)
1	Max	0.1	1.3	1.7	1.8	4.6
	Min	-2.9	-2.2	-2.8	-0.8	-0.9
	Rng	3.0	3.5	4.5	2.6	5.5
	Avg±Rms	-1.2 ±0.8	-0.6 ± 0.7	-0.6 ± 0.8	3.6 ± 0.6	1.9 ± 1.2
2	Max	0.3	1.6	1.7	1.6	3.8
	Min	-3.7	-4.1	-3.1	-4.0	-3.8
	Rng	4.0	5.7	4.8	5.6	7.6
	Avg±Rms	-1.5 ± 0.8	-0.7 ± 1.3	-1.1 ± 1.1	-0.7 ± 1.4	0.4 ± 2.1
3	Max	0.6	3.2	3.2	2.9	5.5
	Min	-2.1	-1.0	-1.0	0.5	0.8
	Rng	2.7	4.2	4.2	2.4	4.7
	Avg±Rms	-0.4 ± 0.6	1.0 ± 0.9	1.0 ± 1.1	1.8 ± 0.6	2.9 ± 1.3
4	Max	1.0	0.3	2.3	3.0	4.9
	Min	-2.1	-3.6	-1.3	-0.8	-0.7
	Rng	3.1	3.9	3.6	3.8	5.6
	Avg±Rms	-2.8 ± 0.8	-1.2 ± 0.9	0.4 ± 1.0	1.5 ± 0.8	2.7 ± 1.1
5	Max	5.1	3.6	7.5	1.5	4.3
	Min	1.4	0.1	-1.3	-2.9	-3.0
	Rng	3.6	3.5	8.8	4.4	7.3
	Avg±Rms	3.6 ± 0.8	1.8 ± 0.8	2.2 ± 2.0	-0.9 ± 1.1	0.4 ± 1.9
6	Max	0.2	-0.3	1.3	4.0	6.3
	Min	-2.7	-4.7	-3.7	0.0	1.3
	Rng	2.9	4.4	4.0	4.0	5.0
	Avg±Rms	-0.8 ± 0.7	-1.9 ± 0.9	-1.0 ± 1.3	1.6 ± 0.8	3.4 ± 1.4
7	Max		5.8			
	Min		-2.2			
	Rng		8.0			
	Avg±Rms		0.7 ± 1.9			
Avg(Rng)		3.2	4.9	5.0	3.8	5.9
Avg(Rms)		0.75	1.0	1.2	0.9	1.5
Max(|Avg|)		3.6	1.8	2.2	3.6	3.4
Period		1 hour	2 hours 38 mins	1 hour	1 hour	1 hour
AREA		40.35/Greece	37.9/Greece	51.71/London	40.35/Greece	40.35/Greece
TIME		25/09/98 12:30:00-13:29:30	13/07/98 09:16:00-11:54:30	19/08/99 11:11:00-12:10:30	25/09/98 12:30:00-13:29:30	25/09/98 12:30:00-13:29:30

Baselines: PSMS-SEMA(12.8km), CG54-KRPI(15km), INED-SHEN(21km), PSMS-PLAT(25km), PSMS-SOHO(33km).

Ion: Double differenced Ionospheric errors in unit of cm. Max and Min are the maximum And minimum of double differenced Ionospheric errors in the period of surveying.

SVs: The number of the satellite pair (the highest SV- SV),
PSMS-SEMA, PSMS-PLAT, and PSMS-SOHO: 1:18-4, 2:18-13, 3:18-16, 4:18-19, 5:18-24, and 6:18-27.
CG54-KRPI: 1:21-1, 2:21-3, 3:21-15 4:21-22, 5:21-23, 6:21-29, and 7:21-31.
INED-SHEN: 1:14-1, 2:14-4, 3:14-7, 4:14-16, 5:14-18, and 6:14-25.

Rng: =Max(Ion)-Min(Ion).

Avg±Rms: The average ± the root mean squares.

Avg(Rng): The average of the Rng.

Avg(Rms): The average of the Rms.

Max(|Avg|): The maximum of the absolute Avg.

AREA: The surveying area, latitude/location.

TIME: The time of data collection, month/year.

Table 5.3 Results of the investigation on the double differenced tropospheric errors based on the linear combination approach

Unit: cm

Tro / SVs		PSMS-SEMA (12.8km)		CG54-KRPI (15km)		INED-SHEN (21km)		PSMS-PLAT (25km)		PSMS-SOHO (33km)	
1	Max / Min	8.5	2.9	9.5	-4.7	0.8	-3.2	7.6	-0.4	5.4	1.2
	Rng	5.6		14.2		4.0		8.0		4.2	
	Avg±Rms	5.0 ± 1.3		1.8 ± 3.4		-0.6 ± 0.8		2.1 ± 1.6		2.8 ± 1.2	
2	Max / Min	13.1	1.7	1.6	-6.3	-0.2	-10.4	2.0	-2.6	0.0	-0.8
	Rng	11.4		7.9		10.2		4.6		0.8	
	Avg±Rms	6.9 ± 2.9		-1.4 ± 1.7		-3.3 ± 2.0		-0.1 ± 1.0		-0.5 ± 0.2	
3	Max / Min	4.8	-0.5	9.3	-3.8	1.8	-2.7	4.3	-1.1	3.6	1.2
	Rng	5.3		13.1		4.5		5.4		2.4	
	Avg±Rms	-1.4 ± 1.2		1.8 ± 3.7		-0.2 ± 1.0		0.8 ± 1.1		2.2 ± 0.7	
4	Max / Min	2.7	-3.4	4.2	-0.7	2.7	-2.3	3.0	-2.1	2.0	0.6
	Rng	6.1		4.9		5.0		5.1		1.4	
	Avg±Rms	-0.4 ± 1.4		1.6 ± 0.9		0.5 ± 1.1		0.2 ± 1.1		1.3 ± 0.4	
5	Max / Min	-0.2	-7.9	12.3	1.7	6.1	-0.9	1.2	-2.7	-0.2	-3.7
	Rng	7.7		11.6		7.0		3.9		3.5	
	Avg±Rms	-3.8 ± 1.4		5.2 ± 2.3		1.9 ± 1.3		-0.8 ± 0.8		-1.7 ± 1.0	
6	Max / Min	13.0	0.0	4.8	-6.1	-1.6	-6.2	10.1	0.9	7.8	2.0
	Rng	13.0		10.9		4.6		9.2		5.8	
	Avg±Rms	5.4 ± 3.4		-0.9 ± 2.4		-3.6 ± 1.0		3.6 ± 2.1		4.1 ± 1.6	
7	Max / Min			10.2	-6.5						
	Rng			16.7							
	Avg±Rms			0.5 ± 4.0							
Avg(Rng)		8.2		11.3		5.9		6.0		3.0	
Avg(Rms)		1.9		2.6		1.2		1.3		0.8	
Max(|Avg|)		6.9		5.2		3.6		3.6		4.1	
Period		1 hour		2 hours 38 mins		1 hour		1 hour		1 hour	
AREA		40.35/Greece		37.9/Greece		51.71/London		40.35/Greece		40.35/Greece	
TIME		25/09/98 12:30:00-13:29:30		13/07/98 09:16:00-11:54:30		19/08/99 11:11:00-12:10:30		25/09/98 12:30:00-13:29:30		25/09/98 12:30:00-13:29:30	

Baselines: PSMS-SEMA(12.8km), CG54-KRPI(15km), INED-SHEN(21km), PSMS-PLAT(25km), PSMS-SOHO(33km).

Tro: Double differenced Ionospheric errors in unit of cm. Max and Min are the maximum and minimum of double differenced Ionospheric errors in the period of surveying.

SVs: The number of the satellite pair (the highest SV- SV),
PSMS-SEMA, PSMS-PLAT, and PSMS-SOHO: 1:18-4, 2:18-13, 3:18-16, 4:18-19, 5:18-24, and 6:18-27.
CG54-KRPI: 1:21-1, 2:21-3, 3:21-15 4:21-22, 5:21-23, 6:21-29, and 7:21-31.
INED-SHEN: 1:14-1, 2:14-4, 3:14-7, 4:14-16, 5:14-18, and 6:14-25.

Rng: =Max(Rng)-Min(Rng).

Avg±Rms The average ± the root mean squares.

Avg(Rng): The average of the Rng.

Avg(Rms): The average of the Rms.

Max(|Avg|): The maximum of the absolute Avg.

AREA: The surveying area at the base station, latitude/location.

TIME: The time of data collection, month/year.

From the results of Figure A.29 to A.33, the investigation on the double differenced tropospheric errors, their variation, and the related effect of multipath is implemented by the same way as described in the previous paragraph. The statistics including the maximum, the minimum, the average, and the RMS are summarized in Table 5.3, and demonstrated with the following figures of 5.7 to 5.12. Included are

1. The effect of phase multipath after the process of ionosphere free combination (Figure 5.3),
2. The average effect of phase multipath for each on various distance baselines (Figure 5.4),
3. The distance dependence of double differenced tropospheric variation (Figure 5.9),
4. The distance dependence of double differenced tropospheric maximum variation (Figure 5.10),
5. The distance dependence of double differenced tropospheric errors (Figure 5.11),
6. The distance dependence of double differenced tropospheric maximum errors (Figure 5.12).

From the results of these figures, three main effects of errors including the phase multipath, the ionospheric delays, and the tropospheric delays are concluded as follows.

- The effect of phase multipath

1. As shown the results of Figure 5.1, 5.2, 5.3, and 5.4, it can be concluded (not surprisingly) that the multipathing effects including those after the process of ionospheric combination and after the process of ionosphere free combination are independent of the baseline distance, and their variation of these trials is more likely dependent of the surveying environments. For instance, in the trial of baseline CG54-KRPI, the multipathing errors can be originated from the reflections in the direction of three satellites (i.e. SV: 1, 15, and 27 as shown in Figure 5.3). In average, this effect can be a level of ±1-2cm for a form of ionospheric combination and ±1-4cm for a form of ionosphere free combination.
2. In Figure 5.2 and 5.4, the multipathing errors after the process of ionosphere free combination is larger than these after the process of ionospheric combination in the first two trials of baseline 12.8km and baseline 15km and this matches the theoretic analysis of observation errors in chapter two. However, a reverse phenomenon is

shown in the rest of the trials. This can be because the result (RMS) is biased by the effect of troposphere.

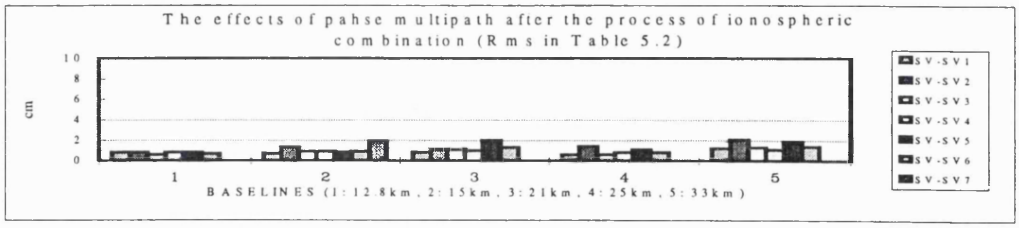

Figure 5.1 The effects of phase multipath after the process of ionospheric combination (Rms)

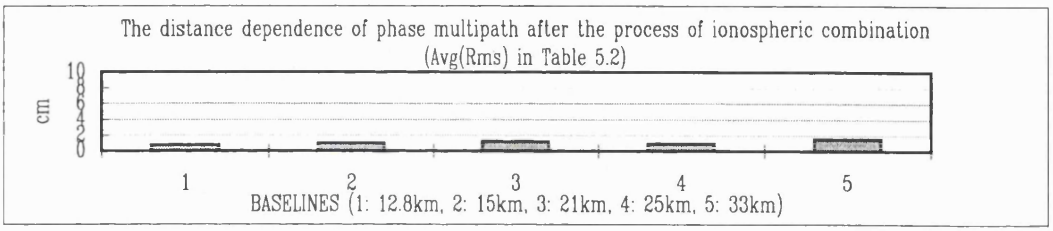

Figure 5.2 The distance dependence of phase multipath after the process of ionospheric combination (Avg(Rms))

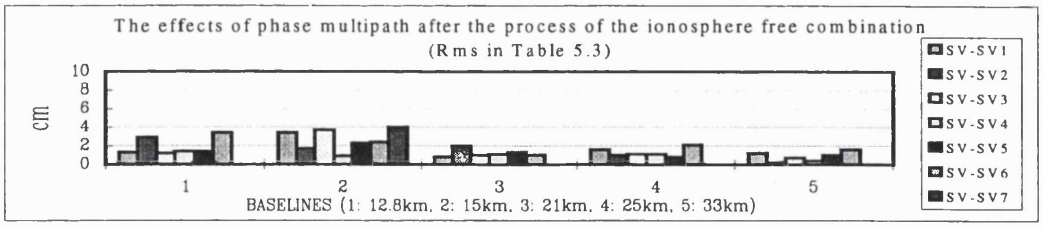

Figure 5.3 The effects of phase multipath after the process of ionosphere free combination

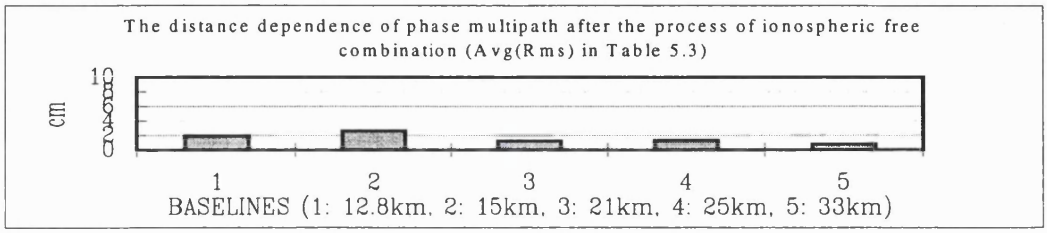

Figure 5.4 The distance dependence of phase multipath after the process of ionosphere free combination

- Behaviour of the "true" double differenced ionospheric errors

1. In Table 5.2, the result of item Avg(Rng) has indicated that the range of double differenced ionospheric errors including the bias of multipathing effect is about 3.2cm (the average for all available satellites) in the area of the shortest distance trial, and about 5.9cm (the average for all available satellites) in the area of the longest distance one for an hourly variation. In general, as the baseline distance increases the ionospheric effect is slightly increased as shown in Figure 5.5 and 5.6. The increasing rate on average is a level of around 2-3 cm per hour from a baseline length of 12.8 km to a baseline length of 33km (see the cases of baselines between 12.8km and 33km). An increasing rate with a function of a constant scale cannot be seen in the cases of baselines between 12.8km and 15km (i.e.3.2cm for an hour to 4.9 cm for 2.63 hours).
2. Figure 5.7 has indicated that the double differenced ionospheric delay including the bias of multipathing effect is a level of about –2.8cm to 3.6cm in the trial of the shortest baseline, and about 0.4cm to 3.4cm in the trial of the longest one for an hour period. The maximum local effect of double differenced ionospheric delays at the surveying area of the trials, shown in Figure 5.8, is a level of 3.6cm, 1.8cm, 2.2cm, 3.6cm, and 3.4cm respectively.

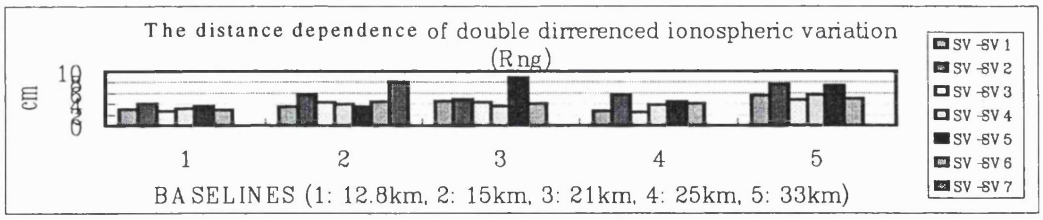

Figure 5.5 The distance dependence of double differenced ionospheric variation (Rng)

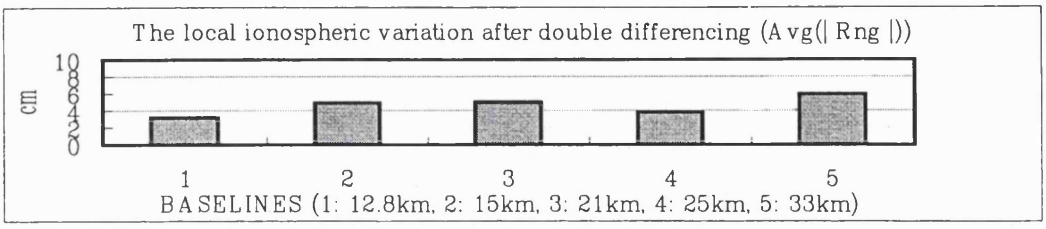

Figure 5.6 The local ionospheric variation after double differencing (Avg(Rng))

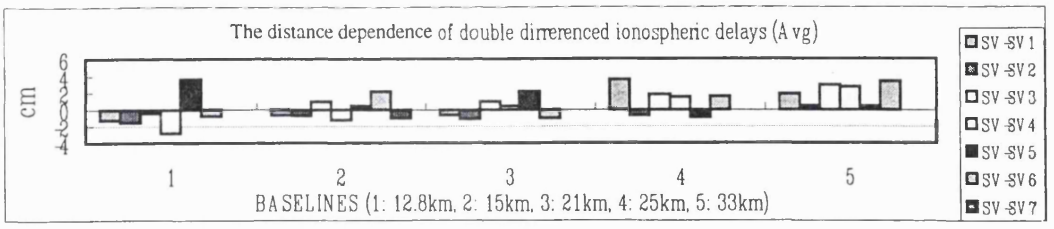

Figure 5.7 The distance dependence of double differenced ionospheric delays (Avg)

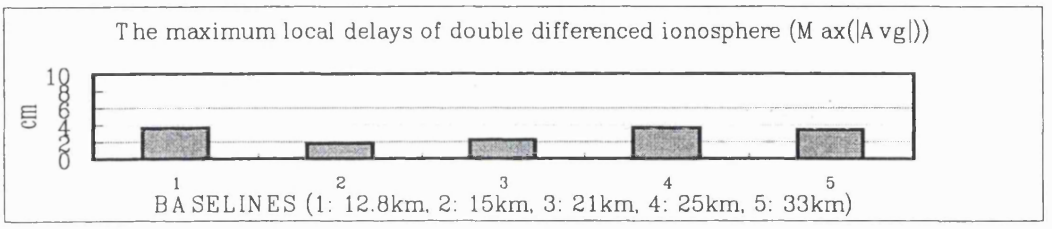

Figure 5.8 The maximum local delays of double differenced ionosphere (Max(|Avg|))

- Behaviour of the "true" double differenced tropospheric errors

1. From the result of Figure 5.9-10, the area of greatest variation of tropospheric errors about 11.3cm is located at the stations, CG54-KRPI, which is a trial of 15km baseline, and the area of smallest one about 3.0cm is located at stations, PSMS-SOHO, which is a trial of 33km baseline. It seems that the variation of tropospheric errors is more dependent of local environments including the pressure, water vapor, and the height of operation stations, and the distance dependence of this error can hardly be seen in these trials.
2. Figure 5.11 has indicated that the double differenced tropospheric delay including the bias of multipathing effect is a level of about –1.4cm to 6.9cm, -1.4cm to 5.2cm, -3.6cm to 1.9cm, -0.8cm to 3.6cm, and –1.7cm to 4.1cm for the trials tested over an hour period. The maximum local effect of double differenced tropospheric delays at the surveying area of the trials, shown in Figure 5.12, is a level of 6.9cm, 5.2cm, 3.6cm, 3.6cm, and 4.1cm respectively.

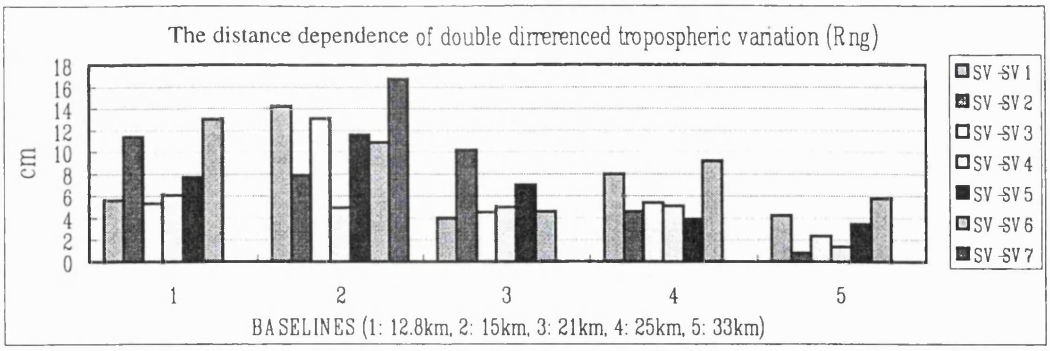

Figure 5.9 The distance dependence of double differenced tropospheric variation (Rng)

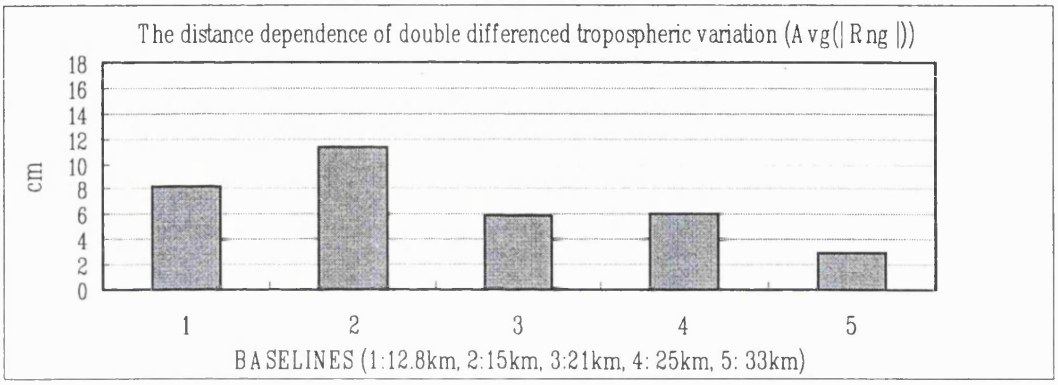

Figure 5.10 The local tropospheric variation after double differencing (Avg(Rng))

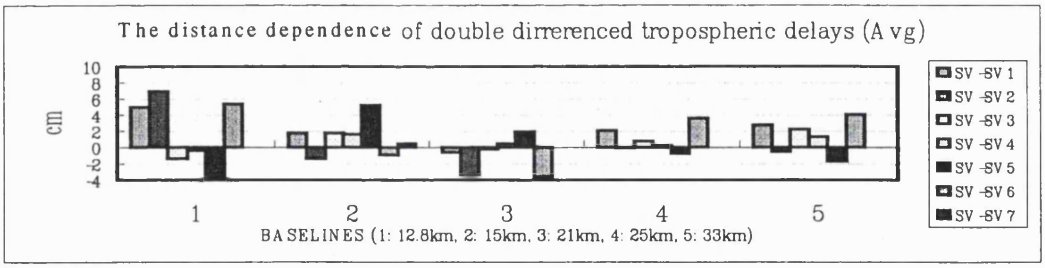

Figure 5.11 The distance dependence of double differenced tropospheric delays (Avg)

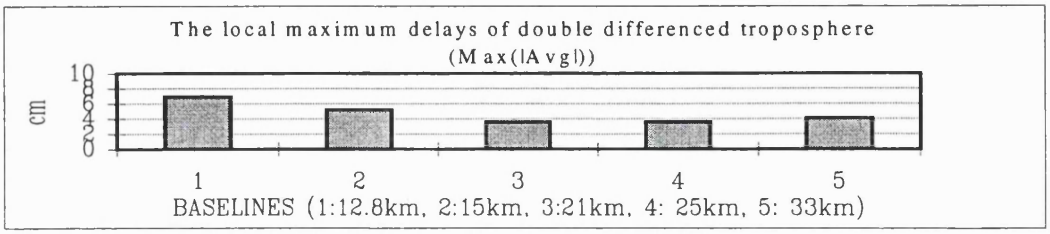

Figure 5.12 The local maximum delays of double differenced troposphere (Max(|Avg|))

- Overview of these errors discussed

1. Comparing Figure 5.2 to Figure 5.8 or 5.12, it is found that the multipathing effect, in general, is much smaller than the effect of tropospheric or ionospheric error after double differencing. Therefore, it can be denoted that as the baseline distance extends to greater than 10km the effect of ionosphere and troposphere cannot be ignored for the RTK GPS applications.
2. Comparing the variation of troposphere to ionosphere (see Figure 5.6 and 5.10), the former is larger than the latter. Even though this can be due to the bias of multipath after the process of ionosphere free combination, but however it can be seen in these figures that the double differenced tropospheric errors are still large even if taking the bias of multipath off. This therefore can indicate that after the process of double difference the variation of troposphere may not be smaller than that of ionosphere.
3. From the results of Figure 5.7 and 5.11, the sign of ionospheric error for each pair of satellites is not always the same as that of tropospheric error. If both errors have an opposite sign, then the combined effect on L1 or L2 observable can increase. On the contrary, this combined effect (the tropospheric and ionospheric effect) on L1 or L2 observable can be reduced because of the elimination of both errors when having the same sign. The different propagation nature of both errors on radio signals has been introduced in the previous chapter. In addition, the magnitude of L1 and L2 ionospheric errors is respectively about 1.5457 and 2.5457 times this calculated ionospheric error. After double differencing, this combined effect of atmospheric error may even be smaller or much larger than the multipathing effect. However, as the baseline distance increases, the increasing effect of ionospheric errors is obvious and cannot be ignored.

Above all, although all results are biased by the effect of multipath, it seems that the ionospheric effect is more dependent of the baseline length, and the tropospheric effect is highly related to the effects of local atmospheric environments at the working stations. As the baseline distance extends to more than 10km, the errors of both the ionosphere and the troposphere may have an effect of few centimetres much larger than the multipathing effect, and their effects on the AFT performance may hence become dominant. For longer distance GPS applications, the effects of these errors can no longer

be ignored and have to be reduced. Moreover, the multipathing effect concerning the surveying environments is still of importance to the final results of the AFT. The AFT implementation in GASP (and probably in most other RTK processing packages) assumes that there are no errors introduced into the double differences by the ionosphere. These results show that this assumption is not always valid. In addition, to face the increasing effect of troposphere, whether or not the applied tropospheric model in GASP can handle this problem is still a question.

5.5.3 EVALUATION OF THE CURRENT TROPOSPHERIC MODEL IN GASP

In recent years, many composite tropospheric models have tried to refine the mapping function with current models so as to increase the modelling accuracy. The recent investigation results in Collin et. al., 1998 has indicated that

1. "The residual range delay error due to an incompletely modelled tropospheric propagation delay can usually be ignored by the average user of wide area differential GPS" was reported.
2. The new-generated tropospheric model is based on the zenith delay algorithms of Saastamoinen, a refined mapping function, and a table of atmospheric parameters (more details see Collin al. et., 1997). For this model, only 7 in 100,000 predictions resulted in residual zenith delay errors outside the range of ±20cm.

In this thesis, of great concern is whether or not the current model applied in AFT positioning can exactly estimate the tropospheric errors as the baseline distances increases. As investigated in the previous subsection, the increasing double differenced effects are achievable at a level of about ±3.6cm (±5.56cm on L_1 and ±9.16cm on L_2) for the ionosphere and about ±6.9cm for the troposphere for the trials of 12.8km to 33km baselines. These effects may become the dominant problems of causing the poor performance of AFT positioning over the various length baselines for test. Currently, the Saastamoinen model has been used in the algorithm of AFT positioning to handle the problem of the tropospheric effects. For short distance GPS applications, no further investigation on the effect of this error or the evaluation of this model was reported at the previous two stages of researches (Corbett, 1994, Corbett al. et., 1995, AL-Haifa, 1996, AL-Haifi al. et., 1996). This may be because the effects of atmospheric errors

were insignificant and the multipathing effect plays a more important role. In this section, the performance of this model over various length baselines will be evaluated with comparisons of the true double differenced tropospheric results obtained from the approach based on two known stations, which have been implemented in Section 5.5. The following conclusions of the investigations on the evaluation of the tropospheric model can be drawn.

1. As shown in Figure A.34 to A.38, the performance of the Saastamoinen model for the trials over the observation period is denoted as a dotted line where the true one from the LCA is denoted as a solid line. By a screening of these figures, an improper fitting of both lines has apparently been shown in most cases and a reverse estimation trend for some have even resulted. Exceptionally, the estimations have been badly performed as the satellite (the lower one of the satellite pair) remains at a position of low elevation angle. Over the observation period, the maximum modelling errors are achievable at a level of 15.2cm, 12.7cm, -4.81cm, 5.81cm, and 7.47cm for these trials respectively. Although the results involving the effect of the ionosphere-free multipath may be overestimated, the limited accuracy of current tropospheric model applied can however be confirmed.
2. The averaging results of the true values, the estimations, and their difference over the observation period are summarized in Table 5.4. From the results of the true and the difference, a worse performance can be seen after the corrections with the tropospheric model. For example, the size can be increased from the original level of 6.91cm, 1.65cm, 0.48cm, -0.78cm, and 1.64cm to a level of 8.22cm, 5.08cm, 0.72cm, 1.09cm, and 3.31cm in some exceptional cases of the trials.
3. From the results of the difference, the modelling errors on each available satellite pair for the trials have been demonstrated as shown in Figure 5.13. In general, the modelling errors can be a level of ±8.22cm, ±5.08cm, ±2.64cm, ±1.34cm, and ±3.31cm on average respectively

Table 5.4 Comparisons of double differenced tropospheric delays obtained from the linear combination approach and the Saastamoinen model

Unit: cm

Tro	Baseline(12.8)			Baseline(15)			Baseline(21)			Baseline(25)			Baseline(33)		
SVs	true	Saas	Diff	true	Saas	Diff	true	Saas	Diff	true	Saas	Diff	true	Saas	Diff
1	5.01	-1.04	6.05	1.81	-1.32	3.13	-0.65	-0.29	-0.36	2.12	1.26	0.86	5.37	2.85	2.52
2	6.91	-1.31	8.22	-1.43	-1.07	-0.36	-3.34	-2.78	-0.56	-0.14	-1.18	1.04	2.66	-0.53	3.19
3	1.39	0.10	1.29	1.85	-1.32	3.17	-0.20	0.00	-0.20	0.83	1.58	-0.75	2.27	2.24	0.03
4	-0.42	-0.21	-0.21	1.65	-3.43	5.08	0.48	-0.24	0.72	0.25	0.75	-0.50	1.78	1.30	0.48
5	-3.85	-1.18	-2.67	5.20	1.87	3.33	1.92	1.97	-0.05	-0.78	-1.87	1.09	1.64	-1.67	3.31
6	5.45	-0.84	6.29	-0.88	-2.62	1.74	-3.57	-0.93	-2.64	3.58	2.24	1.34	7.22	4.13	3.09
7				0.53	-0.43	0.96									

Baselines: PSMS-SEMA(12.8km), CG54-KRPI(15km), INED-SHEN(21km), PSMS-PLAT(25km), PSMS-SOHO(33km).

Tro: double differenced tropospheric delays (in unit of cm), based on the linear Combination approach.

SVs: the number of the satellite pair (the highest SV- SV),
PSMS-SEMA, PLAT and SOHO: 18-4, 18-13, 18-16, 18-19, 18-24, and 18-27.
CG54-KRPI: 21-1, 21-3, 21-15 21-22, 21-23, 21-29, and 21-31.
INED-SHEN: 14-1, 14-4, 14-7, 14-16, 14-18, and 14-25.

True The average of double differenced tropospheric errors obtained from the Linear Combination Approach

Sass The average double differenced tropospheric errors estimated with the Saastamoinen tropospheric model

Diff: The average of difference between the "true" and the "Saas".

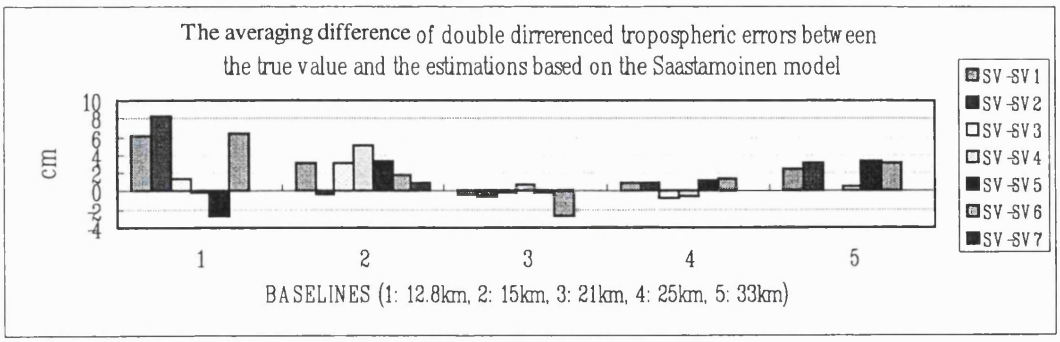

Figure 5.13 The averaging difference of double differenced tropospheric errors between the true value and the estimations based on the Saastamoinen model

As a consequence, the way proposed in this thesis to verify the estimation results of tropospheric model is capable of evaluating the accuracy of tropospheric model. The current model applied in the AFT positioning, irrespective of the difference or the fitting between the true values and the estimations, cannot efficiently resolve the tropospheric problem, exceptionally as the satellite remains at low elevation angle. This comes to the same conclusion as other investigations did (Coster et. al., 1997, Gregorius et. al., 1998, Collin et. al., 1998). For a high precision RTK survey, the current tropospheric modelling needs to be refined and the focus may be on resolving the problem of tropospheric modelling for the low elevation satèllites.

5.6 CONCLUSIONS

In order to know the behaviour of both ionospheric and tropospheric delays and the size of these errors affecting the RTK GPS over long baselines, two approaches based on two known stations, the geometry free approach and the linear combination approach, have been used for the investigations of this chapter. The GFA is used to investigate the behaviour of single path ionospheric delays and the LCA is used to investigate the behaviour of double differenced ionospheric delays with the observable of ionospheric combination and the behaviour of double differenced tropospheric delays with the observable of ionosphere free combination. Meanwhile, the results of double differenced tropospheric delays obtained from the LCA can be used to verify the estimation results with the current tropospheric model in AFT positioning. Since the investigations of this chapter have to rely on the dual frequency GPS data collected at two known stations over a period of at least an hour, hence the preprocessing of cycle slip detection and repair is necessary and accomplished by a reliable software package, the TurboEdit. Through this preprocessing, a 100% "clean" data set for each trial has been confirmed. So, it can be confirmed that there is no effect of cycle slips on the subsequent investigation results. From the investigation results on these typical trials, the following conclusions can be drawn.

1. The behaviour of single path ionospheric delays

- Generally, the lower the elevation angle of the satellite the greater the rate of change of the ionospheric delays.
- The ionospheric delays change very slowly if the satellite maintains at the same elevation, irrespective of whether it is low or high.
- The maximum ionospheric change in the hourly period has been found to be about 3.5m.

2. The behaviour of double differenced ionospheric delays

- The double differenced ionospheric delay including the bias of multipathing effect is a level of about –2.8cm to 3.6cm in the trial of the shortest baseline, and about 0.4cm to 3.4cm in the trial of the longest one for an hour period. The maximum local effect of double differenced ionospheric delays at the surveying area of the trials is a level of 3.6cm, 1.8cm, 2.2cm, 3.6cm, and 3.4cm respectively.
- The range of double differenced ionospheric errors including the bias of multipathing effect is about 3.2cm in the area of the shortest distance trial, and about 5.9cm in the area of the longest distance one for an hourly variation. In general, as the baseline distance increases the ionospheric effect is slightly increased and the increasing rate on average is a level of around 2-3 cm per hour from a baseline length of 12.8 km to a baseline length of 33km. An increasing rate with a function of a constant scale cannot be seen in the cases of baselines between 12.8km and 15km (i.e.3.2cm for an hour to 4.9 cm for 2.63 hours).

3. The behaviour of double differenced tropospheric delays

- The area of greatest variation of tropospheric errors about 11.3cm is located at the stations, CG54-KRPI, which is a trial of 15km baseline, and the area of smallest one about 3.0cm is located at stations, PSMS-SOHO, which is a trial of 33km baseline. It seems that the variation of tropospheric errors is more dependent of local environments including the pressure, water vapor, and the height of operation stations, and the distance dependence of this error can hardly be seen in these trials.
- The double differenced tropospheric delay including the bias of multipathing effect is a level of about –1.4cm to 6.9cm, -1.4cm to 5.2cm, -3.6cm to 1.9cm, -0.8cm to 3.6cm, and –1.7cm to 4.1cm for the trials tested over an hour period. The maximum

local effect of double differenced tropospheric delays at the surveying area of the trials is a level of 6.9cm, 5.2cm, 3.6cm, 3.6cm, and 4.1cm respectively.

4. The evaluation of double differenced tropospheric estimations

- Although the evaluation of estimation results with the LCA involving the effect of the ionosphere-free multipath may be overestimated, the limited accuracy of current tropospheric model applied in GASP can be confirmed from the improper fitting of the estimation results. The maximum modelling errors over the observation period may respectively have a level of 15.2cm, 12.7cm, -4.81cm, 5.81cm, and 7.47cm for these trials tested, exceptionally in the cases of low elevation satellites.
- On average, the modelling errors can be a level of ±8.22cm, ±5.08cm, ±2.64cm, ±1.34cm, and ±3.31cm respectively for the trials of 12.8km to 33km. Therefore, the tropospheric modelling over long distances may have less dependence of baseline length but seemingly it has high correlation with the effects of local atmospheric environments at the working stations.

Above all, for the RTK survey over long baselines, the behaviour of ionosphere and troposphere have been investigated by the GFA and the LCA using the linear combination observations based on two known stations. The investigation results have found that the actual double differenced effects of both errors, achievable at the maximum level of 3.6cm and 6.9cm on average, may become the dominant problems of RTK positioning with the AFT. This technique requires the modelling of both errors for reducing the correspondent effects so as to enhance its performance over long distances. Currently, the Saastamoinen model has been used to handle the tropospheric problem in GASP, but unfortunately this model, being evaluated with comparisons of the true values obtained from the LCA, cannot efficiently reduce the tropospheric effects, especially as the satellite remains at low elevation angles. However, a precise ionospheric model expected for reducing the ionospheric effects is crucial for extending the use of single epoch AFT positioning to longer distances.

CHAPTER SIX

LOCAL IONOSPHERIC MODELLING AND ITS PERFORMANCE OVER LONG BASELINES

6.1 INTRODUCTION

From the initial investigations on the AFT performance in Chapter 3, a poor performance and a decreasing positioning accuracy of AFT, even after the correction of tropospheric effects with a self-contained tropospheric model, have been found for the experimental trials over baseline lengths more than 10km. In the subsequent investigations of Chapter 5, the results have indicated that the level of the effects after double differencing, can be 3.6-6.9cm for the troposphere, and 2.8-5.6cm on L_1 and 4.6-9.2cm on L_2 for the ionosphere, with a bias of multipathing effect about 1-2cm on average. For the RTK survey, the effects of ionospheric and troposphere apparently play a dominant role as the baseline extends to a distance more than 10km. In order to enhance the AFT performance for long distances, currently a self-contained tropospheric model (Saastamoinen model) is used to handle the tropospheric problem and an ionospheric model is crucial for the AFT to figure out the ionospheric problems currently. Up to date, many ionospheric models have been generated, but these models however as analyzed in Chapter 4, can hardly satisfy with current requirements of RTK survey, irrespective of on the modelling accuracy or on a consideration of RTK operation.

In this chapter, several novel ionospheric models, based on a modelling of a single known station (e.g. the base station) called the Local Ionospheric Model (LIM), will be introduced. The methodology and procedures of the modelling are introduced in Section 2. Pointing at the key factors of ionospheric modelling such as the mapping function and the remaining error effects, several different modes of LIM are generated for testing. These are introduced in Section 3. The performance of these models with the same experiment trials as shown in Chapter 3 are demonstrated and discussed in the following section. After this section, the verification of these models, carried out with comparisons of the apparent true ionosphere obtained from the LCA, is carried on in Section 5. Further work in RTK applications with the LIMs are described in Section 6. Finally, the conclusions of the modelling are drawn in the last section,

6.2 LOCAL IONOSPHERIC MODELLING (LIM)

Many ionospheric models have been developed to estimate the ionospheric delays based on the GPS data collected at the reference stations or networks. Depending on the sky coverage of available satellites from the reference stations or networks, usually it can be divided into global, regional, and local modelling. The global ionospheric modelling (GIM) is based on the networks covering the whole world, the regional model (RIM) is based on the continental or national networks covering large areas, and the local model (LIM) is based on the local networks or a single reference station covering small area. Considering the practical problems such as computation, update rate, and the broadcast of ionospheric corrections at the pierce points during the RTK operation, the computation of contemporary corrections can hardly be implemented in time if using current models based on multi-stations or networks (described in section 2.1). As a consequence, the best strategy of ionospheric modelling for the RTK survey can hence be the one based on a single reference station. In addition, the limitation of modelling accuracy and the necessity of preprocessing the ambiguities or hardware biases for current ionospheric models can be the greatest disadvantages which cannot satisfy with current requirements of high precision RTK GPS.

For precise ionospheric modelling, the initial analysis of ionospheric delay and modelling in Chapter 4 has indicated that a deterministic ionospheric modelling basically is based on the concept of ionospheric single layer, but has to consider many factors, which include

1. the cycle slip detection and repair for a time series of data,
2. the observable of modelling,
3. the spatial variation of ionosphere,
4. the time variation of ionosphere,
5. the verification of modelling.

With considerations of these problems as described above, considered and practical processing strategy of ionospheric modelling based on a single reference station (so-called the LIM), is carried out with the dual frequency GPS data collected at the base

station over a period of at least an hour. The preprocessing of cycle slip detection and repair has been implemented with the reliable software TurboEdit in Chapter 5. There is no effect of cycle slips on the modelling for each set of trial data and this can be ensured from the smooth ionospheric estimation results. For other factors, the processing strategies of the LIM will respectively be introduced in the following subsections.

6.2.1 THE OBSERVABLE OF MODELLING

Currently, two types of observables, the L_C observable and the L4 observable, have been used for an ionospheric modelling as described in Table 4.2. The analysis of the observations used for the current ionospheric modelling (see section 4.4.1.1 and section 4.7) has indicated that the L4 or L_C observable cannot solve the problems of the constant biases including the hardware biases and the ambiguities. The L4 observable after double differencing can handle the problem of hardware biases but the remaining problem of the ambiguities is necessary to be resolved and at least two reference stations are required. Without any preprocessing of the ambiguities, the L_C observable can handle the problem of the ambiguities however the preprocessing of the hardware biases can be a time consuming process although it is based on a single reference station only. To deal with the problems of the ambiguities and the hardware biases, the differential L4 observable (between two adjoining epochs) may be a good candidate for an ionospheric modelling because of the following advantages:

1. Since the parameters of range, clock, and troposphere have been cancelled after the process of ionospheric combination with dual frequency GPS observations, the L4 observable is free of the effect of these errors.
2. After the secondary differencing process of L4 observable between two epochs, the parameters of ambiguity and hardware biases are removed. This differential L4 observable, without any preprocessing of hardware calibration and ambiguity fixing, can totally eliminate the possible effect of the estimation errors during the preprocessing and save the assessing time of data.
3. This differential L4 observable can be used for the ionospheric modelling just using the data based on a single-reference station only. So, with considering the practical problems of RTK operation, the update and broadcast of temporary ionospheric variation in a local area may no longer be a problem.

This differential L4 observable over the period of observations can be expressed as

$$L4_{i,i+1} = L4_{i+1} - L4_i, \quad i = 1, n\text{-}1 \qquad (6.1)$$

where

L4 is the ionospheric combination observable,

n is the number of observing epochs.

Nevertheless, this observable has to be under the pre-assumptions that the hardware biases are constant and the data are "clean" (no cycle slips) for a period of at least an hour observing time. Consequently, the remaining errors in this observable only include the ionosphere and the phase multipath.

Usually, the effect of phase multipath is considered as an irrelevant effect and neglected for most of current ionospheric models. This has been investigated in Chapter 5 and the results have shown that the effect of multipath (in a form of ionospheric combination) can be a level of 1-2cm for the trials tested. For the users of L_C observable, the averaging process has been applied to reduce the effect of multipath so as to achieve a high precision ionospheric modelling (see Chapter 4). If the multipath really follows the Gausian distribution, then equation (6.1) after the processing of averaging process can be written as

$$L7 = (n\text{-}1) \times AVG(L4_{i,i+1}) \qquad (6.2.a)$$

$$AVG(L4_{i,i+1}) = \sum L4_{i+1} / (n\text{-}1) - \sum L4_i / (n\text{-}1), \quad i = 1, n\text{-}1 \qquad (6.2.b)$$

where

L7 is the observable used for the ionospheric modelling,

AVG is the operator of averaging process,

n is the number of observing epochs (relating to the observing interval and the period of observing time).

In order to increase the geometric strength and the sky coverage of satellites, the observing data of at least half an hour is necessary to be used for this ionospheric modelling. After the averaging process of the differential L4, this derived observable can be expressed with another form as follows:

$$L7 = I_n - I_1 \qquad (6.3)$$

Obviously, if neglecting the phase multipath, this derived observable, only consisting of the parameter of ionosphere delays at the first and last observing epochs, can be considered as an optimal observable for an ionospheric modelling where the remaining

problem is to resolve this observation equation of the ionosphere between the first and the last epochs. Therefore, to construct the correlation between the ionospheric delays at different observing epochs can be the key point to resolve this equation. This may concern the problems of dealing with the spatial and time variation of ionospheric delays for a period of observing time, which will be introduced in the following subsections.

6.2.2 DEALING WITH SPATIAL VARIATION OF IONOSPHERIC DELAYS

When GPS signals traverse in the dispersive region the ionospheric effects vary with space (location and viewing direction) and time. The spatial variation of ionospheric delays at a certain surveying epoch can be dealt with the concept of single ionospheric layer described in section 4.4.1.3. The ionospheric profile is constructed with the pierce points on the single ionospheric layer. At each pierce point on the ionospheric profile, the slant ionospheric delay from the satellite to the receiver can be divided into the mapping function (the horizontal scalar), and the vertical ionospheric delay (the vertical TEC) as expressed in equation (4.9). The equation (6.3) can hence be rewritten as

$$L7 = M_n V_n - M_1 V_1 \quad \text{.....(6.4)}$$

where

M_1, M_n are the mapping function of the pierce points at the first and last epochs,

V_1, V_n are the vertical ionospheric delay of the pierce points at the first and last epochs.

After converting (3D to 2D), the correlation between the vertical ionospheric delays at these IPPs on the (vertical) profile would be easier to construct on the basis of the corresponding location of each pierce point. Obviously, the equation (6.4) will be resolved if the correlation between the vertical ionospheric delays of V_1 and V_n can be found. This concerns the problem of time variation of ionosphere since the ionosphere is changing by time, which will however be introduced in section 6.2.3. In this section, introduced are more details about the pierce points, the mapping function and the vertical TEC and their computation.

6.2.2.1 PIERCE POINTS

The pierce point is defined as the intersection of the signal path from the satellite to the receiver at the base station or the rover station and the spherical shell (single ionospheric layer or ionospheric profile), as shown point p1 to p6 and s1 to s6 in Figure 4.1. Usually the height of the shell is defined to be the mean ionospheric height and a height of 350 km above the sea level is often used. The location of these pierce points on this profile is to describe the geometrical relationship of the vertical ionosphere (or TEC). Therefore, the location of pierce points on the ionospheric (density) profile can be obtained on the basis of satellite coordinates, station coordinates, and the height of the shell, as follows.

1. The satellite, the pierce point, and the station in Cartesian coordinate system have a relationship as expressed in the following equations (Spiegel, 1959):

   $y - [(y_s - y_a) / (x_s - x_a)] x - y_a - [(y_s - y_a) / (x_s - x_a)] x_a = 0$ .....(6.5.a)

   $z - [(z_s - z_a) / (x_s - x_a)] x - z_a - [(z_s - z_a) / (x_s - x_a)] x_a = 0$ .....(6.5.b)

   where

   x_a, y_a, z_a are the coordinates of station,

   x_s, y_s, z_s are the coordinates of satellite,

   x, y, z are the coordinates of pierce point.

2. The relationship between the Cartesian coordinates (x, y, z) and the geodetic coordinates (φ, λ, h) is

   $x = (N + h) \cos\varphi \cos\lambda$ .....(6.6.a)

   $y = (N + h) \cos\varphi \sin\lambda$ .....(6.6.b)

   $z = [N (1-e^2) + h] \cos\varphi \cos\lambda$ .....(6.6.c)

   where $N = a / (1-e^2 \sin^2\varphi)^{1/2}$, $e^2 = 2f - f^2$, a and f is the length of the semi-major and the flattening respectively (Leick, 1995).

3. Based on equations (6.5) and (6.6), the simultaneous equations with two parameters of the longitude and the latitude can be derived as follows.

   $f_1(\varphi,\lambda) = 0$ .....(6.7.a)

   $f_2(\varphi,\lambda) = 0$ .....(6.7.b)

   After being linearized, the equations can be resolved with an iteration method (see the textbook of numeric analysis), and the unique solution of pierce points can be obtained. The transformation between the geodetic and the Cartesian coordinate systems can be implemented by Equation (6.6).

6.2.2.2 THE MAPPING FUNCTION AND THE VERTICAL TOTAL ELECTRON CONTENT (TEC)

Based on the concept of single ionospheric layer, the slant ionospheric delay at each pierce point on the profile can be expressed as a function of the mapping function and the vertical ionospheric delay (or the vertical TEC). For all available satellites, the observation equation (6.4) applied in this local ionospheric modelling can be rewritten as the following expression of the mapping function and the vertical ionospheric delay over a period of time.

$$L7_k = M_{k,n(k)} V_{k,n(k)} - M_{k,1} V_{k(i),1} \quad i = 1,n(k) , k = 1, m \qquad (6.8)$$

where

$L7_k$ is the derived observation based on the broadcast radio signals from satellite k,

$M_{k,1}$, $M_{k,n(k)}$ are the mapping function of the pierce points at the first epoch and the last epoch for satellite k,

$V_{k,1}$, $V_{k,n(k)}$ are the vertical ionospheric delays at the pierce points of the first epoch and the last epoch for satellite k,

n(k) is the number of available epochs for satellite k,

m is the number of available satellites.

Regarding the mapping function of each pierce point, currently many functions have been derived based on the spherical shell for the ionospheric modelling (see Chapter 4). This parameter is so important to define the relationship between the slant and the vertical, and the modified mapping function expressed as the equation (6.9) is often used for the modelling of ionosphere such as the JPL's Global Ionospheric Model. However, two different mapping functions are tested in this research. One, called mapping function I, is a modified mapping function as follows.

$$M(\theta) = \{1-[cos(\theta)/(1+h/R)]^2\}^{-1/2} \qquad (6.9)$$

where

θ is the elevation angle,

R is the radius of the earth,

h is the height of spherical shell (350km).

Another, expressed as the equation (6.10), is based on the concept of density of ionosphere suggested by the JPL (Wilson et. Al., 1993). Based on the concept of single

ionospheric layer, the actual length of the slant ionospheric delay is the distance from the pierce point to the station and the length of the vertical delay is the height of spherical shell. In a local area, the density of the slant ionospheric delay can be assumed to be the same as the density of the vertical delay as given by the following expression.

$$I / d = V / h \quad \text{.....(6.10.a)}$$

$$I = (d / h)\, V \quad \text{.....(6.10.b)}$$

$$= M\, V \quad \text{.....(6.10.c)}$$

Then, the mapping function Π can be obtained as follows.

$$M(d,h) = d(x_p, y_p, z_p, x_a, y_a, z_a) / h \quad \text{.....(6.11.a)}$$

$$d(x_p, y_p, z_p, x_a, y_a, z_a) = [(x_p-x_a)^2 + (y_p-y_a)^2 + (z_p-z_a)^2]^{-1/2} \quad \text{.....(6.11.b)}$$

where

d is the range between the pierce point $(x_p, y_p, z_p)$and the station (x_a, y_a, z_a),

h is the height of spherical shell,

M is the mapping function of the pierce point.

6.2.3 DEALING WITH TIME VARIATION OF IONOSPHERE

The construction of the vertical ionospheric profile is based on the vertical ionospheric delays (or called the vertical TEC) of the pierce points on the single ionospheric layer. Supposing there were lots of satellites available in the sky above the operating station or many receivers were set up around the surveying area, then the (vertical) ionospheric profile could be constructed instantly from a single epoch of received data. At least, currently it is impossible (maybe possible in the future). Usually a period time of data collection is necessary for the construction of vertical ionospheric profile with these data. Hence, this raises another problem of ionospheric modelling due to the ionosphere changing with time which means at the same location (pierce point) on the profile, the vertical ionosphere at the first epoch can be different from the one at the next epoch.

Currently the ways to deal with the time variation of ionosphere include the following.

1. The ionospheric behaviour is assumed to be relatively constant over a few hours.
2. It is assumed to be time independent in a sun-earth reference system (Lanyi, 1988).

In fact, the ionosphere is changing even in the sun-earth reference system, thus a time span of the fit should be minimised in order to optimise the accuracy and temporal resolution of the vertical TEC (Wilson et. Al., 1993). For an accurate ionospheric

modelling, the time variation of ionosphere cannot be ignored, especially when the location of surveying area is under an anomalous region of ionosphere such as the equatorial and polar regions (see section 4.3.2). In this research, a weighting function and a transformation have been used to deal with the problem of time variation of the ionosphere. This is introduced in the next two subsections.

6.2.3.1 THE WEIGHTING FUNCTION

Supposing that the behaviour of the ionosphere during a very short time of the observing interval such as 30 seconds is frozen, then the correlation between the vertical ionospheric delays of pierce points at two adjacent epochs can be established by a weighting function on the basis of the pierce point's location on the ionospheric profile. For a time series of the vertical ionospheric delays can be expressed as

$V_{i+1} = W_{i+1,i} V_i$, i = 1 , n-1.....(6.12)

where

V_i is the vertical ionospheric delay at epoch i,

$W_{i+1,i}$ is the weighting function which is a coefficient matrix of the correlation between the vertical ionospheric delays of pierce points on the ionospheric profile at epoch i and the next epoch i+1.

The matrix of weighting function for each pair of epochs can be expressed as

$$W_{k2,k1} = \begin{bmatrix} \omega_{1,1} & \cdots & \omega_{1,n1-1} & \omega_{1,n1} \\ \vdots & \ddots & \vdots & \vdots \\ \omega_{n2-1,1} & \cdots & \omega_{n2-1,n1-1} & \omega_{n2-1,n1} \\ \omega_{n2,1} & \cdots & \omega_{n2,n1-1} & \omega_{n2,n1} \end{bmatrix}$$

The weight function of each pierce point at the next epoch is given by the ratio of reciprocal of the distance between this point and the corresponding points at the first epoch and the summation of reciprocal of the distances between this point and all pierce points at the first epoch. Put it in a formal way,

$\omega_{k2,k1} = (1 / D_{k2,k1}) / \Sigma (1 / D_{k2,k1})$, $k2 = 1, m_2, k1 = 1, m_1$ .....(6.13)

where

m_1 is the number of pierce points (satellites) at the first epoch,

m_2 is the number of pierce points (satellites) at the next epoch,

$D_{k2,k1}$ is the distance between two pierce points.

By this way, it can be easily seen that the closer is a pierce point at the next epoch relative to another one at first epoch, the lager weight is placed upon the previous point.

6.2.3.2 TRANSFORMATION OF VERTICAL TEC

Based on equation (6.12), the transformation between the vertical ionospheric delays at the pierce points of two adjacent epochs for a period of time can be obtained as follows.

$V_2 = W_{2,1} V_1$ .....(6.14.1)

$V_3 = W_{3,2} V_2$ .....(6.14.2)

...

$V_n = W_{n,n-1} V_{n-1}$ .....(6.14.n-1)

Hence, the vertical ionospheric delays at epoch n can be transformed to the vertical ionospheric delays at the first epoch as the following expression.

$V_n = (W_{n,n-1} W_{n-1,n-2} \cdots W_{2,1}) V_1$ .....(6.15)

$$= \left(\prod_{i=1}^{n-1} W_{i+1,i} \right) \cdot V_1$$

For all available satellites in the period of observing time, equation (6.15) can be expressed as

$V_{n(k)} = (W_{n(k),n-1(k)} W_{n-1(k),n-2(k)} \cdots W_{2(k),1(k)}) V_1$ ...k = 1 , m.....(6.16)

$$= \left(\prod_{i=1}^{n-1(k)} W_{i+1(k),i(k)} \right) \cdot V_1$$

where n(k) is the number of available epochs for satellite k.

6.2.4 ESTIMATION OF THE (VERTICAL) IONOSPHERIC PROFILE AND IONOSPHERIC CORRECTIONS

With the weight function and the transformation, the observation equations can be rewritten as

$L7_k = [M_{k,,n} (W_{n,n-1} W_{n-1,n-2} \cdots W_{2,1}) - M_{k,1}] V_{k,1}$ k = 1, m.....(6.17)

In a form of matrix, this observation equation can be written as

$L7_m = A_{m\times m}\, V_{m,1}$ .....(6.18)

where m is the number of available satellites at the first epoch (with a subscript of 1). Then the vertical ionospheric delays of each pierce point at the first epoch for each satellite can be obtained after resolving this observation equation as follows.

$V_{m,1} = (A_{m\times m})^{-1}\, L7_m$ .....(6.19)

Finally, the vertical ionospheric delays for the other epochs can sequentially be computed with the weighting function based on the vertical ionospheric delay at the first epoch.

$V_2 = W_{2,1}\, V_1$ .....(6.20.1)

$V_3 = W_{3,2}\, V_2$ .....(6.20.2)

... ...

$V_n = W_{n,\,n-1}\, V_{n-1}$ .....(6.20.n-1)

Based on the calculated vertical ionospheric delays with the corresponding mapping function, the slant ionospheric delays can therefore be obtained as follows.

$I_{k,i} = M_{k,i}\, V_{k,i}$ $\quad k = 1, m\,,\, i = 1, n(k)$.....(6.21)

This calculated slant ionospheric delays are respectively scaled with the corresponding wavelength of L1and L2 to obtain the L_1 and L_2 frequency ionospheric delays (corrections) expressed as

$I_{L1} = \Upsilon_1\, I$ .....(6.22.a)

$I_{L2} = \Upsilon_2\, I$ .....(6.22.b)

6.2.5 PROCEDURES AND ERROR ANALYSIS

As described in the previous section, the local ionospheric modelling (LIM) has been carefully constructed with consideration of many factors such as the drawbacks of current ionospheric models, the problem of cycle slips, the formation of observable, and the spatial and time variation of ionosphere. An optimal ionospheric model can be expected to satisfy current requirements of high precision RTK GPS with this modelling. The procedure of LIM is however summarized as the following steps.

1. Preprocessing of cycle slip detection and repair for a time series of GPS data (TurboEdit),
2. Formation of observable L7 (equation 6.1-6.3),
3. Computation of the location of pierce point (equation 6.5-6.7) and the mapping function (equation 6.9-6.11),

4. Generation of the weighting function (equation 6.12-6.13),
5. Transformation of the vertical ionospheric delays between epochs (equation 6.16),
6. Formation of the coefficient matrix of observation equations (equation 6.17),
7. Estimation of the unknown parameters (equation 6.18-6.19),
8. Generation of the vertical ionospheric profile (equation 6.20),
9. Computation of the slant ionospheric delays (equation 6.21),
10. Computation of the ionospheric corrections on L_1 and L_2 frequency (equation 22).

As can be seen, most effects of observation errors on this modelling have been considered and resolved during the construction of LIM. The unresolved problems such as the effect of (ionospheric combination) multipath on phase can be the main error source of this modelling. In recent years, the effect of code multipath has been widely investigated, but the investigation of phase multipath with using the method of signals to noise ratio has begun. From the initial investigation of ionospheric behaviour in Chapter 5, the multipathing effect after double differencing may have a level of ±1-2 cm in a form of ionospheric combination for these trials tested. The accuracy of this modelling can therefore be limited due to this effect. Besides, the suitability of two mapping functions still needs to be evaluated. In order to obtain a more accurate ionospheric model, several LIMs, based on two mapping functions with consideration of the multipathing effects, are tested in the following section.

6.3 DIFFERENT MODES OF LOCAL IONOSPHERIC MODEL (LIMs)

In order to reduce the multipathing effect on the LIM, two methods using the ionospheric combination of observations on code and phase are used to estimate the phase multipath in this research.

$$M1_{phase} = P4_n/100.0 - P4_1/100.0 \quad \text{.....(6.23)}$$

$$M2_{phase} = (L4_n - \cdot_{j=n-9,\,n} L4_j/10) - (L4_1 - \cdot_{i=1,10} L4_i/10) \quad \text{.....(6.24)}$$

The concept of the first method to obtain the corrections of phase multipath is that equation (6.23) is dominated only by the code multipath where the hardware biases in the observable of P4 are eliminated after the differencing of ionospheric combination observations between two epochs. Supposing that the ratio of the multipath between code and phase (theoretically, the maximum of multipath is about 5m for the code and

5cm for the phase) is 100, the phase multipath can be obtained from equation (6.23). The second method is based on the residual of ionospheric combination observations on phase where the constant biases including the ambiguity and the hardware biases are cancelled after subtracting L4 observations with the correspondent average on itself. The residual of observable, $M2_{phase}$, for each epoch in equation (6.24), dominated by the phase multipath, can hence be used to obtain the corrections of phase multipath.

In order to reduce the ionospheric effect for the high precision RTK GPS applications, several LIMs, based on two mapping functions with consideration of the multipathing effects, are supposed to be tested in the following sections.

1. LIM1: based on the mapping function of JPL with ignorance of the multipathing effect.
2. LIM2: based on the new mapping function with ignorance of the multipathing effect.
3. LIM3: based on the mapping function of JPL with consideration of the multipathing effect by using the first method.
4. LIM4: based on the new mapping function with consideration of the multipathing effect by using the first method.
5. LIM5: based on the mapping function of JPL with consideration of the multipathing effect by using the second method.
6. LIM6: based on the new mapping function with consideration of the multipathing effect by using the second method.

6.4 PERFORMANCE OF LIMs

After the computation of LIMs with the dual frequency GPS data collected at the base stations, PSMS, CG54, and INED for the trials tested, the ionospheric delays of each trial above the survey area at these known stations can be obtained and respectively shown in Figure 6.1 to 6.3. In each figure, the curves for single path ionospheric delays are supposed to demonstrate the performance of LIMs. The difference of the averaged ionospheric delays between LIMs is summarized as shown the item LIMs of Table 6.1.

From the results of Figures 6.1-3 and Table 6.1, it can be concluded:

1. Basically, two main types of modelling, one based on the mapping function I and the other based on the mapping function II, can be seen from the discrepancy of results in these figures (the black, darker one, represents the former and the red, lighter one, represents the latter). In each type of modelling, the elimination of the multipathing effect with two methods can result to, in general, an estimation of about a ten centimeter difference with comparison of the results based on the modelling with ignorance of the multipathing effect. This difference, in theory, is dependent of the size of multipathing effect (relating to the survey environments), the geometry of satellite constellation and the operation station, and by all means the efficiency of the method to eliminate the multipathing effect is crucial. However, results indicate that the mapping function, concerning of the determination of coefficient matrix of observation equations, may play a dominant role of ionospheric modelling, and the multipathing effect cannot be ignored for an accurate ionospheric modelling.
2. The single path ionospheric estimations may have a size of about 4m to 7m over the period of an hour observation as the satellite passes the position at the elevation angle from 26.8° to 52.3°, for example, in a case of SV: 27 for the trial of 12.8km baselines. At the same observing epoch, for example, the first epoch of the same trial above, the highest satellite only has a delay of about 2.5m where the lowest satellite has a delay of about 7m. These have indicated that the single path ionospheric delay is highly dependent of the elevation angle of observing satellite, and the hourly ionospheric variation cannot be ignored for the RTK survey.
3. For the two survey areas at the same observing time (e.g. the first epoch), in general, the trail of PSMS-SEMA has a range of ionospheric delays, about 1.9m to 8.6m where the trail of INED-SHEN has a range about 1.6m to 3.9m. The ionospheric delays have shown quite a different effect at two surveying areas, the former at the area of 35°-43° latitudes and the latter at the area of 46°-54° latitudes. This has indicated that the area near anomaly area of ionosphere (±30° latitudes) may have a higher effect of ionosphere. However, the ionospheric effect on the RTK survey is also independent of the surveying area.
4. For the trial of INED-SHEN, the satellites even at the same low elevation angle of about 20°, such as SV: 18 and SV: 25, can respectively have the delays of about 5.2m and 3.1m. This has indicated that the ionospheric delays on the satellites at a

different azimuth may have great difference effects. Hence, the ionospheric effect on each satellite available is dependent of the azimuth of satellite.

5. From the smooth curves in these figures, 100% "clean" observations used for the modelling can be confirmed. In other words, there is no effect of cycle slips on LIMs for the trials tested.
6. For the LIMs generated, the similarity of LIM2, LIM4, and LIM5 is generally shown in these figures.

Above all, the single path ionospheric effects, depending on the elevation angle and azimuth of the satellite, and the surveying area, may have a level of up to near 8.6 meters (13.3m on L_1 and 21.9m on L_2) on average over the observation period for these typical trials. For the modelling of ionosphere with the LIMs, the mapping function, a scalar to determine the slant ionosphere, may play a dominant role, and the multipathing effects may decrease the modelling accuracy. Apparently, the estimation results from the LIMs basically can be divided into two groups, one is based on the mapping function I and another is based on the mapping function II. For each group, the ionospheric estimations between the modes of LIM with/without the elimination of multipathing effects may have a slight difference of couples of tens centimeters.

- In the case of trials, PSMS-SEMA, PSMS-PLAT, and PSMS-SOHO

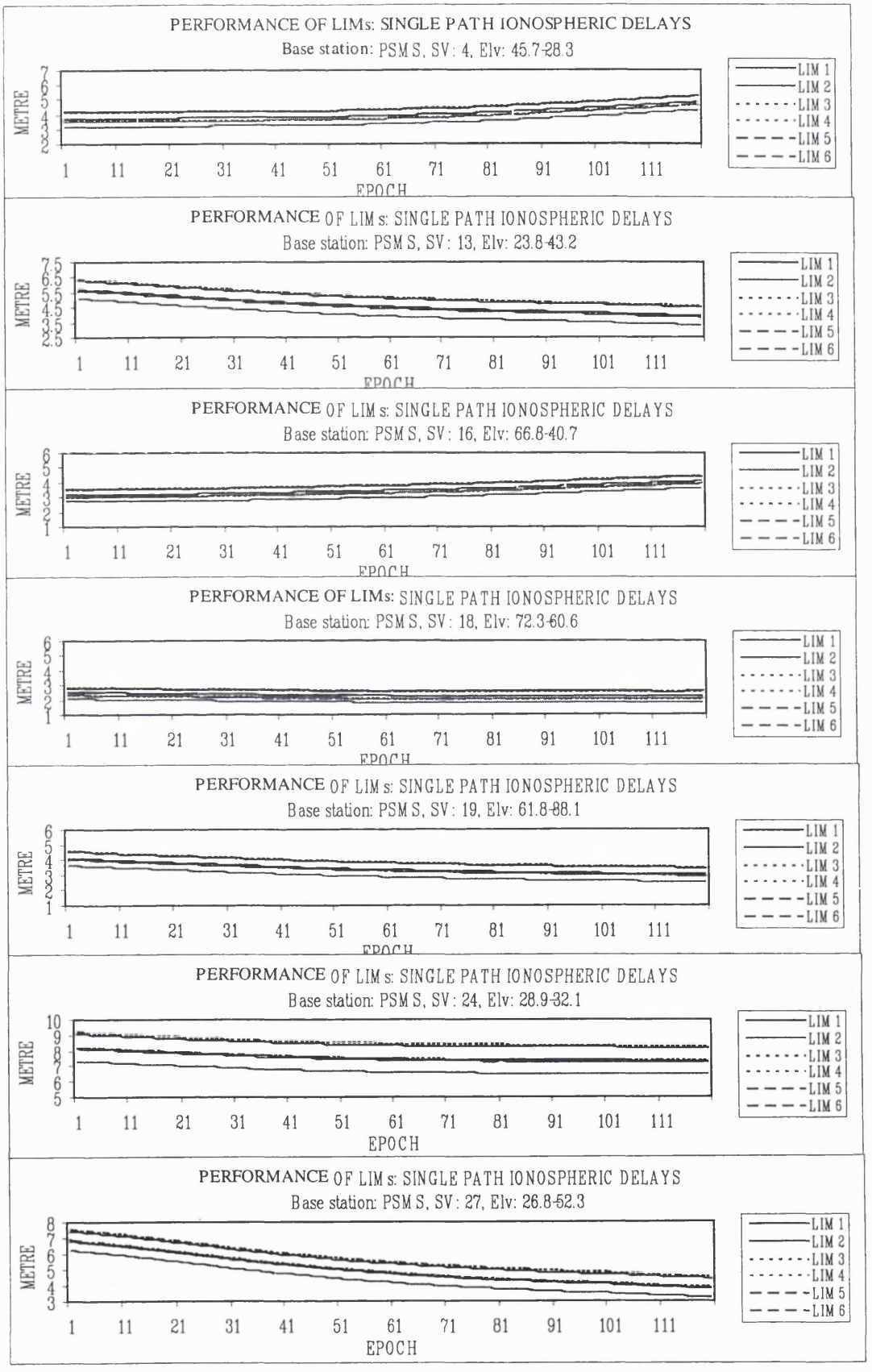

Figure 6.1 The performance of single path ionospheric delays based on LIMs in the case of trials, PSMS-SEMA, PSMS-PLAT, and PSMS-SOHO

- In the case of trial, CG54-KRPI

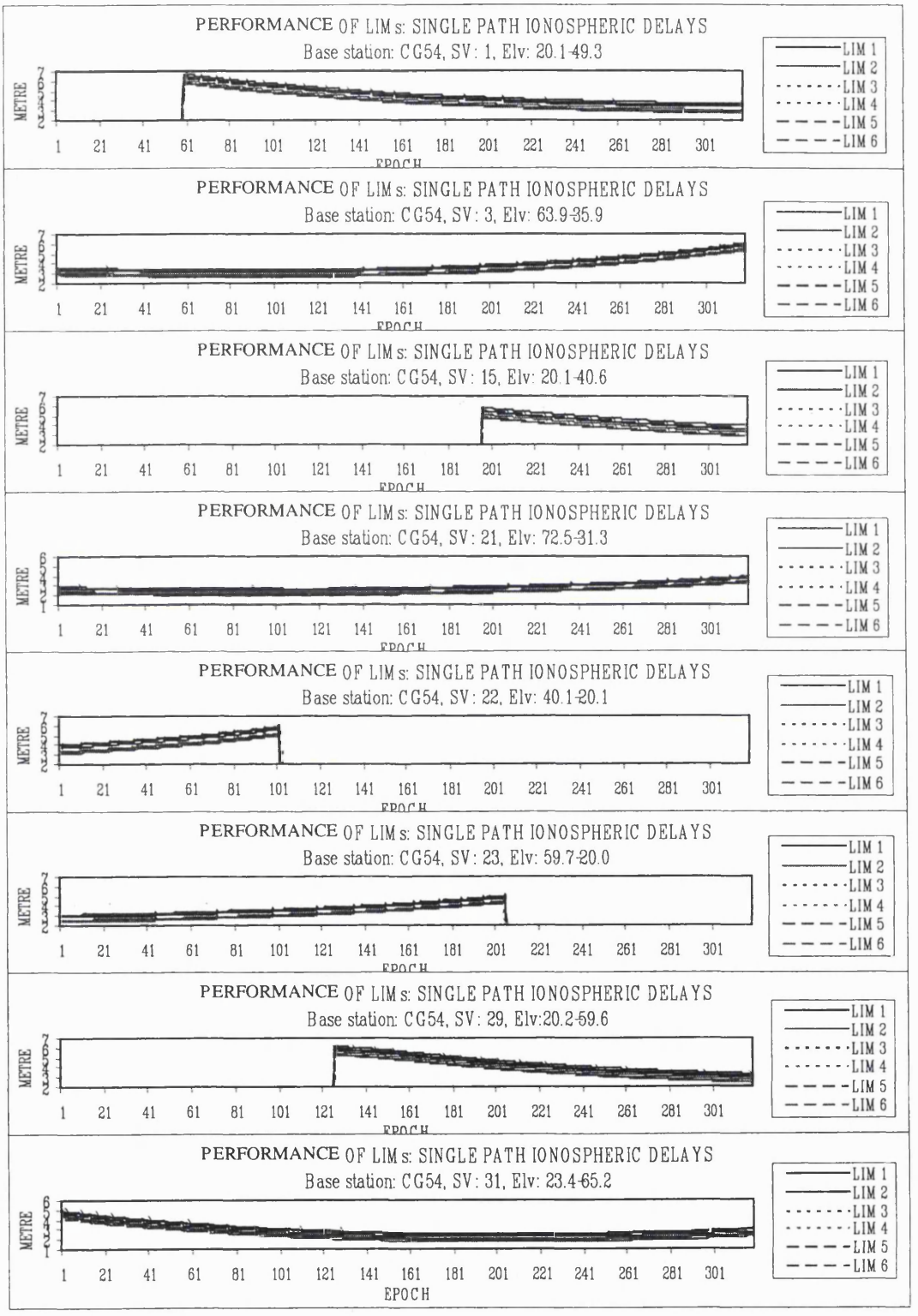

Figure 6.2 The performance of single path ionospheric delays based on LIMs in the case of trial, CG54-KRPI

- In the case of trial, INED-SHEN

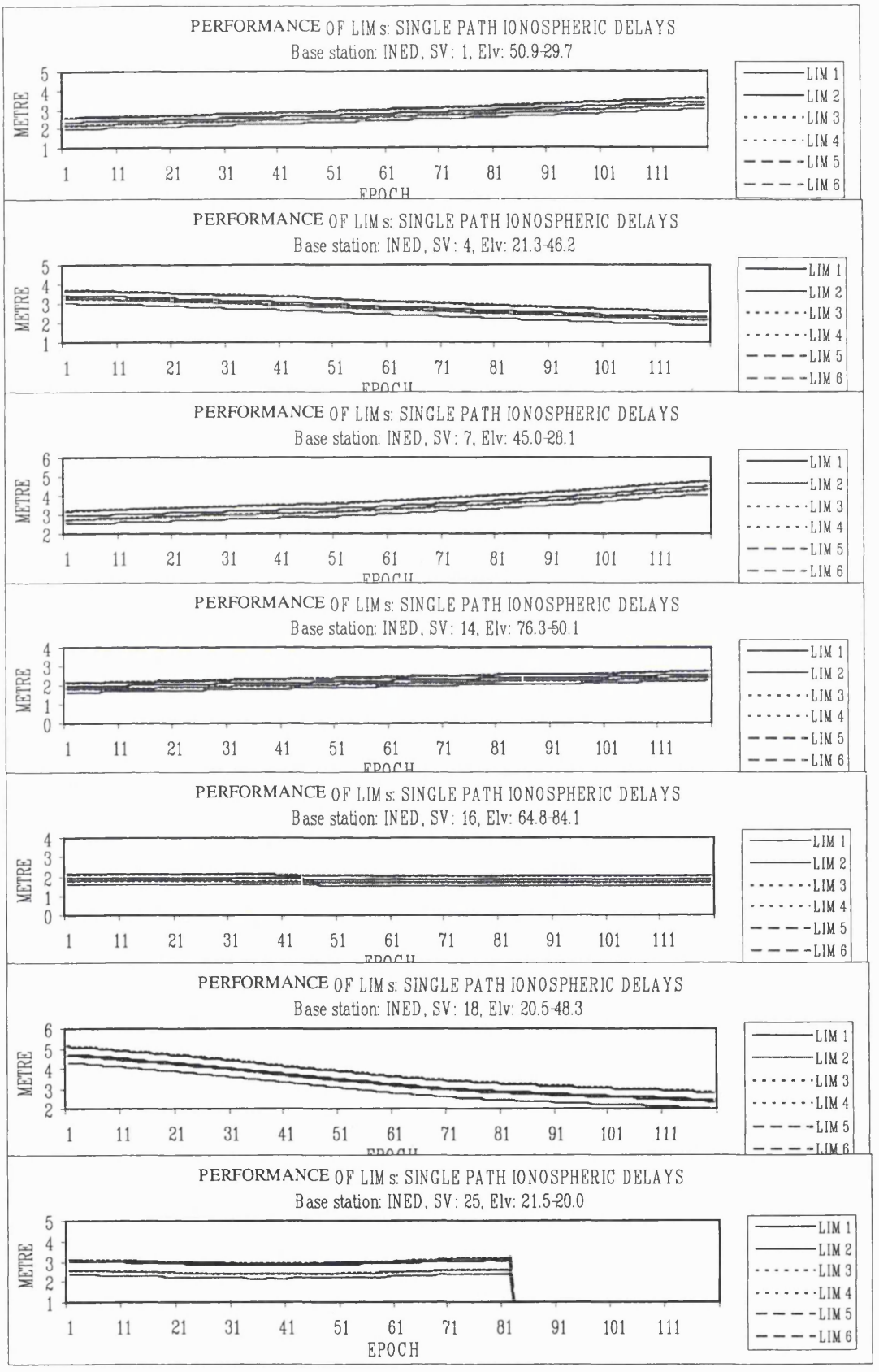

Figure 6.3 The performance of single path ionospheric delays based on LIMs in the case of trial, INED-SHEN

6.5 EVALUATION OF LIMs

As a matter of fact, the evaluation of LIMs seems difficult to be accomplished without knowledge of the true ionospheric delays. Usually, the ways to verify the estimation results of ionospheric modelling are carried out by

1. Analyzing the positioning results of RTK technique with/without the ionospheric corrections estimated by the ionospheric model generated.
2. Comparing with the results of other ionospheric models.

Since the algorithm of RTK techniques involves some uncertain factors, such as accuracy of the tropospheric and other related error modeling, the former way would hardly get the work done. In particular for the case of tropospheric estimation as discussed in Chapter5, the current approach verified by this criterion may even lead to spurious results. The latter way is to place one model under comparison against a benchmark model, while, provided that the choice of baseline itself is arguable, the results of comparison will be subject to skeptics as well. Therefore, to get over the weakness inherent in these two methods, an alternative verification procedure is called for.

In this thesis, two steps for verification are proposed to evaluate the performance of the LIMs. The first step of verification is just to check the estimation trend of single path ionospheric delays estimated by the LIMs with comparisons of the apparent true values obtained from the GFA. This will be carried out in this section. At the second step, the "true" double differenced ionospheric delays obtained from the LCA can be used for the verification of double differenced ionospheric delays estimated by the LIMs and the subsequent ionospheric prediction. After two steps of verification to ensure the modelling accuracy and correctness of the LIMs, the computation of AFT positioning with these ionospheric corrections is then carried on to know the efficiency of the LIMs on the AFT positioning. These will be discussed in the next chapter.

As introduced in the previous chapter, the geometry free approach (GFA) has been used to investigate the behaviour of single path ionospheric delays for these trials tested. With this approach, the apparent true value of single path ionospheric delay calculated only consists of the true ionospheric delay, the hardware bias (which is a constant over a short period of time such as few hours), and the small phase multipathing effects. With

comparisons of this result, the estimations with the LIMs must be incorrect if both estimation curves over the observation period are not apparently parallel. By this way, it can accurately evaluate the estimation trend of ionospheric modelling.

As shown in Figure 6.4 to 6.6, the ionospheric estimations with the LIMs are denoted as several types of black and red lines for each mode of LIM where the apparent true ionospheric results obtained from GFA are denoted as the blue line. The averaging results of GFA, LIMs, and their difference over the whole observation period are summarized in Table 6.1. The following conclusions can be drawn.

1. In these figures of 6.4 to 6.6, these estimation curves of ionospheric delays generated by the LIMs for the trials tested apparently follow the trend of the true one obtained from the GFA. Basically, the correctness of estimating the single path ionospheric delays with the LIMs has first been evaluated at least on the estimation trend.
2. From the results of item Diff in Table 6.1, the differences between two results from the LIMs and the GFA have indicated that the constant hardware biases may have half of the quantity, in general about 1-3 meters depending on each available satellite and the operating receiver. From here, the hardware bias is hence isolated where isolation of the satellite hardware bias and the receiver hardware bias included cannot be accomplished.

As of a consequence, the definiteness of LIM for these modes generated, at least from the evaluation of modelling trend, can first be ensured.

- In the case of trials, PSMS-SEMA, PSMS-PLAT, and PSMS-SOHO

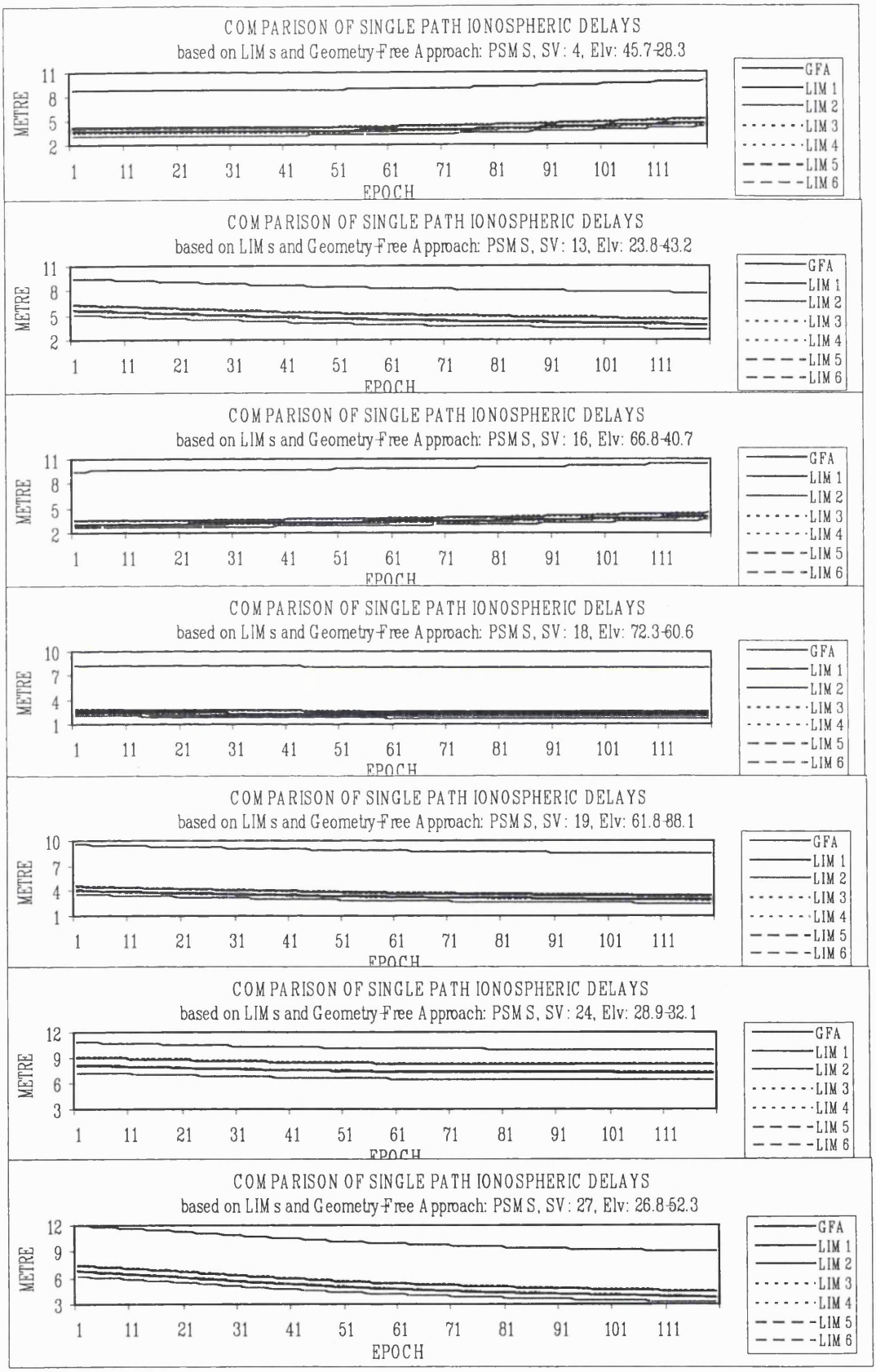

Figure 6.4 Comparison of the single path ionospheric delays based on LIMs and GFA in the case of trials, PSMS-SEMA, PSMS-PLAT, and PSMS-SOHO

- In the case of trial, CG54-KRPI

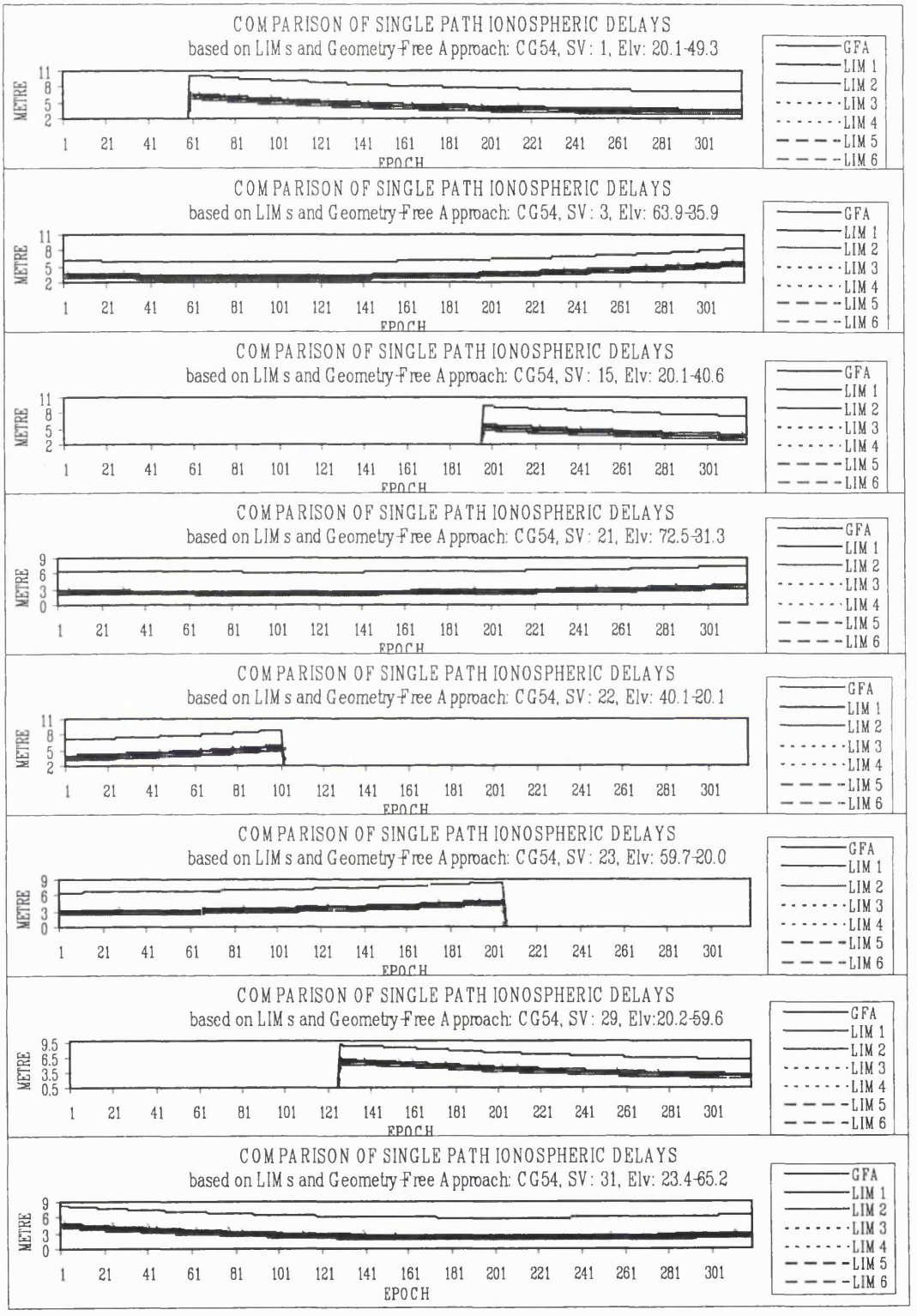

Figure 6.5 Comparison of the single path ionospheric delays based on LIMs and GFA in the case of trial, CG54-KRPI

- In the case of trial, INED-SHEN

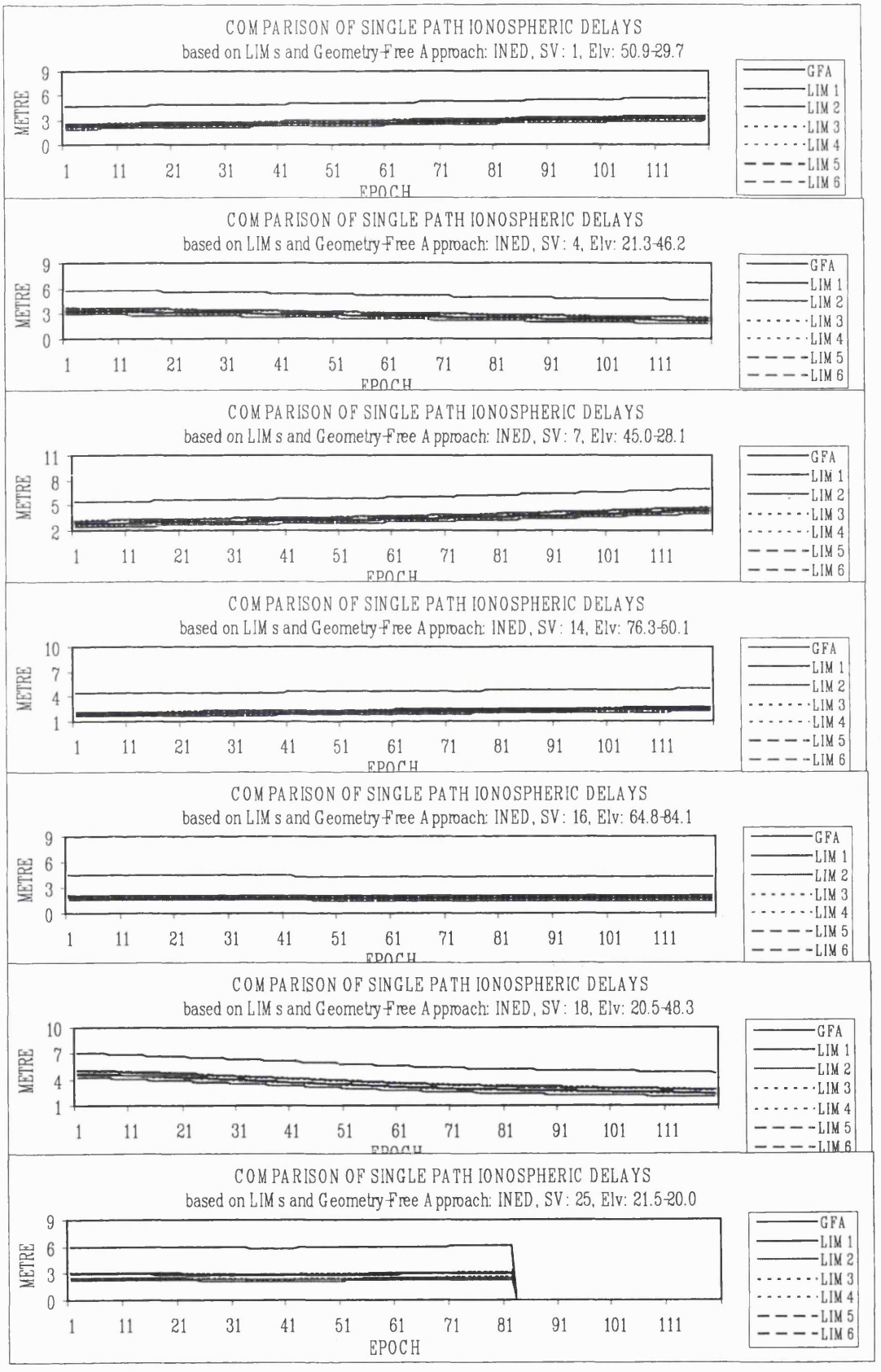

Figure 6.6 Comparison of the single path ionospheric delays based on LIMs and GFA in the case of trial, INED-SHEN

Table 6.1 The comparison of the ionospheric delays obtained from the Geometry Free Approach (GFA) and LIMs

Unit: meter

Ion	Baseline(12.8)			Baseline(15)			Baseline(21)			Baseline(25)			Baseline(33)		
SVs	GFA	LIMs	Diff	GFA	LIMs	Diff	GFA	LIMs	Diff	GFA	LIMs	Diff	GFA	LIMs	Diff
1	9.102	4.434	4.667	8.122	4.863	3.439	5.164	3.020	2.144	9.102	4.434	4.667	9.102	4.434	4.667
		3.824	5.278		4.049	4.073		2.634	2.530		3.824	5.278		3.824	5.278
		4.517	4.585		4.587	3.536		3.057	2.108		4.517	4.585		4.517	4.585
		3.894	5.208		3.960	4.162		3.665	2.499		3.894	5.208		3.894	5.208
		4.085	5.017		4.318	3.704		2.841	2.323		4.085	5.017		4.085	5.017
		3.525	5.576		3.810	4.312		2.475	2.689		3.525	5.576		3.525	5.576
2	8.424	5.210	3.214	6.445	3.937	2.509	5.206	3.125	2.081	8.424	5.210	3.214	8.424	5.210	3.214
		3.534	3.890		3.411	3.034		2.704	2.502		3.534	3.890		3.534	3.890
		5.344	3.080		3.918	3.527		3.178	2.208		5.344	3.080		5.344	3.080
		4.653	3.771		3.400	3.045		2.751	2.455		4.653	3.771		4.653	3.771
		4.695	3.729		3.796	2.649		2.885	2.321		4.695	3.729		4.695	3.729
		4.075	4.349		3.291	3.155		2.482	2.724		4.075	4.349		4.075	4.349
3	9.865	3.857	6.009	8.310	4.780	3.530	6.054	3.828	2.226	9.865	3.857	6.009	9.865	3.857	6.009
		3.338	6.527		4.097	4.213		3.380	2.673		3.338	6.527		3.338	6.527
		3.931	5.934		4.544	3.766		3.869	2.184		3.931	5.934		3.931	5.934
		3.402	6.463		3.876	4.434		3.415	2.638		3.402	6.463		3.402	6.463
		3.565	6.300		4.456	3.854		3.601	2.453		3.565	6.300		3.565	6.300
		3.090	6.776		3.804	4.506		3.176	2.878		3.090	6.776		3.090	6.776
4	8.111	2.633	5.478	6.548	2.934	3.614	4.639	2.433	2.206	8.111	2.633	5.478	8.111	2.633	5.478
		2.131	5.980		2.437	4.111		2.098	2.541		2.131	5.980		2.131	5.980
		2.691	5.420		2.923	3.625		2.464	2.175		2.691	5.420		2.691	5.420
		2.178	5.933		2.432	4.116		2.125	2.514		2.178	5.933		2.178	5.933
		2.390	5.721		2.818	3.730		2.284	2.355		2.390	5.721		2.390	5.721
		1.929	6.182		2.341	4.207		1.969	2.670		1.929	6.182		1.929	6.182
5	8.853	3.851	5.001	7.803	4.818	2.985	4.393	2.061	2.332	8.853	3.851	5.001	8.853	3.851	5.001
		3.329	5.524		4.135	3.669		1.724	2.669		3.329	5.524		3.329	5.524
		3.951	4.902		4.829	2.974		2.094	2.299		3.951	4.902		3.951	4.902
		3.418	5.435		4.151	3.652		1.752	2.641		3.418	5.435		3.418	5.435
		3.469	5.384		4.599	3.205		1.913	2.480		3.469	5.384		3.469	5.384
		2.990	5.683		3.950	3.853		1.592	2.801		2.990	5.683		2.990	5.683
6	10.22	8.436	1.788	7.233	3.767	3.466	5.736	3.767	1.970	10.22	8.436	1.788	10.22	8.436	1.788
		7.495	2.730		3.227	4.006		3.314	2.422		7.495	2.730		7.495	2.730
		8.623	1.602		3.764	3.469		3.849	1.888		8.623	1.602		8.623	1.602
		7.662	2.562		3.228	4.005		3.389	2.347		7.662	2.562		7.662	2.562
		7.625	2.600		3.635	3.598		3.437	2.299		7.625	2.600		7.625	2.600
		6.765	3.459		3.118	4.115		3.005	2.731		6.765	3.459		6.765	3.459
7	10.15	5.595	4.554	7.388	4.477	2.911	5.937	3.000	2.937	10.15	5.595	4.554	10.15	5.595	4.554
		4.962	5.187		3.912	3.476		2.472	3.466		4.962	5.187		4.962	5.187
		5.757	4.392		4.332	3.056		3.055	2.882		5.757	4.392		5.757	4.392
		5.111	5.039		3.775	3.613		2.517	3.420		5.111	5.039		5.111	5.039
		5.044	5.106		4.206	3.182		2.961	2.976		5.044	5.106		5.044	5.106
		4.462	5.688		3.665	3.723		2.307	3.630		4.462	5.688		4.462	5.688
8				6.444	3.037	3.407									
					2.520	3.925									
					3.078	3.366									
					2.564	3.880									
					2.843	3.602									
					2.346	4.098									

Baselines:	Base-Rover stations—PSMS-SEMA(12.8km), CG54-KRPI(15km), INED-SHEN(21km), PSMS-PLAT(25km), PSMS-SOHO(33km).
Ion:	The single path ionospheric delays (in unit of m), based on the Geometry Free Approach and LIMs.
SVs:	the number of satellite, PSMS, SEMA, PLAT and SOHO: 1:4, 2:13, 3:16, 4:18, 5:19, 6:24, and 7:27. CG54, KRPI: 1:1, 2:3, 3:15, 4:21, 5:22, 6:23, 7:29, and 8:31. INED, SHEN: 1:1, 2:4, 3:7, 4:14, 5:16, 6:18, and 7:25.
GFA:	The single path ionospheric errors obtained from the Linear Combination Approach
LIMs:	The single path ionospheric errors estimated by the Local Ionospheric Models.
Diff:	The difference of single path ionospheric errors between the LCA and the LIMs.

6.6 THE RTK APPLICATIONS OF LIM

In this research, the generation of LIM is mainly to obtain the ionospheric corrections for reducing the ionospheric effects and thus increase the RTK positioning accuracy for long distance applications. To achieve this goal, the ionospheric delay is first modelled based on the concept of ionospheric profile with the dual frequency GPS phase data at the known (base) station over at least an hour period. After the generation of LIM, the vertical ionospheric profile above the survey area can hence be constructed, and the L1 and L2 ionospheric corrections for the base station can also be obtained from the estimations of single path ionospheric delays. Based on this vertical ionospheric profile constructed, the prediction of ionospheric delays for the rover station surrounding the base station can thus be carried out. In practice, once the ionospheric profile is constructed, the ionospheric corrections for the base and the rover at the following epoch can be obtained based on Equation (6.1) as long as the corresponding satellite is still on lock. As of a consequence, the single epoch AFT with these ionospheric corrections can be performed to see the efficiency of the LIMs for the RTK applications over long baselines. These will be introduced in the next chapter.

In the previous sections, the ionospheric estimation results with the LIMs have been computed and verified. Basically, the LIMs have been found to be successful on the estimation of single path ionospheric delays after checking the trend of ionospheric curve estimated over the observation period. Nevertheless, the complete verification on the correctness and efficiency of the LIMs can hardly be accomplished until the implementation of the AFT with the ionospheric corrections over the various baselines tested.

6.7 CONCLUSIONS

From the investigations of previous chapters, it has been confirmed that the ionospheric effect may become a dominant problem of current RTK GPS as the baseline distance increases. This effect after double differencing can be a level of 2.8-5.6cm on L_1 and 4.6-9.2cm on L_2 over the baseline distances of 12.8km to 33km. The generation of precise ionospheric model is essential to obtain the ionospheric corrections for reducing the ionospheric effects and thus enhance the performance of RTK positioning for long distances. Unfortunately, the current ionospheric models such as LIM, RIM, and GIM cannot satisfy with the requirements of high precision RTK. In this chapter, several refined ionospheric models are hence proposed for test. From the investigations of this chapter, the following conclusions can however be drawn as follows.

1. Disadvantages of current ionospheric models for the RTK applications:

- The preprocessing of ambiguity resolution or hardware calibration is necessary and time consuming, and an incorrect or incomplete preprocessing may however degrade the modelling accuracy.
- The computation, update, and transmission of contemporary ionospheric corrections can hardly be accomplished by current models based on the multi-stations or the networks. Besides, currently only hourly ionospheric corrections are provided on the Web. These cannot satisfy with the requirements of the high precision RTK GPS users.
- The definition of so-called sun-earth system to resolve the time variation of ionosphere is not consistent for current models.
- The modelling accuracy of current models is still limited.

2. The improvements of ionospheric modelling with the LIMs

- The processing strategies of LIM, such as adoption of the optimal software for cycle slip detection and repair and the use of observable L7, can minimize the possibility of the effects of all observation errors on modelling except the phase multipath.
- Resolving the problem of ambiguity resolution and hardware calibration with using the L7 observable, the LIM has the following benefits:

(1) Saving the processing time of resolving the ambiguities and hardware biases,

(2) Evading the possible problems and effects of ambiguities unresolved or hardware biases false-calibration.

- Instead of the transformation of sun-earth system (often used in current ionospheric models but the definition of the system is not consistent), the concept of transformation with a weighting function between two adjoining epochs is used to figure out the problem of time variation of ionosphere for the modelling.
- With using a modelling based on a single known station, the LIM may work out the practical problems such as the processing, updating, and transmission of ionospheric corrections during the RTK operation.
- By the testing of several LIMs based on two types of mapping functions and two methods for the elimination of the unresolved phase multipathing effects, an optimal ionospheric modelling can be obtained.
- The verification of LIMs on single path and double differenced results is considered and carried out with comparison of the results from the GFA and the LCA based on two known stations. The evaluation of LIMs can hence be more accurate and reliable than the usual ways with using the positioning results or with comparisons of other models.

3. The performance of LIMs

- For these typical trials operated at the base stations of PSMS, CG54, and INED over the observation period of at least an hour, the estimation results of single path ionospheric delays with the LIMs on average may respectively have a level of up to near 8.6m, 4.8m, and 3.8m. These effects on the dual frequency signals can be a level of 13.3m, 7.4m, 5.9m on L_1 and 21.9m, 12.2m, 9.7m on L_2. The ionospheric effects on GPS positioning obviously cannot be ignored over the baselines of more then 10km. For the RTK positioning with the AFT over long distances, what is of great concerns is this effect after double differencing which will be investigated in the subsequent chapter. However, the investigation results of this chapter have found that the ionospheric effect is highly dependent of the elevation angle and the azimuth of observing satellites and the surveying area (or maybe time).
- For the modelling of ionosphere with the LIMs, the mapping function, a scalar to determine the slant ionosphere, may play a dominant role, and the multipathing

effect can be the only effect from the observation errors, which is also essential to increase the modelling accuracy. Basically, the modes of LIM for the tests proposed in this thesis can be divided into two groups: one is based on the mapping function I, another is based on the mapping function II. In each group, the ionospheric estimations on single path between the modes of LIM with/without the elimination of multipathing effects may have a slight difference of couples of tens centimeters.

- The smooth curves of ionospheric estimations have indicated that 100% "clean" data are available after the preprocessing of cycle slips with the TurboEdit. In other words, the results of LIMs are not affected by the effect of cycle slips.

4. The evaluation of LIMs performances

- The verification of ionospheric modelling using current ways may take a risk of a false evaluation because the verification, with using irrespective of the positioning results or the results of other ionospheric models, has involved the uncertainty of other error effects or the accuracy of the model comparable.

- In this thesis, two steps of verifications proposed to evaluate the performance of the LIMs cannot have the drawbacks of using current ways, and are far more accurate and reliable. The first step of verification, by checking the estimation trend of single path ionospheric delays with comparisons of the apparent true values obtained from the GFA, has found that the LIMs on the estimation trend of single path ionospheric delays have properly performed over the observation period. The second step of verification with using the "true" double differenced ionospheric delays obtained from the LCA is able to verify the double differenced ionospheric delays estimated with the LIMs, which will be discussed in the next chapter.

5. The RTK applications of LIMs

- For the RTK applications over long distances, the generation of LIMs is for two purposes:
  (1) Obtaining the ionospheric corrections at the base station for reducing the corresponding ionospheric effects,

(2) Constructing the vertical ionospheric profile above the surveying area for predicting the ionospheric delays (or corrections) at the rover station.

- The estimation results with the LIMs have been verified and found that the single path ionospheric errors can be properly modelled at least on the estimation trend over the observation period for the trials tested. This ensures that the corresponding ionospheric profile above the survey area for each trial can be appropriately constructed for the subsequent ionospheric prediction at the rover station.

For the RTK survey with the single epoch AFT, reducing the ionospheric effects is crucial for extending the use of this technique over long distances. The LIM for each mode, proposed in this chapter, is generated to estimate the ionospheric delays and to construct the ionospheric profile with the estimations covering the surveying area on the basis of GPS dual frequency data collected at the base station for at least hourly observation period. Based on the (vertical) ionospheric profile constructed, the ionospheric predictions for obtaining the corrections of ionospheric effects at any site of the rover surrounding the base station can hence be carried out during the RTK operation period. With these ionospheric corrections for both the base and rover stations, the RTK positioning with the single epoch AFT can be expected to be improved, but how efficient the AFT positioning can be achieved after the ionospheric corrections based on the LIMs still needs further investigations. With the same trials for test, the complete investigations on the AFT positioning over various length baselines will be introduced in the next chapter.

CHAPTER SEVEN

PERFORMANCE OF SINGLE-EPOCH AFT WITH IONOSPHERIC CORRECTIONS OVER LONG BASELINES

7.1 INTRODUCTION

To date, shortening the time of initialisation or re-initialisation and expanding the use of current RTK techniques for long distances are the two main challenge facing the RTK GPS currently. The advantage of using the single epoch AFT is that this technique with an ability to provide the instantaneous positions is free of the problem of initialisation or re-initialisation, which is a limitation of other techniques for long range RTK applications (details see Chapter 2). For short distance applications, currently centimeter level positioning accuracy is available with the AFT in a benign environment and limited only by the multipathing problem. As the distance increases, other errors such as ionosphere and troposphere begin to decorrelate.

Through the investigations of previous chapters, the answer for an attempt to extend the use of this technique over long distances may concern the modelling of two dominant errors of ionosphere and troposphere. For reducing the tropospheric effects with a self-contained tropospheric model, the modelling accuracy, however limited, has been found exceptionally as the satellite remains at low elevation angle. To achieve this goal, the focus on a precise ionospheric modelling has been accomplished with the generation of several LIMs for testing. At the first step of evaluation of the LIMs as discussed in the previous chapter, the proper estimations of single path ionospheric delays with the LIMs have been confirmed at least on the estimation trend.

In this chapter, the focus of the research work is on the following.

1. the prediction of ionospheric delays for the rover station based on the ionospheric profile constructed with the LIMs, (in Section 2)
2. the verification of the estimation results based on the LIMs (the second step of evaluation of the LIMS), (in Section 3)
3. the AFT positioning with the ionospheric corrections and the evaluation of final results. (in Section 4)

In Section 5, the improvements of single epoch AFT with the LIM will be summarized and discussed. For the RTK positioning with the AFT over long distances, all conclusions of the investigation results will be drawn in the last section.

7.2 PREDICTION OF IONOSPHERIC DELAYS FOR THE ROVER STATION

During the RTK operation, the L1 and (or) L2 observations for each station at the base and the rover are affected by the ionosphere. On the basis of the dual frequency GPS data collected at the base station, the corrections for these ionospheric effects on the observations of the base station can be obtained with using the LIMs generated in Chapter 5. Meanwhile, the ionospheric profile, consisting of the vertical one and the corresponding scalar of mapping function, is hence constructed for the survey area above the base station. Based on this vertical ionospheric profile constructed, the prediction of ionospheric delays can be accomplished for any site of the rover around the base during the period of RTK survey.

The procedures of ionospheric prediction for the rover station is carried out as follows and respectively introduced in the following subsections.

1. Construction of the vertical ionospheric profile,
2. The initial solution of rover station,
3. The computation of pierce points,
4. The calculation of mapping function and vertical total electron Content (TEC),
5. The computation of ionospheric corrections for the L1 and L2 observations of the rover.

7.2.1 THE CONSTRUCTION OF IONOSPHERIC PROFILE

For the rover station(s), the prediction of ionospheric delays has to rely on the ionospheric profile covering the survey area at the height of 350km above the base station. As described in Chapter 6, the construction of ionospheric profile has been implemented in a post-processing mode by the LIMs, with the dual frequency GPS data collected at the base station over a period of time about an hour at least. Depending on

the coverage of this profile in the air, the area of vertical ionospheric delays (or TEC) locally provided concerns of the baseline length of RTK applications.

For the trials of different length baselines tested in this research, the results from the LIMs have been evaluated on the trend of the estimated ionospheric curves and a proper estimate of ionospheric delays for the base station has been found. This also indicates that the (vertical) ionospheric profile based on the base (a single) station is, in practice, generated appropriately for the prediction of ionospheric delays of the rover at any site (pierce points) surrounding the base for the RTK survey at any epoch around the operation period.

7.2.2 THE INITIAL SOLUTION OF ROVER STATION

Based on the concept of ionospheric profile, the accumulated ionospheric delays from each satellite available to the rover station (receiver) can also be divided into a scalar of mapping function and the vector of vertical ionospheric delay at each corresponding pierce point on the profile. The vertical ionospheric delay at each corresponding pierce point for the rover can be obtained from the known vertical delays at those pierce points previously constructed based on the base. This computation has to rely on the relationship between the positions of those pierce points on the profile for the base and the rover. To obtain the position of the pierce points, requires the station coordinates of the rover.

The initial solution of rover station can be obtained from the single epoch AFT by several ways (see Al-Haifai, 1995) as follows:

1. by processing the data with an independent GPS software and adding the solutions to the NXF file,
2. in the initialisation file either from provisional coordinates (if the unknown receiver data was collected on a known monument) or obtained by another software (e.g. Ashtech's GPPS software) in a static mode,
3. from the built-in single epoch code solution algorithm accomplished by the RINTONXF program.

In a scenario of RTK GPS, only the third method can satisfy the requirement of self-contained. However the more accurate the estimation of the rover station, the less the

effect on the computation of the pierce point position. This effect is considered negligible if the estimation error of the rover station can be within few meters.

7.2.3 PIERCE POINTS

As described in Chapter 6, the definition of pierce point for both of the rover and the base is exactly the same. For the rover station, the computation of the position at each pierce point on the ionospheric profile is based on the satellite coordinates and the initial solution of rover station implemented in the previous subsection. The procedure of this computation follows the one for the base as described in section 6.2.3.1.

On the ionospheric profile at the height of 350km above the survey area, the geometrical relationship between all pierce points of the base and the rover can therefore be established with these computed positions of pierce points for further use of the prediction of vertical ionospheric delays.

7.2.4 PREDICTION OF THE VERTICAL IONOSPHERIC DELAYS WITH THE WEIGHTING FUNCTION

The correlation between the vertical ionospheric delays at the pierce points of base station and rover station can be established by a weighting function on the basis of the pierce point's positions on the ionospheric profile. As expressed below, the vertical ionospheric delays at the pierce points of rover station, V_k, can be obtained based on the vertical ionospheric profile generated by LIM, V_j.

$$V_k = \sum_{j=1}^{m_j} \left(W_{k,j} \cdot V_j \right)$$

$$k = 1, m_k \quad \text{.....(7.1)}$$

where

$$W_{k,j} = \frac{(1/D_{k,j})}{\sum_{l=1}^{m_l} (1/D_{k,l})}$$

$$D_{k,j} = \{[x_S(k) - x_p(j)]^2 + [y_S(k) - y_p(j)]^2 + [z_S(k) - z_p(j)]^2\}^{-1/2}$$

and

x_p, y_p, z_p are the coordinates of pierce points for the base,

x_S, y_S, z_S are the coordinates of pierce points for the rover,

m is the number of pierce points (satellites) of the base station,

m_k is the number of pierce points (satellites) of the rover station.

7.2.5 COMPUTATION OF THE IONOSPHERIC CORRECTIONS WITH THE MAPPING FUNCTION

In order to obtain the ionospheric corrections for the L1 and L2 observations of the rover, the vertical ionospheric delay, one of the two parameters to construct the slant ionospheric delay, is first computed by a procedure of ionospheric prediction with the weighting function implemented in the previous subsection. The mapping function, the other parameter, is an important scalar to define the relationship of ionospheric delays between the slant and the vertical. With the same definition of the two mapping functions used for the generation of LIM introduced in previous Chapter, the following equations are respectively used to obtain the mapping functions for the computation of ionospheric corrections of the rover.

$$M(\theta) = \{1-[cos\ (\theta)/(1+h/R)]^2\}^{-1/2} \quad (7.2)$$

$$M(d,h) = d(x_p, y_p, z_p, x_a, y_a, z_a) / h \quad (7.3a)$$

$$d(x_p, y_p, z_p, x_a, y_a, z_a) = [(x_p-x_a)^2 + (y_p-y_a)^2 + (z_p-z_a)^2]^{-1/2} \quad (7.3b)$$

where

θ is the elevation angle,

R is the radius of the earth,

d is the range between the pierce point $(x_p, y_p, z_p)$and the station (x_a, y_a, z_a),

h is the height of spherical shell (350km),

M(d,h) is the mapping function of the pierce point.

After the computation of vertical ionospheric delays and the corresponding mapping function for each epoch of the rover, the ionospheric delays for each epoch of the rover can be calculated by the following equation (7.4). The ionospheric corrections for the L_1 and L_2 frequency observations of the rover can hence be obtained respectively based on the equation (7.5.a) and (7.5.b).

$$I_k = M_k V_k \quad (7.4)$$

$$I1_k = \Upsilon_1 I_k \quad (7.5.a)$$

$$I2_k = \Upsilon_2 I_k \quad (7.5.b)$$

Where k=1,m, and m is the number of the processing epochs.

7.2.6 ERROR ANALYSIS

For the ionospheric prediction, there are two main error sources:

1. One is from the ionospheric profile constructed by the LIMs with the GPS data collected at the base. The accuracy of these estimated ionospheric delays for the construction of ionospheric profile hence determines the accuracy of the subsequent ionospheric prediction for the rover.
2. Another is from the initial solution of rover station. The accuracy of this solution, concerning the subsequent computations such as the position of pierce points, the weighting function, and the mapping function, can also affect the results of the ionospheric prediction for the rover.

Besides, the ionospheric corrections for the rover are also dependent on two methods for the elimination of multipathing effects and two types of mapping functions for test.

For the trials tested in this research, the estimation of ionospheric delays with the LIMs has been evaluated in the previous chapter. Basically this estimation can be concluded to be proper at least on the trend of the estimated ionospheric curves. In addition, the accuracy of initial solution for the rover station using the built-in single epoch code solution algorithm is, in general, achievable at a level of few meters for the trials of longer baselines tested. This effect, for instance, on the mapping function can be an error at a level below few digits after the decimal point. Due to the error of initial solution, the effects on the prediction of ionospheric delays for the rover are considered negligible.

7.2.7 PERFORMANCES OF THE IONOSPHERIC ESTIMATION BASED ON THE LIMs

As introduced in Chapter 6, the (vertical) ionospheric profiles have been generated with the LIMs on the basis of dual frequency GPS data collected at the base station. With comparisons of the results of GFA based on two known stations, a proper estimation of the single path ionospheric delays for the baseline trials has been found at least on the estimation trend. Based on the corresponding ionospheric profile generated by each LIM

for test, the prediction of single path ionospheric delays for the rover is carried out as the procedure of ionospheric prediction introduced in the previous subsections. From each corresponding single path ionospheric estimation, the L_1 and L_2 ionospheric corrections for the base and for the rover can hence be calculated. The double differenced estimation results for each trial over the observation period are demonstrated with the dot curve as shown in Figure B.1 to B.38 (summarized in Appendix B). For further analysis of the performance of double differenced ionospheric estimations based on the LIMs, the computed statistics of the mean, the standard deviation, the maximum, the minimum, and the variation for each available satellite pair over the period of surveying epochs are summarized in Table 7.1 to 7.6. From the statistic of the mean, for example, in a case of the LIM1, the estimated double differenced ionospheric delays on each couple of satellites for the trials of various baselines from 12.8km to 33km are demonstrated in Figure 7.1.

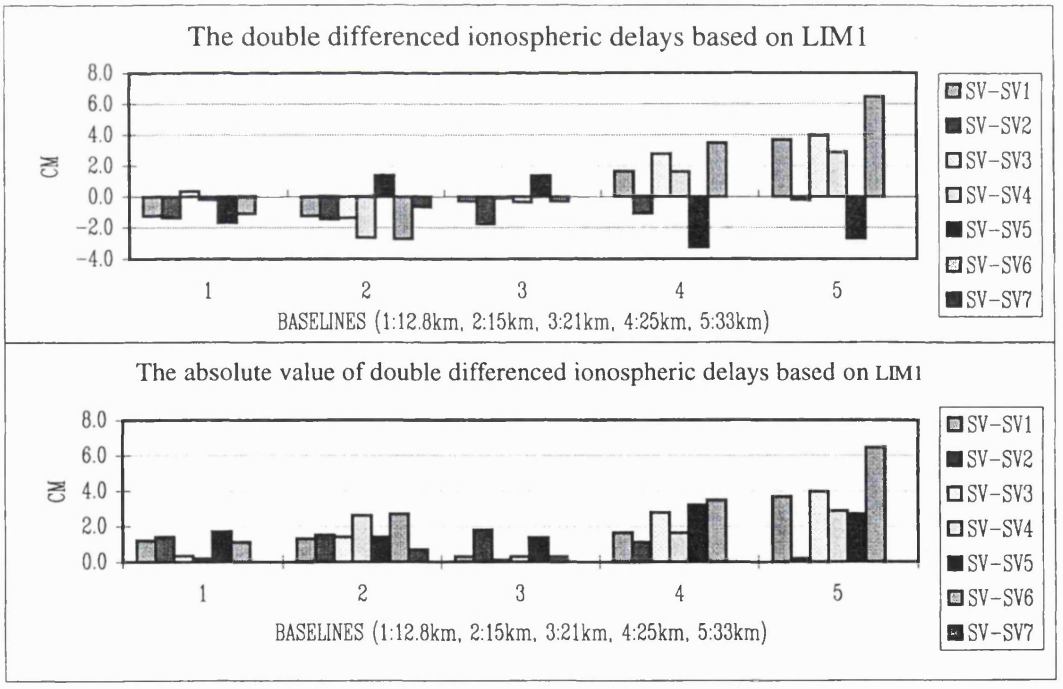

Figure 7.1 The double differenced ionospheric delays for various length baselines tested

From the results of these figures and the table, it can be concluded.

1. From a viewpoint of the relationship between the ionospheric effect and the baseline length, the effect of double differenced ionosphere apparently increases as the baseline length increases. The effects on average can be a level of ±1.7cm, ±2.7cm, ±1.8cm, ±3.5cm, and ±6.5cm respectively for the trial of 12.8km, 15km, 21km, 25km, and 33km baselines. Obviously, the ionospheric effect after double differencing is highly dependent of the baseline length.
2. From the results of the maximum and the minimum based on LIM1 in Table 7.1, the variation of double differenced ionospheric delays can be a range of –2.1~0.5, -4.6~1.5, -1.9~2.0, -4.7~5.2, -5.4~9.2 in unit of centimeters respectively for the trials above. The largest effect for each individual observing epoch over the period of survey can be a level of 2.1cm, 4.6cm, 2.0cm, 5.2cm, and 9.2cm respectively. For the RTK survey, the actual effect on L_1 and L_2 observations can be a size of 1.5 time and 2.5 time the effects above. This indicates that the ionospheric effects for each individual epoch over the observation period cannot be ignored, and the individual effect of each epoch after double differencing is also dependent of the baseline length.
3. Among the trials, two exceptional cases of 15km and 21km baselines either from the average or from the individual epoch have shown an unusual phenomenon of the longer baseline with a smaller effect (or the shorter baseline with a larger effect). This may be because that the surveying area of 21km baseline case located at the middle latitude (further away from the anomaly area of ionosphere: -15 to 15 latitude) may have a steady ionospheric and hence the effect is smaller. This indicates that the ionospheric effect is also independent of the surveying area.
4. In each trial, the double differenced ionospheric effects on these satellite pair are quite different. This can be because of the geometrical position of these satellites at different elevation angle. For example, a larger effect has been shown for the fifth pair of satellites in the case of 12.8km baseline since the position of this pair is located respectively at the highest and the lowest elevation angle.
5. For the ionospheric modelling with the LIMs, the multipath is the only effect from the observation errors, but this effect on the estimation results can hardly be distinguished without comparisons of the true values of ionosphere. The multipathing effects over the observation period can be transferred into a form of a constant bias or a drift for the ionospheric modelling with the LIMs. This will be discussed in the next section.

6. For the LIMs tested, there is a slight difference of millimeter level for the estimated double differenced ionospheric delays between the LIMs. The analysis of the modelling results for other modes, in general, has the same conclusions as those made based on the estimation results of LIM1. The evaluation of these LIMs however cannot be accomplished until a further comparison.

Overall, the ionospheric estimations based on the LIMs can be determined by the factors such as the multipathing effects, the location of surveying area, the elevation angle of the satellite, and the baseline length. Except these factors, the time of survey is also an important factor from some related literatures, but however there is no investigation on this for these trials tested. With no doubt, the ionospheric effects after double differencing with a size of 9.2cm maximum for the 33km baseline (a larger size of 1.5457 and 2.5457 time for L_1 and L_2 GPS signals) cannot be ignored for the RTK survey. However, the ionospheric effects after double differencing may become too sensitive to be accurately modelled without consideration of these factors during the modelling. The verification of ionospheric modelling results with the LIMs will be introduced in the following section. "Whether or not the LIM for each mode tested with the ionospheric prediction (being deliberately constructed) are accurate enough for the application of RTK GPS?" and "of which mode can be the optimal model?" need further evaluations.

Table 7.1 Comparison of double differenced ionospheric delays between the true value and the estimation based on LIM1

Unit: centimeter

Ion		Baseline(12.8)			Baseline(15)			Baseline(21)			Baseline(25)			Baseline(33)		
SVs		LIM1	True	Diff	LIM1	True	Diff	LIM1	True	Diff	LIM1	True	Diff	LIM1	True	Diff
	Mean	-1.2	-1.2	0.0	-1.3	-0.7	-0.6	-0.3	-0.6	0.3	1.6	0.4	1.3	3.7	1.9	1.8
	±σ	0.2	0.8	0.7	0.3	0.7	0.8	0.3	0.9	0.7	0.4	0.6	0.6	0.8	1.2	1.1
1	Max	-0.9	0.1	1.6	-0.7	1.3	1.0	0.2	1.7	2.1	2.4	1.8	3.0	5.1	4.6	4.7
	Min	-1.6	-2.9	-1.2	-1.8	-2.2	-2.7	-0.8	-2.8	-1.5	0.9	-0.8	0.1	2.2	-0.9	-1.0
	Rng	0.6	3.0	2.8	1.1	3.5	3.7	1.0	4.5	3.6	1.5	2.6	2.9	2.8	5.5	5.6
	Mean	-1.4	-1.5	0.1	-1.5	-0.7	-0.8	-1.8	-1.1	-0.6	-1.1	-0.7	-0.3	-0.2	0.4	-0.6
	±σ	0.1	0.8	0.8	1.7	1.3	0.7	0.1	1.1	1.1	0.4	1.4	1.7	0.6	2.1	2.6
2	Max	-1.1	0.3	2.4	1.1	1.6	0.8	-1.6	1.7	1.3	-0.4	1.6	3.4	0.9	3.8	4.4
	Min	-1.6	-3.7	-1.5	-4.6	-4.1	-2.4	-1.9	-3.1	-3.4	-1.7	-4.0	-3.1	-1.2	-3.8	-4.7
	Rng	0.5	4.0	3.9	5.7	5.7	3.3	0.3	4.8	4.7	1.3	5.6	6.5	2.1	7.6	9.1
	Mean	0.3	-0.4	0.8	-1.4	1.0	-2.4	-0.1	1.0	-1.1	2.8	1.8	1.0	4.0	2.9	1.0
	±σ	0.1	0.6	0.6	0.0	0.9	1.0	0.2	1.1	1.0	0.5	0.6	0.6	0.8	1.3	1.1
3	Max	0.5	0.6	2.5	-1.3	3.2	-0.4	0.2	3.2	0.9	3.6	2.9	2.5	5.3	5.5	3.8
	Min	0.2	-2.2	-0.3	-1.5	-1.0	-4.6	-0.5	-1.0	-3.1	2.0	0.5	-0.2	2.6	0.8	-1.1
	Rng	0.3	2.8	2.8	0.1	4.2	4.2	0.7	4.1	4.0	1.7	2.5	2.7	2.7	4.6	4.9
	Mean	-0.2	-0.3	0.1	-2.6	-1.2	-1.4	-0.3	0.4	-0.8	1.6	1.5	0.1	2.9	2.7	0.2
	±σ	0.0	0.8	0.8	0.6	0.9	0.6	0.1	1.0	1.1	0.7	0.8	0.6	1.1	1.1	1.1
4	Max	-0.2	1.0	1.9	-1.6	0.3	0.1	-0.2	2.3	1.0	3.0	3.0	1.4	4.9	4.9	2.0
	Min	-0.2	-2.1	-1.2	-3.5	-3.6	-3.0	-0.5	-1.3	-2.7	0.4	-0.9	-1.8	1.1	-0.7	-3.0
	Rng	0.0	3.1	3.1	1.9	3.9	3.1	0.3	3.5	3.7	2.6	3.9	3.2	3.9	5.6	5.0
	Mean	-1.7	3.6	-5.2	1.4	1.9	-0.4	1.4	2.2	-0.9	-3.2	-0.9	-2.4	-2.7	0.4	-3.1
	±σ	0.2	0.8	0.8	0.1	0.8	0.8	0.5	2.0	2.0	0.8	1.1	0.8	1.5	1.9	1.2
5	Max	-1.3	5.0	-3.2	1.5	3.6	1.1	2.0	7.5	3.1	-1.8	1.5	-0.0	-0.2	4.3	0.4
	Min	-2.1	1.4	-6.6	1.1	0.1	-2.3	0.6	-1.3	-5.5	-4.7	-2.9	-4.0	-5.4	-3.0	-6.3
	Rng	0.8	3.5	3.4	0.3	3.5	3.4	1.5	8.8	8.6	2.9	4.4	4.0	5.2	7.4	6.6
	Mean	-1.1	-0.8	-0.3	-2.7	-1.9	-0.8	-0.3	-1.0	0.7	3.5	1.6	1.9	6.5	3.4	3.0
	±σ	0.1	0.7	0.7	0.3	0.9	0.8	0.2	1.3	1.4	1.0	0.8	1.1	1.5	1.4	2.0
6	Max	-1.0	0.3	1.7	-2.2	-0.3	1.6	0.1	1.3	3.2	5.2	4.0	4.3	9.2	6.3	5.9
	Min	-1.3	-2.7	-1.4	-3.1	-4.7	-2.7	-0.7	-3.7	-2.0	1.9	-0.0	-0.3	4.0	1.3	-1.0
	Rng	0.3	3.0	3.1	0.9	4.4	4.3	0.8	5.0	5.2	3.4	4.0	4.6	5.1	5.0	6.9
	Mean				-0.7	0.7	-1.4									
	±σ				1.2	1.9	0.8									
7	Max				1.2	5.9	0.1									
	Min				-2.8	-2.2	-4.7									
	Rng				4.0	8.1	4.8									

Baselines: PSMS-SEMA(12.8km), CG54-KRPI(15km), INED-SHEN(21km), PSMS-PLAT(25km), PSMS-SOHO(33km).

Ion: The double differenced ionospheric delays (in unit of cm), based on the Linear Combination Approach (LCA) and the Local Ionospheric Model, LIM1.

SVs: The number of satellite pairs,
PSMS-SEMA, PSMS-PLAT and PSMS-SOHO:
1:18-4, 2:18-13, 3:18-16, 4:18-19, 5:18-24, and 6:18-27.
CG54-KRPI: 1:21-1, 2:21-3, 3:21-15, 4:21-22, 5:21-23, 6:21-29, and 7:21-31.
INED-SHEN: 1:14-1, 2:14-4, 3:14-7, 4:14-16, 5:14-18, and 6:14-25.

True: The double differenced ionospheric delays obtained from the LCA, which are considered as the true values

LIM1: The double differenced ionospheric errors estimated by the LIM1.

Diff: The difference of single path ionospheric errors between the LIM1 and the Ture.

Mean The average of all data.

σ The standard deviation of all data.

Max The maximum of all data based on LIM1, LCA, and Diff.

Min The minimum of all data based on LIM1, LCA, and Diff.

Rng =Max-Min.

Table 7.2 Comparison of double differenced ionospheric delays between the true value and the estimation based on LIM2

Unit: centimeter

Ion		Baseline(12.8)			Baseline(15)			Baseline(21)			Baseline(25)			Baseline(33)		
SVs		LIM2	True	Diff	LIM2	True	Diff	LIM2	True	Diff	LIM2	True	Diff	LIM2	True	Diff
	Mean	-1.0	-1.2	0.2	-1.0	-0.7	-0.4	-0.2	-0.6	0.3	1.3	0.4	1.0	3.0	1.9	1.1
	±σ	0.1	0.8	0.7	0.3	0.7	0.8	0.2	0.9	0.7	0.4	0.6	0.6	0.7	1.2	1.1
1	Max	-0.8	0.1	1.8	-0.6	1.3	1.2	0.2	1.7	2.2	2.0	1.8	2.6	4.2	4.6	3.8
	Min	-1.3	-2.9	-0.9	-1.5	-2.2	-2.5	-0.7	-2.8	-1.6	0.7	-0.8	-0.3	1.9	-0.9	-1.3
	Rng	0.5	3.0	2.8	0.8	3.5	3.6	0.8	4.5	3.7	1.2	2.6	2.9	2.3	5.5	5.2
	Mean	-1.1	-1.5	0.4	-1.2	-0.7	-0.6	-1.4	-1.1	-0.3	-0.9	-0.7	-0.2	-0.2	0.4	-0.6
	±σ	0.1	0.8	0.8	1.4	1.3	0.6	0.1	1.1	1.1	0.3	1.4	1.6	0.5	2.1	2.5
2	Max	-0.9	0.3	2.6	0.9	1.6	0.9	-1.3	1.7	1.7	-0.3	1.6	3.5	0.7	3.8	4.3
	Min	-1.3	-3.7	-1.3	-3.9	-4.1	-1.9	-1.5	-3.1	-3.1	-1.4	-4.0	-2.8	-1.0	-3.8	-4.5
	Rng	0.4	4.0	3.9	4.9	5.7	2.8	0.2	4.8	4.8	1.1	5.6	6.4	1.8	7.6	8.8
	Mean	0.3	-0.4	0.8	-1.1	1.0	-2.2	-0.1	1.0	-1.1	2.3	1.8	0.6	3.3	2.9	0.4
	±σ	0.0	0.6	0.6	0.0	0.9	0.9	0.2	1.1	1.0	0.4	0.6	0.5	0.7	1.3	1.1
3	Max	0.4	0.6	2.5	-1.1	3.2	-0.1	0.2	3.2	0.9	3.1	2.9	2.0	4.5	5.5	3.0
	Min	0.2	-2.2	-0.3	-1.2	-1.0	-4.3	-0.4	-1.0	-3.1	1.6	0.5	-0.6	2.2	0.8	-1.7
	Rng	0.2	2.8	2.8	0.1	4.2	4.2	0.6	4.1	4.0	1.4	2.5	2.6	2.4	4.6	4.7
	Mean	-0.1	-0.3	0.2	-2.1	-1.2	-0.9	-0.3	0.4	-0.7	1.4	1.5	-0.1	2.4	2.7	-0.2
	±σ	0.0	0.8	0.8	0.4	0.9	0.6	0.1	1.0	1.0	0.7	0.8	0.6	1.0	1.1	1.1
4	Max	-0.1	1.0	2.0	-1.3	0.3	0.9	-0.2	2.3	1.0	2.6	3.0	1.3	4.3	4.9	1.7
	Min	-0.1	-2.1	-1.1	-2.8	-3.6	-2.4	-0.4	-1.3	-2.6	0.3	-0.9	-2.0	0.9	-0.7	-3.3
	Rng	0.0	3.1	3.1	1.4	3.9	3.2	0.3	3.5	3.7	2.2	3.9	3.3	3.4	5.6	5.0
	Mean	-1.4	3.6	-5.0	1.1	1.9	-0.7	1.1	2.2	-1.1	-2.7	-0.9	-1.9	-2.3	0.4	-2.7
	±σ	0.2	0.8	0.8	0.1	0.8	0.8	0.4	2.0	2.0	0.7	1.1	0.8	1.3	1.9	1.2
5	Max	-1.1	5.0	-2.9	1.2	3.6	0.9	1.6	7.5	2.8	-1.5	1.5	0.3	-0.2	4.3	0.4
	Min	-1.7	1.4	-6.3	0.8	0.1	-2.6	0.4	-1.3	-5.9	-4.0	-2.9	-3.6	-4.5	-3.0	-6.0
	Rng	0.6	3.5	3.4	0.4	3.5	3.4	1.2	8.8	8.6	2.4	4.4	3.9	4.3	7.4	6.4
	Mean	-0.9	-0.8	-0.1	-2.3	-1.9	-0.3	-0.2	-1.0	0.8	2.9	1.6	1.4	5.5	3.4	2.0
	±σ	0.1	0.7	0.7	0.2	0.9	0.8	0.2	1.3	1.3	0.9	0.8	1.0	1.3	1.4	1.9
6	Max	-0.8	0.3	1.8	-1.8	-0.3	2.1	0.1	1.3	3.3	4.4	4.0	3.6	7.7	6.3	4.8
	Min	-1.1	-2.7	-1.2	-2.6	-4.7	-2.2	-0.5	-3.7	-1.8	1.6	-0.0	-0.7	3.4	1.3	-1.8
	Rng	0.3	3.0	3.1	0.7	4.4	4.3	0.6	5.0	5.1	2.9	4.0	4.3	4.4	5.0	6.6
	Mean				-0.6	0.7	-1.3									
	±σ				1.0	1.9	1.0									
7	Max				1.0	5.9	0.4									
	Min				-2.3	-2.2	-4.9									
	Rng				3.3	8.1	5.3									

Baselines: PSMS-SEMA(12.8km), CG54-KRPI(15km), INED-SHEN(21km), PSMS-PLAT(25km), PSMS-SOHO(33km).

Ion: The double differenced ionospheric delays (in unit of cm), based on the Linear Combination Approach (LCA) and the Local Ionospheric Model, LIM2.

SVs: The number of satellite pairs,
PSMS-SEMA, PSMS-PLAT and PSMS-SOHO:
1:18-4, 2:18-13, 3:18-16, 4:18-19, 5:18-24, and 6:18-27.
CG54-KRPI: 1:21-1, 2:21-3, 3:21-15, 4:21-22, 5:21-23, 6:21-29, and 7:21-31.
INED-SHEN: 1:14-1, 2:14-4, 3:14-7, 4:14-16, 5:14-18, and 6:14-25.

True: The double differenced ionospheric delays obtained from the LCA, which are considered as the true values

LIM2: The double differenced ionospheric errors estimated by the LIM2.

Diff: The difference of single path ionospheric errors between the LIM2 and the Ture.

Mean The average of all data.

σ The standard deviation of all data.

Max The maximum of all data based on LIM2, LCA, and Diff.

Min The minimum of all data based on LIM2, LCA, and Diff.

Rng =Max-Min.

Table 7.3 Comparison of double differenced ionospheric delays between the true value and the estimation based on LIM3

Unit: centimeter

Ion		Baseline(12.8)			Baseline(15)			Baseline(21)			Baseline(25)			Baseline(33)		
SVs		LIM3	True	Diff	LIM3	True	Diff	LIM3	True	Diff	LIM3	True	Diff	LIM3	True	Diff
	Mean	-1.3	-1.2	-0.0	-1.3	-0.7	-0.6	-0.3	-0.6	0.3	1.7	0.4	1.3	3.7	1.9	1.8
	±σ	0.2	0.8	0.7	0.3	0.7	0.8	0.3	0.9	0.7	0.4	0.6	0.6	0.8	1.2	1.1
1	Max	-1.0	0.1	1.6	-0.8	1.3	1.0	0.2	1.7	2.0	2.4	1.8	3.0	5.2	4.6	4.8
	Min	-1.6	-2.9	-1.2	-1.8	-2.2	-2.7	-0.8	-2.8	-1.5	0.9	-0.8	0.1	2.3	-0.9	-0.9
	Rng	0.7	3.0	2.7	1.0	3.5	3.7	1.0	4.5	3.6	1.5	2.6	2.9	2.9	5.5	5.7
	Mean	-1.4	-1.5	0.1	-1.5	-0.7	-0.8	-1.8	-1.1	-0.7	-1.1	-0.7	-0.4	-0.2	0.4	-0.6
	±σ	0.1	0.8	0.8	1.6	1.3	0.7	0.1	1.1	1.1	0.4	1.4	1.7	0.6	2.1	2.6
2	Max	-1.2	0.3	2.3	1.1	1.6	0.8	-1.6	1.7	1.3	-0.4	1.6	3.4	0.9	3.8	4.4
	Min	-1.7	-3.7	-1.5	-4.6	-4.1	-2.4	-1.9	-3.1	-3.4	-1.7	-4.0	-3.1	-1.2	-3.8	-4.7
	Rng	0.5	4.0	3.9	5.7	5.7	3.3	0.3	4.8	4.7	1.3	5.6	6.5	2.2	7.6	9.1
	Mean	0.3	-0.4	0.8	-1.4	1.0	-2.4	-0.1	1.0	-1.1	2.8	1.8	1.1	4.0	2.9	1.1
	±σ	0.1	0.6	0.6	0.0	0.9	0.9	0.2	1.1	1.0	0.5	0.6	0.6	0.8	1.3	1.1
3	Max	0.5	0.6	2.5	-1.4	3.2	-0.4	0.2	3.2	0.9	3.7	2.9	2.6	5.4	5.5	3.9
	Min	0.2	-2.2	-0.3	-1.5	-1.0	-4.6	-0.5	-1.0	-3.1	2.0	0.5	-0.2	2.7	0.8	-1.1
	Rng	0.3	2.8	2.8	0.1	4.2	4.2	0.7	4.1	4.0	1.7	2.5	2.8	2.8	4.6	5.0
	Mean	-0.2	-0.3	0.1	-2.6	-1.2	-1.4	-0.3	0.4	-0.8	1.7	1.5	0.2	2.9	2.7	0.3
	±σ	0.0	0.8	0.8	0.6	0.9	0.6	0.1	1.0	1.1	0.8	0.8	0.6	1.1	1.1	1.2
4	Max	-0.2	1.0	1.9	-1.6	0.3	0.1	-0.2	2.3	1.0	3.1	3.0	1.4	5.0	4.9	2.1
	Min	-0.2	-2.1	-1.2	-3.5	-3.6	-3.0	-0.5	-1.3	-2.7	0.4	-0.9	-1.8	1.1	-0.7	-3.0
	Rng	0.0	3.1	3.1	1.9	3.9	3.1	0.3	3.5	3.7	2.6	3.9	3.2	3.9	5.6	5.0
	Mean	-1.7	3.6	-5.3	1.4	1.9	-0.4	1.4	2.2	-0.8	-3.3	-0.9	-2.4	-2.8	0.4	-3.2
	±σ	0.2	0.8	0.8	0.1	0.8	0.8	0.5	2.0	2.0	0.9	1.1	0.8	1.5	1.9	1.2
5	Max	-1.3	5.0	-3.2	1.5	3.6	1.1	2.1	7.5	3.1	-1.9	1.5	-0.1	-0.2	4.3	0.4
	Min	-2.1	1.4	-6.6	1.1	0.1	-2.3	0.6	-1.3	-5.4	-4.8	-2.9	-4.1	-5.5	-3.0	-6.3
	Rng	0.8	3.5	3.4	0.3	3.5	3.4	1.5	8.8	8.6	3.0	4.4	4.0	5.3	7.4	6.7
	Mean	-1.1	-0.8	-0.3	-2.7	-1.9	-0.8	-0.3	-1.0	0.7	3.6	1.6	2.0	6.6	3.4	3.2
	±σ	0.1	0.7	0.7	0.3	0.9	0.8	0.2	1.3	1.4	1.0	0.8	1.1	1.6	1.4	2.1
6	Max	-1.0	0.3	1.6	-2.2	-0.3	1.6	0.1	1.3	3.2	5.4	4.0	4.4	9.3	6.3	6.1
	Min	-1.3	-2.7	-1.4	-3.1	-4.7	-2.6	-0.7	-3.7	-2.0	1.9	-0.0	-0.2	4.1	1.3	-0.9
	Rng	0.3	3.0	3.1	0.9	4.4	4.3	0.8	5.0	5.2	3.4	4.0	4.6	5.2	5.0	7.0
	Mean				-0.7	0.7	-1.4									
	±σ				1.2	1.9	0.8									
7	Max				1.2	5.9	0.1									
	Min				-2.8	-2.2	-4.6									
	Rng				4.0	8.1	4.8									

Baselines: PSMS-SEMA(12.8km), CG54-KRPI(15km), INED-SHEN(21km), PSMS-PLAT(25km), PSMS-SOHO(33km).

Ion: The double differenced ionospheric delays (in unit of cm), based on the Linear Combination Approach (LCA) and the Local Ionospheric Model, LIM3.

SVs: The number of satellite pairs,
PSMS-SEMA, PSMS-PLAT and PSMS-SOHO:
1:18-4, 2:18-13, 3:18-16, 4:18-19, 5:18-24, and 6:18-27.
CG54-KRPI: 1:21-1, 2:21-3, 3:21-15, 4:21-22, 5:21-23, 6:21-29, and 7:21-31.
INED-SHEN: 1:14-1, 2:14-4, 3:14-7, 4:14-16, 5:14-18, and 6:14-25.

True: The double differenced ionospheric delays obtained from the LCA, which are considered as the true values

LIM3: The double differenced ionospheric errors estimated by the LIM3.

Diff: The difference of single path ionospheric errors between the LIM3 and the Ture.

Mean The average of all data.

σ The standard deviation of all data.

Max The maximum of all data based on LIM3, LCA, and Diff.

Min The minimum of all data based on LIM3, LCA, and Diff.

Rng =Max-Min.

Table 7.4 Comparison of double differenced ionospheric delays between the true value and the estimation based on LIM4

Unit: centimeter

Ion		Baseline(12.8)			Baseline(15)			Baseline(21)			Baseline(25)			Baseline(33)		
SVs		LIM4	True	Diff	LIM4	True	Diff	LIM4	True	Diff	LIM4	True	Diff	LIM4	True	Diff
	Mean	-1.0	-1.2	0.2	-1.0	-0.7	-0.3	-0.2	-0.6	0.3	1.4	0.4	1.0	3.1	1.9	1.2
	±σ	0.2	0.8	0.7	0.2	0.7	0.8	0.2	0.9	0.7	0.4	0.6	0.6	0.7	1.2	1.1
1	Max	-0.8	0.1	1.8	-0.7	1.3	1.2	0.2	1.7	2.2	2.0	1.8	2.6	4.2	4.6	3.9
	Min	-1.3	-2.9	-1.0	-1.4	-2.2	-2.4	-0.7	-2.8	-1.6	0.7	-0.8	-0.2	1.9	-0.9	-1.3
	Rng	0.5	3.0	2.8	0.7	3.5	3.6	0.8	4.5	3.7	1.3	2.6	2.9	2.4	5.5	5.2
	Mean	-1.2	-1.5	0.4	-1.2	-0.7	-0.5	-1.5	-1.1	-0.3	-0.9	-0.7	-0.2	-0.2	0.4	-0.6
	±σ	0.1	0.8	0.8	1.4	1.3	0.6	0.1	1.1	1.1	0.3	1.4	1.7	0.5	2.1	2.5
2	Max	-0.9	0.3	2.6	0.9	1.6	0.9	-1.3	1.7	1.7	-0.3	1.6	3.5	0.8	3.8	4.3
	Min	-1.3	-3.7	-1.3	-3.8	-4.1	-1.8	-1.5	-3.1	-3.1	-1.5	-4.0	-2.9	-1.1	-3.8	-4.6
	Rng	0.4	4.0	3.9	4.7	5.7	2.7	0.2	4.8	4.8	1.1	5.6	6.4	1.8	7.6	8.9
	Mean	0.3	-0.4	0.8	-1.1	1.0	-2.2	-0.1	1.0	-1.1	2.4	1.8	0.6	3.4	2.9	0.5
	±σ	0.1	0.6	0.6	0.0	0.9	0.9	0.2	1.1	1.0	0.4	0.6	0.5	0.7	1.3	1.1
3	Max	0.4	0.6	2.5	-1.1	3.2	-0.1	0.2	3.2	0.9	3.1	2.9	2.0	4.6	5.5	3.1
	Min	0.2	-2.2	-0.3	-1.2	-1.0	-4.3	-0.4	-1.0	-3.1	1.7	0.5	-0.5	2.2	0.8	-1.6
	Rng	0.2	2.8	2.8	0.1	4.2	4.2	0.6	4.1	4.0	1.5	2.5	2.6	2.4	4.6	4.7
	Mean	-0.1	-0.3	0.2	-2.0	-1.2	-0.8	-0.3	0.4	-0.7	1.4	1.5	-0.1	2.5	2.7	-0.2
	±σ	0.0	0.8	0.8	0.4	0.9	0.6	0.1	1.0	1.0	0.7	0.8	0.6	1.0	1.1	1.1
4	Max	-0.1	1.0	2.0	-1.2	0.3	1.0	-0.2	2.3	1.0	2.6	3.0	1.3	4.4	4.9	1.8
	Min	-0.1	-2.1	-1.1	-2.7	-3.6	-2.3	-0.4	-1.3	-2.6	0.4	-0.9	-2.0	0.9	-0.7	-3.3
	Rng	0.0	3.1	3.1	1.4	3.9	3.3	0.3	3.5	3.7	2.3	3.9	3.3	3.5	5.6	5.0
	Mean	-1.4	3.6	-5.0	1.1	1.9	-0.7	1.2	2.2	-1.1	-2.8	-0.9	-1.9	-2.4	0.4	-2.8
	±σ	0.2	0.8	0.8	0.1	0.8	0.8	0.4	2.0	2.0	0.7	1.1	0.8	1.3	1.9	1.2
5	Max	-1.1	5.0	-2.9	1.2	3.6	0.8	1.7	7.5	2.8	-1.6	1.5	0.2	-0.2	4.3	0.4
	Min	-1.8	1.4	-6.4	0.8	0.1	-2.6	0.5	-1.3	-5.8	-4.1	-2.9	-3.7	-4.6	-3.0	-6.0
	Rng	0.7	3.5	3.4	0.4	3.5	3.4	1.2	8.8	8.6	2.5	4.4	3.9	4.4	7.4	6.5
	Mean	-0.9	-0.8	-0.1	-2.2	-1.9	-0.2	-0.2	-1.0	0.8	3.0	1.6	1.4	5.6	3.4	2.2
	±σ	0.1	0.7	0.7	0.2	0.9	0.8	0.2	1.3	1.3	0.9	0.8	1.0	1.3	1.4	1.9
6	Max	-0.8	0.3	1.8	-1.8	-0.3	2.2	0.1	1.3	3.3	4.5	4.0	3.7	7.9	6.3	5.0
	Min	-1.1	-2.7	-1.2	-2.4	-4.7	-2.1	-0.5	-3.7	-1.8	1.6	-0.0	-0.6	3.5	1.3	-1.7
	Rng	0.3	3.0	3.1	0.7	4.4	4.3	0.6	5.0	5.1	2.9	4.0	4.3	4.4	5.0	6.6
	Mean				-0.5	0.7	-1.3									
	±σ				0.9	1.9	1.0									
7	Max				0.9	5.9	0.5									
	Min				-2.2	-2.2	-4.9									
	Rng				3.2	8.1	5.4									

Baselines: PSMS-SEMA(12.8km), CG54-KRPI(15km), INED-SHEN(21km), PSMS-PLAT(25km), PSMS-SOHO(33km).

Ion: The double differenced ionospheric delays (in unit of cm), based on the Linear Combination Approach (LCA) and the Local Ionospheric Model, LIM4.

SVs: The number of satellite pairs,
PSMS-SEMA, PSMS-PLAT and PSMS-SOHO:
1:18-4, 2:18-13, 3:18-16, 4:18-19, 5:18-24, and 6:18-27.
CG54-KRPI: 1:21-1, 2:21-3, 3:21-15, 4:21-22, 5:21-23, 6:21-29, and 7:21-31.
INED-SHEN: 1:14-1, 2:14-4, 3:14-7, 4:14-16, 5:14-18, and 6:14-25.

True: The double differenced ionospheric delays obtained from the LCA, which are considered as the true values

LIM4: The double differenced ionospheric errors estimated by the LIM4.

Diff: The difference of single path ionospheric errors between the LIM4 and the Ture.

Mean The average of all data.

σ The standard deviation of all data.

Max The maximum of all data based on LIM4, LCA, and Diff.

Min The minimum of all data based on LIM4, LCA, and Diff.

Rng =Max-Min.

Table 7.5 Comparison of double differenced ionospheric delays between the true value and the estimation based on LIM5

Unit: centimeter

Ion		Baseline(12.8)			Baseline(15)			Baseline(21)			Baseline(25)			Baseline(33)		
SVs		LIM5	True	Diff	LIM5	True	Diff	LIM5	True	Diff	LIM5	True	Diff	LIM5	True	Diff
	Mean	-1.1	-1.2	0.1	-1.2	-0.7	-0.6	-0.3	-0.6	0.3	1.5	0.4	1.1	3.4	1.9	1.5
	±σ	0.2	0.8	0.7	0.3	0.7	0.8	0.3	0.9	0.7	0.4	0.6	0.6	0.8	1.2	1.1
1	Max	-0.9	0.1	1.7	-0.8	1.3	1.0	0.2	1.7	2.1	2.2	1.8	2.8	4.7	4.6	4.3
	Min	-1.5	-2.9	-1.0	-1.7	-2.2	-2.6	-0.8	-2.8	-1.6	0.8	-0.8	-0.1	2.1	-0.9	-1.1
	Rng	0.6	3.0	2.8	1.0	3.5	3.7	0.9	4.5	3.6	1.4	2.6	2.9	2.7	5.5	5.5
	Mean	-1.3	-1.5	0.3	-1.4	-0.7	-0.7	-1.6	-1.1	-0.5	-1.0	-0.7	-0.2	-0.2	0.4	-0.6
	±σ	0.1	0.8	0.8	1.6	1.3	0.7	0.1	1.1	1.1	0.3	1.4	1.7	0.6	2.1	2.6
2	Max	-1.0	0.3	2.5	1.1	1.6	0.9	-1.4	1.7	1.4	-0.4	1.6	3.5	0.8	3.8	4.4
	Min	-1.5	-3.7	-1.4	-4.5	-4.1	-2.3	-1.7	-3.1	-3.2	-1.5	-4.0	-2.9	-1.1	-3.8	-4.5
	Rng	0.5	4.0	3.9	5.6	5.7	3.2	0.3	4.8	4.7	1.1	5.6	6.4	1.9	7.6	8.9
	Mean	0.3	-0.4	0.8	-1.3	1.0	-2.4	-0.1	1.0	-1.1	2.6	1.8	0.8	3.6	2.9	0.7
	±σ	0.1	0.6	0.6	0.0	0.9	0.9	0.2	1.1	1.0	0.5	0.6	0.6	0.8	1.3	1.1
3	Max	0.4	0.6	2.5	-1.3	3.2	-0.4	0.2	3.2	0.9	3.4	2.9	2.3	5.0	5.5	3.4
	Min	0.2	-2.2	-0.3	-1.4	-1.0	-4.5	-0.4	-1.0	-3.1	1.8	0.5	-0.4	2.4	0.8	-1.4
	Rng	0.2	2.8	2.8	0.1	4.2	4.2	0.7	4.1	4.0	1.6	2.5	2.7	2.6	4.6	4.8
	Mean	-0.2	-0.3	0.1	-2.5	-1.2	-1.3	-0.3	0.4	-0.7	1.5	1.5	-0.0	2.6	2.7	-0.1
	±σ	0.0	0.8	0.8	0.5	0.9	0.6	0.1	1.0	1.1	0.7	0.8	0.6	1.0	1.1	1.1
4	Max	-0.2	1.0	1.9	-1.5	0.3	0.3	-0.2	2.3	1.0	2.7	3.0	1.3	4.5	4.9	1.8
	Min	-0.2	-2.1	-1.2	-3.4	-3.6	-2.8	-0.5	-1.3	-2.7	0.4	-0.9	-1.9	1.0	-0.7	-3.2
	Rng	0.0	3.1	3.1	1.8	3.9	3.1	0.3	3.5	3.7	2.4	3.9	3.3	3.6	5.6	5.0
	Mean	-1.5	3.6	-5.1	1.4	1.9	-0.5	1.2	2.2	-1.0	-2.9	-0.9	-2.1	-2.4	0.4	-2.9
	±σ	0.2	0.8	0.8	0.1	0.8	0.8	0.5	2.0	2.0	0.8	1.1	0.8	1.4	1.9	1.2
5	Max	-1.2	5.0	-3.0	1.4	3.6	1.1	1.9	7.5	2.9	-1.6	1.5	0.2	-0.2	4.3	0.4
	Min	-1.9	1.4	-6.5	1.1	0.1	-2.3	0.5	-1.3	-5.6	-4.3	-2.9	-3.7	-4.9	-3.0	-6.1
	Rng	0.7	3.5	3.4	0.3	3.5	3.4	1.4	8.8	8.5	2.7	4.4	3.9	4.7	7.4	6.5
	Mean	-1.0	-0.8	-0.2	-2.6	-1.9	-0.7	-0.3	-1.0	0.7	3.1	1.6	1.6	5.8	3.4	2.4
	±σ	0.1	0.7	0.7	0.3	0.9	0.8	0.2	1.3	1.4	1.0	0.8	1.1	1.5	1.4	2.0
6	Max	-0.9	0.3	1.8	-2.1	-0.3	1.7	0.1	1.3	3.3	4.8	4.0	3.9	8.5	6.3	5.2
	Min	-1.2	-2.7	-1.3	-3.0	-4.7	-2.6	-0.7	-3.7	-1.9	1.6	-0.0	-0.6	3.5	1.3	-1.6
	Rng	0.3	3.0	3.1	0.8	4.4	4.3	0.7	5.0	5.2	3.2	4.0	4.5	4.9	5.0	6.8
	Mean				-0.7	0.7	-1.4									
	±σ				1.1	1.9	0.9									
7	Max				1.2	5.9	0.2									
	Min				-2.7	-2.2	-4.7									
	Rng				3.9	8.1	4.9									

Baselines: PSMS-SEMA(12.8km), CG54-KRPI(15km), INED-SHEN(21km), PSMS-PLAT(25km), PSMS-SOHO(33km).

Ion: The double differenced ionospheric delays (in unit of cm), based on the Linear Combination Approach (LCA) and the Local Ionospheric Model, LIM5.

SVs: The number of satellite pairs,
PSMS-SEMA, PSMS-PLAT and PSMS-SOHO:
1:18-4, 2:18-13, 3:18-16, 4:18-19, 5:18-24, and 6:18-27.
CG54-KRPI: 1:21-1, 2:21-3, 3:21-15, 4:21-22, 5:21-23, 6:21-29, and 7:21-31.
INED-SHEN: 1:14-1, 2:14-4, 3:14-7, 4:14-16, 5:14-18, and 6:14-25.

True: The double differenced ionospheric delays obtained from the LCA, which are considered as the true values

LIM5: The double differenced ionospheric errors estimated by the LIM5.

Diff: The difference of single path ionospheric errors between the LIM5 and the Ture.

Mean The average of all data.

σ . The standard deviation of all data.

Max The maximum of all data based on LIM5, LCA, and Diff.

Min The minimum of all data based on LIM5, LCA, and Diff.

Rng =Max-Min.

Table 7.6 Comparison of double differenced ionospheric delays between the true value and the estimation based on LIM6

Unit: centimeter

Ion		Baseline(12.8)			Baseline(15)			Baseline(21)			Baseline(25)			Baseline(33)		
SVs		LIM6	True	Diff	LIM6	True	Diff	LIM6	True	Diff	LIM6	True	Diff	LIM6	True	Diff
	Mean	-0.9	-1.2	0.3	-1.0	-0.7	-0.3	-0.2	-0.6	0.4	1.5	0.4	1.1	3.7	1.9	1.8
	±σ	0.1	0.8	0.7	0.2	0.7	0.8	0.2	0.9	0.7	0.4	0.6	0.6	0.8	1.2	1.1
1	Max	-0.7	0.1	1.9	-0.7	1.3	1.2	0.1	1.7	2.2	2.2	1.8	2.8	5.1	4.6	4.7
	Min	-1.2	-2.9	-0.9	-1.4	-2.2	-2.4	-0.6	-2.8	-1.6	0.8	-0.8	-0.1	2.2	-0.9	-1.0
	Rng	0.5	3.0	2.8	0.7	3.5	3.6	0.8	4.5	3.8	1.4	2.6	2.9	2.8	5.5	5.6
	Mean	-1.0	-1.5	0.5	-1.2	-0.7	-0.5	-1.3	-1.1	-0.2	-1.0	-0.7	-0.2	-0.2	0.4	-0.5
	±σ	0.1	0.8	0.8	1.4	1.3	0.6	0.1	1.1	1.1	0.3	1.4	1.7	0.5	2.1	2.5
2	Max	-0.8	0.3	2.7	0.9	1.6	0.9	-1.2	1.7	1.8	-0.4	1.6	3.5	0.7	3.8	4.3
	Min	-1.2	-3.7	-1.2	-3.8	-4.1	-1.8	-1.4	-3.1	-3.0	-1.5	-4.0	-2.9	-0.9	-3.8	-4.4
	Rng	0.4	4.0	3.9	4.7	5.7	2.7	0.2	4.8	4.7	1.1	5.6	6.4	1.6	7.6	8.7
	Mean	0.3	-0.4	0.8	-1.1	1.0	-2.2	-0.1	1.0	-1.1	2.6	1.8	0.8	3.1	2.9	0.1
	±σ	0.0	0.6	0.6	0.0	0.9	0.9	0.2	1.1	1.0	0.5	0.6	0.6	0.7	1.3	1.1
3	Max	0.4	0.6	2.5	-1.1	3.2	-0.1	0.2	3.2	0.9	3.4	2.9	2.3	4.2	5.5	2.7
	Min	0.2	-2.2	-0.3	-1.2	-1.0	-4.3	-0.4	-1.0	-3.1	1.8	0.5	-0.4	2.0	0.8	-2.0
	Rng	0.1	2.8	2.8	0.1	4.2	4.2	0.6	4.1	4.0	1.6	2.5	2.7	2.2	4.6	4.7
	Mean	-0.1	-0.3	0.2	-2.0	-1.2	-0.8	-0.3	0.4	-0.7	1.5	1.5	-0.0	2.2	2.7	-0.5
	±σ	0.0	0.8	0.8	0.4	0.9	0.6	0.1	1.0	1.0	0.7	0.8	0.6	0.9	1.1	1.1
4	Max	-0.1	1.0	2.0	-1.2	0.3	1.0	-0.1	2.3	1.0	2.7	3.0	1.3	3.9	4.9	1.6
	Min	-0.1	-2.1	-1.1	-2.7	-3.6	-2.3	-0.4	-1.3	-2.6	0.4	-0.9	-1.9	0.8	-0.7	-3.5
	Rng	0.0	3.1	3.1	1.4	3.9	3.3	0.3	3.5	3.6	2.4	3.9	3.3	3.1	5.6	5.1
	Mean	-1.3	3.6	-4.8	1.1	1.9	-0.7	1.0	2.2	-1.2	-2.9	-0.9	-2.1	-2.1	0.4	-2.5
	±σ	0.2	0.8	0.8	0.1	0.8	0.8	0.4	2.0	2.0	0.8	1.1	0.8	1.2	1.9	1.3
5	Max	-1.0	5.0	-2.8	1.2	3.6	0.8	1.5	7.5	2.7	-1.6	1.5	0.2	-0.2	4.3	0.5
	Min	-1.5	1.4	-6.2	0.8	0.1	-2.6	0.4	-1.3	-6.0	-4.3	-2.9	-3.7	-4.1	-3.0	-5.8
	Rng	0.6	3.5	3.4	0.4	3.5	3.4	1.2	8.8	8.6	2.7	4.4	3.9	3.9	7.4	6.3
	Mean	-0.8	-0.8	-0.0	-2.2	-1.9	-0.2	-0.2	-1.0	0.8	3.1	1.6	1.6	4.9	3.4	1.5
	±σ	0.1	0.7	0.7	0.2	0.9	0.8	0.2	1.3	1.3	1.0	0.8	1.1	1.3	1.4	1.9
6	Max	-0.7	0.3	1.9	-1.8	-0.3	2.2	0.1	1.3	3.4	4.8	4.0	3.9	7.2	6.3	4.2
	Min	-1.0	-2.7	-1.1	-2.4	-4.7	-2.1	-0.5	-3.7	-1.8	1.6	-0.0	-0.6	2.9	1.3	-2.3
	Rng	0.3	3.0	3.1	0.7	4.4	4.3	0.6	5.0	5.1	3.2	4.0	4.5	4.2	5.0	6.5
	Mean				-0.5	0.7	-1.3									
	±σ				0.9	1.9	1.0									
7	Max				0.9	5.9	0.5									
	Min				-2.2	-2.2	-4.9									
	Rng				3.2	8.1	5.4									

Baselines: PSMS-SEMA(12.8km), CG54-KRPI(15km), INED-SHEN(21km), PSMS-PLAT(25km), PSMS-SOHO(33km).

Ion: The double differenced ionospheric delays (in unit of cm), based on the Linear Combination Approach (LCA) and the Local Ionospheric Model, LIM6.

SVs: The number of satellite pairs,
PSMS-SEMA, PSMS-PLAT and PSMS-SOHO:
1:18-4, 2:18-13, 3:18-16, 4:18-19, 5:18-24, and 6:18-27.
CG54-KRPI: 1:21-1, 2:21-3, 3:21-15, 4:21-22, 5:21-23, 6:21-29, and 7:21-31.
INED-SHEN: 1:14-1, 2:14-4, 3:14-7, 4:14-16, 5:14-18, and 6:14-25.

True: The double differenced ionospheric delays obtained from the LCA, which are considered as the true values

LIM6: The double differenced ionospheric errors estimated by the LIM6.

Diff: The difference of single path ionospheric errors between the LIM6 and the Ture.

Mean The average of all data.

σ The standard deviation of all data.

Max The maximum of all data based on LIM6, LCA, and Diff.

Min The minimum of all data based on LIM6, LCA, and Diff.

Rng =Max-Min.

7.3 THE VERIFICATION OF DOUBLE DIFFERENCED IONOSPHERIC ESTIMATIONS BASED ON THE LIMS

As described in the previous chapter and the previous section of this chapter, the estimations of ionospheric delays for the base and for the rover have been accomplished respectively with the LIMs and with the ionospheric prediction on the basis of the results of each LIM for test. In the following sections, the ionospheric prediction based on the LIMs is also called the LIMs with no further description. With these ionospheric estimations, the performance of single epoch AFT over long baselines is supposed to be enhanced for the high precision RTK applications after the correction of ionospheric effects. Before applying these ionospheric corrections to the AFT, the verification of these estimation results is still of importance to insure the accuracy and the efficiency of the modelling since the combined effect on the RTK positioning results has involved many sources of observation errors. From the models for reducing the corresponding effect, the distinguishing of the correctness for each model involved may need further considerations.

As popularly used for the verification of many current ionospheric models, the ways to verify the results of ionospheric modelling are carried out by

1. The analysis of the performance of RTK techniques with/without the ionospheric corrections.
2. The comparison with the results of other ionospheric models.

In fact, the first way concerning the algorithm of RTK techniques with some uncertain factors involved, such as the accuracy of the tropospheric and other related error modelling, can hardly verify the results of ionospheric modelling. This also indicates that the efficiency of the modelling does not exactly equal the accuracy of the modelling. The second way has to stand on the assurance of better results with one model comparable.

In this research, two main dominant models based on the Saastamoinen model and the LIMs are essential to reduce the corresponding effect of troposphere and ionosphere for the RTK survey with the AFT over long baselines. Obviously, the verification of tropospheric and ionospheric modelling with current ways may lead to a false

evaluation. A novel concept of verification with the results calculated based on two known stations may be more voracious to evaluate the results of correspondent modelling. As introduced in Chapter 5, the GFA and the LCA based on two known stations, being used for the investigations of the ionospheric and tropospheric behaviour, can respectively obtain the apparent true values of ionospheric and tropospheric delays on the single path and/or the double differenced. With comparisons of the LCA tropospheric results, the tropospheric estimations based on the current model in GASP can hence be evaluated as discussed in Chapter 5. As implemented in Chapter 6, the single path ionospheric results of the GFA even with a constant bias can be used for the evaluation of the results of LIMs on the trend of the single path ionospheric curves estimated. In this section, the ionospheric results of the LCA with a small effect of phase multipath can be used for the verification of double differenced ionospheric delays estimated by the LIMs and the ionospheric prediction.

For the trials of various baselines tested, the double differenced ionospheric delays, estimated by the LCA and the LIMs with the ionospheric prediction, are demonstrated as respectively shown the solid curve and the dot curve in these figures summarized in Appendix B. In each figure, the difference between the curves of the solid and the dot is to demonstrate the fitting of double differenced ionospheric estimations on the apparent true value of ionospheric delays. In addition, from the results of each LIM for test, the related statistics of the mean, the standard deviation, the maximum, the minimum, and the range (the variation) for each pair of satellites over the period of at least an hour are computed for the evaluation of LIMs. These statistics are respectively summarized in Table 7.1 to Table 7.6. From the results of these figures and the statistics, it can be concluded as follows.

1. By a screening of these figures in Appendix B, a proper fitting of the results of LIMs on the true ionospheric results, in general, has shown in each trial for test. The differences between the estimations and the true values have shown the modelling errors with types of a drift or a constant over the period of survey. From a check on the elevation angle of each related satellite shown in Appendix A, a larger bias or drift of modelling errors may occur when the observing satellite is located at the lower angle of about 20°-30°. These cases can be seen, for example,

from the SV: 18-24 in the trial of 12.8km baseline, the SV: 21-31 in the trial of 15km baseline.

2. From the statistic of the mean in Table 7.1 to 7.6, the accuracy of ionospheric modelling and prediction after double differencing can be achieved, in general, at a level of millimeters in a benign environment, but however it can be degraded to a level of more than one centimeter at the following situations:
   (1) As the baseline extends to a distance more than 21km.
   (2) As the path of satellites remains at a low elevation angle of about 20°.
   (3) As the RTK survey operates in a severe multipathing environment.

   For example, the result of Figure 7.2 (an example based on the LIM1) has shown few exceptional cases with low accuracy of ionospheric modelling. For these exceptional cases, the correspondent information, concerning of the factors affecting the modelling accuracy such as the baseline length, the elevation angles, and the multipathing effects, are summarized in Table 7.7. Apparently, the dominant effect of multipath is the unique source of observation error for the ionospheric modelling with the LIMs. As the elevation angle of satellite decreases, the multipathing effect on the modelling may increase and the modelling accuracy can thus be degraded. In addition, as the baseline length increases, the probability of causing the low modelling accuracy (see the item of No.) may increase. As of a consequence, the accuracy of ionospheric modelling with the LIMs is dependent of the multipathing effects, the elevation angle of satellites, and the baseline length. The factor of satellite elevation angle may concerns the determination of the mapping function.
3. As shown in the figures of Appendix B, the high frequency portion of each true ionospheric curve is denoted as the multipathing effects. With a statistic, as shown the standard deviation of item DIFF in Table 7.1 to 7.6, the level of multipathing effects on each satellite pair of the baselines tested can roughly be indicated. For these specific trials, the range of this effect can be a size in average from few millimeters to about 2cm. As shown in these figures of Appendix B, the multipathing effects on the modelling of ionosphere with the LIMs may result to an error of a constant bias and/or a drift. The size of this error can be determined by the structure of coefficient matrix of observation equations, which are related to the geometry of observing satellites and the parameters such as the mapping function and the weighting function for the construction of the accumulated ionospheric delays.

4. The maximum or the minimum in Table 7.1 to 7.6 is a statistic to indicate the actual size of the largest value of ionospheric estimation with the LIMs, the true ionospheric delays, and the difference between the estimation and the true value over the observation period. For instance, the largest modelling error of ionospheric estimation irrespective of overestimated or underestimated based on the LIM1 may have a size of –6.6cm, -4.7cm, -5.5cm, 4.3cm, -6.3cm respectively for the various baseline trials from the statistic of the maximum or the minimum of item DIFF in Table 7.1. With using this statistic, an idea of the actual maximum effects of ionospheric modelling error with the LIMs can therefore be obtained. In general, the larger effect of ionospheric modelling error is shown for each individual epoch.
5. From the item of range (= the maximum - the minimum) in Table 7.1, this statistic is used to demonstrate the variation of ionosphere after double differencing at the surveying area. For these baselines tested, the size of double differenced ionospheric delays may vary from few millimeters in the trial of 12.8km baseline to few centimeters in the trial of 33km baseline. It also indicates that the ionospheric variation after double differencing is highly dependent of the baseline length and the surveying area. Comparing to the variation of the troposphere at the same surveying area (see section in Chapter 5), the ionospheric variation has shown more steady in these specific baselines for test.
6. For the LIMs tested, the results based on the statistic of the maximum or the minimum have shown a slight difference of about few millimeters to 1.5 centimeters between the ionospheric estimations based on the LIMs for test.

Overall, a high precision ionospheric modelling can be accomplished with the LIMs on the basis of a concept of ionospheric profile. In general, the accuracy of the LIMs on double differenced estimations in average, is achievable at a level of millimeters in a benign environment, but however degraded to a level of few centimeters depending on the multipathing effects, the elevation angle of satellites, and the baseline length. Basically, the multipath can be the only source of observation error for the ionospheric modelling with the LIMs. For these longer baselines of 25km and 33km, the degradation of estimation accuracy may be possible due to the effect of improper position of pierce points calculated from the initial solution of rover station whose accuracy can be greatly decreased as the baseline distance increases. The results of the LIM for each mode

shown a slight difference cannot be evaluated until the implementation of the single epoch AFT with the ionospheric corrections on the basis of these results.

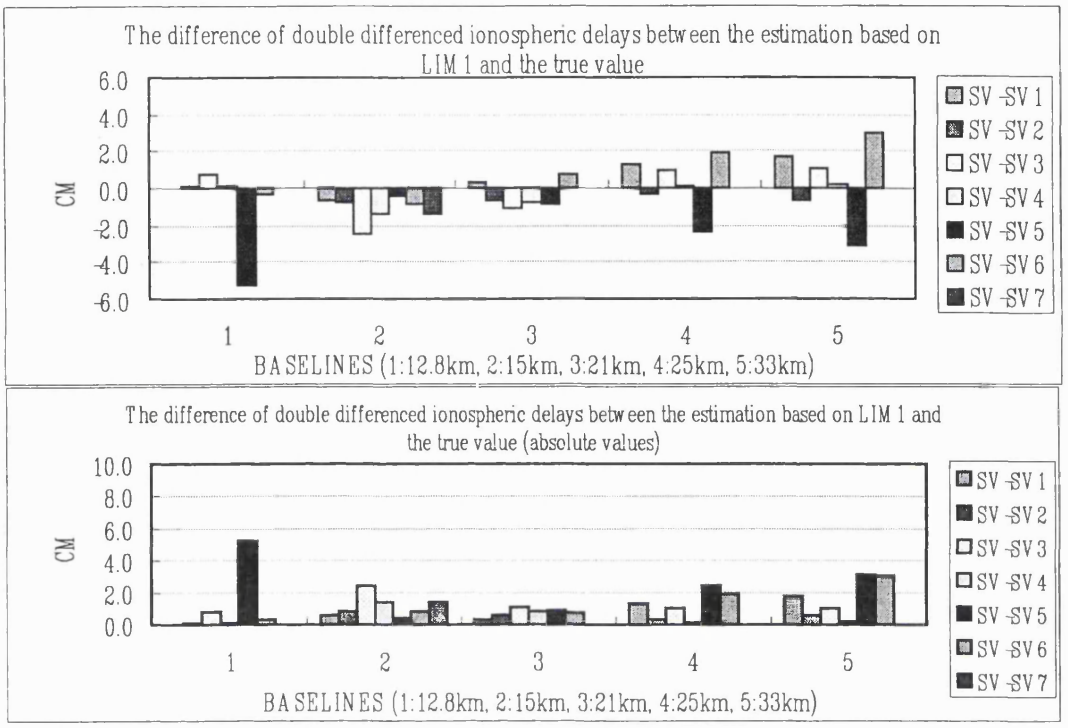

Figure 7.2 The difference of double differenced ionospheric delays between the estimation based on the LIM1 and the true value (absolute values)

Table 7.7 Analysis of ionospheric modelling for the exceptional cases of low accuracy

BASELINES		Length	SV	Accuracy	Multipath	Elevation	No.
BASE	ROVER	(km)		(cm)	(cm)	angle	
PSMS	SEMA	12.8	18-24	-5.2	0.8	28.9-32.1	1
CG54	KRPI	15	21-15	-2.4	1.0	20.0-40.5	1
INED	SHEN	21	—	—	—	—	0
PSMS	PLAT	25	18-24	-2.4	0.8	29.2-32.2	2
			18-27	1.9	1.1	26.6-52.2	
PSMS	SOHO	33	18-24	-3.1	1.2	29.2-32.2	2
			18-27	3.0	2.0	26.5-52.0	

Accuracy: the largest value of the mean in Table 7.1 for all of satellite pair.
Multipath: the largest value of the standard deviation of item DIFF in Table 7.1 for all of satellite pair.
Elevation angle: the elevation angles of the lower satellite on SV (i.e. 24, 15, and 27) from the first epoch to the end epoch.
No.: the total number of the cases of low modelling accuracy for the trials tested.

7.4 THE SINGLE-EPOCH AFT WITH IONOSPHERIC CORRECTIONS

For the adaptation of a wide variety of different receivers, most geodetic GPS processing software developed are able to accept an international format, the Receiver Independent Exchange Format (RINEX, see Gurtner, 1993), which is a well-defined format of GPS data exchange from a binary file to an ASCII file. For the use of single epoch AFT, the exchange of the RINEX file to a compact file, the file of Newcastle Exchange Format (NXF) is required and accomplished by the software of RINTONXF.

At present, there are many segments in current version of the single epoch AFT software where the Saastamoinen model, an empirical modelling on a process of epoch by epoch basis, is suitable to be developed as a segment of the AFT algorithm for reducing tropospheric effects. With the need of a period time of GPS data, the LIMs or the ionospheric prediction seems only suitable to be developed as an independent software for obtaining the ionospheric corrections. Before applying to the AFT for reducing the ionospheric effects, the ionospheric corrections generated by the LIMs and the ionospheric prediction are necessary to be added to the correspondent measurements in the NXF files for the base and the rover respectively.

7.4.1 THE NXF FILE WITH IONOSPHERIC CORRECTIONS

The NXF format has been designed to reduce the files contained in RINEX format to a file type of data required for the use of GPS positioning with the single epoch AFT. The NXF consists of the necessary information, such as the measurements for each type included, the computation of Cartesian coordinates of the satellites in WGS84 based on the broadcast ephemeris or the precise ephemeris (SP3 format), and the basic information of file header (Corbett, 1995).

With the ionospheric corrections for the L_1 and L_2 frequency observations on code and phase generated based on the LIMs and the ionospheric prediction, the new NXF files for the base and the rover are re-constructed to reduce the ionospheric effects based on the following equations:

$P1=P1-\Upsilon_1 I$ .....(7.6.a)

$P2=P2-\Upsilon_2 I$ .....(7.6.b)

$L1=L1+\Upsilon_1 I$ .....(7.7.a)

$L2=L2+\Upsilon_2 I$ .....(7.7.b)

where

P1, and P2 are the L_1 and L_2 frequency observations on code,

L1, and L2 are the L_1 and L_2 frequency observations on phase

I is the ionospheric estimation of the base or the rover.

7.4.2 PERFORMANCES OF SINGLE EPOCH AFT WITHOUT/WITH IONOSPHERIC CORRECTIONS

Based on Equation (7.6) and (7.7), the new NXF files for each mode of the LIM over the baselines tested are generated after adding the correspondent ionospheric corrections into the source file. With these new files, the positioning results of single epoch AFT, over the baselines of 12.8km to 33km, are obtained after the process of GASP as described in Chapter 3. The performances of GASP results represented with the forms of x, y, and z coordinates and baseline length are respectively demonstrated for each LIM on the trials of various length baselines tested as shown the figures of C.6-10, C.11-15, C.16-20, C.21-25, C.26-30, and C.31-35, which are summarized in Appendix C. In these figures, GASP results are denoted with two types of dot line. The curved ones show the individual GASP results and the straight ones show the average of GASP estimation for the period of observation. The average process of GASP estimation has been taken to reduce the effect of multipath since the average of this effect, with a characteristic of sinusoid for a period of observing time, is assumed near zero. Besides, the estimations for these epochs apparently unfixed are excluded for obtaining an unbiased result and thus the subsequent correct evaluations and conclusions.

The precise positioning results, calculated based on processing with GIPSY in a static mode for all experiment baselines, are also shown in the same format as described above in each correspondent figure. These true values, denoted with a solid line in these figures, are used for the evaluation of the estimation results of the AFT. The averaging results of the unbiased estimation, the true, and their difference are summarized in Table 7.8. By comparing the difference between the true values and the unbiased estimation results as demonstrated in Figure 7.3, the performance of AFT without/with ionospheric

corrections (respectively denoted as LIM0, and LIM1 to LIM6 for each mode) may hence be evaluated for the trials tested as follows.

1. For the trials of various length baselines, in general, the performances of AFT on the baseline length for the trials of 12.8km, 15km, and 21km baselines are enhanced after the correction of ionospheric effects based on the LIMs. The level of the positioning accuracy for all fixed epochs can be upgraded from about 3 centimeters to few millimeters for the trials of 12.8km and 21km baselines and from 4 centimeters to 2-3 centimeters for the trial of 15km baseline. The comparison between the results of 15km and 21km baseline trials has found that a slight degradation of positioning results can be resulted even in the shorter baseline. The reason for this can be that a larger error of modelling for the ionosphere and notably for the troposphere have been found in the trial of 15km baseline (see Figure 5.9 in Chapter 5). However, as the baseline distance extends to 25km and more, the process of ionospheric correcting may even lead to a poorer performance. In general, a great degradation of positioning results can be generated for these cases of 25km and 33km baselines.
2. The evaluation of AFT performance, irrespective of using the positioning results of Cartesian coordinates or baseline length (both are summarized in Table 7.8), basically comes to the same conclusions as described above for the successful trials. Depending on the geometry of the contemporary satellite constellation, the degradation of positioning performance on x, y and z co-ordinates can hence be variable after the propagation of the remaining errors of modelling, in particular for the trials of 15km, 25km, and 33km.
3. From the previous evaluation of AFT performance over the baselines for test, it has been found that a nearly unbiased positioning result for the trials of 12.8km and 21km baselines is achievable with the AFT after the correction of ionospheric effects. The evaluation of the LIMs would be more accurate to be accomplished with an analysis of these results from these trials. For the LIMs tested, the results of baseline length over the 12.8km and 21km baselines in Table 7.8 have indicated that the modes of LIM based on the mapping function II apparently have a more accurate positioning result. Among these modes of LIM, the LIM2 with a result of smallest difference for both trials, can be the optimal modelling of ionosphere.

Table 7.8 Difference between the GASP estimation and the true values for the LIMs over the baselines

Unit: cm

BASELINES		Length	LIM	X	Y	Z	Baseline
BASE	ROVER	(km)					length
PSMS	SEMA	12.8	LIM0	0.46	2.36	1.40	-2.97
			LIM1	0.14	-0.55	0.36	0.73
			LIM2	0.23	-0.09	0.60	0.16
			LIM3	0.11	-0.62	0.33	0.80
			LIM4	0.20	-0.15	0.57	0.22
			LIM5	0.28	-0.29	0.54	0.44
			LIM6	0.36	0.13	0.75	-0.08
CG54	KRPI	15	LIM0	-6.31	-4.72	-1.86	-4.08
			LIM1	-7.77	-11.33	-12.23	-2.71
			LIM2	-7.90	-9.75	-9.96	-3.48
			LIM3	-7.83	-10.57	-11.00	-3.08
			LIM4	-7.28	-8.66	-8.71	-3.36
			LIM5	-6.85	-8.72	-9.22	-2.92
			LIM6	-3.00	-5.19	-6.72	-0.72
INED	SHEN	21	LIM0	3.33	0.56	-4.76	-2.99
			LIM1	0.33	-1.22	-0.56	0.93
			LIM2	0.86	-0.91	-0.60	0.23
			LIM3	0.27	-1.25	-0.50	1.01
			LIM4	0.82	-0.93	-0.54	0.29
			LIM5	0.48	-1.07	-0.35	0.68
			LIM6	-2.28	-2.83	1.61	4.39
PSMS	PLAT	25	LIM0	4.41	0.97	0.84	-3.79
			LIM1	-2.58	-2.42	5.65	4.23
			LIM2	2.79	-6.49	2.75	5.62
			LIM3	-60.67	28.7	-69.68	4.02
			LIM4	-2.54	-0.13	3.4	2.97
			LIM5	-6.44	0.6	-9.27	3.15
			LIM6	-0.25	-5.52	-9.34	6.34
PSMS	SOHO	33	LIM0	-16.59	18.71	-10.97	-1.38
			LIM1	58.88	-55.50	37.17	-3.93
			LIM2	24.26	-30.42	5.28	4.44
			LIM3	36.80	-34.09	13.31	-2.93
			LIM4	21.90	-26.68	3.65	3.38
			LIM5	18.50	-18.36	4.08	-0.28
			LIM6	28.47	-34.83	-21.07	4.50

X, Y, Z, and Baseline length: difference between the estimated x, y, z, and baseline length based on the LIMs, and the true x, y, z, and baseline length.

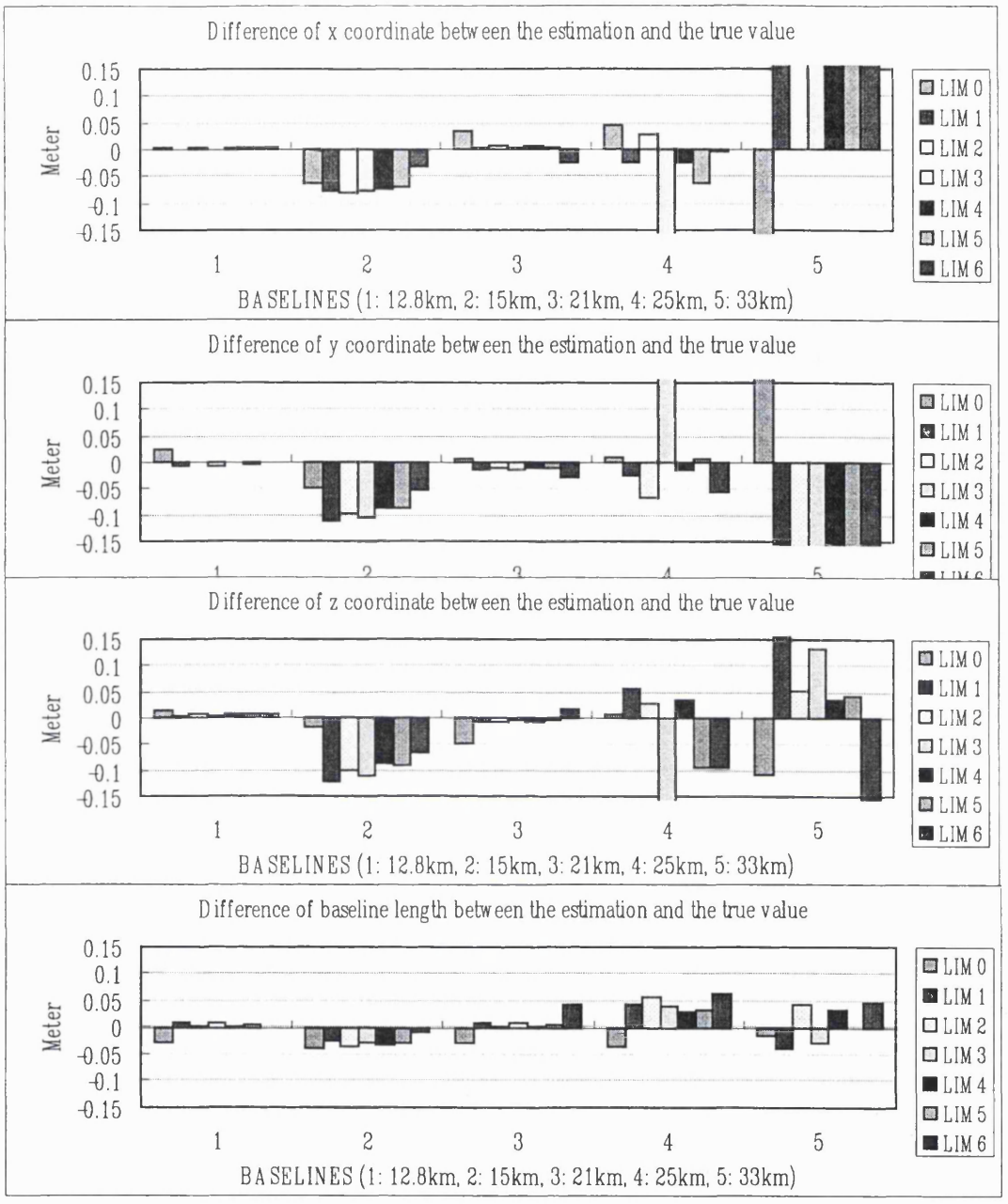

Figure 7.3 The difference between the estimation and the true value on the positioning results of x, y, and z coordinates, and baseline length

7.4.3 THE SUCCESS RATE OF SINGLE EPOCH AFT BEFORE/AFTER THE CORRECTION OF IONOSPHERIC EFFECTS

After the correction of ionospheric effects with the LIMs, the performance of AFT over the baselines from 12.8 km to 33 km have been evaluated with comparisons of the true

values for all of unbiased ionospheric estimations in the forms of x, y, and z coordinates and baseline length. In general, after the ionospheric corrections based on the LIMs, the positioning accuracy of AFT over the baselines below 21km can be upgraded to a level of few centimeters and even millimeters, but a degradation of AFT positioning accuracy is however found as the baseline distance extends to about 25km. For the applications of RTK over long baselines, much concern is not only the positioning accuracy but also the success rate of AFT positioning over the observation period.

In this section, the percentage of success positioning of AFT over the observation period will be pointed out for the trials of various length baselines before/after the correction of ionospheric effects as summarized in Table 7.9 and demonstrated in Figure 7.4 to 7.5. In order to see the improvements after applying the ionospheric model, the criteria (2cm for baselines <13km and 5cm for baselines >13km) used in this chapter are the same as used in Chapter 3.

1. From the results of baseline length in Figure 7.5, two opposite results have been shown for the baseline trials after the correction of ionospheric effects. For instance, the optimal case of LIM2 has indicated that:
   (1) A significant improvement of the success percentage has been made from 17%, 17%, and 60% to about 99%, 65%, and 86% respectively for the trials of 12.8km, 15km, and 21km baselines.
   (2) A degradation of the success percentage has shown a drop respectively from 19% and 33% to below 10% for the trials of 25km and 33km baselines.

   The results also indicate that the AFT positioning even with the ionospheric corrections may result to a failure as the baseline distance extends to more than about 25km. The possible reasons for this will, however, be discussed in the next section.
2. From the results of x, y, and z coordinates as shown in Figure 7.4, the success percentage of the baselines below 21km, in general, has been increased after the ionospheric correction, but the level, due to the geometry of satellites available for the positioning, has shown a variable performance. This can hence indicate that the evaluation of the ionospheric modelling can hardly be accomplished by the analysis of AFT results on x, y, and z coordinates.

3. Among the LIMs for the baselines below 21km, the largest percentage of success rate achievable is the LIM2. The success percentages between the modes for each LIM may have a range of difference about 10 %. These can be seen from the results listed in Table 7.9.

Table 7.9 Percentage of success epochs of AFT over different baselines

BASELINES		Length	LIM	X(%)	Y(%)	Z(%)	Baseline
BASE	ROVER	(km)					length(%)
PSMS	SEMA	12.8	LIM0	80	28	71	17
			LIM1	83	98	90	91
			LIM2	85	99	87	99
			LIM3	85	98	90	91
			LIM4	83	99	89	98
			LIM5	84	99	88	97
			LIM6	85	99	85	99
CG54	KRPI	15	LIM0	2	39	53	17
			LIM1	35	29	22	76
			LIM2	30	30	32	65
			LIM3	35	29	22	76
			LIM4	30	30	33	65
			LIM5	33	30	24	74
			LIM6	40	24	2	46
INED	SHEN	21	LIM0	57	82	51	60
			LIM1	80	90	81	83
			LIM2	76	90	75	86
			LIM3	80	90	82	80
			LIM4	76	89	75	85
			LIM5	76	90	78	84
			LIM6	65	75	68	55
PSMS	PLAT	25	LIM0	44	58	65	19
			LIM1	7	10	1	3
			LIM2	17	20	17	10
			LIM3	6	8	0	2
			LIM4	15	20	15	10
			LIM5	11	17	11	10
			LIM6	11	17	11	10
PSMS	SOHO	33	LIM0	30	45	22	33
			LIM1	4	1	4	3
			LIM2	2	5	7	0
			LIM3	5	0	4	4
			LIM4	3	5	7	2
			LIM5	4	3	5	2
			LIM6	3	10	12	4
Criteria: difference between the estimated x, y, z, and baseline length, and the true x, y, z, and baseline length: < 2 cm (baseline length < 13 km), < 5 cm (baseline length > 13 km).							

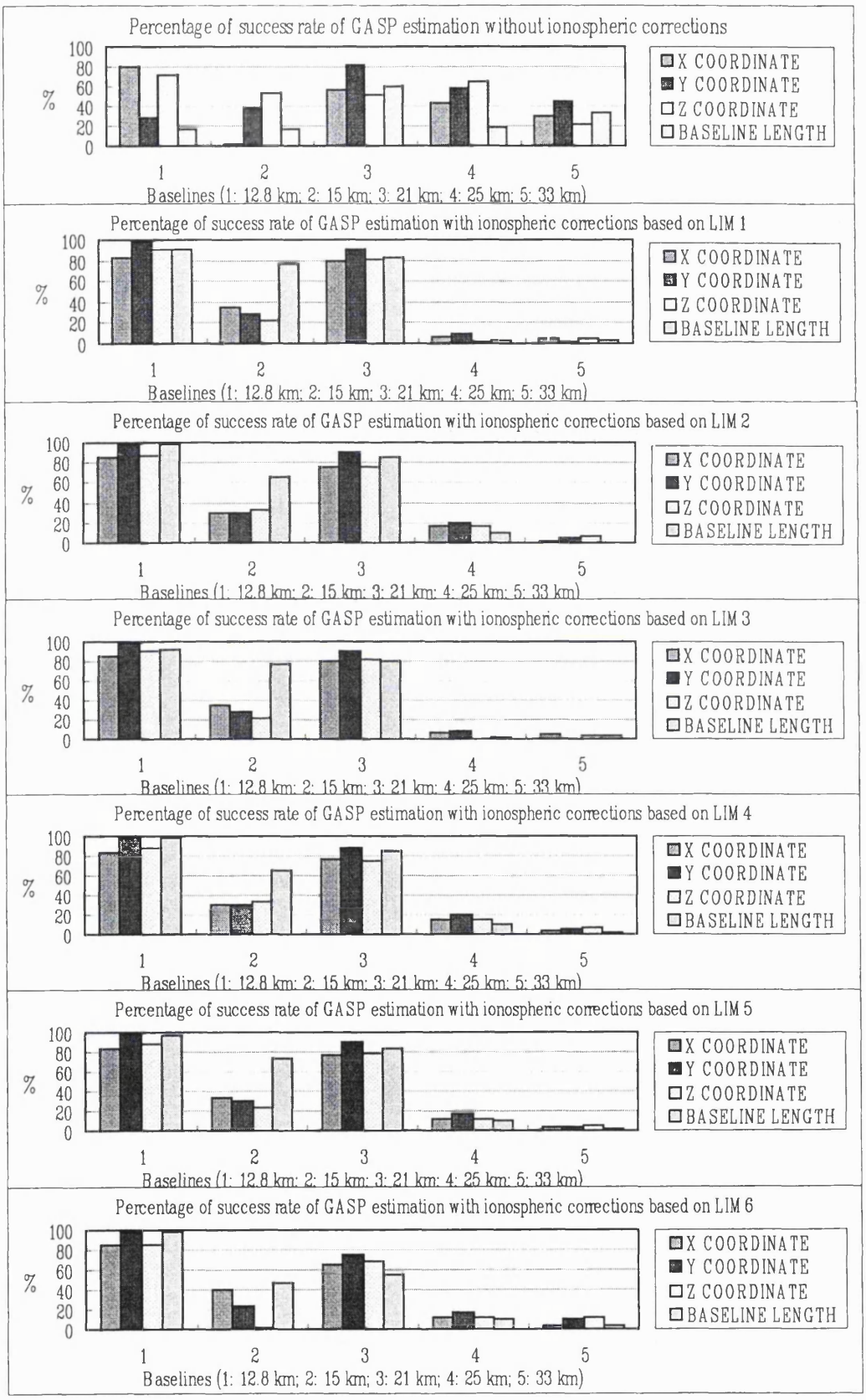

* Criteria: 2cm, baseline length < 13km; 5cm, baseline length > 13km

Figure 7.4 Percentage of success rate of GASP estimation for the LIMs tested

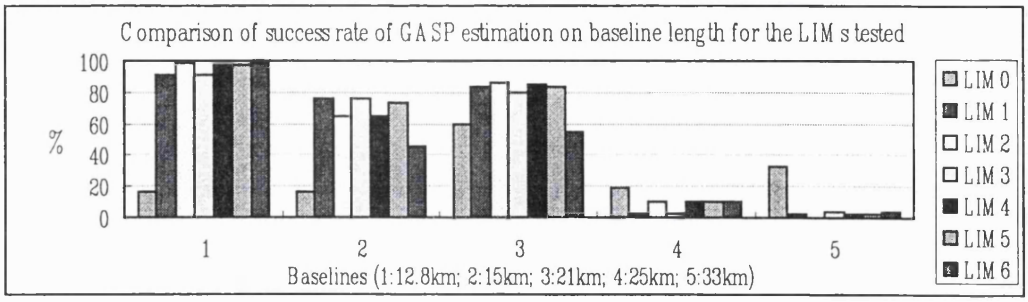

* Criteria: 2cm, baseline length < 13km; 5cm, baseline length > 13km

Figure 7.5 Percentage of success rate of GASP estimation on baseline length for the LIMs tested

7.4.4 SUMMARY OF THE AFT POSITIONING RESULTS AND ERROR ANALYSIS

From the analysis of the AFT performance on the positioning accuracy and the success positioning rate in the previous two subsections, the consistent results of AFT positioning over long baselines can be concluded as follow:

1. The positioning accuracy of AFT over the baselines below 21km can significantly be improved after the correction of ionospheric effects based on the LIMs. As the baseline distance extends to more than about 25km, a worse result with the AFT on both the positioning accuracy and the success positioning rate can be caused even after the ionospheric corrections with the LIMs.
2. Among the LIMs, the second mode of LIM, an ionospheric modelling based on the mapping function II, is the optimal ionospheric modelling to achieve the AFT positioning at a high precision positioning accuracy and with a great improvement of success positioning rate.

Nevertheless, a goal of 100% success rate is still hardly achievable over the baselines below 21km, and a total failure even occurs in the cases of baselines over 25km and 33km, although the modelling accuracy of the LIMs has been evaluated to be accurate. What can be the main problems for these?

As well known, the effects of observation errors on the performance of AFT are mainly from the ionosphere, the troposphere, and the multipath during the transmission of GPS signals to the receivers. The modelling of these errors have been expected to reduce these effects for the enhancement of RTK positioning performance with this technique over longer baselines. In this research, the single epoch AFT has been carried out by the software of GASP with a self-contained model of Saastamoinen for the elimination of tropospheric effects, with several LIMs generated for the elimination of ionospheric effects, and with ignorance of the multipathing effects. The following analysis is hence carried out on the basis of the main effects of three types of errors.

1. As discussed in Section 7.3, the estimation results of ionosphere with the LIMs have been verified with the apparent true values after double differencing. For the trials of various baselines, an accuracy of ionospheric estimation about few millimeters to few centimeters can however be achieved with the LIMs. Nevertheless, the modelling accuracy is highly dependent of the multipathing effects, the elevation angle of satellites, and the baseline length where the multipathing effects can be dominant for the ionospheric modelling with the LIM.
2. The multipathing effect on phase, according to the results investigated in Chapter 5, generally has a size of 1-2cm in average for the baselines tested, which is considered small and usually neglected by current RTK techniques including the AFT. However, the multipathing effects and the derived effects from the multipath during the ionospheric modelling can still be of importance for the AFT positioning.
3. As shown the figures in Appendix A, the fitting of the tropospheric estimations on the apparent true values for the observing epochs is badly performed with the current tropospheric model in GASP. For most cases, even the trends of the tropospheric curves for the estimated and the true are improperly fit. Apparently, the accuracy of this model listed in Table 5.2, in general, is not accurate enough to reduce the tropospheric effects. For example, the large effects of tropospheric modelling errors over about 10cm for most of satellite pairs can be the main reason for the degradation of success rate in this specific case of 15km baseline, comparing to the case of 21km baseline. On the contrary, with the smaller effects of the tropospheric modelling error below 4.81cm in general, the case of longer baseline,

INED-SHEN (21km) can even have a percentage of success rate about 60% before the correction of ionospheric effects. Therefore, the large effects due to the improper tropospheric modelling can be the main problem for the degradation of success rate of these trials. Especially, the cases of longer distance baselines such as the trials of 25km and 33km baselines. The most possible reasons for this can be concluded as follows:

(1) From the investigations on the behaviour of troposphere and ionosphere in Chapter 4, the propagation characteristics of GPS signals for phase along the path of the ionosphere and the troposphere are characterized respectively as the advance and the delay of the L1 and L2 carrier phase observations. In other words, the effects of troposphere and ionosphere on the AFT performance have a quantity of opposite sign and can hence be self-eliminated for portion. As the ionospheric effects have been reduced with the ionospheric model, the effects of tropospheric delays are therefore revealed on the combined effects if the tropospheric model is not accurate enough to reduce the effect itself. Besides, the effects of both errors may increase as the baseline distance increases although the tropospheric effects may have a high correlation with the variation of local atmospheric conditions such as pressure, temperature, and humidity. A larger combined effect due to the reasons above can eventually result to a degradation of success rate of AFT positioning over the baselines of 25km and 33km.

(2) As the baseline distance extends to more than 25km, the ionospheric prediction can be overestimated due to the improper results of all related computations such the position of pierce points, mapping function, and weight function which are originated from the decreasing accuracy of initial solution of rover station. The original situation of self-elimination for the ionospheric and tropospheric effects can become a reverse situation. The combined effect of both modelling errors can hence become much larger, and this may result to a degradation of success rate of AFT positioning.

In fact, a fully successful positioning of AFT over the longer baselines has to rely on an accurate modelling of not only the ionosphere but also the troposphere. The elimination of phase multipathing effects is beneficial to increase the modelling accuracy of the LIM and enhance the AFT performance. In particular, a refined tropospheric model instead of

current one is extremely essential for one to achieve a goal of high precision AFT positioning result with 100% success rate for the RTK applications over long baselines.

7.5 IMPROVEMENTS OF SINGLE-EPOCH AFT WITH THE LIM

For the RTK survey over long baselines, there are two major issues involving the generation of ionospheric model and the AFT positioning with the ionospheric corrections estimated based on the model generated in this research. With considering the practical requirements during the RTK operation, the processing strategies, the accuracy, and the verification of ionospheric modelling are essential to fully reduce the ionospheric effects, and thus enhance the AFT performance for long distance applications of RTK GPS. Based on the results of two issues, the improvements can be summarized as follows.

- The ionospheric modelling and prediction

Over long distances, the disadvantages of using current ionospheric models for the RTK GPS can be concluded as follows.

1. The preprocessing of ambiguity resolution or hardware calibration is necessary and time consuming, and an incorrect or incomplete preprocessing may however degrade the modelling accuracy.
2. The computation, update, and transmission of contemporary ionospheric corrections can hardly be accomplished by current models base on the multi-stations or the networks. Besides, only the hourly ionospheric corrections are provided on the Web. and this cannot satisfy with current requirements of RTK.
3. The definition of so-called sun-earth system to resolve the time variation of ionosphere is not consistent for current models.
4. The modelling accuracy of current models is still limited.

The first problem has been resolved by the LIM with using the L7 observable, which is able to cancel the parameters of ambiguities and hardware biases. The LIM is a modelling on a single known (base) station basis, which can work out the second problem. With considering the spatial and time variation of ionosphere, the mapping

function and the weighting function are used to solve the problem of spatial variation, and the transformation of ionosphere between two epochs is used to handle the problem of time variation. With these processing strategies of the LIM, it may be possible to accurately model the quite sensitive effects of ionosphere as shown in Table 7.10, and also satisfies the requirements of RTK survey.

In addition, the verification of ionospheric modelling as current ways may take a risk of a false evaluation because the verification, with using irrespective of the positioning results or the results of other ionospheric models, has involved the uncertainty of other error effects or the accuracy of the model comparable. In this research, the results obtained from the GFA and the LCA based on two known stations are more accurate and reliable to verify the ionospheric estimation results of LIM. At the first stage of verification with comparisons of the results of GFA, the single path ionospheric estimations based on the LIM have found to be proper at least on the estimation trend. This ensures that the subsequent ionospheric prediction is on a correct ionospheric profile basis. At the second stage of verification with comparisons of the results of LCA, the double differenced ionospheric estimations based on the LIM and the ionospheric prediction are achievable at a centimeter level of modelling accuracy for these typical trials of various baseline distances. As shown in Table 7.10 which is an example of the optimal modelling among the LIMs, the modelling accuracy and the largest effect of LIM2 over the observation period may depend on the multipathing effects, the location of survey area, the elevation angle of observing satellites, and the baseline length.

Table 7.10 The ionospheric estimation and modelling accuracy based on the results of LIM2

Unit: cm

Baseline / LIM	12.8km	15km	21km	25km	33km
Ionospheric estimation	±(1.4±0.2)	±(2.3±0.2)	±(1.4±0.1)	±(2.9±0.9)	±(5.5±1.3)
Modelling accuracy	-5.0 ± 0.8	-2.2 ± 0.9	1.1 ± 0.4	-1.9 ± 0.8	-2.7 ± 1.2
The largest effect	-6.3	-4.9	-5.9	-3.6	-6.0
Results from Table 7.2: Ionospheric estimation, ±(Mean ±.) on item LIM2, Modelling accuracy, Mean ±.on item DIFF, The largest effect, the maximum or minimum on item DIFF.					

- The improvements of AFT performance

Apparently, a centimeter level of modelling accuracy is achievable with the LIM after two stages of verifications. With these precise ionospheric corrections, the AFT performance over these longer baselines can hence be improved. A proper evaluation of the AFT positioning results, accomplished with comparisons of the results obtained from the very precise GPS software, GYPSY II, in a static mode, is first of sure. Moreover, since the AFT positioning has involved two models of troposphere and ionosphere for reducing the correspondent effects, the evaluation of one model with the way of using the AFT positioning results has to stand on the assurance of another model. This is the reason why the popular ways used in current ionospheric models may have a risk of false evaluation. In this research, the verification of tropospheric modelling, similar to the way for the verification of ionospheric modelling, has been implemented with comparisons of the results of LCA based on two known stations in Chapter 5. The results of the tropospheric verification have shown that the tropospheric model applied in GASP is not accurate enough to reduce the tropospheric effects. The performance and the success rate of AFT can therefore affected by the tropospheric modelling errors, which may cause the difficulty of further evaluation for the efficiency of ionospheric modelling on the AFT positioning results. In order to exactly evaluate the efficiency of ionospheric modelling, the statistics of AFT positioning results, such as the mean, standard deviation, the maximum, and the minimum, are first computed before/after the correction of ionospheric effects based on the LIM for all fixed epochs over the observation period. Next, the percentages of AFT success positioning over the observation period are statistically summarized for the trials tested before/after the correction of ionospheric effects.

Table 7.11 The improvements of AFT positioning accuracy and success rate after the correction of ionospheric effect based on the LIM2

Baseline	12.8km		15km		21km		25km		33km	
AFT Positioning	-LIM	LIM	-LIM	LIM	-LIM	LIM	-LIM	LIM	-LIM	LIM
Accuracy(cm)	-2.96	0.16	-4.08	-3.48	-2.99	0.23	-3.79	5.62	-1.38	4.44
Success rate(%)	17	99	17	65	60	86	19	10	33	0

Results from Table 7.9:
-LIM: AFT Positioning before the correction of ionospheric effects based on the LIM2.
LIM: AFT Positioning after the correction of ionospheric effects based on the LIM2.

As shown in Table 7.11, the improvements of AFT positioning accuracy after the correction of ionospheric effects with the LIM have indicated that indeed the LIM can efficiently work on the elimination of ionospheric effects and enhance the AFT performance over the baselines of 12.8km, 15km, and 21km. However, as the baseline distance extends to more than about 25km, the causes of leading to a worse positioning result can be due to the increasing effects of tropospheric modelling errors, the ionospheric modelling errors, and the multipath where the dominant effect can be from the tropospheric modelling errors. Meanwhile, a similar result of success rate of AFT performance is also shown in the same table.

Overall, a significant improvement of AFT with the ionospheric corrections based on the LIM2 can be concluded, if comparing to the achievements of current commercial RTK technique, an initialisation of about 30 seconds and a success rate of 99.93% over the baseline of 14km for the newly LEICA system 500 (Leica, 1999). However, a 100% success positioning results can hardly fully accomplished without the completion of a refined tropospheric modelling.

7.6 CONCLUSIONS

For RTK GPS over long baselines, the limitations of current techniques such as an initialisation or re-initialisation process of at least about 30 seconds cannot satisfy current requirements for a wide range of applications. This problem can be resolved by the single epoch AFT, which is a technique with an ability of instantaneous positioning on the basis of the GPS dual frequency data for a single epoch only. Currently, this technique can be achieved at a level of a centimeter in a benign environment but is however still limited to short baseline applications. For short baselines, multipath is considered as the dominant effect. As the baseline distance increases, other errors such as the ionosphere and troposphere start to decorrelate.

In order to extend the use of this technique for long distance applications, both the ionospheric modelling and the tropospheric modelling are expected to resolve the two dominant problems of this technique over long baselines. Currently, a self-contained

tropospheric model is used to handle the tropospheric problem, and so the modelling of ionosphere is crucial for this to be possible. The LIM for each mode on testing, generated in the previous chapter, is used for the construction of ionospheric profile above the survey area and the ionospheric estimations for the base. Based on the correspondent (vertical) ionospheric profile, the ionospheric prediction to obtain the ionospheric estimations for the rover has been carried out as the procedures described in Section 7.2 for each baseline trial. From the investigation results of double differenced ionospheric effects, the following conclusions can be drawn:

1. The double differenced ionospheric effects on AFT performance

- The double differenced ionospheric effects on average are at a level of ±1.7cm, ±2.7cm, ±1.8cm, ±3.5cm, and ±6.5cm respectively for the trials of 12.8km, 15km, 21km, 25km, and 33km baselines. Obviously, the ionospheric effect after double differencing is highly dependent of the baseline length.
- The largest effect for each individual observing epoch over the period of survey is at a level of 2.1cm, 4.6cm, 2.0cm, 5.2cm, and 9.2cm respectively. For the RTK survey, the actual effect on L_1 and L_2 observations can be a size of 1.5 time and 2.5 time the effects above. This indicates that the ionospheric effects for each individual epoch over the observation period cannot be ignored, and the individual epoch effect after double differencing is also dependent of the baseline length.
- For the LIMs tested, there is a slight difference of millimeter level for the estimated double differenced ionospheric delays between the LIMs.

2. The verification of double differenced ionospheric estimation results

- The verification of ionospheric modelling using current methods may take a risk of a false evaluation because the verification, with using irrespective of the positioning results or the results of other ionospheric models, has involved the uncertainty of other error effects or the accuracy of the model comparable.
- At the second stage of verification with comparisons of the results of LCA, the double differenced ionospheric estimations based on the LIM and the ionospheric prediction are achievable at centimeter level of modelling accuracy for these typical trials of various baseline distances.

- In general, the estimation results with the LIMs are fitted properly on the true ionospheric results in each case of the trials. The differences between the estimations and the true values have shown the modelling errors with types of a drift and/or a constant over the period of survey.
- The accuracy of ionospheric modelling and prediction after double differencing can be achieved, in general, at a level of millimeters in a benign environment, but however it can be degraded to a level of more than one centimeter at the following situations:
  (1) As the baseline extends to a distance more than 21km.
  (2) As the path of satellites remains at a low elevation angle of about 20°.
  (3) As the RTK survey operates in a severe multipathing environment.
- The largest modelling error of ionospheric estimation irrespective of overestimated or underestimated based on the LIM1 may have a size of –6.6cm, -4.7cm, -5.5cm, 4.3cm, -6.3cm respectively for the various baseline trials.

3. Error analysis of ionospheric modelling

- The modelling accuracy of LIMs can be determined by the factors such as the multipathing effects, the location of survey area, the elevation angle of observing satellites, and the baseline length. As the baseline extends to more than 25km, the decreasing accuracy of initial solution of the rover station, concerning of the subsequent computations such as the position of pierce points, the weighting function, and the mapping function, can also affect the results of the ionospheric prediction for the rover.
- Comparing to the variation of the troposphere at the same surveying area, the ionospheric variation has shown steady in these specific baselines for test.

4. The performance of AFT

- The level of the positioning accuracy for all fixed epochs can be upgraded from about 3 centimeters to few millimeters for the trials of 12.8km and 21km baselines and from 4 centimeters to 2-3 centimeters for the trial of 15km baseline. A degradation of positioning results can be generated for the cases of 25km and 33km baselines.

- A significant improvement of the success percentage has been made from 17%, 17%, and 60% to about 99%, 65%, and 86% respectively for the trials of 12.8km, 15km, and 21km baselines. On the contrary, a degradation of the success percentage has shown a drop respectively from 19% and 33% to below 10% for the trials of 25km and 33km baselines.
- The positioning accuracy of AFT over the baselines below 25km can significantly be improved after the correction of ionospheric effects based on the LIMs. As the baseline distance extends to more than about 25km, a worse result with the AFT on both the positioning accuracy and the success positioning rate can be caused even after the ionospheric corrections with the LIMs.
- Among the LIMs for the baselines below 25km, the second mode of LIM, an ionospheric modelling based on the mapping function II, is the best ionospheric modelling to achieve the AFT positioning at a high precision positioning accuracy and with a great improvement of success positioning rate. The success percentages between the modes for each LIM may have a range of difference about 10 %.

5. The evaluation of AFT performance

- An accurate evaluation of the AFT positioning results, accomplished with comparisons of the results obtained from the very precise GPS software, GYPSY II, in a static mode, is first of sure. The evaluation with this way can only be available for the efficiency, but not for the exactness, of the ionospheric model. Since the AFT positioning has involved two models of troposphere and ionosphere for reducing the correspondent effects, the evaluation of one model with the way of using the AFT positioning results has to stand on the assurance of another model. This is the reason why the popular ways used in current ionospheric models may have a risk of false evaluation.
- The verification of tropospheric modelling, similar to the way for the verification of ionospheric modelling, has been implemented with comparisons of the results of LCA based on two known stations in Chapter 5. The results of the tropospheric verification have shown that the tropospheric model applied in GASP is not accurate enough to reduce the tropospheric effects.
- In order to exactly evaluate the efficiency of ionospheric modelling, the statistics of AFT positioning results, such as the mean, standard deviation, the maximum, and

the minimum, are computed before/after the correction of ionospheric effects based on the LIM for all fixed epochs over the observation period

- Next, the percentages of AFT success positioning over the observation period are statistically summarized for the trials tested before/after the correction of ionospheric effects.

6. Error analysis of AFT positioning

- The effects of observation errors on the performance of AFT are mainly from the ionosphere, the troposphere, and the multipath during the transmission of GPS signals to the receivers.
- For the trials of various baselines, an accuracy of ionospheric estimation about few millimeters to few centimeters can however be achieved with the LIMs. Nevertheless, the modelling accuracy is highly dependent of the multipathing effects, the elevation angle of satellites, and the baseline length where the multipathing effects can be dominant for the ionospheric modelling with the LIM.
- The multipathing effect on phase generally has a size of 1-2cm in average for the baselines tested, which is considered small and usually neglected by current RTK techniques including the AFT. However, the multipathing effects and the derived effects from the multipath during the ionospheric modelling can still be of importance for the AFT positioning.
- The fitting of the tropospheric estimations on the apparent true values for the observing epochs is badly performed with the current tropospheric model in GASP. For most cases, even the trends of the tropospheric curves for the estimated and the true are improperly fit.
- Exceptionally, the cases of longer distance baselines such as the trials of 25km and 33km baselines. The most possible reasons for this can be concluded as follows:
  (1) As the ionospheric effects have been reduced with the ionospheric model, the effects of tropospheric delays are therefore revealed on the combined effects if the tropospheric model is not accurate enough to reduce the effect itself. A reverse positioning result can hence be performed.
  (2) The decreasing accuracy of initial solution of rover station, also concerning of the subsequent computations such as the position of pierce points, the weighting function, and the mapping function, may affect the results of the

ionospheric prediction for the rover and the subsequent AFT positioning. These effects may also cause the degradation of success rate and accuracy of AFT positioning.

Overall, a precise ionospheric modelling, crucial for extending the use of single epoch AFT over long distances, can hardly be accomplished without a complete at each step irrespective of the generation and the verification. Through two steps of verification, undoubtedly the LIM proposed in this thesis can actually reduce the ionospheric effects and its accuracy, in general, is achievable at a centimeter level, depending on the multipathing effects, the location of survey area, the elevation angle of observing satellites, and the baseline length. Two methods for the elimination of multipathing effects applied to the LIM cannot work the multipathing problem for increasing the modelling accuracy. The LIM2, on the basis of the mapping function II, is considered as the optimal ionospheric model. Due to this successful ionospheric modelling with the LIM, significant improvements of AFT performance on positioning accuracy and success rate have been made over the baseline distance below 25km. As the distance extends to more than 25km, a worse performance of AFT even occurs after the correction of ionospheric effects. The most possible reason for this can be because of the improper tropospheric modelling effects with the model currently applied. As of a consequence, the elimination of phase multipathing effects is beneficial to increase the modelling accuracy of the LIM and enhance the AFT performance. In particular, a refined tropospheric model instead of current one is essential for one to achieve a goal of fully successful positioning of AFT over the longer baselines for a wide range of RTK applications.

CHAPTER EIGHT
CONLUSIONS AND SUGGESTIONS

8.1 INTRODUCTION

Since GPS has been established, the growing applications on land, sea, and in space have been continuously exploited via improvements to the various positioning techniques. To date, centimetre-level positioning is achievable with many of the current techniques, but nevertheless the precise RTK survey can only operate within a short range and the bottleneck of initialisation or re-initialisation process limits its applications. However, many applications, (especially offshore application and those for which the density and the cost of installation and maintenance, of operating reference stations are important) require RTK to operate over longer distances. Among current techniques, the single epoch AFT with the ability of instantaneously positioning on the basis of single epoch dual frequency GPS data is free of the initialisation or re-initialisation problem. This technique, following research over short baselines (less than 10km) can achieve single centimetre level positioning accuracy, but is, however, limited in application (due to its short range).

In order to extend the single epoch RTK GPS technique to longer distances, and so increase it applications, this research has focused on baselines of about 10km to 30km. The research work presented in this thesis has concentrated on:

1. Current achievements and requirements of RTK GPS
2. The performance of AFT over long baselines
3. The propagation errors and current ionospheric models
4. The behaviour of the ionosphere and troposphere
5. The generation of a high precision local ionospheric model
6. The ionospheric prediction based on the ionospheric profile
7. The performance of AFT with the ionospheric corrections

The investigations on current RTK GPS over long distances have been carried out with consideration of the technical and operational problems. At each stage of the investigation, the exploration of problems, the analysis of error effects, the proposing of

an optimal processing strategy and the evaluation of investigation results were essential to achieve the objects of this research. Consequently, with a self-contained tropospheric model and the generation of an accurate and practical ionospheric model for reducing the corresponding error effects, the aim of this research to extend RTK GPS with single epoch AFT for long distance applications has been achieved to a limited extent.

8.2 CONCLUSIONS

From the investigation results over various length baselines for test, the conclusions drawn can be summarized as follows.

1. GPS relative positioning over long baselines

- Shortening the time of initialisation or re-initialisation, and extending the use of current RTK techniques for long distances are two main challenges of achieving the goal for a wide range of high precision RTK applications. Current RTK GPS requires considering many aspects in terms of the technology and the operation, such as the capability, the reliability, and the accuracy of the technique, the computation, update, and communication of corrections, and the cost of establishment and maintenance of operating reference stations.
- The LRK with a processing strategy of triple differenced positioning, the DGPS with the corrections based on the networks, and the commercial RTK software with an achievement of few tens second initialisation over the baselines of less than about 14km, cannot fully satisfy the requirements of current RTK GPS. The single epoch AFT, with an ability of providing the instantaneous positions on the basis of a single epoch of GPS dual frequency data, is potentially the optimal for RTK GPS. Without the problem of initialisation or re-initialisation, this technique is immune to cycle slips and can currently achieve a centimeter-level positioning accuracy over the baseline of less than 10km. It, however, requires an ionospheric model to reducing the corresponding effects so as to enhance its positioning performance for long distances.
- In terms of the practical and technical requirements of RTK GPS, the following conclusions can be drawn.

  (1) The optimal strategy of RTK GPS is based on single epoch AFT positioning.

(2) The reduction of the effect of measurement errors such as the ionospheric and tropospheric delays can be expected to extend the use of current techniques to long distances, and a more accurate modelling of these errors is necessary for this to be possible.

(3) For modelling these errors, using single a reference station would be more practical than using networks.

(4) For ionospheric modelling, using the delta range $L4$ would be more practical and could possibly lead to the achievement of a highly accurate modelling.

2. The single epoch AFT over long distances

- From the investigation carried out with the AFT and an existing tropospheric model, a poor performance, in general, has be shown in baseline trials of 12.8km to 33km. Basically, the main effects of observation errors on these consist of the tropospheric, the ionospheric, and the phase multipathing. The dominant effects for this may be due to the ionospheric delays (perhaps also including the error of imperfect tropospheric modelling).
- The criteria to evaluate the investigation results at this stage has been carried out with the GPS software, GIPSY II, in a static mode on the basis of the (at least) hourly dual frequency data.
- Irrespective from the short baseline investigation or from the long baseline investigation, both of the results have indicated that the tolerable error size of the AFT is quite narrow and it appears to be less than about two centimeters. This also indicates that the success of AFT positioning over long baselines requires an accurate modelling of the dominant errors for exactly reducing the correspondent effects.

3. The propagation errors and current ionospheric models

- The propagation characteristics of GPS signals for code and for phase along the path of the ionosphere can be characterized as the delay of the code (called *group delay*) and the advance of the carrier phase (called *phase advance*). This is mainly because the phase velocity based on binary phase modulated is larger than the

vacuum speed and the group (code) velocity based on the modulation or the energy is smaller than vacuum speed by the same amount but opposite sign.

- In the non-dispersive region of the atmosphere the effect on GPS code and phase measurements is the same because refraction in a neutral medium is not dispersive for the radio signals below 30 GHz frequency. Usually this effect of tropospheric propagation can be expressed as a function of temperature, pressure, and relative humidity.
- The ionospheric effect changes with the time of the day, season, location of the receiver, viewing direction, solar activity, the state of the earth's magnetic field. The severe scintillation can occur during the solar maximum or strong magnetic storm periods and cause severe problems such as loss of signal lock. Therefore, monitoring and broadcasting the ionosphere by an accurate, reliable, and practical ionospheric model is necessary for many GPS operations possibly even over short baselines.
- At present, global and regional ionosphere maps (broadcast on the web) based on global ionosphere models (GIM) and regional ionosphere models (RIM) are available for wide area DGPS (WADGPS) and worldwide DGPS (WWDGPS). Because of the limited accuracy of these models, a local ionosphere model (LIM) using local GPS networks has been developed to see whether it would be possible to enhance the performance of RTK GPS. To date local area DGPS (LADGPS) using a single-reference station has been attempted but the accuracy decreases with increasing distance from the base station (WARSAW, 1998). Nevertheless, LADGPS may become mainstream DGPS method for GPS services in the future.
- The ionospheric modelling based on the single ionospheric layer at the height of spherical shell about 350km is carried out with using phase data better than using code data of dual frequency GPS measurements under the pre-assumption of the instrument biases being constant in a few hour period of time. Preprocessing of cycle slip detection and repair is necessary for the ionospheric modelling, therefore the software dealing with the problem of the cycle slips has to be very reliable and able to get a time series of data 100% "clean".
- The preprocessing of ambiguity resolution or hardware calibration is necessary for current ionospheric modelling using the observable of either $L4$ or L_C. However, the calibration of hardware biases is time consuming and a 100% success of ambiguity fixing is not always fully accomplished. The construction of the ionosphere with the

mapping function and the vertical TEC to deal with the spatial variation of ionosphere can be the key problems of the ionospheric modelling. In current models, the definition of the origin of the so-called sun-earth reference system used for dealing the time variation of ionosphere is not identical. The drawbacks above of current models lead to the degradation of modelling accuracy.

- Although the positioning accuracy or the success percentage of ambiguity resolution is the popular way to evaluate the ionospheric modelling, it can be affected by the other remaining errors like the tropospheric modelling errors. However it may be a good way to verify the estimation results of ionospheric modelling if taking two steps, a refined approach for the exactness of the modelling and the positioning accuracy (or the percentage of ambiguity resolution) for its efficiency when applying to DGPS or RTK GPS.

4. The behaviour of ionospheric delays and tropospheric delays over long distances

- The investigation on the behaviour of the atmosphere delays over long baselines has been carried out with using two approaches based on two known stations for the same trials as tested in previous chapter. The result of GFA, even biased by a constant hardware error, is still useful for investigating the behaviour of single path ionospheric delays. The LCA is used to obtain the apparent true double differenced ionosphere with using the observable of ionospheric combination and the apparent true double tropospheric delays with using the observable of ionosphere-free combination. Both investigation results of double differenced ionosphere and troposphere are respectively affected by the phase multipath of ionospheric combination and ionosphere-free combination.
- The behaviour of single path ionospheric delays over long baselines tested has the following characteristics. Generally, the lower the elevation angle of the satellite the greater the rate of change of the ionospheric delays. The ionospheric delays change very slowly if the satellite maintains at the same elevation, irrespective of whether it is low or high. The maximum hourly ionospheric change has been found to be about 3.5m.
- The range of double differenced ionospheric errors including the bias of multipathing effect is about 3.2cm in the area of the shortest distance trial, and about 5.9cm in the area of the longest distance one for an hourly variation. In

general, as the baseline distance increases, the ionospheric effect slightly increases, and the increasing rate on average is a level of around 2-3 cm per hour from a baseline length of 12.8 km to 33km

- The effect of double differenced tropospheric errors can be a level of about –3.6cm to 6.9cm on average for these trials. The area of greatest variation of double differenced tropospheric errors about 11.3cm is located at the stations, CG54-KRPI, which is a 15km baseline, and the smallest one, of about 3cm, is located at stations, PSMS-SOHO, which is a trial of 33km baseline. It seems that the variation of tropospheric errors is more dependent of local environments including the pressure, the temperature, the water vapor, and the height of operation stations, and the distance dependence of this error can hardly be seen in these trials.

5. The evaluation of tropospheric model

- Currently, the Saastamoinen model has been used to handle the tropospheric problem in GASP, but unfortunately this model, being evaluated with comparisons of the true values, obtained from the LCA, cannot efficiently reduce the tropospheric effects, especially when the satellite is at low elevation angles.
- The evaluation of the tropospheric modelling results, estimated with the exiting model in AFT algorithm, has been carried out with comparisons of the true results obtained from the LCA. Although the true results involving the effect of the ionosphere-free multipath may be overestimated, the limited accuracy of tropospheric model currently applied in GASP can be confirmed from the improper fitting of the estimation results on the true values.
- On average, the modelling errors can be a level of ±8.22cm, ±5.08cm, ±2.64cm, ±1.34cm, and ±3.31cm respectively for the trials of 12.8km to 33km. As a result, a refined tropospheric model instead of current one may be required for successful AFT positioning over long distance.

6. Local ionospheric modelling

- As well as the drawbacks relating to the technical problems concluded in the previous investigation on current ionospheric models, the following practical problems associated with RTK or DGPS operations means that it can hardly satisfy

current accuracy and range requirements. If the ionosphere changes too quickly, the time to compute, update, and transmit the temporal ionospheric corrections for grid can hardly be implemented with a model based on multi-stations the networks. Besides, currently only hourly corrections are provided on the Web.

- Pointing to the drawbacks of current ionospheric models, a novel modelling based on a single reference (base) station has been carried out with the following refinements.
  (1) The processing strategies of LIM, such as adoption of the optimal software for cycle slip detect and repair and the use of observable L7, can minimize the possibility of the effects of observation errors. The remaining effects on modelling can only be the phase multipathing.
  (2) Resolving the problem of ambiguity resolution or hardware calibration with using the L7 observable, the LIM has the following benefits: saving the processing time of resolving the ambiguities and hardware biases and avoiding the possible problems and effects of ambiguities unresolved or false-calibration of hardware biases.
  (3) Instead of the transformation of the sun-earth system (often used in current ionospheric models but the definition of the system is not consistent), the concept of transformation with a weighting function between two adjoining epochs is used to deal with the problem of time variation of ionosphere for the modelling.
  (4) The testing of several LIMs based on two types of mapping functions and two methods for the elimination of the unresolved phase multipathing effects has been carried out.
  (5) The verification of LIMs on single path and double differenced results is considered and carried out with comparison of the results from the GFA and the LCA based on two known stations. The evaluation of LIMs can hence be more accurate and reliable than that carried out in the usual ways using positioning results or via comparisons of other models.
- The estimation results with the LIMs have found that the ionospheric effect is highly dependent of the elevation angle and the azimuth of observing satellites and the surveying area (or maybe time). For these typical trials operated at the base stations of PSMS, CG54, and INED over the observation period of at least an hour, the estimation results of single path ionospheric delays with the LIMs on average

may respectively have a level of up to near 8.6m, 4.8m, and 3.8m. These effects on the dual frequency signals can be a level of 13.3m, 7.4m, 5.9m on L_1 and 21.9m, 12.2m, 9.7m on L_2.

- Basically, the modes of LIM for test proposed in this thesis can be divided into two groups: one is based on mapping function I, and another is based on the mapping function II. In each group, the ionospheric estimations on single path between the modes of LIM with/without the elimination of multipathing effects may have a slight difference of couples of tens centimeters.
- The smooth curves of ionospheric estimations have indicated that 100% "clean" data are available after the preprocessing of cycle slips with the TurboEdit. In other words, it can be assured that the estimation results of LIMs were not affected by cycle slips in any the trials carried out.

7. The evaluation of LIMs performances

- The verification of ionospheric modelling using current methods may risk a false evaluation because the verification, irrespective of the positioning results or the results of other ionospheric models, has involved the uncertainty of other error effects or the accuracy of the model used for the comparison. The two steps of verification proposed in this thesis to evaluate the performance of the LIMs does not have the drawbacks of using current ways, and are far more accurate and reliable.
- The first step of verification, by checking the estimation trend of single path ionospheric delays with comparisons of the apparent true values obtained from the GFA, has found that the LIMs on the estimation trend of single path ionospheric delays have properly performed over the observation period.

8. The RTK applications of LIMs

- For RTK applications over long distances, the generation of LIMs is for two purposes:
  (1) Obtaining the ionospheric corrections at the base station for reducing the correspondent ionospheric effects,

(2) Constructing the vertical ionospheric profile above the surveying area for predicting the ionospheric delays (or corrections) at the rover station.

- The estimation results with the LIMs have been verified and found that the single path ionospheric errors can be properly modelled at least on the estimation trend over the observation period for the trials tested. This ensures that the corresponding ionospheric profile above the survey area for each trial can be appropriately constructed for the subsequent ionospheric prediction at the rover station.

9. The ionospheric prediction (The double differenced ionospheric effects on AFT performance)

- Based on the (vertical) ionospheric profile constructed with the LIM for each mode, the ionospheric prediction to obtain the ionospheric estimations for the rover has been carried out as the procedures described in Section 7.2 for each baseline trial. For the RTK positioning, the ionospheric effects for the base and the rover can hence be reduced on the basis of the correspondent ionospheric estimations (corrections).
- The investigation results have found that the ionospheric effect after double differencing is highly dependent of the baseline length. The double differenced ionospheric effects in average can be a level of ±1.7cm, ±2.7cm, ±1.8cm, ±3.5cm, and ±6.5cm respectively for the trials of 12.8km, 15km, 21km, 25km, and 33km baselines. The largest effect for each individual observing epoch over the period of survey can be a level of 2.1cm, 4.6cm, 2.0cm, 5.2cm, and 9.2cm where the actual effect on L_1 and L_2 observations can be a size of 1.5 time and 2.5 time the effects above for the RTK survey. For the modes of LIMs tested, there is a slight difference at the millimeter level for the estimated double differenced ionospheric delays between the LIMs.

10. The verification of double differenced ionospheric estimation results

- The second stage of ionospheric modelling verification has been carried out via comparisons of the apparent true results obtained from the LCA. The results have found that the double differenced ionospheric estimations based on the LIM and the

ionospheric prediction can be achieved at a centimeter level of modelling accuracy for these typical trials of various baseline distances.

- In general, the estimation results with the LIMs fit properly to the true ionospheric results in each case of the trials. The differences between the estimations and the true values have shown the modelling errors with types of a drift and/or a constant over the period of survey. The largest modelling error of ionospheric estimation irrespective of overestimated or underestimated based on the LIM1 may have a size of –6.6cm, -4.7cm, -5.5cm, 4.3cm, -6.3cm respectively for the various baseline trials.
- The accuracy of ionospheric modelling and prediction after double differencing can be achieved, in general, at a level of millimeters in a benign environment, but however it can be degraded to a level of more than one centimeter at the following situations:
  (1) As the baseline extends to a distance more than 21km,
  (2) As the path of satellites remains at a low elevation angle of about 20°,
  (3) As the RTK survey operates in a severe multipathing environment.
- The modelling accuracy of LIMs can be determined by the factors such as the multipathing effects, the location of survey area, the elevation angle of observing satellites, and the baseline length. As the baseline extends to more than 25km, the decreasing accuracy of initial solution of the rover station, issues concerning of the subsequent computations such as the position of pierce points, the weighting function, and the mapping function, can also affect the results of the ionospheric prediction for the rover.

11. The evaluation and the performance of AFT with ionospheric corrections

- An accurate evaluation of the AFT positioning results, accomplished with comparisons of the results obtained from the very precise GPS software, GYPSY II, in a static mode, is first of sure. This evaluation can only available for the efficiency, but not for the exactness, of the ionospheric model. Since the AFT positioning has involved two models of troposphere and ionosphere for reducing the correspondent effects, the evaluation of one model with this method of using the AFT positioning results has to stand on the assurance of another model. This is the

reason why the popular ways used in current ionospheric models may have the risk of a false evaluation.

- The positioning accuracy of AFT over the baselines below 25km can significantly be improved after the correction of ionospheric effects based on the LIMs. As the baseline distance extends to more than about 25km, a worse result with the AFT on both the positioning accuracy and the success positioning rate can be caused even after the ionospheric corrections with the LIMs. The level of the positioning accuracy for all fixed epochs can be upgraded from about 3 centimeters to few millimeters for the trials of 12.8km and 21km baselines and from 4 centimeters to 2-3 centimeters for the trial of 15km baseline. A degradation of positioning results can be generated for these cases of 25km and 33km baselines.
- A significant improvement of the success percentage has been made from 17%, 17%, and 60% to about 99%, 65%, and 86% respectively for the trials of 12.8km, 15km, and 21km baselines. On the contrary, a degradation of the success percentage has shown a drop respectively from 19% and 33% to below 10% for the trials of 25km and 33km baselines.
- Among the LIMs for the baselines below 25km, the second mode of LIM, an ionospheric modelling based on the mapping function II, is the best ionospheric modelling to achieve the AFT positioning at a high precision positioning accuracy and with a great improvement of success positioning rate. The success percentages between the modes for each LIM may have a range of difference about 10 %.

12. Error analysis of AFT positioning after the correction of ionospheric effects

- The effects of observation errors on the performance of AFT are mainly from the ionosphere, the troposphere, and the multipath during the transmission of GPS signals to the receivers. For the trials of various baselines, an accuracy of ionospheric estimation about few millimeters to few centimeters can however be achieved with the LIMs. Nevertheless, the modelling accuracy is highly dependent of the multipathing effects, the elevation angle of satellites, and the baseline length where the multipathing effects can be dominant for the ionospheric modelling with the LIM.
- The multipathing effect on phase generally has a size of 1-2cm on average for the baselines tested, which is considered small and usually neglected by current RTK

techniques including the AFT. However, the multipathing effects and the derived effects from the multipath during the ionospheric modelling can still be of importance for the AFT positioning.

- The fitting of the tropospheric estimations on the apparent true values for the observing epochs is badly performed with the current tropospheric model in GASP. For most cases, even the trends of the tropospheric curves for the estimated and the true are improperly fit.
- Exceptions to this are the cases of longer distance baselines such as the trials of 25km and 33km baselines. The most probable reasons for this are thought to be as follows:
  (1) As the ionospheric effects have been reduced with the ionospheric model, the effects of tropospheric delays are therefore revealed on the combined effects if the tropospheric model is not accurate enough to reduce the effect itself. A reverse positioning result can hence be performed.
  (2) The decreasing accuracy of the initial solution of the rover station, also impacts on the subsequent computations such as the position of pierce points, the weighting function, and the mapping function, may affect the results of the ionospheric prediction for the rover and the subsequent AFT positioning. These effects may also cause the degradation of success rate and accuracy of AFT positioning.

Over all, the research work represented in this thesis has participated in increasing the capability of current techniques over long distances for a wide range of high precision RTK GPS applications. To date, the bottlenecks of current RTK GPS, the initialisation or re-initialisation process and the limitation of short range applications, require to be resolved for a wide range applications. The greatest advantage of using the single epoch AFT can substantially resolve the problem of initialisation or re- initialisation which is the bottleneck of using other techniques. Even with an existing tropospheric model for reducing the effects, the degradation of AFT performance as the baseline distance increases can be seen from the investigation results in Chapter Three. Over short baselines, the problem is limited to multipathing effects, but as the distance increases the ionospheric errors (maybe including the tropospheric modelling errors) begin to decorrelate. This has been confirmed from the investigation on the behaviour of ionospheric and tropospheric errors over long distances in Chapter Five. The effects of

both errors may become dominant over the baseline distance more than 10km. To extend the use of AFT over long distances, a self-contained tropospheric model is used for reducing the tropospheric effects, and several modes of local ionospheric models with the ionospheric prediction for test are expected for the reduction of ionospheric effects, implemented in Chapter Six and Seven. From the final results, a significant improvement of the AFT positioning with the second mode of LIM can be achieved in the trials of baselines below 21km, but a worse a result is however found in the trials of baselines more than 25km.

8.3 SUGGESTIONS FOR FUTURE WORK

For the RTK survey over long distances, an attempt of extending the use of single epoch AFT for long distances on the basis of single epoch dual frequency data was carried out with a existing tropospheric model and the ionospheric model generated for reducing the correspondent effects. The significant improvement of AFT performance over the baseline length of less than 21km is achievable after the ionospheric correction with the ionospheric model generated, but a fully successful positioning result over the observation period can still not be obtained. As the baseline distances extend to more than 25km, the positioning after the ionospheric correction performance can actually be degraded. The reason for this, as described in conclusions, can be mainly because of the imperfect modelling of troposphere since the ionospheric modelling accuracy can be achieved at a level of few centimeters. Therefore, for achieving a goal of 100% success AFT positioning over longer distances, specific suggestions for further research work are as follows

1. The first essential work, which is being carried out by many researchers, is to refine the tropospheric models. Currently, a combination modelling with the empirical tropospheric model and a refined mapping function is widely being tested. From the investigation on the behaviour of troposphere, the results have indicated that the variation of tropospheric errors is more dependent of local atmospheric environments. Due to this local characteristic of troposphere, a concept of local tropospheric modelling based on a single reference station may be possible for achieving an accurate model (as is carried out for instance in some static GPS processing).

2. Increasing the accuracy of the ionospheric model proposed in this thesis has to rely on the elimination of multipathing effects (the main remaining error effect on the modelling), which can be very difficult task in a scenario of RTK. From the testing results of mode 3 to 6 of LIM, two methods for reducing the multipathing effects cannot work. Currently, investigations based on the phase multipath with Signal-to-Noise Ratio (SNR) may find a solution. A well-designed antenna such as the choke ring ought to be used for reducing the multipathing effects during the RTK survey.
3. The tolerable error size of the AFT has been found to be quite narrow either from the short distance investigation in the previous research or from the long distance investigation in this research. For the AFT itself, the algorithm may be modified as follows.
   (1) As concluded in the previous research on the AFT over short baselines, the approximate solution has to be good for fully appreciating the benefits of the flexible search process. Hence, the computation of the approximate solution with the observable of widelane or ionosphere-free combination may obtain a better result.
   (2) In the investigation of AFT positioning over short baselines, the combination of the L_1 with a scaled L_2 phase data was one of the important factors to achieve the success of final results. For short distance AFT, this combined observable is suitable but as the baseline distance increases, the effects of tropospheric and ionospheric errors become the dominant problems for the AFT to fix the ambiguities successfully. Refining the current tropospheric model applied in AFT is one way to handle the problem of imperfect modelling. If an accurate tropospheric model still cannot be obtained, another way is using a combination such as $L_1 - 0.8\ L_2$, which is able to reduce the tropospheric effects substantially. By this way, the geometry strength of satellite constellation may become much weaker but the use of lower elevation satellites may compensate for this.

REFERENCES

Aarons J. and Basu S. (1994), "Ionospheric Amplitude and Phase Fluctuation at the GPS Frequencies", Proceedings of ION GPS-94, Salt Lake City, Utah USA, pp. 1569-1578.

Abidin H. Z. (1993a), "On-the-Fly Ambiguity Resolution: Formulation and Results", Manuscripta Geodaetica, 18, pp. 380-405.

Abidin H. Z. (1993b), "On-the-Fly Ambiguity Resolution", GPS World, April 1994, pp. 40-50.

Al-Haifi Y. M. (1996), "Short Range GPS Single Epoch Ambiguity Resolution", PhD Dissertation, University of Newcastle upon Tyne, UK.

Al-Haifi Y. M., Corbett S. J., and Cross, P. A. (1998), "Performance Evaluation of GPS Single-Epoch On-the-Fly Ambiguity Resolution", Journal of The Institute of Navigation, Winter 1997-1998, Vol. 44, No. 4, pp. 479-487.

Ashkenazi V. and Summerfield P. J. (1989), "Rapid Static and Kinematic GPS Surveying with or without Cycle Slips", The Second International Conference on Differential Satellite Navigation System, London, 29 March-2 April 1993.

Ashkenazi V. and Summerfield P. J. (1992), "Wide Area Differential GPS: A Performance Atudy", Proceedings of ION GPS-92, Albuquerque, New Mexico USA, , pp. 589-598.

Axelrad P. and MscDcran P. (1994), "Use of Signal-To-Noise Ratio for Multipath Error Correction in GPS Differential Phase Measurements: Methodology and Experimental Results", Proceedings of ION GPS-94, Salt Lake City, Utah USA, pp. 655-666.

Barboux J. P. (1994), "Practical Real Time Kinematic Applications of GPS", The Third International Conference on Differential Satellite Navigation System, London, April 1994.

Bar-Sever Y. E. (1996), "Strategies for Near Real Time Estimation of Precipitable Water Vapor", Proceedings of the 1996 IGS Workshop, pp. 165-176.

Bar-Sever Y. E. and Kroger P. M. (1996), "Strategies for GPS-Based Estimates of Troposphere Delay", Proceedings of ION GPS-96, Kansas City Convention Center, Missouri USA, pp. 615-622.

Bertiger W. I., Bar-Sever Y. E., Haines B. J., Iijima B. A., Lichten S. M., Lindqwister U. J., Mannucci A. J., Muellerschoen R. J., Munson T.N., Moore A. W., Romans

L. J., Wilson B. D., Wu S. C., and Yunck T. P. (1998), "A Real-Time Wide Area Differential GPS system", Journal of The Institute of Navigation, Winter 1997-1998, Vol. 44, No. 4, pp. 433-447.

Beser J. and Balendra A. (1994), "Ehanced Ionospheric Delay Compensation Using GLONASS", Proceedings of ION GPS-94, Salt Lake City, Utah USA, pp. 1609-1617.

Beutler G., Gurtner W., Hugentobler U., Rothacher M., Schildknecht T. and Wild U. (1989), "Ionosphere and GPS Processing Techniques", Astronomical Institute, University of Berne, Switzerland.

Bishop G., Basu S., Groves K., and Smitham M. (1996), "Upcoming Ionospheric Impacts on GPS at Solar Max, What do we know / What do we need? ", Proceedings of ION GPS-96, Kansas City Convention Center, Missouri USA, Vol. 1, pp. 595-604.

Blewitt G. (1989), "Carrier Phase Ambiguity Resolution for the Global Positioning System Applied to Geodetic Baselines up to 2000 km", Journal of Geophysical Research, Vol. 94, No. B8, pp. 10.187-10.203.

Blewitt G. (1990), "An Automatic Editing Algorithm for GPS data", Geophysics Research Letter, Vol. 17, No. 3, pp. 199-202.

Blewitt G. (1997), "Basics of the GPS Techniques: Observation Equations", Lecture Notes, Department of Geomatics, University of Newcastle upon Tyne, UK.

Barnes J. (1999), " Multipathing Effects on GPS", Personal Communications.

Brunner F. K. and Welsch W. M. (1993), "Effect of the Troposphere on GPS Measurements", GPS World, January 1993, pp. 42-51.

Chao Y. C., Tsai Y. J., Walter T., Kee C., Enge P., and Parkinson B. (1995), "An Algorithm for Inter-frequency Bias Calibration and Application to WAAS Ionosphere Modeling", Proceedings of ION GPS-95, Palm Spring Convention Center, California USA, pp. 639-646.

Chen D. (1994a), "Fast Ambiguity Resolution Approach for Precise Rapid Static and Kinematic GPS Positioning", The Third International Conference on Differential Satellite Navigation System, London, April 1994.

Chen D. (1994b), "Fast Ambiguity Search Filter (FASF): a Novel Concept for GPS Ambiguity Resolution", Proceedings of ION GPS-93, Salt Lake City, Utah USA, Vol. 1, pp. 781-787.

Christie J. R. I., Ko P. Y., Pervan B. S., Enge P. K., Powell J. D., and Parkinson B. W. (1998), "Analytical and Experimental Observations of Ionospheric and Tropospheric Decorrelation Effects for Differential Satellite Navigation during Precision Apporocah", Proceedings of ION GPS-98, Nashville, Tennessee USA, pp. 739-747.

Christle R. I. J., Parkinson B. W., and Enge P. K. (1996), "The Effects of the Ionosphere and C/A Frequency on GPS Signal Shape: Considerations for GNSS-2", Proceedings of ION GPS-96, Kansas City Convention Center, Missouri USA, Vol. 1, pp. 647-653.

Chu C. M. (1993), "Efficient and Effective Handling of Cycle Slips in Global Positioning System Data", PhD dissertation, The University of New South Wales, Australia.

Clynch J.and Henry C. (1994), "Ionospheric Effects on GPS and DGPS in Polar Regions", Proceedings of ION GPS-94, Salt Lake City, Utah USA, pp. 1579-1587.

Cohan C. E., Pervan B., and Parkleson B. W. (1992), "Estimation of Absolute Ionospheric Delay Exclisively through Single-Frequency GPS Measurements", Proceedings of ION GPS-92, Albuquerque, New Mexico USA, pp. 325-330.

Collins J. P. and Langley R. B. (1998), "The residual tropospheric propagation delay: How bad can it get? ", Proceedings of ION GPS-98, Nashville, Tennessee USA, pp. 729-738.

Colombo O.and Evans A. G. (1998), "Testing Decimeter-Level, Kinematic, Differential GPS Over Great Distances at Sea and on Land", Proceedings of ION GPS-98, Nashville, Tennessee USA, pp. 1257-1264.

Conker R. S., El-Arini M. B., and Albertson T. W. (1997), "Description and Assessment of Real-Time Algorithms to Estimate the Ionospheric Error Bounds for WAAS*", Journal of The Institute of Navigation, Winter 1997, Vol. 44, No. 1, pp. 77-87.

Conway A., Macpherson K., and Brown J. (1998), "Predicting the maximum of solar cycle 23", Journal of AOG, April 1998, Vol. 39, pp. 2.22-24.

Corbett S. J. (1994), "GPS Single Epoch Ambiguity Resolution for Airborne Positioning and Orientation", PhD Dissertation, University of Newcastle upon Tyne, UK.

Corbett S. J. (1995), "The Newcastle Exchange Format (NXF)", Department OF Geomatics, University of Newcastle upon Tyne, UK.

Corbett S. J. and Cross P. A. (1995a), "GPS Ambiguity Searching Program (GASP)", Lecture Notes, Department of Geomatics, University of Newcastle upon Tyne, UK.

Corbett S. J. and Cross P. A. (1995b), "GPS Single Epoch Ambiguity Resolution", Journal of Survey Review, July 1995, 33, 257, pp. 149-160.

Corbett S. J. and Cross P. A. (1995c), "The Ambiguity Function Method", Lecture Notes, Department of Geomatics, University of Newcastle upon Tyne, UK.

Coster A. J. and Gaposchkin E. M. (1989) "Use of GPS Pseudo-Range and Phase for Measurement of Ionospheric and Tropospheric Refraction", Proceedings of ION GPS-89, Nashville, Albuquerque, New Mexico USA, pp. 439-442.

Coster A. J., Niell A. E., Sollheim Fendes V. B., Toor P. C., Buchmann K. P., and Upham C.A. (1996), "Measurements of Precipitable Water Vapor by GPS, Radiosondes, and a Microwave Water Vapor Radiometer", Proceedings of ION GPS-96, Kansas City Convention Center, Missouri USA, pp. 625-634.

Counselman C. C. and Gourevitch S. A. (1981), "Miniature Interferometer Terminals for Earth Surveying: Ambiguity and Multipath in Global Positioning System", IEEE Transactions on Geoscience and Remote Sensing, GE-19 (No.: 4), pp. 244-252.

Cross, P. A. (1983), "Advanced Least Squares Applied to Position-Fixing – Working Paper No. 6, London: North East London Polytechnic, Department of Surveying, UK.

Cross, P. A. (1987), "Kalman Filter/Smoother Equations: their Derivation and Implementation", The Royal Institution of Chartered Surveyors/Hydrographic Society Seminar on Kalman Filtering, University of Nottingham, February 1987.

Cross, P. A. (1991), "Steps in FARS Method", Lecture Notes, July 1991, University of Newcastle upon Tyne, UK.

Cross, P. A. (1993), "The Impacts of GPS on Surveying and Mapping", Journal of Surveying and Mapping, South African, 2(part 2), pp. 73-80.

Cross, P. A. (1998), "GPS-Techniques Applied to Geodesy and Surveying", Lecture Notes in Earth Science, No. 19, Springer-Verlag, Berlin, pp. 349-360.

Cross, P. A. and Pritchett C. H. (1986), "A Kalman Filter for Real-time Positioning during Geophysical Surveys at Sea", XVIII International Congress Toronto Canada.

Cross, P. A., Chin W., and Tu Y. (1993), "Ambiguity Resolution for Rapid GPS Relative Positioning", the Tenth Conference of the Southern African Surveyors, Sun City South Africa.

Danaher J., Balendra A., Danaher M., Erpelding E., Gerlach R., and Beser J (1993), "GLONASS Dual Frequency Ionosphere Sounder", Proceedings of ION GPS-93, Salt Lake City, Utah USA, pp. 1363-1372.

Daniell R. E., Brown Jr. L. D., and Simon R. W. (1996), "A New, Improved Ionospheric Corrections Algorithm for Single Frequency GPS Receivers", Proceedings of ION GPS-96, Kansas City Convention Center, Missouri USA, pp. 635-640.

Darin F., Johanaaon J., Carlson R., Elgered G., Jarlemark P., and Ronnang B. (1997), "Continuous Monitoring of the Atmosphere Using GPS", Proceedings of ION GPS-97, Kansas City, Missouri USA, pp. 199-205.

Davis J. L., Herring A., Shapiro I. I., and Rogers E. E. (1985), "Geodesy by radio interferometry: Effects of atmospheric modeling errors on estimates of baseline length", Radio Science, November-December 1985, Vol. 20, No. 6, pp. 1593-1607.

Delikaraoglou D. (1989), "On the stochastic modelling of GPS ionospheric delays", Manuscripta Geodaetica, 14, pp. 100-109.

Delikaraoglou D. and Kleusberg A. (1988), "On the effect of the ionospheric delay on geodetic relative GPS positioning", Manuscripta Geodaetica, 13, pp. 1-8.

Doherty P. and Gendron P. J. (1997), "The Spatial and Temporal Variation in Ionospheric Range Delay", Proceedings of ION GPS-97, Kansas City, Missouri USA, Vol. 1, pp. 231-240.

Doherty P. H., Decker D. T., Klobuchar J. A., Anderson D. N., and Wilson B. D. (1996), "Observed Ionospheric Dependence on Solar Activity: Implications for a New Single Frequency GPS User Algorithm", Proceedings of ION GPS-96, Kansas City Convention Center, Missouri USA, pp. 565-574.

Engler E., Sardon E., Jakowski N., Jungstand A., and Klahn D. (1995), " Real-time Monitoring of the Ionosphere", Proceedings of the 1995 IGS Workshop, pp. 67-76.

Erickson C. (1992), "Analysis of Ambiguity Resolution Techniques for Rapid Static GPS Surveys Using Single Frequency Data", Proceedings of ION GPS-92, Albuquerque, New Mexico USA, pp. 453-462.

Euler H. and Landau H. (1992), "Fast Ambiguity Resolution On-the-Fly for Real-Time Applications", The Sixth International Geodetic Symposium on Satellite Positioning, The Ohio State University, Columbus, Ohio 43210, USA, Vol. 2, pp. 650-659.

Feess W. A. (1987), "Evaluation of GPS Ionospheric Time-Delay Model", IEEE Transactions on Aerospace and Electronic Systems, May 1987, Vol. AES-23, No. 3, pp. 332-338.

Feltens J.(1996), "Ionosphere Maps – A New Product of IGS ? ", Proceedings of the 1996 IGS Workshop, pp. 177-180.

Feltens J., Dow J. M., Mur T. J. M., Martiez C. C., and Bayona-Perez M.A. (1996), "Verification of ESOC Ionosphere Modeling and Status of IGS Intercomparison Activity", Proceedings of the 1996 IGS Workshop, pp. 205-211.

Flechtner F. (1997), "Modelling the Ionosphere with PRARE", pre@dfd.dlr.de

Frei E. and Beutler G. (1990), "Rapid static positioning based on the fast ambiguity resolution approach 'FARA': theory and first results", Manuscripta Geodaetica, 15, pp. 325-356.

Freymueller J. T. (1997), " PhaseEdit 1.1 UserÕs Guide", Department of Geophysics, Stanford University, jeff@pangea.Stanford.EDU.

Fridman A. (1998), "Methods of Filtering in Instant Ambiguity Resolution and Their Application to RTK-OTF Positioning", Proceedings of ION GPS-98, Nashville, Tennessee USA, pp. 381-388.

Gao Y. (1998), "Ionospheric Effect and Modeling for Regional Area Differential DGPS Network", Proceedings of ION GPS-98, Nashville, Tennessee USA, pp. 91-97.

Gendt G. (1996a), "IGS Troposphere Estimations –Summary-", Proceedings of the 1996 IGS Workshop, pp. 147-149.

Gendt G. (1996b), "Comparison of IGS Troposphere Estimations", Proceedings of the 1996 IGS Workshop, pp. 151-162.

Georgiadou Y.and Kleusberg A. (1988), "On the effect of ionospheric delay on the geodetic relative GPS positioning", Manuscripta Geodaetica, 13, pp. 1-8.

Giffard R. P. (1998), "Ionospheric Effects at Nanosecond Level Observed in Common-View Time Transfer", Journal of The Institute of Navigation, Winter 1997-1998, Vol. 44, No. 4, pp. 489-496.

Gounon R. and Erceau F. (1998), "The LRK Real-time Kinematic Technique for a Centimetre Accuracy Domain up to 40km", The Hydrographic Journal, April 1998, No. 88., pp. 3-6.

Gregorius T. (1996), "GIPSY–OASIS II", Department of Geomatics, University of Newcastle upon Tyne, August 1996.

Gurtner W. (1994), "RINEX: The Receiver Independent Exchange Format Version 2", Astronomical Institute, University of Berne, Switzerland.

Han S. (1995), "Ambiguity Recovery for GPS Long Range Kinematic Positioning", Proceedings of ION GPS-95, Palm Spring Convention Center, California USA, September 1995, pp. 349-360.

Hanson P. (1992), "A Real-Time GPS Kinematic Survey System", Proceedings of ION GPS-92, Albuquerque, New Mexico USA, pp. 1005-1013.

Hanson P. (1994), "Real-Time GPS Carrier Phase Navigation", The Third International Conference on Differential Satellite Navigation System, London.

Hatch R. (1986), "Dynamic Differential GPS at the Centimeter Level", The Fourth International Geodetic Symposium on Satellite Positioning, pp. 1287-1298.

Hatch R. (1989), "Ambiguity Resolution in the Fast Lane", Proceedings of ION GPS-89, Colorado Springs, Colorado USA, September 1989, pp. 45-50.

Hatch R. (1990), "Instantaneous Ambiguity Resolution", KIS Symposium 1990, Banff, Canada, September 1990, pp. 229-308.

Herring T. A. (1986), "Precision of Vertical Estimates From Very Long Baseline Interferometry", Journal of Geophysical Research, August 1986, Vol. 91, No. B9, pp. 9177-9182.

Herring T. A. (1990), "Geodesy by Radio Interferometry: The Application of Kalman Filtering to the Analysis of Very Long Baseline Interferometry Data", Journal of Geophysical Research, August 1990, Vol. 95, No. B8, pp. 12,561-12581.

Herring T. A. (1992), "Submillimeter Horizontal Position Determination Using Very Long Baseline Interferometry", Journal of Geophysical Research, February 1992, Vol. 97, No. B2, pp. 1981-1990.

Hofmann-Wellenhof B. and Remondi B. W. (1988), "The Antenna Exchange: One Aspect of High-Precision GPS Kinematic Survey", In Bhattacharji et. al. (Ed),

GPS Techniques Applied to Geodesy and Surveying (Lecture Notes in Earth Scinece: 19), 19 (pp. 261-277) Darmastadt, Germany: Springer-Verlag.

Hofmann-Wellenhof B., Lichtenegger H., and Collins J. (1994), "GPS Theory and Practice, Wien: Springer-Verlag, Third Revised Edition, 355pp.

Hopfield H. S. (1963), "The Effect of Tropospheric Refraction on the Doppler Shift of a Satellite Signal", Journal of Geophysical Research, September 1963, Vol. 68, No. 18, pp. 5157-5168.

Hwang P. Y., McGraw G. A., and Bader J. R. (1998), "Enhanced Differential GPS Carrier-Smoothed Code Processing Using Dual Frequency Measurements", Proceedings of ION GPS-98, Nashville, Tennessee USA, pp. 461-470.

IESSG (1996), "The Accurate Recovery of Cycle Slips", http://www.nottingham.ac.uk/~iszwww/isgres24.htm.

Jakowski N. (1995), "Ionospheric Research and Future Contributions of the IGS Network", Proceedings of the 1995 IGS Workshop, pp. 17-29.

Jakowski N. and Sardou E. (1996), "Comparison of GPS/ICS-derived TEC data with parameters measured by independent ionospheric probing techniques", Proceedings of the 1996 IGS Workshop, pp. 221-230.

Jong Ir. K. (1999), "Permanent GPS Arrays", Journal of GEO, March 1999.

Jonkman N. F. (1998), "The Geometry-Free Approach to Integer GPS Ambiguity Estimation", Proceedings of ION GPS-98, Nashville, Tennessee USA, pp. 369-379.

JPL (1992), "GIPSY–II Manual", NASA/Caltech, hurst@cobra.jpl.nasa.gov.

Kee C. and Yun D. (1998), "Development of Real-time SNUDGPS via Ionospheric and Tropospheric Corrections", Proceedings of ION GPS-98, Nashville, Tennessee USA, pp. 1411-1419.

Kleusberg A. (1986), "Ionospheric propagation effects in geodetic relative GPS positioning", Manuscripta Geodaetica, 11, pp. 256-261.

Klobuchar A. (1991), "Ionospheric Effects on GPS", GPS World, April 1991, pp. 48-51.

Klobuchar J. A. (1987), "Ionospheric Time-Delay Algorithm for Single-Frequency GPS Users", IEEE Transactions on Aerospace and Electronic Systems, May 1987, Vol. AES-23, No. 3, pp. 325-331.

Knight M. and Finn A. (1998), "The Effects of Ionospheric Scintillation on GPS", Proceedings of ION GPS-98, Nashville, Tennessee USA, pp. 673-685

Knight M., and Finn A. (1996), "The Impacts of Ionospheric Scintillation on GPS Performance", Proceedings of ION GPS-96, Kansas City Convention Center, Missouri USA, pp. 555-564.

Komjathy A. and Langley R.B. (1996), "The Effect of Shell Height on High Precision Ionospheric Modelling Using GPS", Proceedings of the 1996 IGS Workshop, pp. 193-203.

Lachapelle G., Cannon M. E., and Lu G. (1992), "Ambiguity Resolution On-the-Fly Comparison of P Code and High Performance C/A Code Receiver Technology", Proceedings of ION GPS-92, Albuquerque, New Mexico USA, pp. 1025-1032.

Landau H. and Euler H. (1992), "On-the-Fly Ambiguity Resolution for Precise Differential Positioning", Proceedings of ION GPS-92, Albuquerque, New Mexico USA, pp. 1025-1032.

Landau H. and Vollath U. (1994), "Differential GPS – New Development on High Precision Positioning with On-the-Fly Ambiguity Resolution", The Third International Conference on Differential Satellite Navigation System, April London.

Langley R. B. (1992), "The Effect of the Ionosphere and Troposphere on Satellite Positioning Systems", Refraction of Transatmospheric Signals in Geodesy, Proceedings of the Symposium, The Hague, The Newtherlands, May 1992, pp. 97.

Lanyi G. E. and Roth T. (1988), "A comparison of mapped and measured total ionospheric electron content using global positioning system and beacon satellite observations", Radio Science, July-August 1988, Vol. 23, No. 4, pp. 483-492.

Leick A. (1995), "GPS Satellite Surveying", Second Edition, John Wiley & Sons Inc., 560pp.

Li Z., and Gao Y. (1998), "Improving Ambiguity Resolution for a Regional Area DGPS System Using Multiple Days of Data", Proceedings of ION GPS-98, Nashville, Tennessee USA, pp. 399-406.

Ma C., Sauser M., Bell L. J., Clark T. A., Gordon D., Himwich W. E., and Ryan J. W. (1990), " Measurement of Horizontal Motions in Alaska Using Very Long Baseline Interferometry", Journal of Geophysical Research, December 1990, Vol. 95, No. B13, pp. 21,991-22,011.

Mader G. L. (1986), "Dynamic Positioning Using GPS Carrier Phase Measurements", The Fourth International Geodetic Symposium on Satellite Positioning, pp. 1131-3283.

Mannucci A. J., Wilson B. D., and Edwards C. D. (1993), "A New Method for Monitoring the Earth's Ionospheric Total Electron Content Using the GPS Global Network", Proceedings of ION GPS-93, Salt Lake City, Utah USA, pp. 1323-1332.

Mannucci A. J., Wilson B. D., Yuan D. N., Lindqwister Ulf J., and Runge T. F. (1995), "Global Monitoring of Ionospheric Total Electron Content Using the IGS Network", Proceedings of the 1995 IGS Workshop, pp. 49-56.

Martin S. and Jahn C. H. (1998), "High Precision Real-Time Differential Correction Network for Geodetic Applications", Proceedings of ION GPS-98, Nashville, Tennessee USA, pp. 23-30.

Michael L. T., Catchpole I., and Hansla A. (1993), "Single Frequency Ionosphere Determination Using GPS", Proceedings of ION GPS-93, Salt Lake City, Utah USA, pp. 1373-1381.

Mikhail E. M. (1981), "Analysis and Adjustment of Survey Measurements", Van Nostrand Reinhold Company Inc., 135 West 50th Street, New York, N. Y. 10020.

Nam Y. S., Kuang D., and Schutz B. E. (1996), "Comparison of GPS Estimates of Wet Tropospheric Delays with WVR Measurements", Proceedings of ION GPS-96, Kansas City Convention Center, Missouri USA, pp. 641-646.

Napier M. (1991), "Kalman Filter for GPS", The Institution of Engineering Surveying and Space Geodesy, University of Nottingham, April 1991.

Niell A. E. (1992), "Global mapping functions for atmospheric delay at radio wavelength", Journal of Geophysical Research, Vol. 101, No. B2, pp. 3247-3268.

Ordnance Survey (1998), "Global Positioning System and mapping in the twenty-first century", http://www.o-s.co.uk/literatu/infopapr/1998/pap1298.html.

Pratt M., Burke B., and Misra P. (1998), "Single-Epoch Integer Ambiguity Resolution with GPS-GLONASS L1-L2 Data", Proceedings of ION GPS-98, Nashville, Tennessee USA, Vol. 1, pp. 389-398.

Pullen S., Opshaug G., Hansen A., Walter T., Enge P., and Parkinson B. (1998), "A Preliminary Study of the Effect of Ionospheric Scintillation on WAAS User

Availability in Equatorial Regions", Proceedings of ION GPS-98, Nashville, Tennessee USA, pp. 687-698.

Remondi B. W. (1986), "Performing Centimeter-Level Surveying in Seconds with GPS Carrier Phase: Initial Results", Proceedings of the Fourth International Geodetic Symposium on Satellite Positioning, Austin USA, 2, pp. 1229-1249.

Remondi B. W. (1988), "Pseudo-Kinematic GPS Results Using the Ambiguity Function Method", National Geodetic Survey (Technical Memo No.: NOAA-TM-NOS-NGS-52, US), Rockville, MD USA.

Remondi B. W. (1992a), "Real-Time Centimeter-Accuracy GPS without Static Initialisation", The Sixth International Geodetic Symposium on Satellite Positioning, The Ohio State University, Columbus, Ohio 43210, USA, pp. 691-701.

Remondi B. W. (1992b), "Real-Time Centimeter-Accuracy GPS: Initialisation While in Motion (Warm Start Versus Cold Start)", Proceedings of ION GPS-92, Albuquerque, New Mexico USA, pp. 1053-1061.

Riley S. and Daly P. (1993), "Performance of the GLONASS P-Code at L1 and L2 Frequencies", Proceedings of ION GPS-93, Salt Lake City, Utah USA, pp. 1353-1362.

Saastamoinen J. (1973), "Contributions to the theroy of atmospheric refraction", In part three parts: Bullentin Geodesique, No. 105, pp. 279-298; No. 106, pp. 383-397; No. 107, pp. 13-34.

Sardon E., Rius A., and Zarraoa N. (1994a), "Estimation of the transmitter and receiver differential biases and the ionospheric total electron content from Global Positioning System observations", Radio Science, May-June 1994, Vol. 29, No. 3, pp. 577-586.

Sardon E., Rius A., and Zarraoa N. (1994b), "Ionospheric calibration of single frequency VLBI and GPS observations using dual GPS data", Bulletin Geodesque, 68, pp. 230-235.

Schaer S., Beutler G., Mervart L., and Rothacher M. (1995), "Global and Regional Ionosphere Models Using the GPS Double Difference Phase Observable", Proceedings of the 1995 IGS Workshop, pp. 77-92.

Schaer S., Beutler G., Rothacher M., and Springer T. A. (1996), "Daily Global Ionosphere Maps Based on GPS Carrier Phase Data Routinely Produced by the Code Analysis Center", Proceedings of the 1996 IGS Workshop, pp. 181-192.

Skone S. (1998), "An Adaptive WADGPS Ionospheric Grid Model for the Auroral Region", Proceedings of ION GPS-98, Nashville, Tennessee USA, pp. 185-194.

Skone S. and Cannon M. E. (1997), "Ionospheric Limitations and Specifications in the Auroral Zone", Proceedings of ION GPS-97, Kansas City, Missouri USA, pp. 187-196.

Skone S. and Cannon M. E. (1998), "Detailed Analysis of Auroral Zone WADGPS Ionospheric Grid Accuracies during Magnetospheric Sunstorm Event", Proceedings of ION GPS-98, Nashville, Tennessee USA, pp. 701-710.

Spiegfl M. R. (1959), "Schaum's Outline Series: Theory and Problems of Vector Analysis", McGRAW-HILL Book Company, New York.

Stewart P. J. (1997), "The Reduction of Differential Ionospheric Delay for GPS Carrier Phase Ambiguity Resolution", Master dissertation, Department of Geodesy and Geomatics Engineering, University of New Brunswick, Canada.

Stewart P. J. and Langley R. B. (1998), "Ionospheric Modeling for WADGPS at Nothern Latitudes", Proceedings of ION GPS-98, Nashville, Tennessee USA, pp. 757-765.

Teunissen P. J. G. and Tiberius C. C. J. M. (1994), "Integer Least-Squares Estimation of the GPS Phase Ambiguities", Proceedings of the International Symposium on Kinematic Systems in Geodesy, Geomatics, and Navigation (KIS94), University of Galgary, Banff, Canana, pp. 221-231.

Tsedilina E.E. and Weitman O. V. (1994), "Time delay of atransionospheric radio signals in a horizontally inhomogeneous ionosphere", Radio Science, May-June 1994, Vol. 29, No. 3, pp. 625-630.

Van Dierendonck A. J., Klobuchar J., and Hua Q. (1993), "Ionospheric Scintillation Monitoring Using Commercial Single Frequency C/A Code Receivers", Proceedings of ION GPS-93, Salt Lake City, Utah USA, pp. 1333-1342.

Vollath U., Birnbach S., Landau H., Fraile-Ordonez J. M., and Martin-Neira M. (1998), "Analysis of Three-Carrier Ambiguity Resolution (TCAR) Technique for Precise Relative Positioning in GNSS-2", Proceedings of ION GPS-98, Nashville, Tennessee USA, Vol. 1, pp. 417-426.

Wanninger L. (1992), "Monitoring Total Ionospheric Electron Content and Ionospheric Irregularities with GPS", Refraction of Transatmospheric Signals in Geodesy, Proceedings of the Symposium, The Hague, The Newtherlands, May 1992, pp. 141-146.

Wanninger L. (1995a), "Improved Ambiguity Resolution BY Regional Differential Modelling of the Ionosphere", Proceedings of ION GPS-95, Palm Spring Convention Center, California USA, pp. 55-62.

Wanninger L. (1995b), "Monitoring Ionospheric Disturbances Using the IGS Network", Proceedings of the 1995 IGS Workshop, pp. 57-66.

Wanninger L. (1995c), "Enhancing differential GPS using regional ionospheric error models", Bullenten Geodesque, 69, pp. 283-291.

Warrnant R. (1997), "Influence of the Ionospheric Refraction on the Repeatability of Distance Computed by GPS", Proceedings of ION GPS-97, Kansas City, Missouri USA, pp. 217-223.

WARSAW University of Technology (1998), "Reports on Geodesy", Institute of Geodesy and Geodetic Astronomy, No. 11 (41), 1998.

Webster I. R. (1993), "A Regional Model for the Prediction of Ionospheric Delay for Single Frequency Users of the Global Positioning System", Master Dissertation, Department of Surveying Engineering, University of New Brunswick, Canada.

Wild U., Beutler G., Fankhauser S., and Gurtner W. (1990), "PROPRIETES STOCHASTIQUES DE L'IONOSPHERE EVALUEES A PARTIR D'OBSERVATIONS DANS LE CADRE DU GPS", GPS'90/SPG'90, September 1990, pp. 412-427.

Wild U., Beutler G., Gurtner W. and Rothacher M. (1989), "Estimating the ionosphere using one or more dual frequency GPS receivers", Proceedings of the 1989 IGS Workshop, pp. 724-735.

Wilson B. D. and Mannucci A. J. (1993) "Instrumental Biases in Ionospheric Measurements Derived from GPS Data", Proceedings of ION GPS-93, Salt Lake City, Utah USA, pp. 1343-1351.

Wu J. and Lin S. G. (1998), "Kinematic Positioning with GPS Carrier Phases by Two Types of Wide Laning", Journal of The Institute of Navigation, Winter 1997-1998, Vol. 44, No. 4, pp. 471-477.

Ziegler C. and Euler H. (1999), " Real-Time Processing Strategies –System 500", Leica, March 1999.

APPENDIX A

SUMMARY OF THE RELATED FIGURES OF CHAPTER FIVE

In Appendix A, it includes the related figures of chapter 5 as follows:

1. the elevation angle of the trials tested (Figure A.1-A.10),
2. the ambiguity resolution of the trials tested (Figure A.11-A.15),
3. the behaviour of single path ionospheric delays of the trials tested (Figure A.16-A.23),
4. the behaviour of double differenced ionospheric delays of the trials tested (Figure A.24-A.28),
5. The behaviour of double differenced tropospheric delays of the trials tested (Figure A.29-A.33),
6. The comparison between the "true" double differenced tropospheric delays obtained from the linear combination approach and the double differenced tropospheric estimation based on the Saastamoinen model (Figure A.34-A.38).

- The elevation angle of the trials tested

1. Trial of baseline PSMS-SEMA

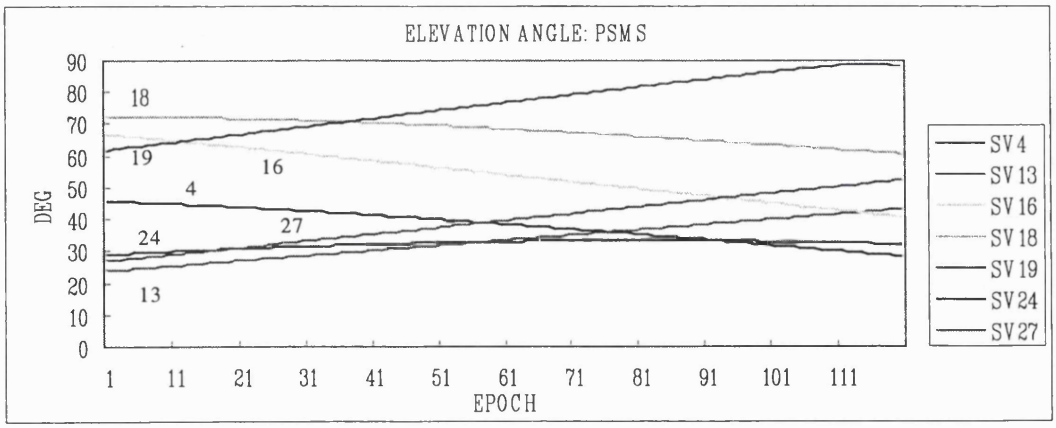

Figure A.1 The elevation angle of available satellites at the station PSMS

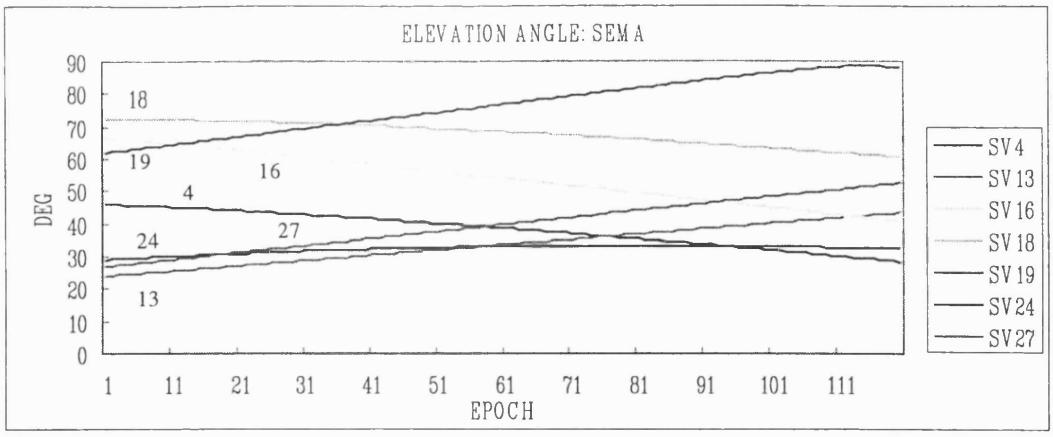

Figure A.2 The elevation angle of available satellites at the station SEMA

2. Trial of baseline CG54-KRPI

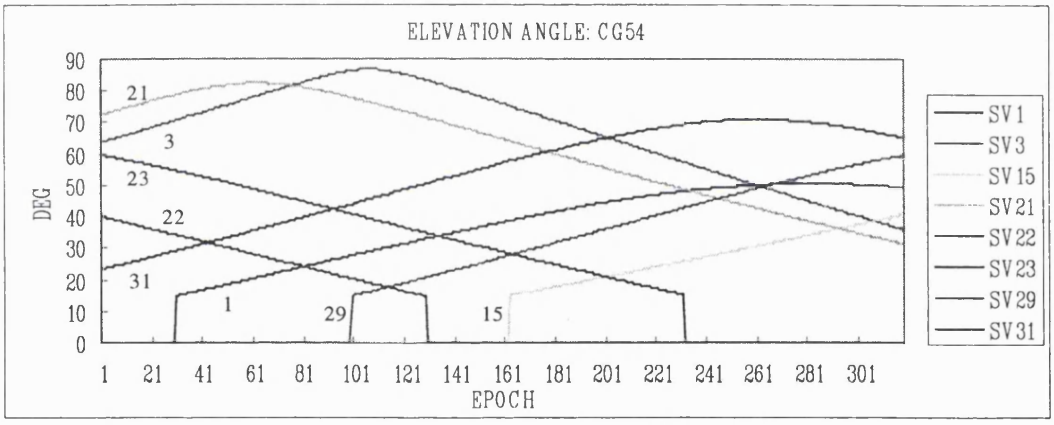

Figure A.3 The elevation angle of available satellites at the station CG54

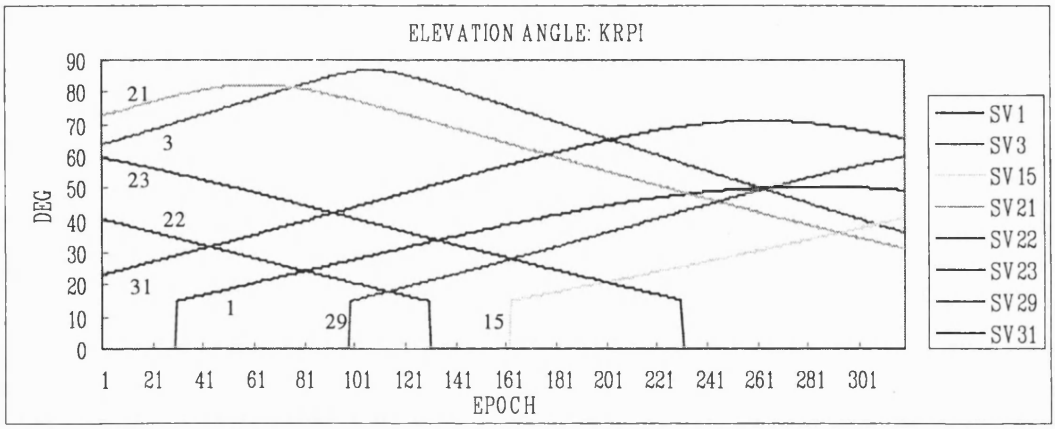

Figure A.4 The elevation angle of available satellites at the station KRPI

3. Trial of baseline INED-SHEN

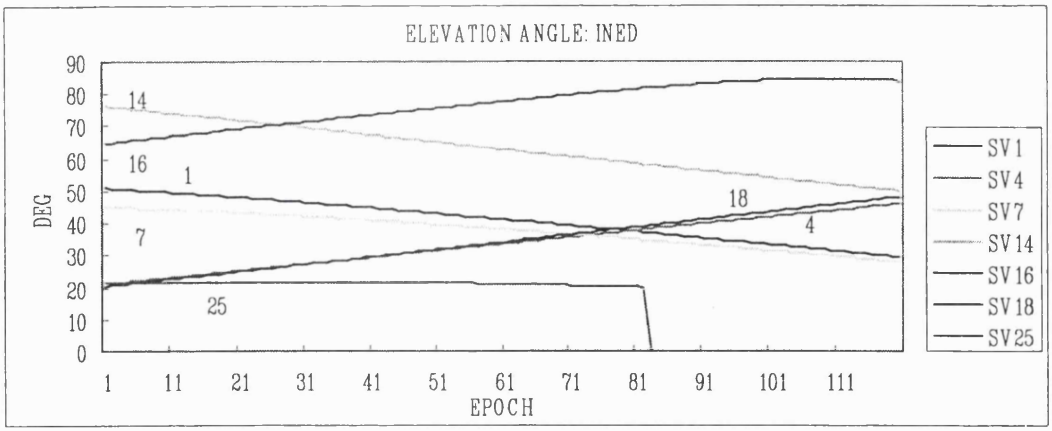

Figure A.5 The elevation angle of available satellites at the station INED

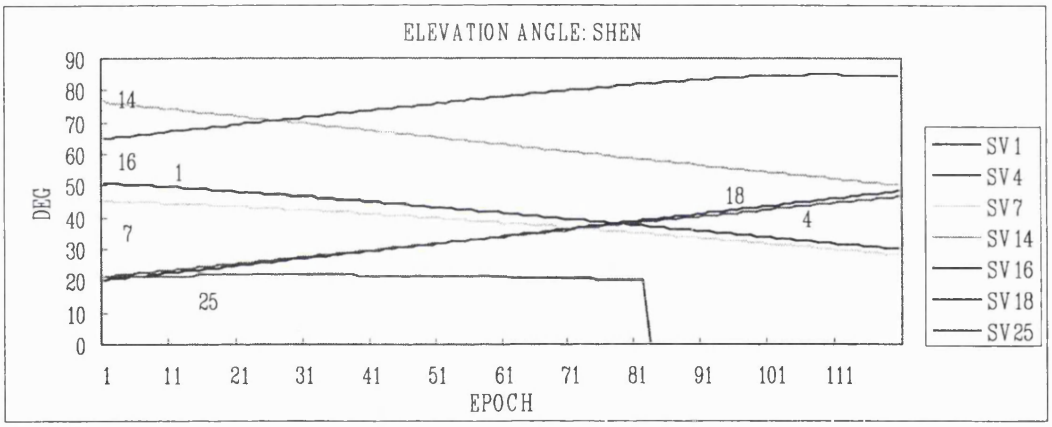

Figure A.6 The elevation angle of available satellites at the station SHEN

4. Trial of baseline PSMS-PLAT

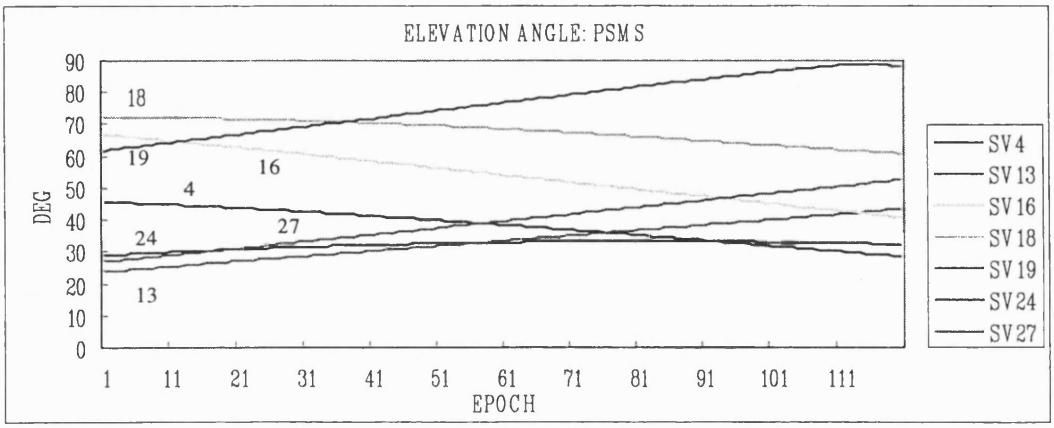

Figure A.7 The elevation angle of available satellites at the station PSMS

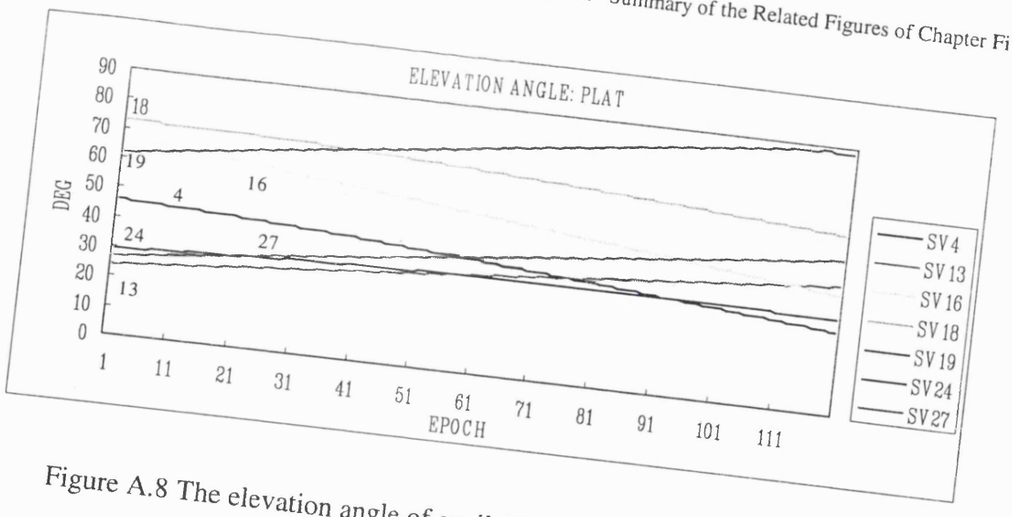

Figure A.8 The elevation angle of available satellites at the station PLAT

5. Trial of baseline PSMS-SOHO

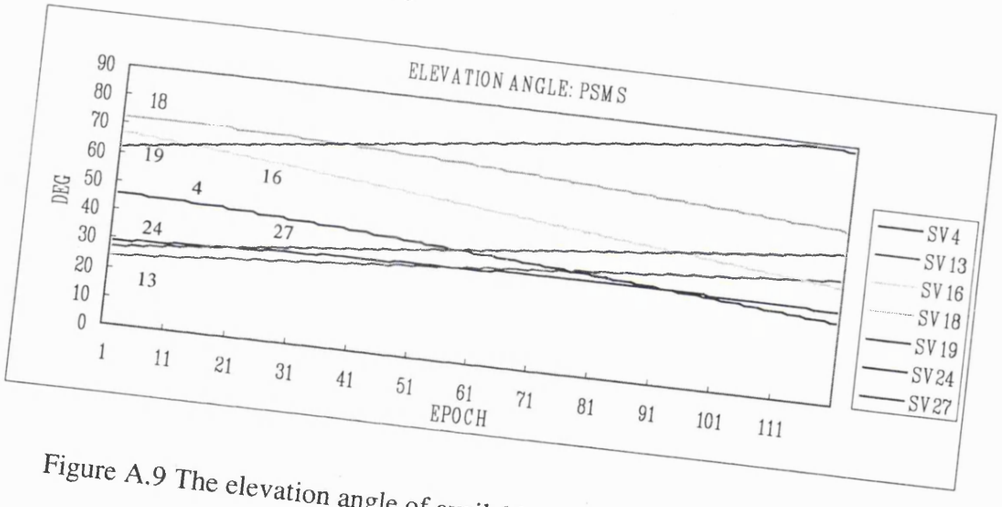

Figure A.9 The elevation angle of available satellites at the station PSMS

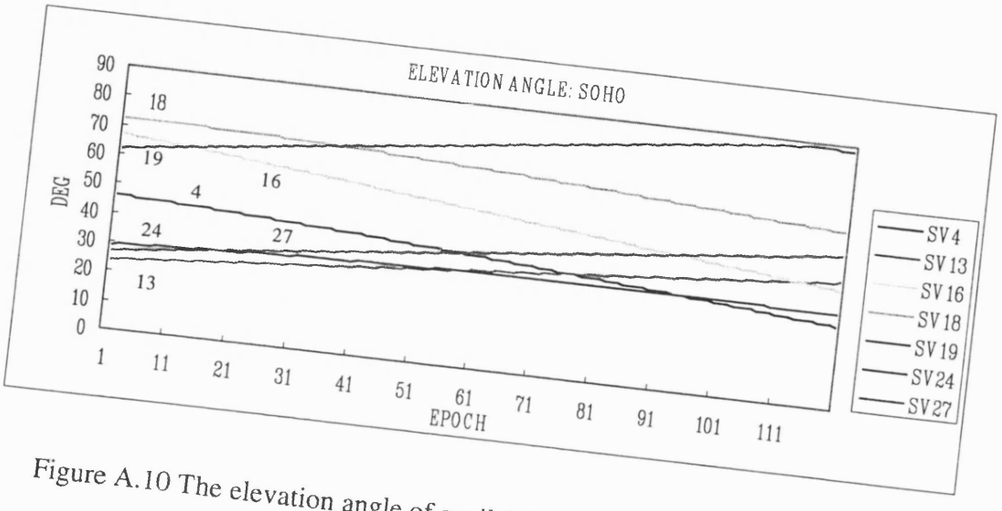

Figure A.10 The elevation angle of available satellites at the station SOHO

- The ambiguity resolution of the trials tested

1. Trial of baseline PSMS-SEMA

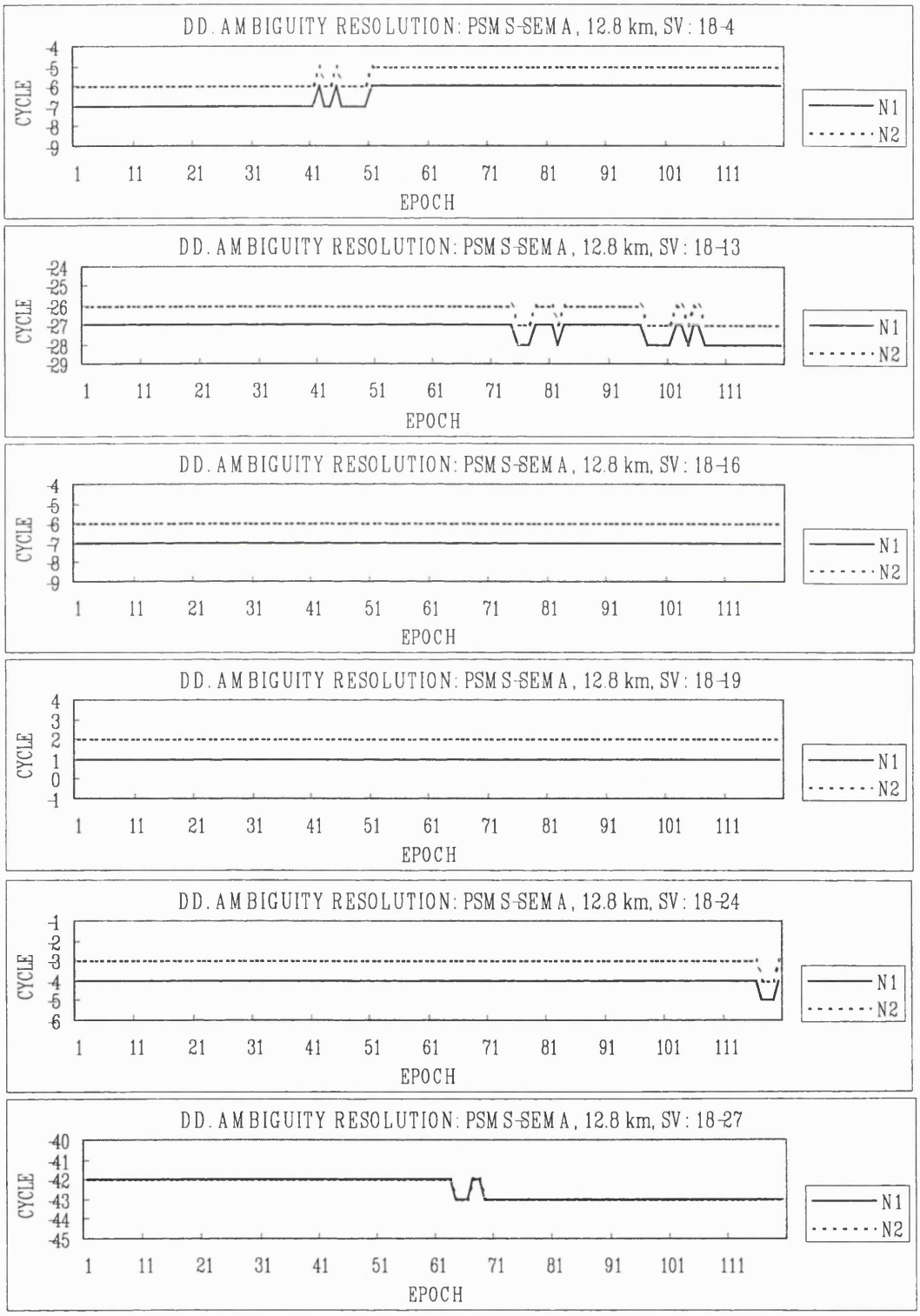

Figure A.11 The double differenced ambiguity resolution in the trial of baseline PSMS-SEMA

2. Trial of baseline CG54-KRPI

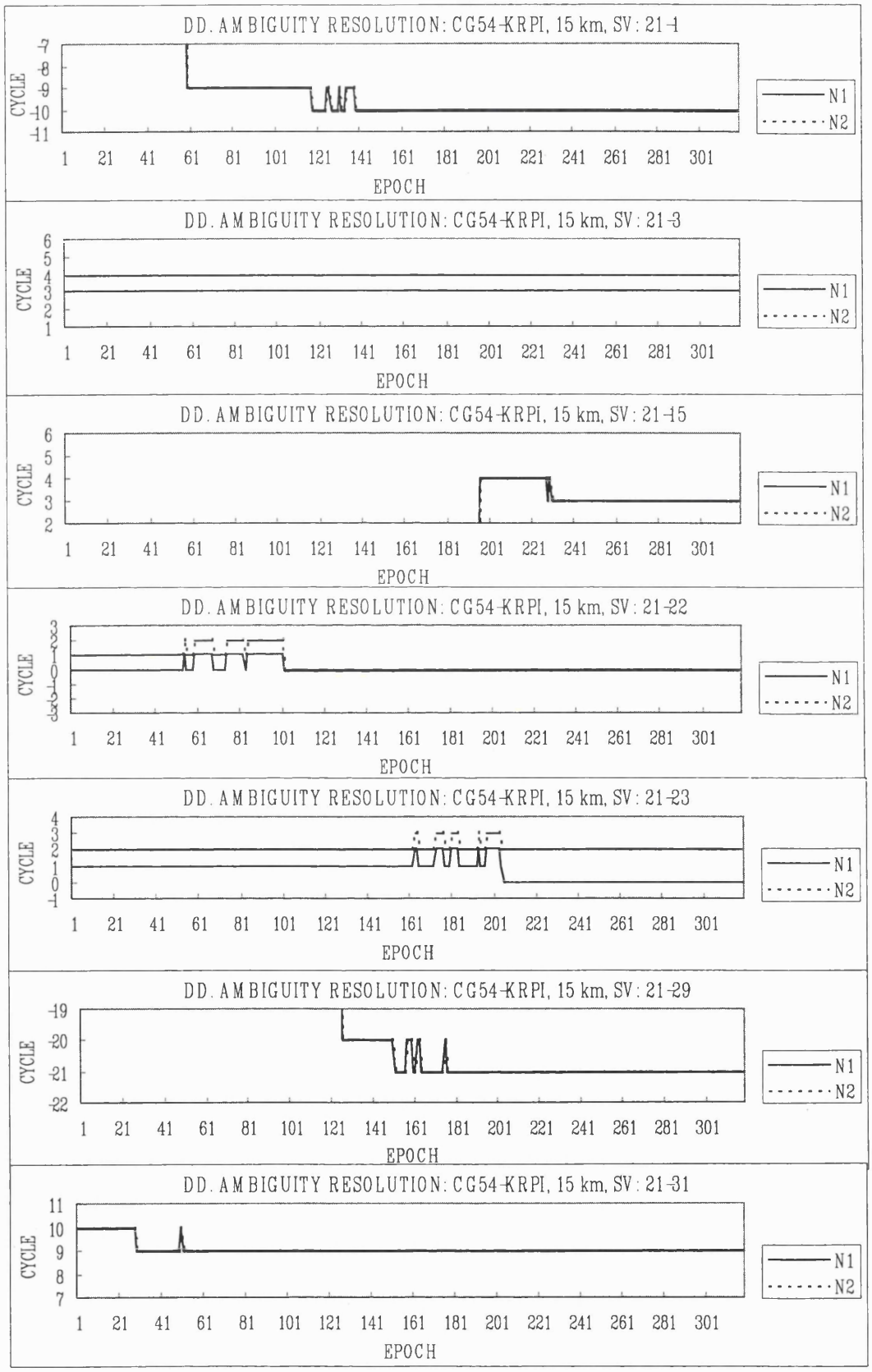

Figure A.12 The double differenced ambiguity resolution in the trial of baseline CG54-KRPI

3. Trial of baseline INED-SHEN

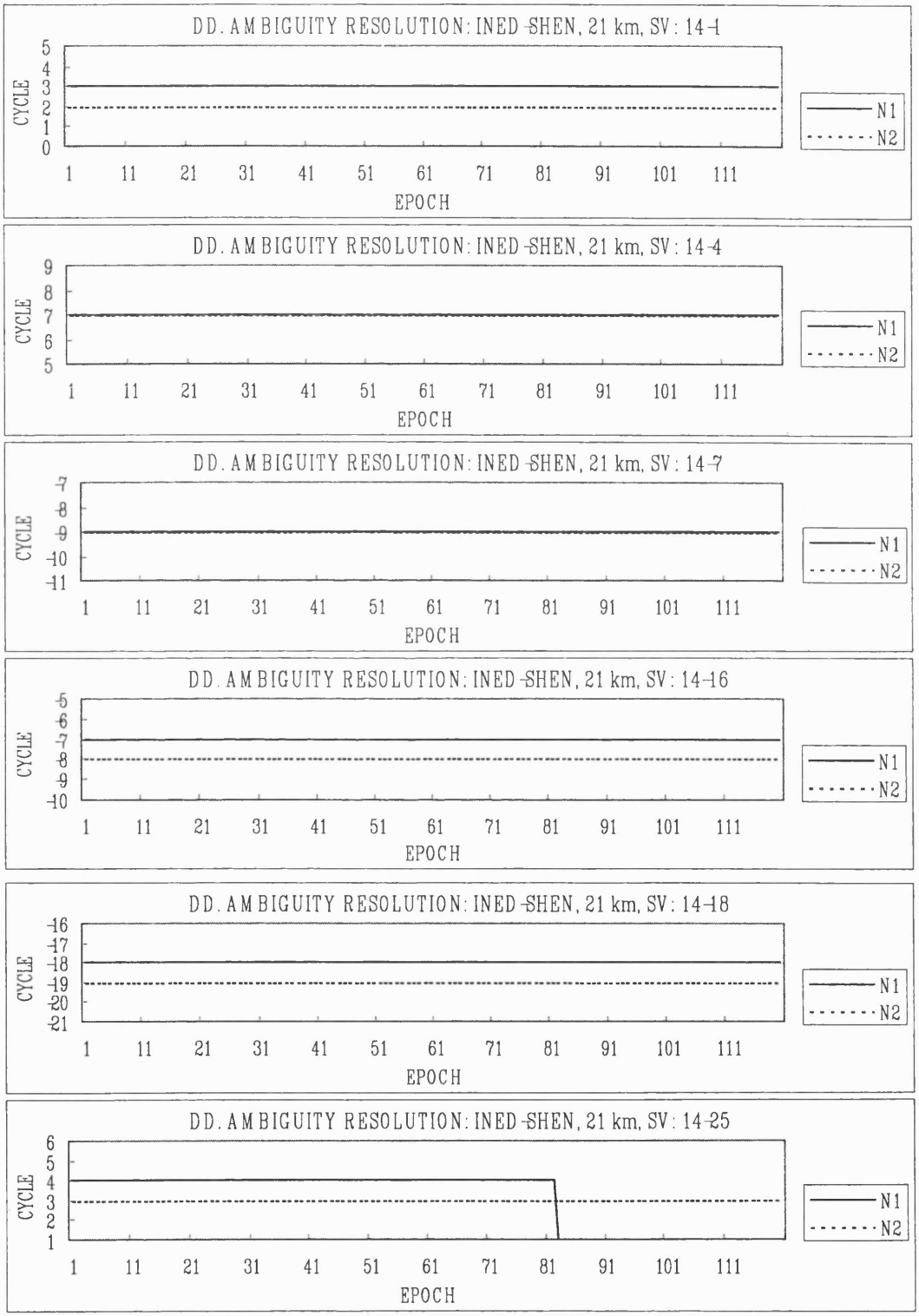

Figure A.13 The double differenced ambiguity resolution in the trial of baseline INED-SHEN

4. Trial of baseline PSMS-PLAT

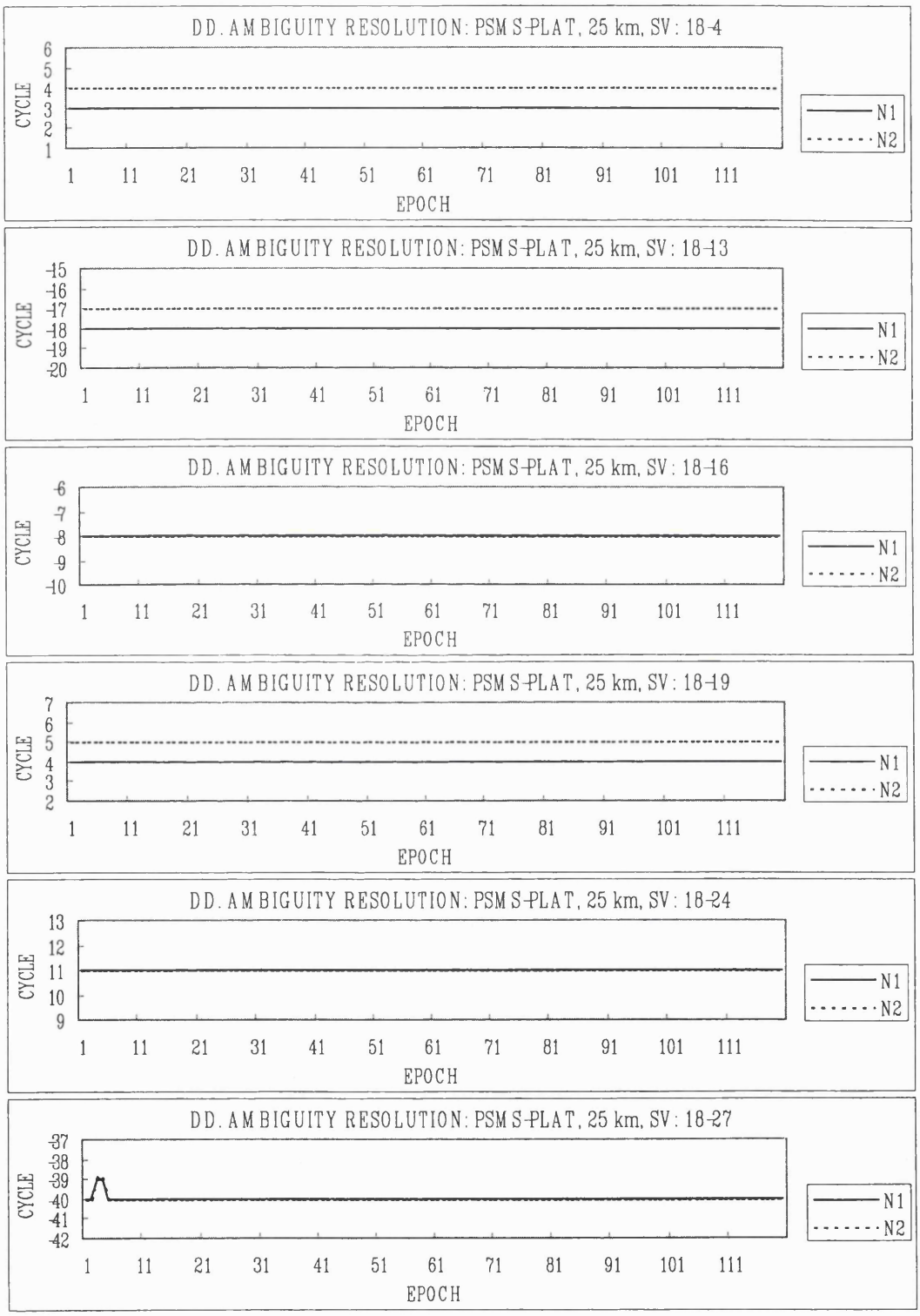

Figure A.14 The double differenced ambiguity resolution in the trial of baseline PSMS-PLAT

5. Trial of baseline PSMS-SOHO

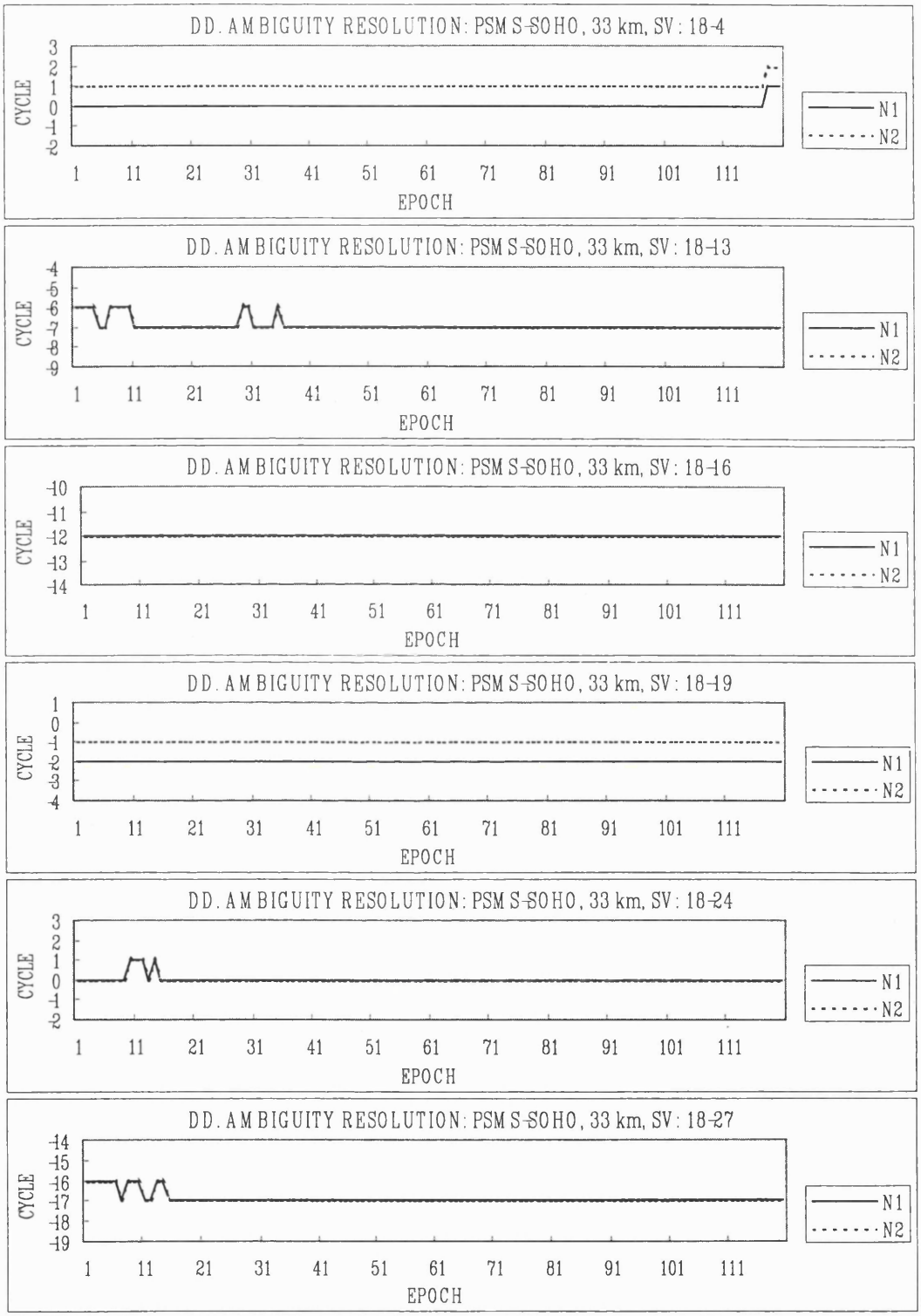

Figure A.15 The double differenced ambiguity resolution in the trial of baseline PSMS-SOHO

- The behaviour of single path ionospheric delays of the trials tested

1. At station PSMS

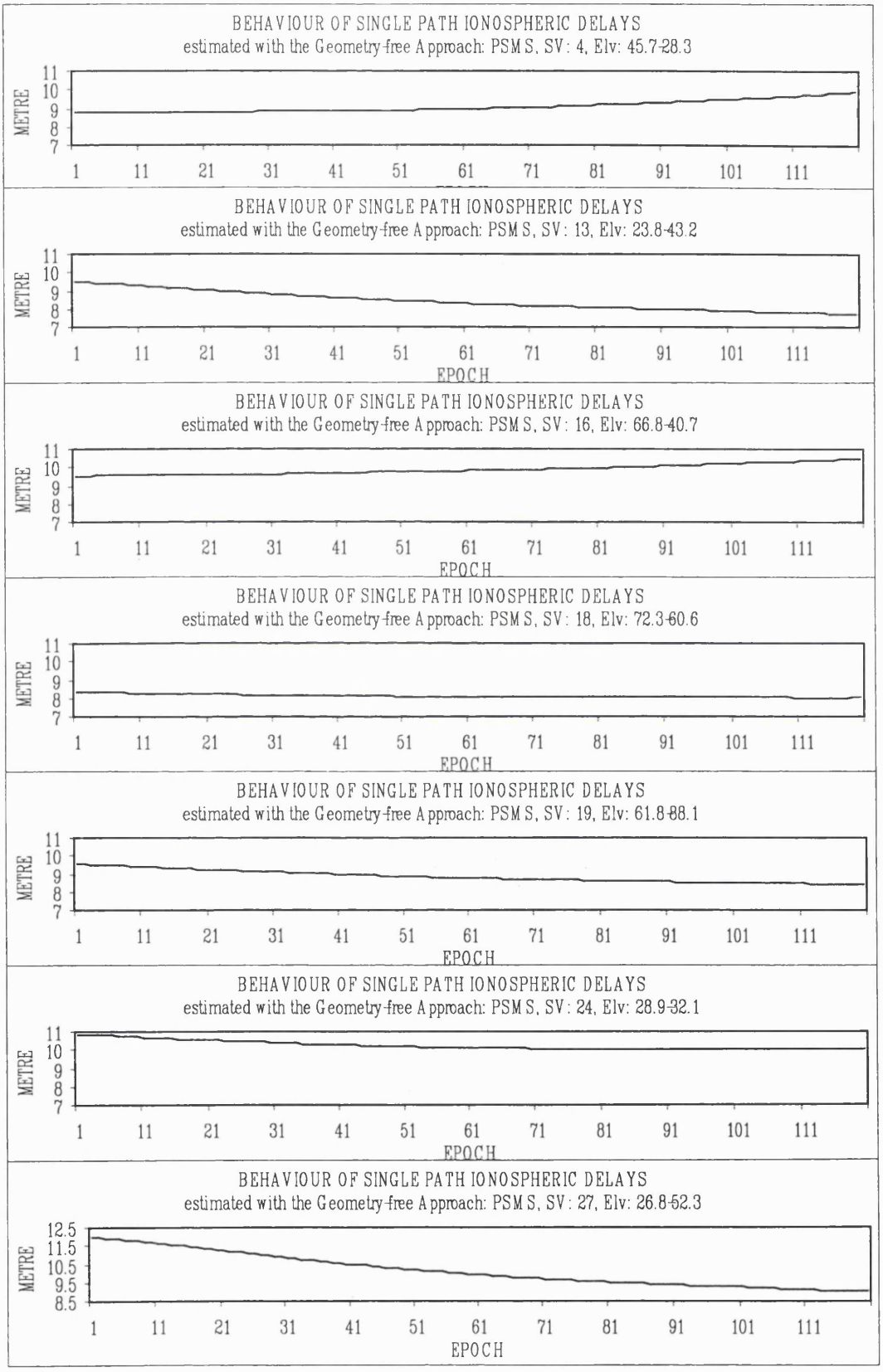

Figure 5.16 The behaviour of single path ionospheric delays at the station PSMS

2. At station SEMA

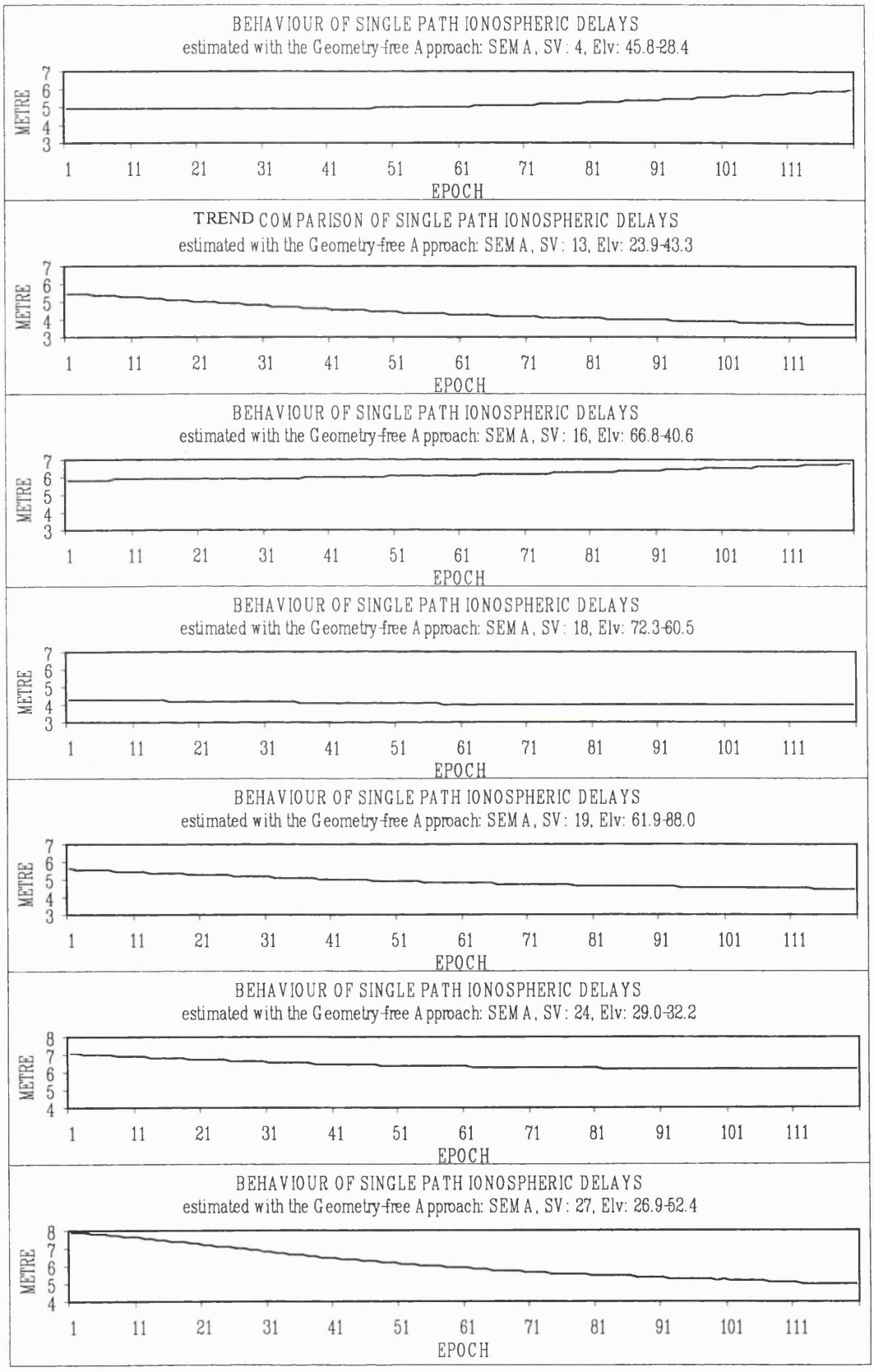

Figure 5.17 The behaviour of single path ionospheric delays at the station SEMA

3. At station CG54

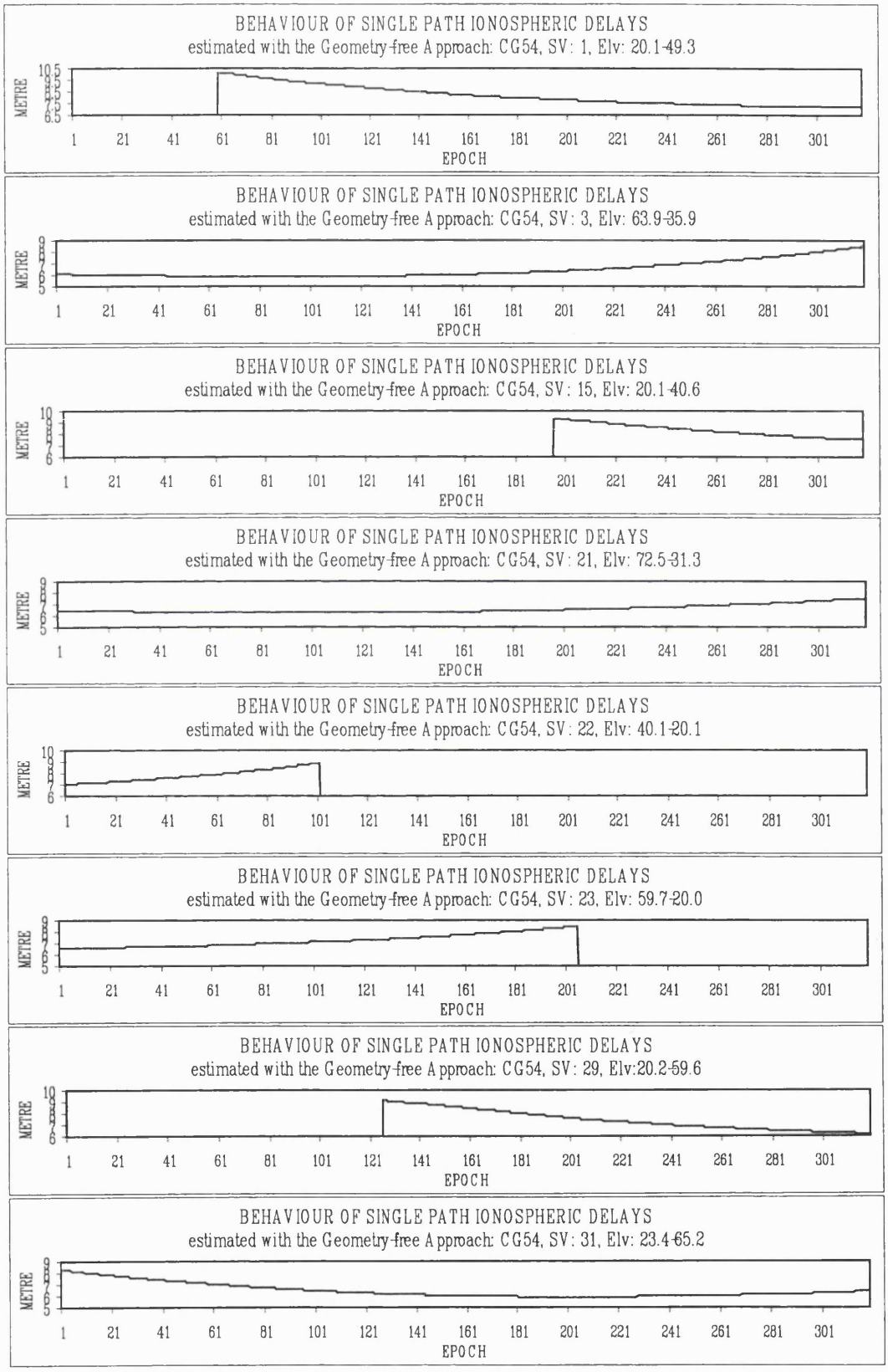

Figure 5.18 The behaviour of single path ionospheric delays at the station CG54

4. At station KRPI

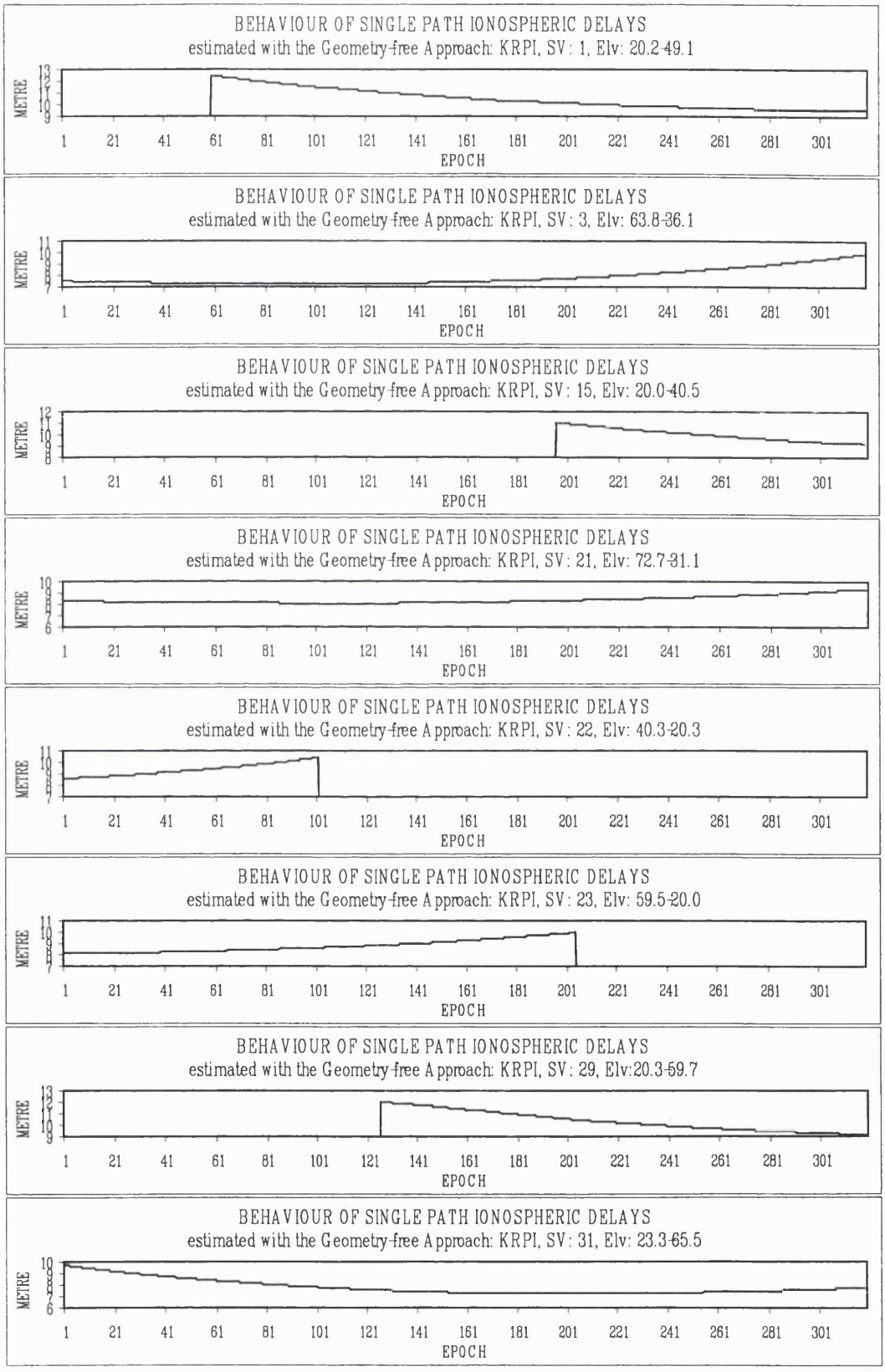

Figure A.19 The behaviour of single path ionospheric delays at the station KRPI

1. At station INED

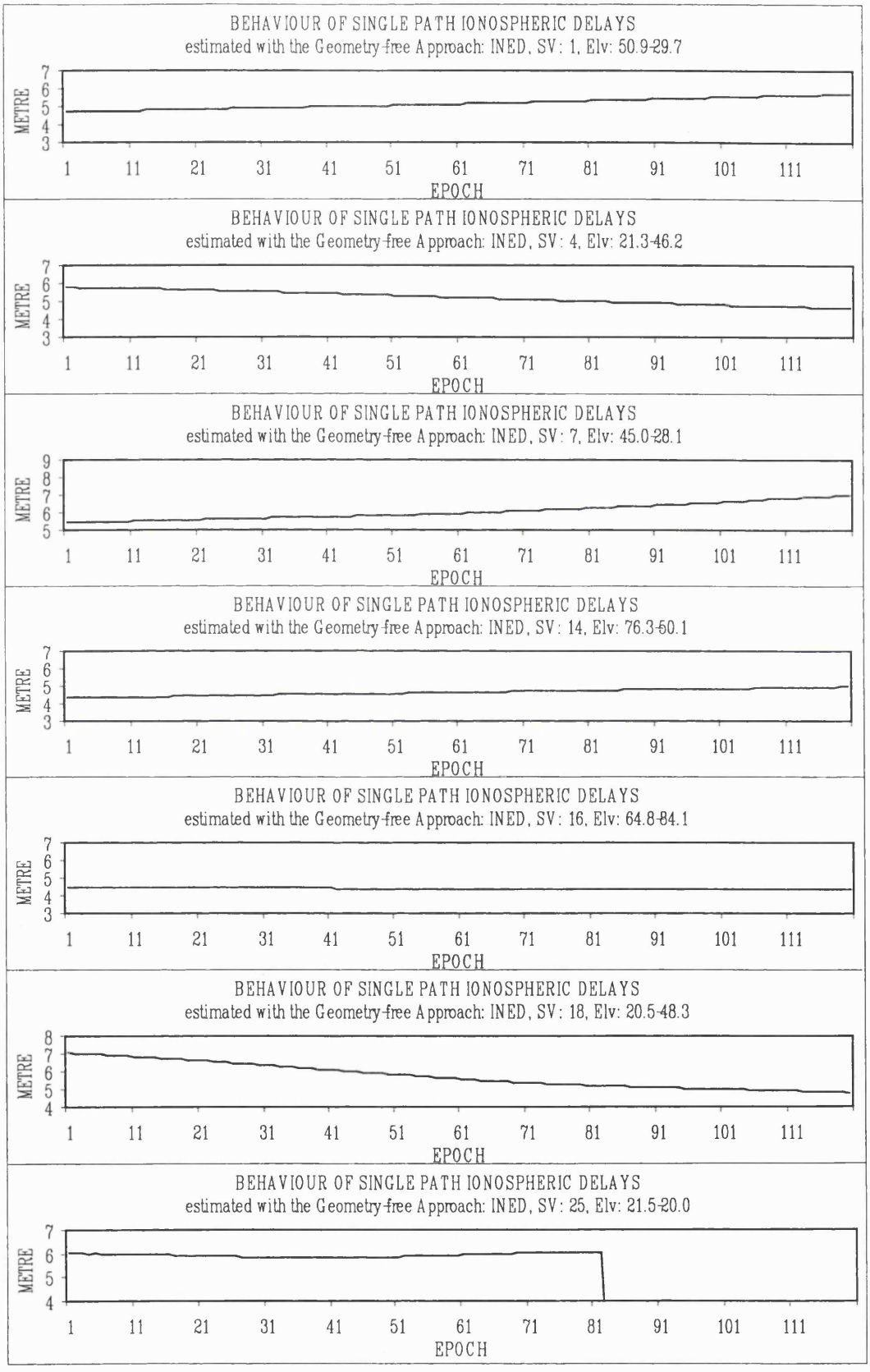

Figure A.20 The behaviour of single path ionospheric delays at the station INED

1. At station SHEN

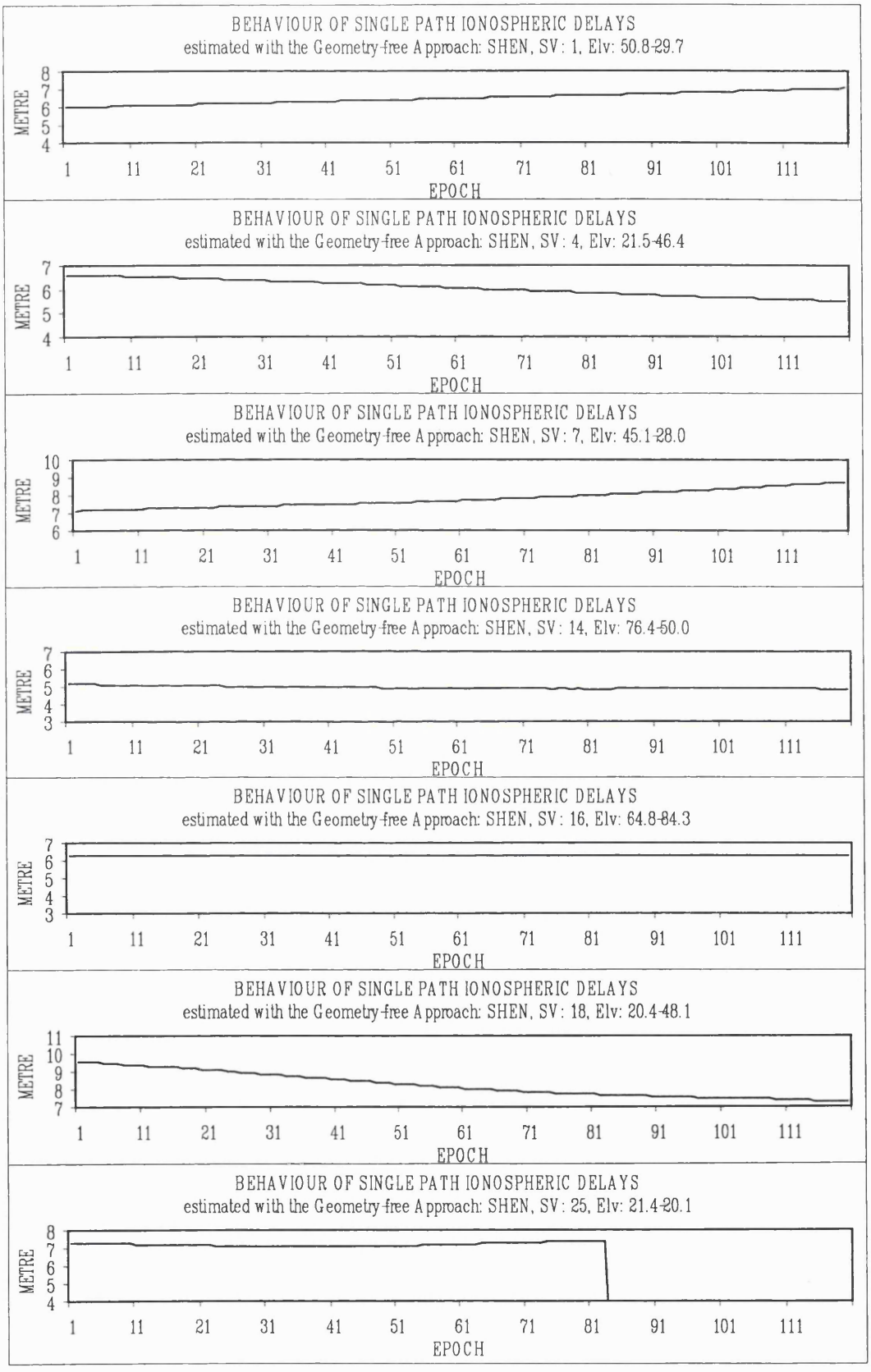

Figure A.21 The behaviour of single path ionospheric delays at the station SHEN

2. At station PLAT

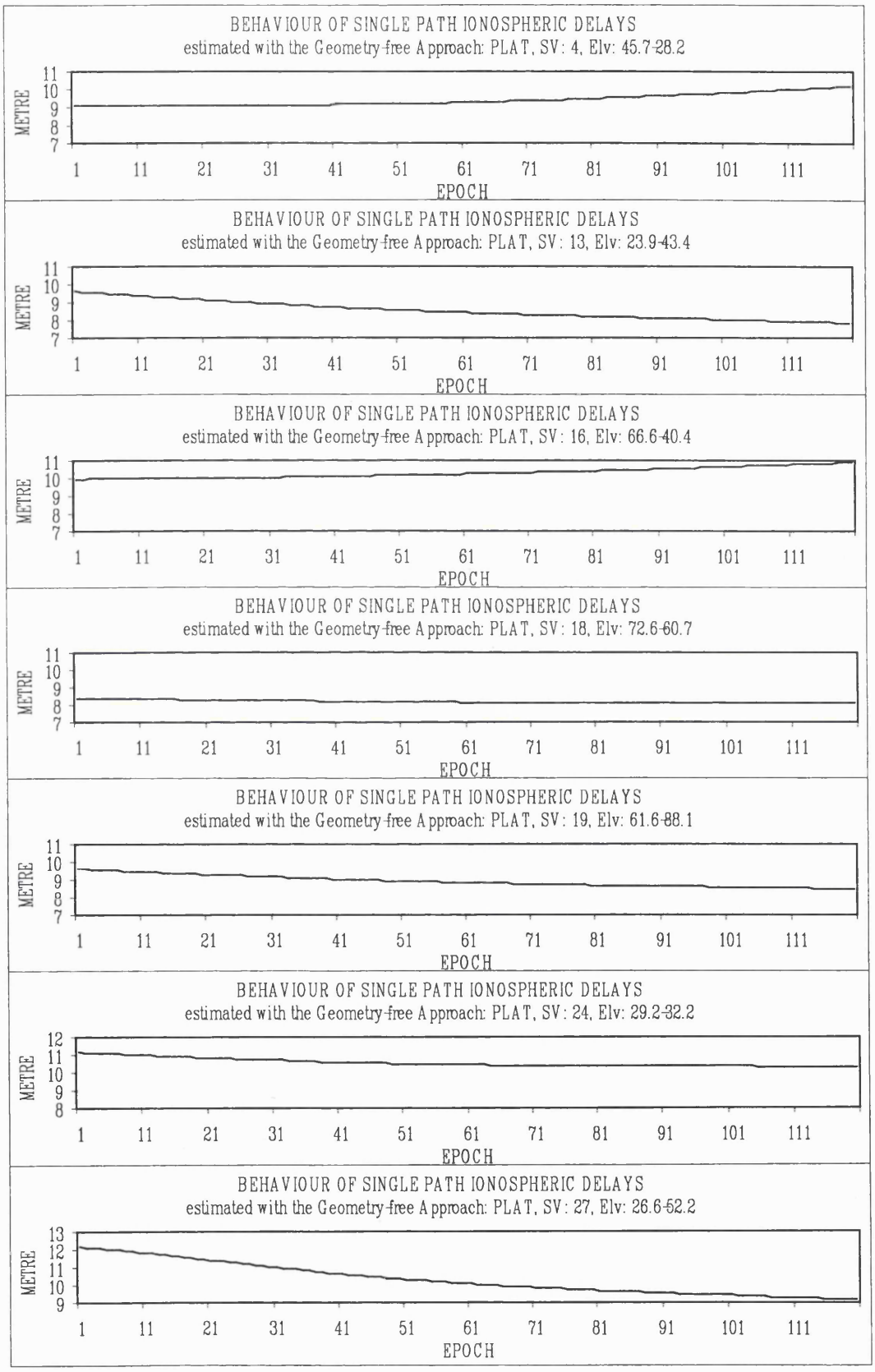

Figure A.22 The behaviour of single path ionospheric delays at the station PLAT

3. At station SOHO

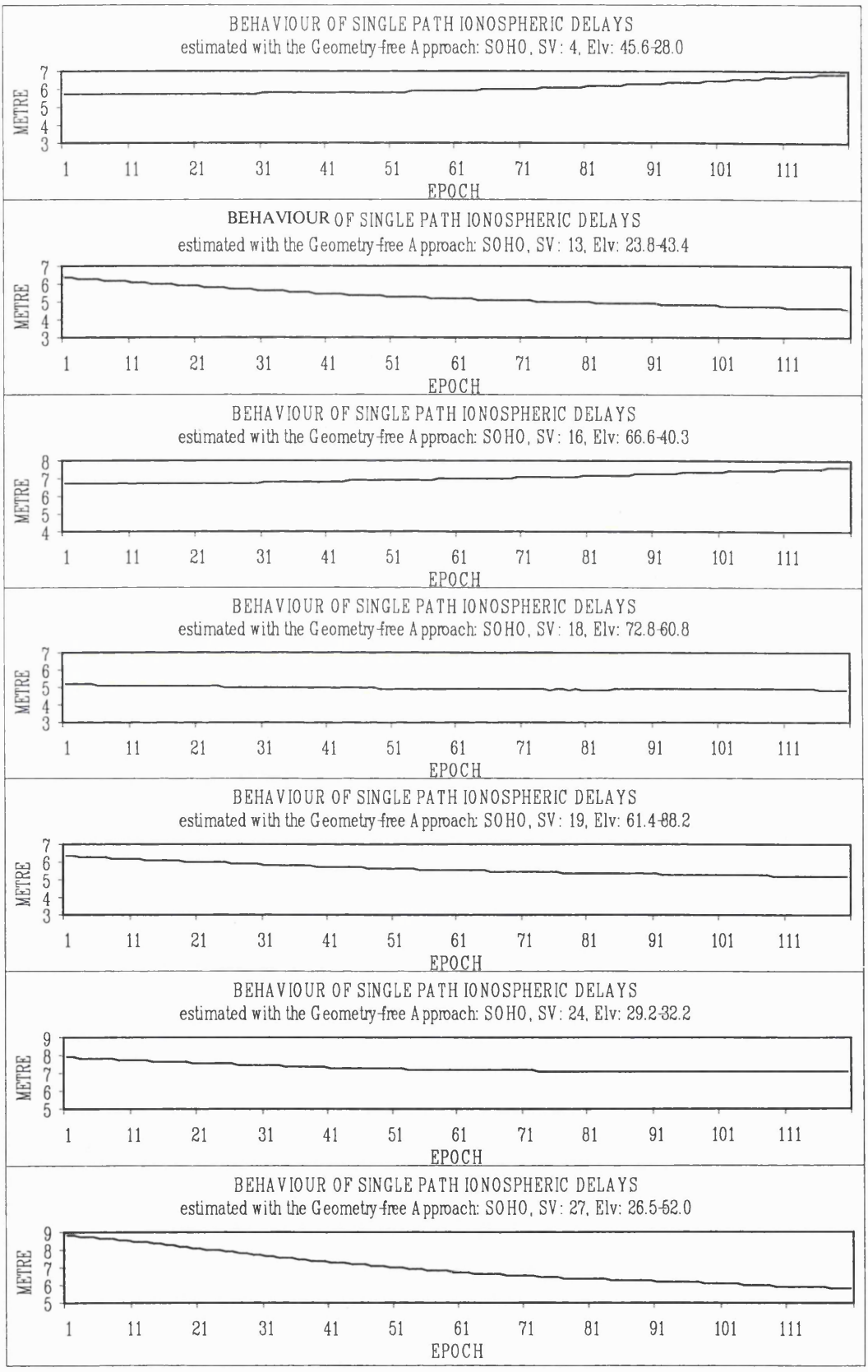

Figure A.23 The behaviour of single path ionospheric delays at the station SOHO

- The behaviour of double differenced ionospheric delays of the trials tested

1. Trial of baseline PSMS-SEMA

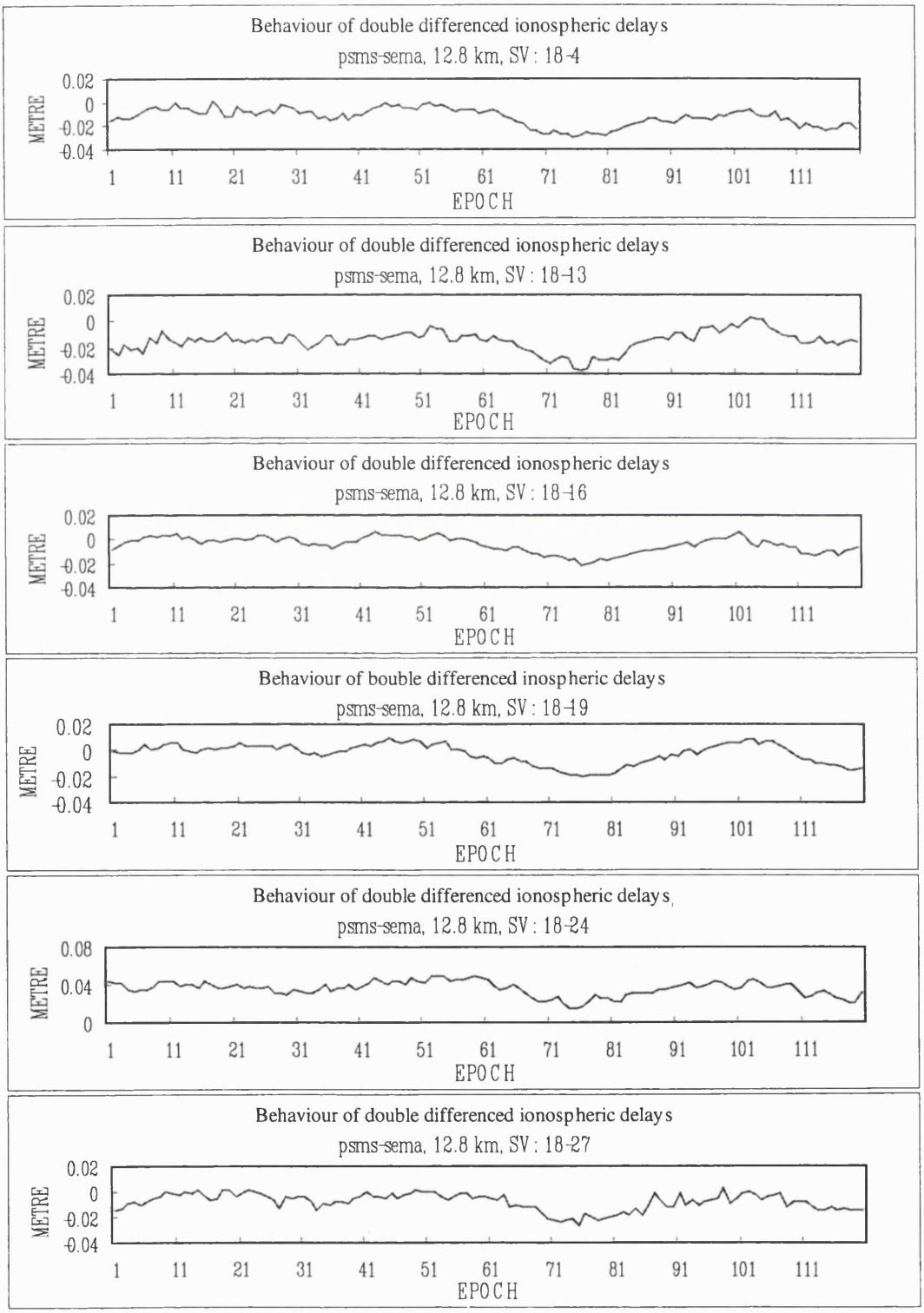

Figure A.24 Behaviour of double differenced ionospheric delays in the trial of baselines PSMS-SEMA

2. Trial of baseline CG54-KRPI

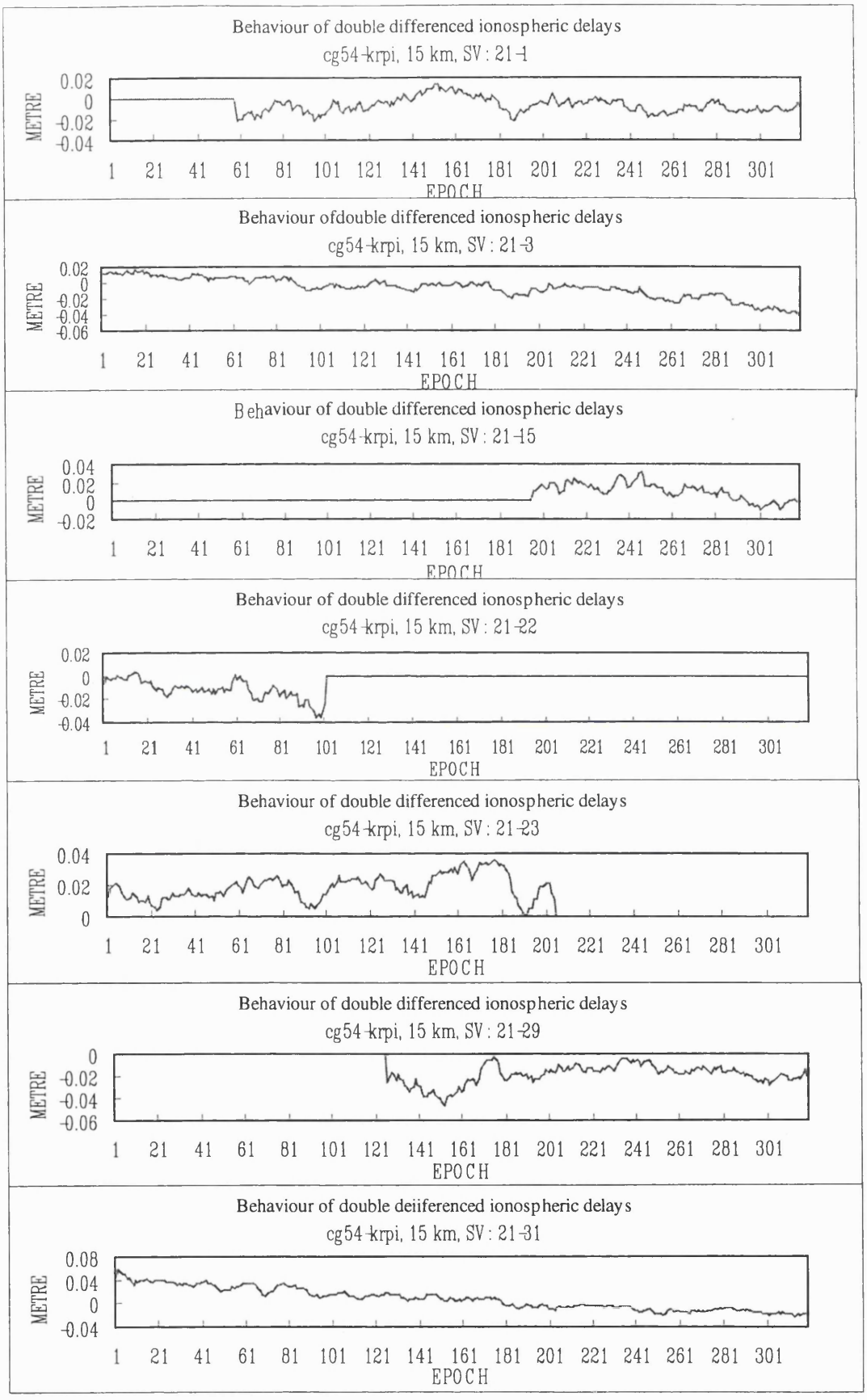

Figure A.25 Behaviour of double differenced ionospheric delays in the trial of baselines CG54-KRPI

3. Trial of baseline INED-SHEN

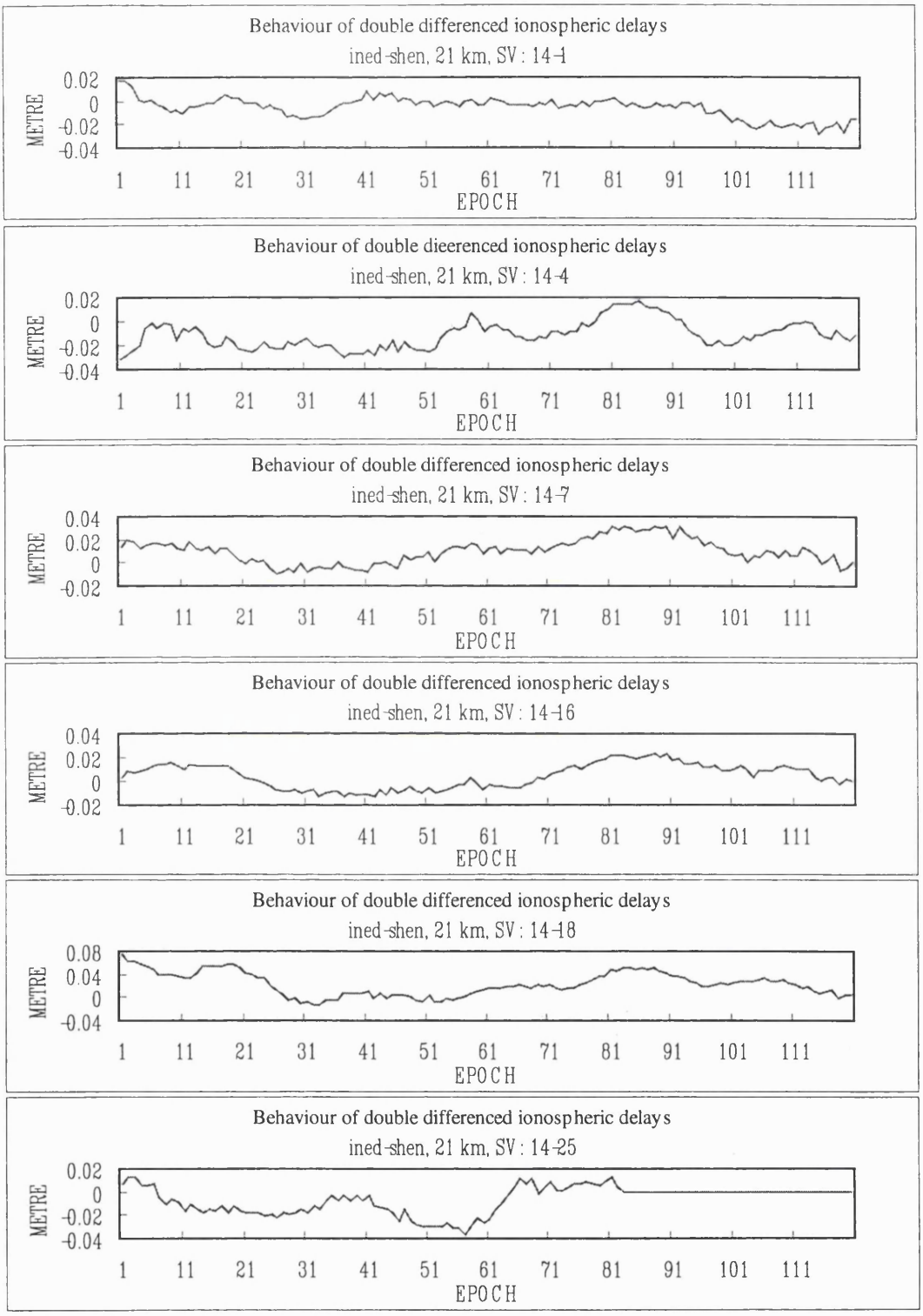

Figure A.26 Behaviour of double differenced ionospheric delays in the trial of baselines INED-SHEN

4. Trial of baseline PSMS-PLAT

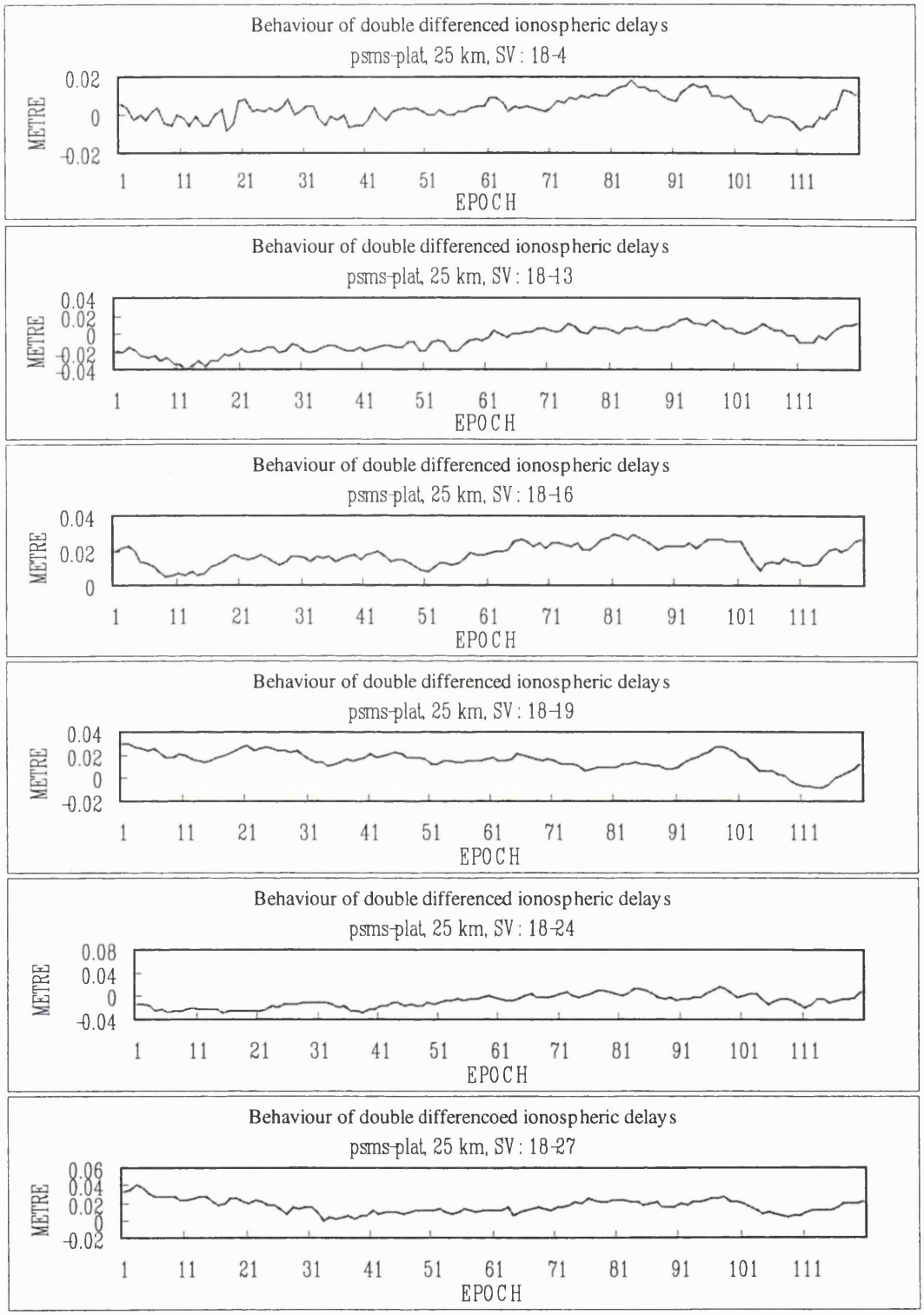

Figure A.27 Behaviour of double differenced ionospheric delays in the trial of baselines PSMS-PLAT

5. Trial of baseline PSMS-SOHO

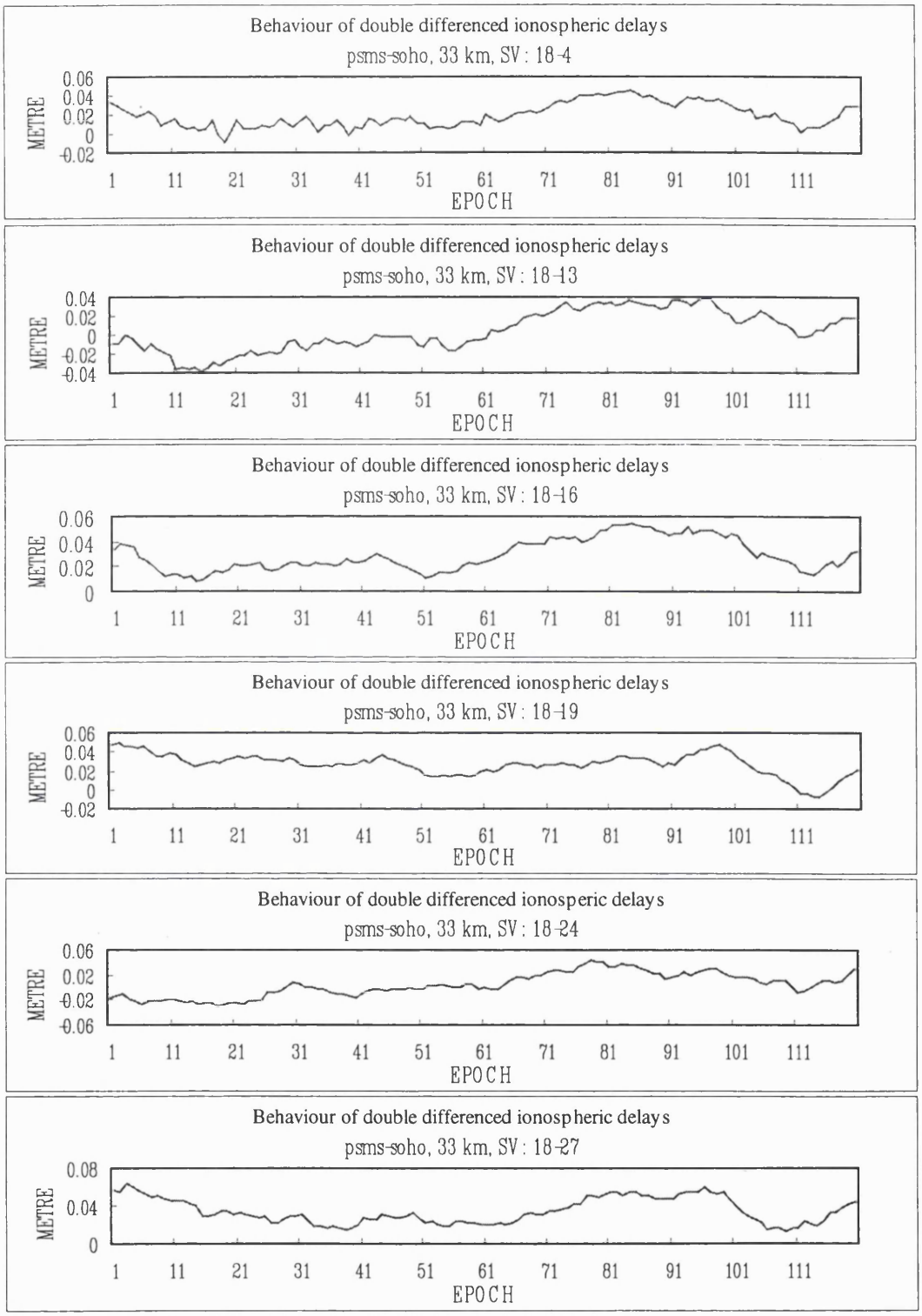

Figure A.28 Behaviour of double differenced ionospheric delays in the trial of baselines PSMS-SOHO

- The behaviour of double differenced tropospheric delays of the trials tested

1. Trial of baseline PSMS-SEMA

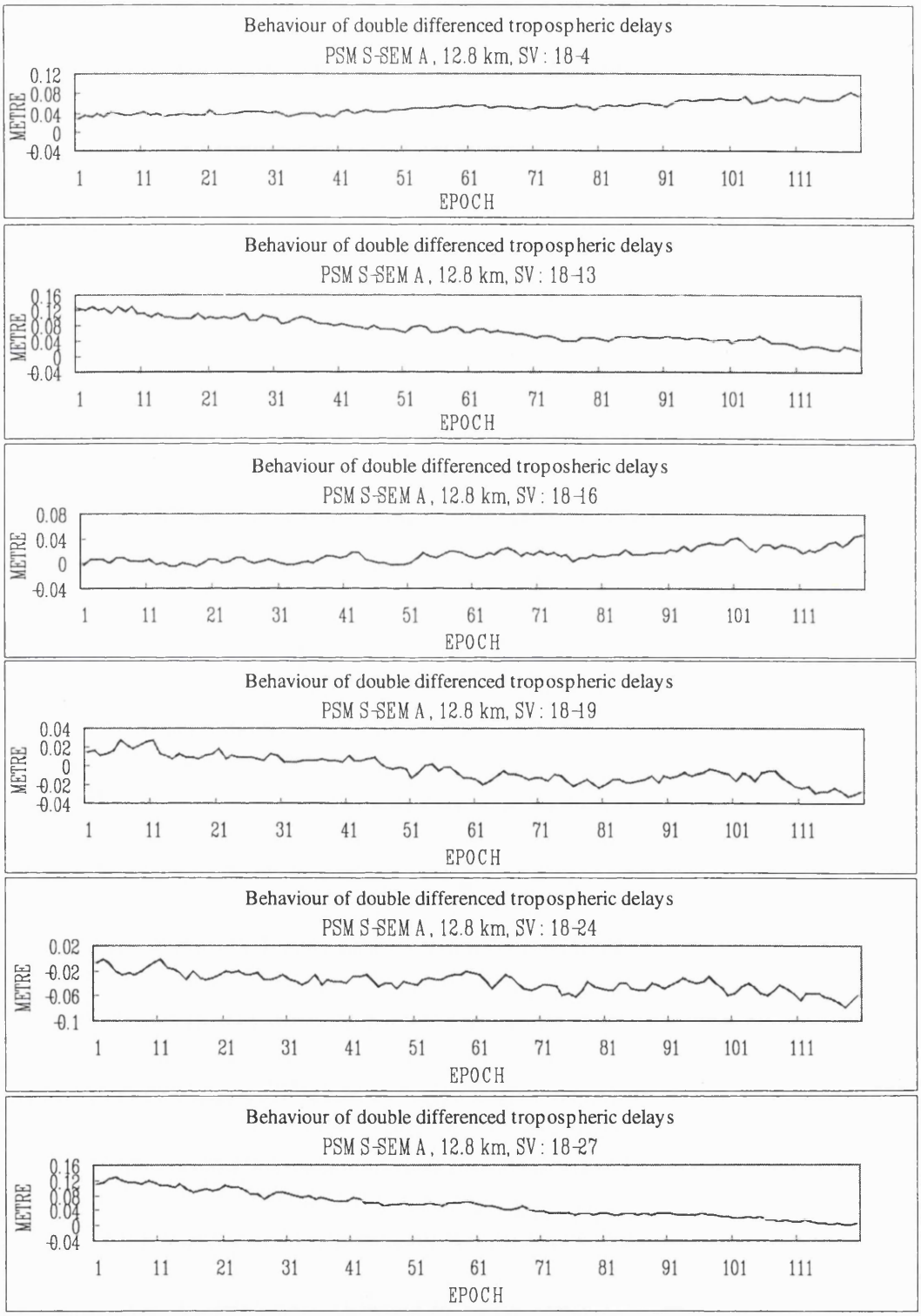

Figure A.29 Behaviour of double differenced tropospheric delays in the trial of baselines PSMS-SEMA

2. Trial of baseline CG54-KRPI

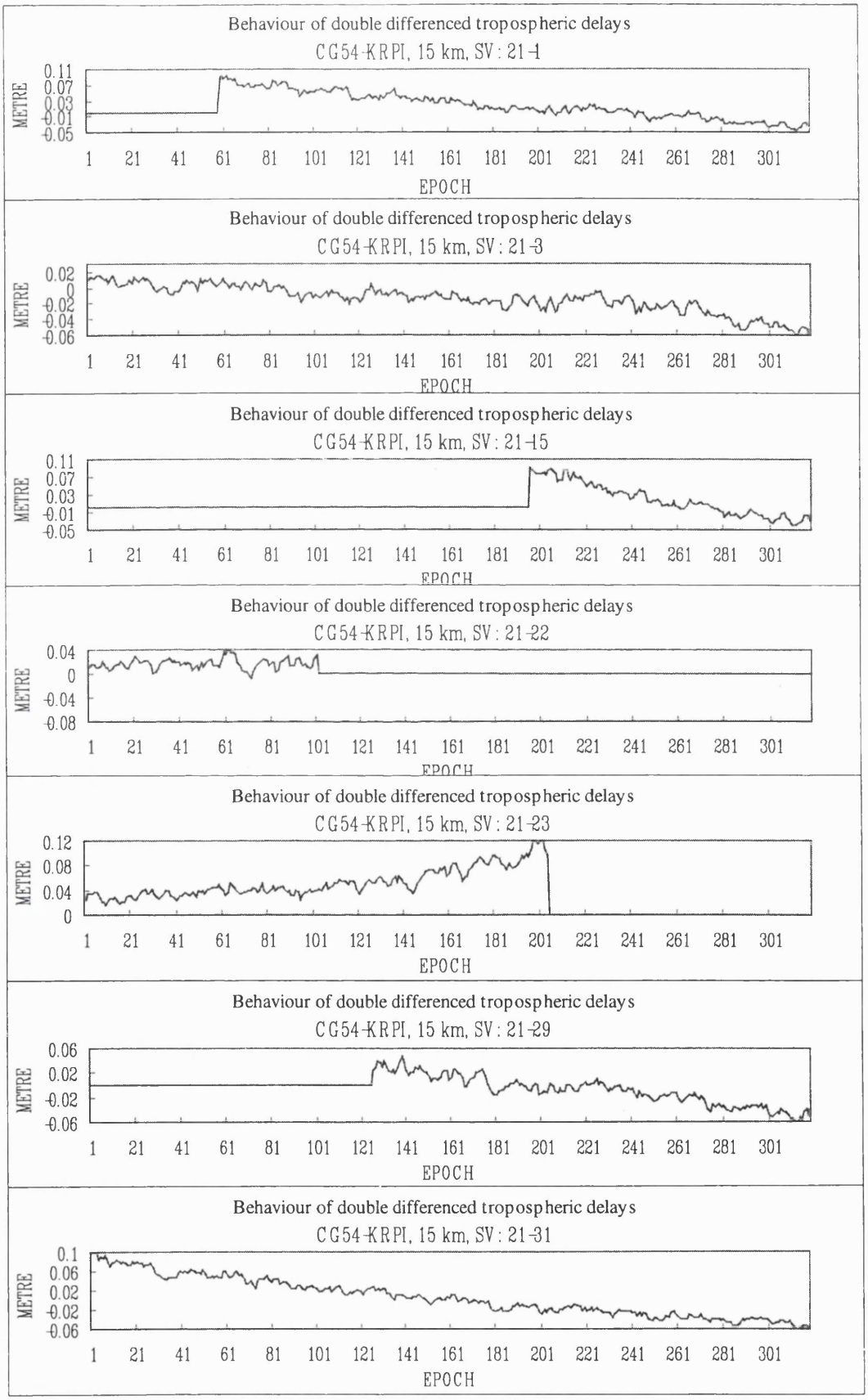

Figure A.30 Behaviour of double differenced tropospheric delays in the trial of baselines CG54-KRPI

3. Trial of baseline INED-SHEN

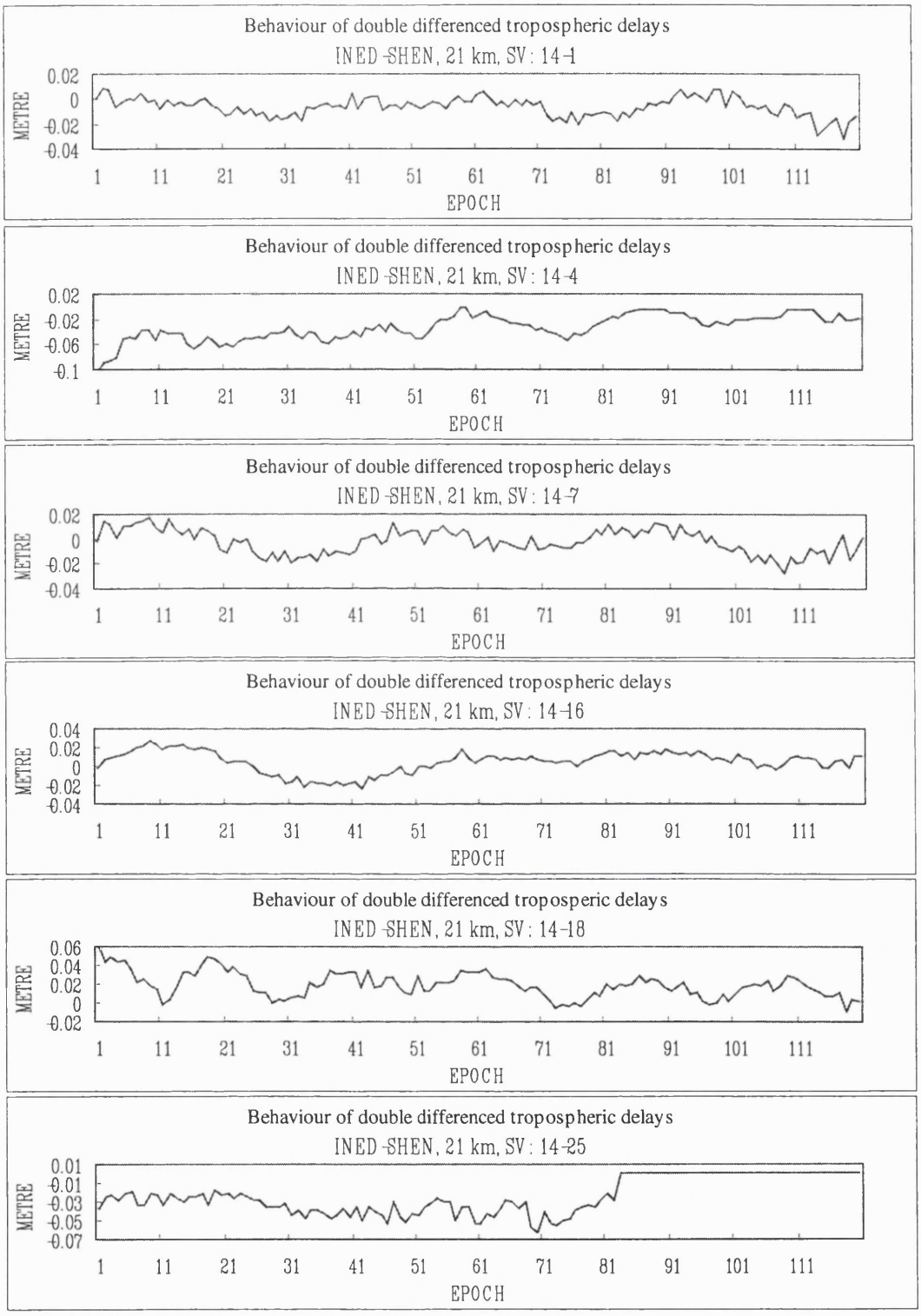

Figure A.31 Behaviour of double differenced tropospheric delays in the trial of baselines INED-SHEN

4. Trial of baseline PSMS-PLAT

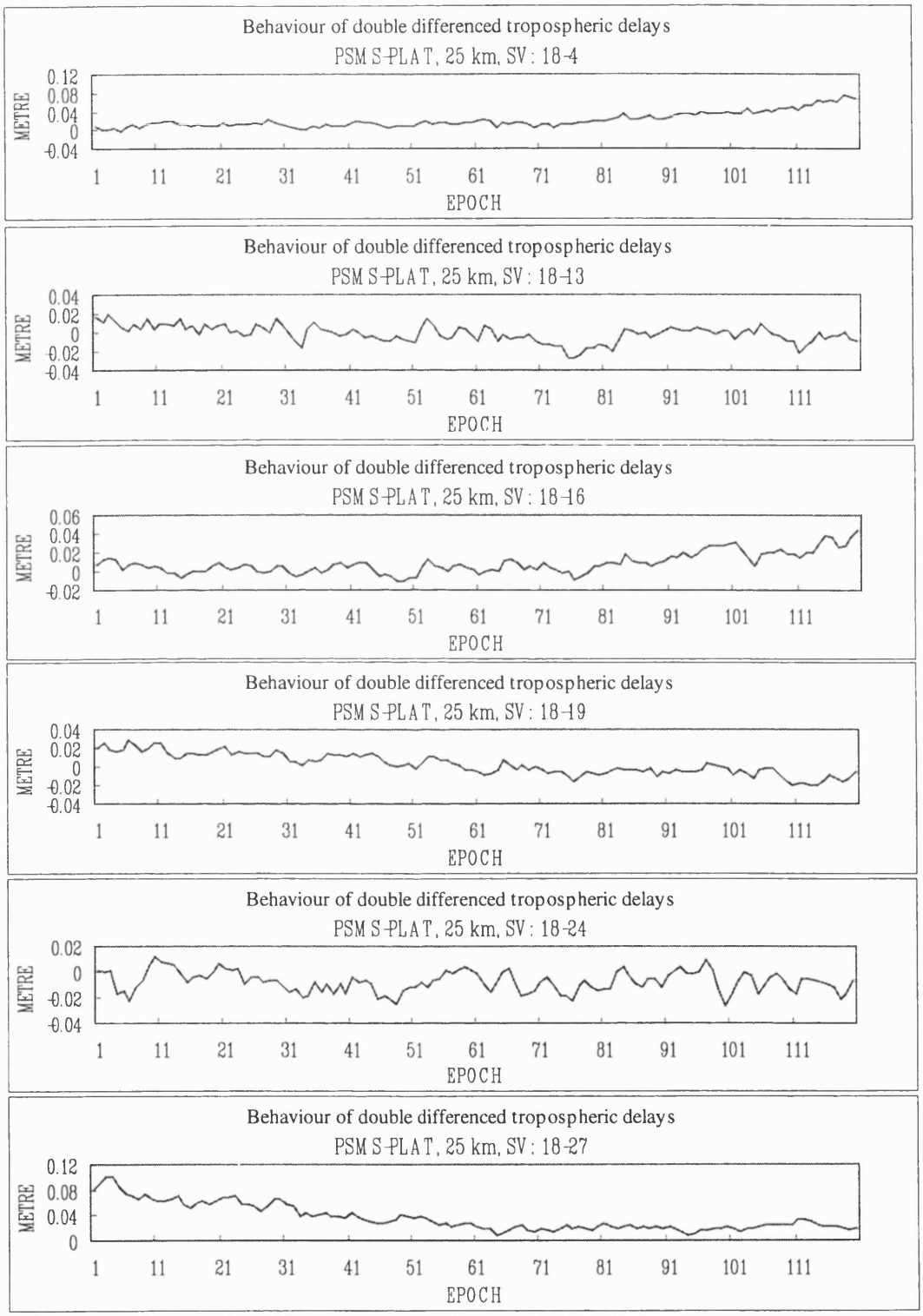

Figure A.32 Behaviour of double differenced tropospheric delays in the trial of baselines PSMS-PLAT

5. Trial of baseline PSMS-SOHO

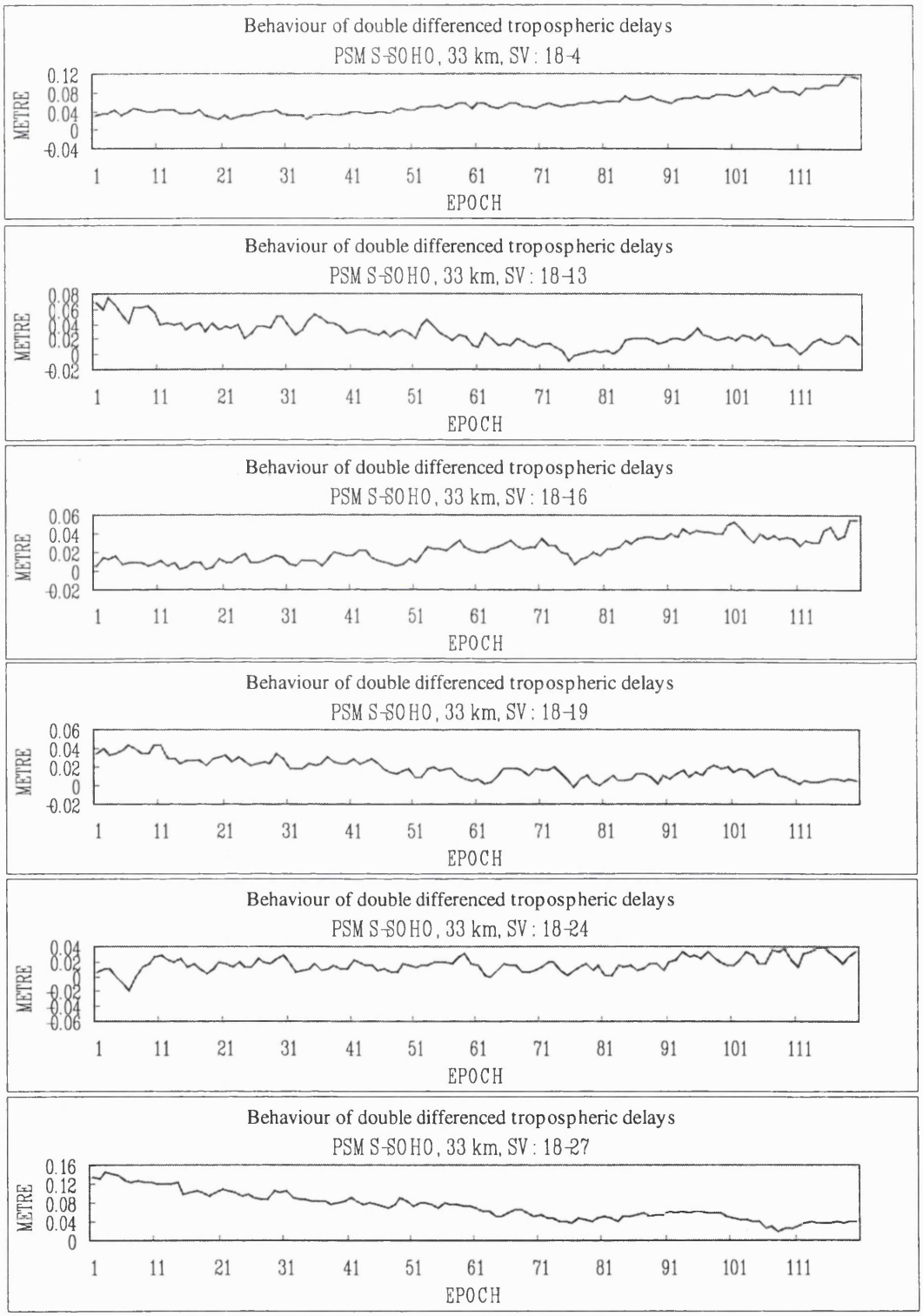

Figure A.33 Behaviour of double differenced tropospheric delays in the trial of baselines PSMS-SOHO

- The comparison between the "true" double differenced tropospheric delays obtained from the linear combination approach and the double differenced tropospheric estimation based on the Saastamoinen model

1. Trial of baseline PSMS-SEMA

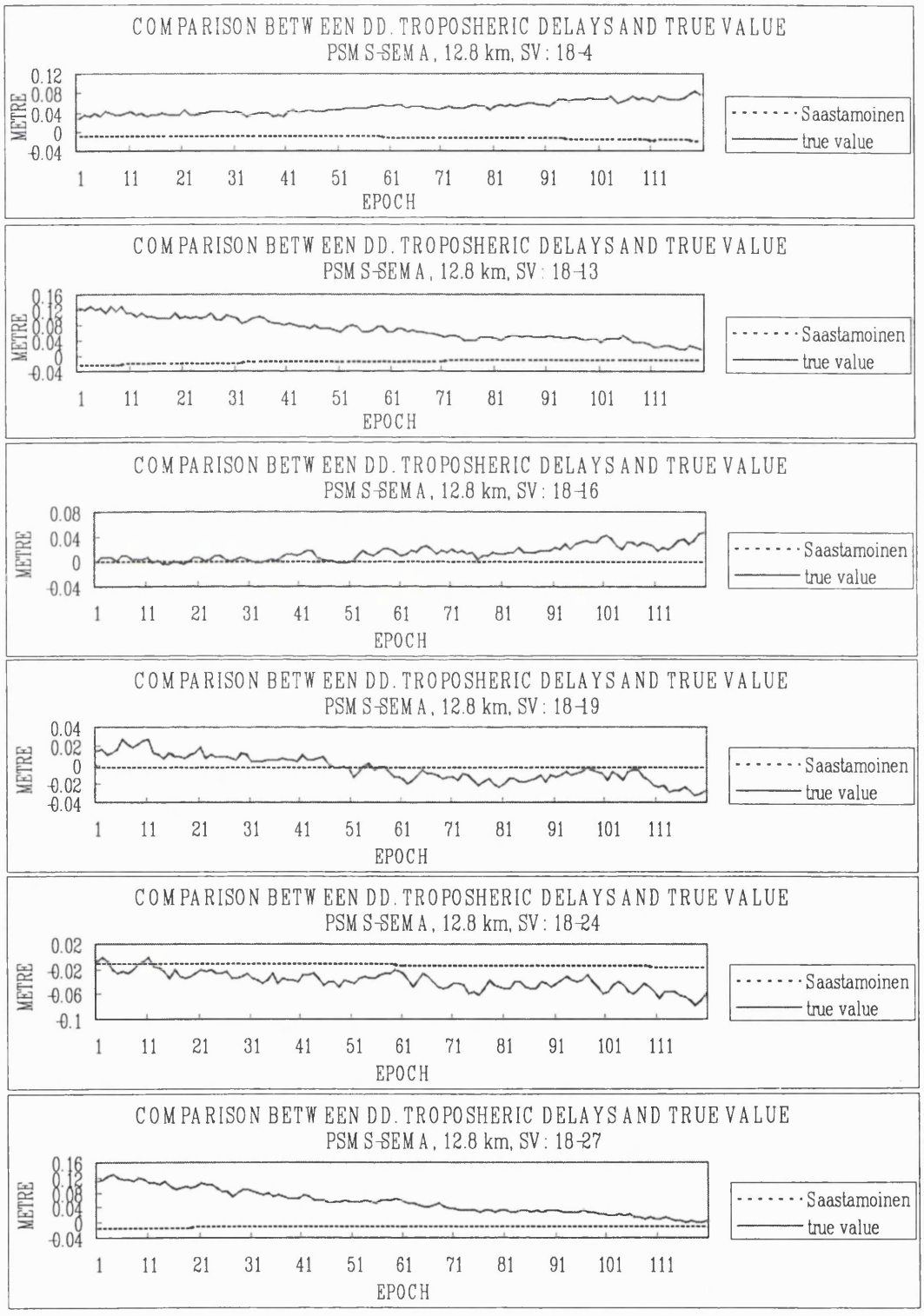

Figure A.34 Comparison between the "true" and the estimation of double differenced tropospheric delays in the trial of baseline PSMS-SEMA

2. Trial of baseline CG54-KRPI

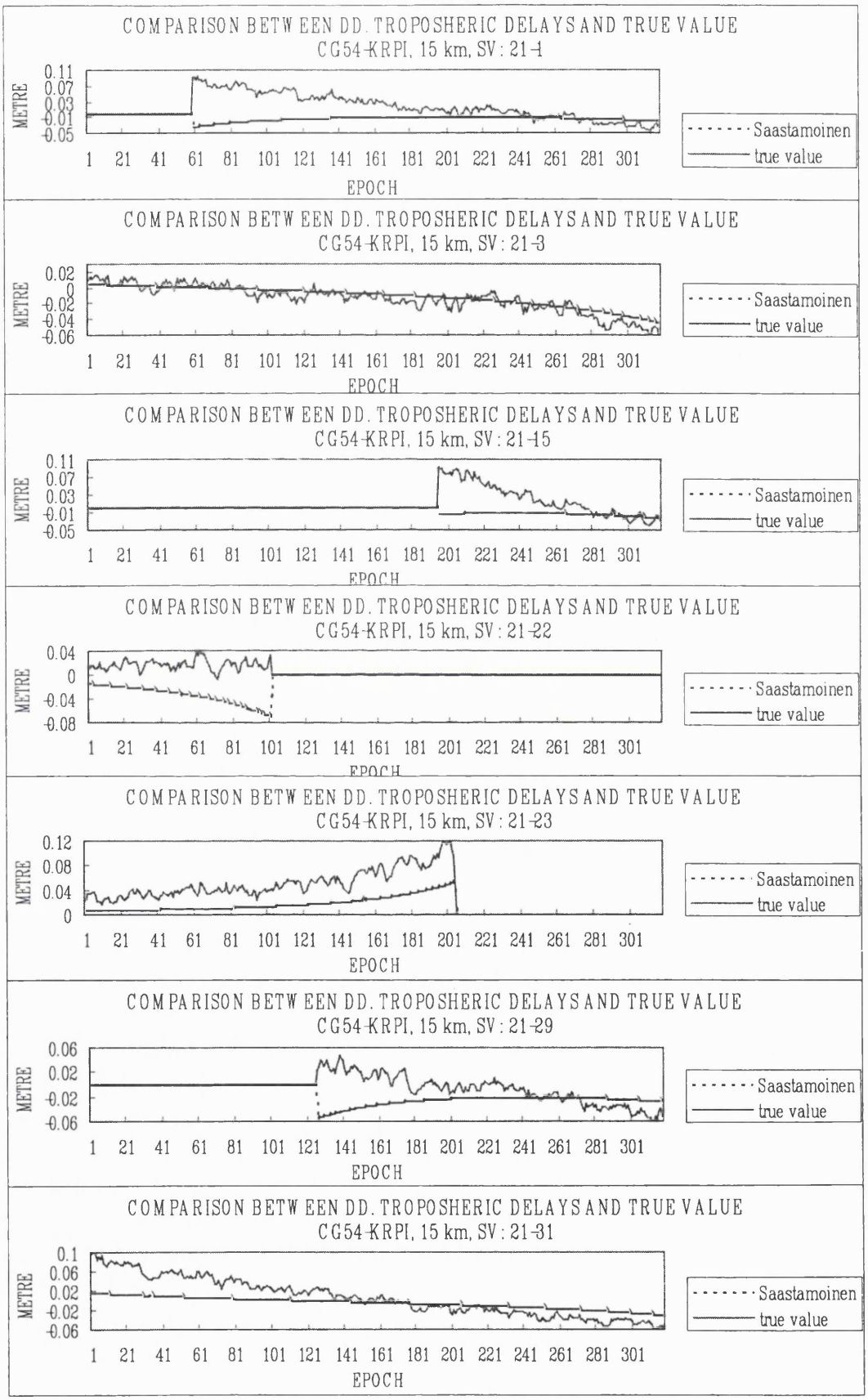

Figure A.35 Comparison between the "true" and the estimation of double differenced tropospheric delays in the trial of baseline CG54-KRPI

3. Trial of baseline INED-SHEN

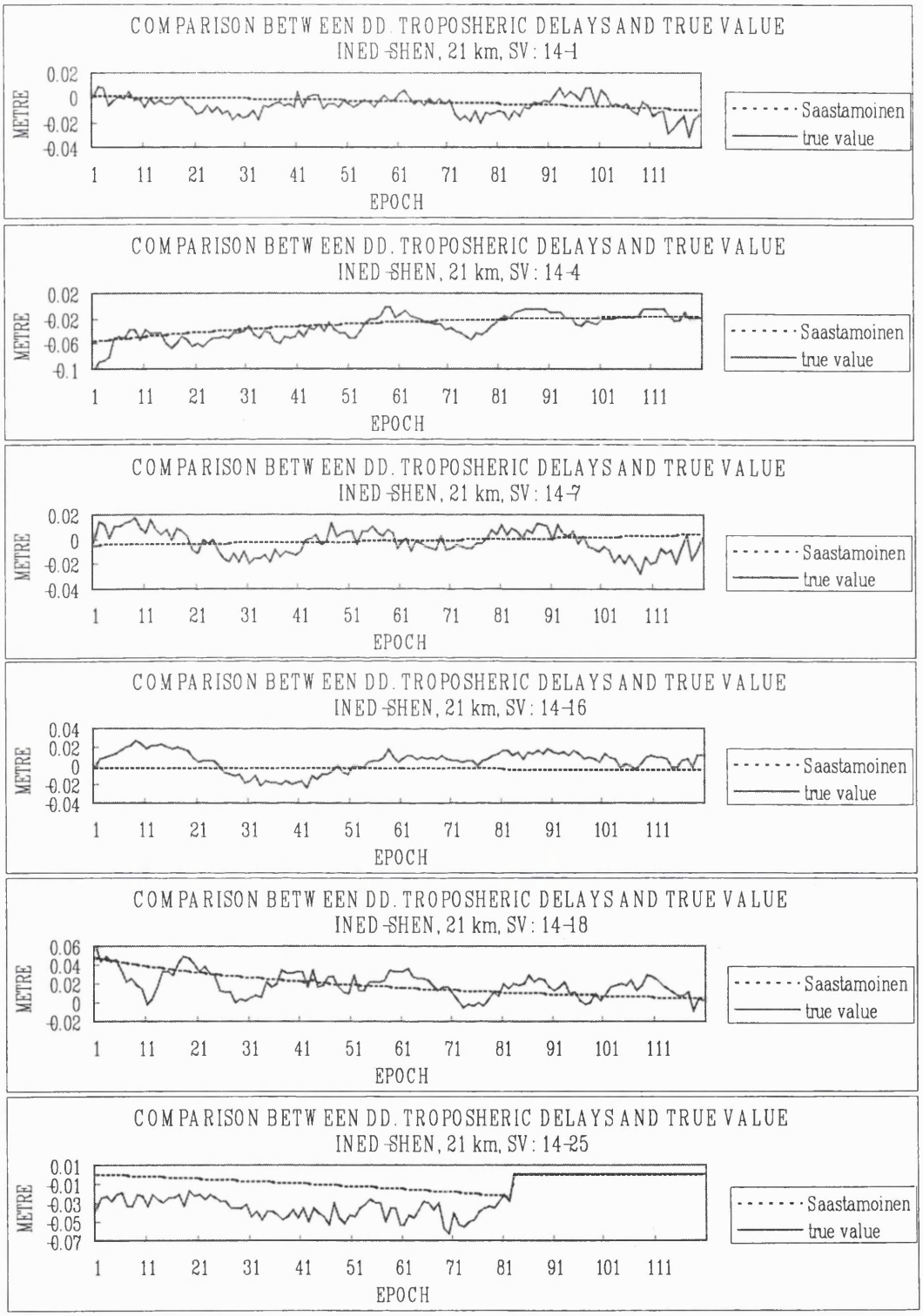

Figure A.36 Comparison between the "true" and the estimation of double differenced tropospheric delays in the trial of baseline INED-SHEN

4. Trial of baseline PSMS-PLAT

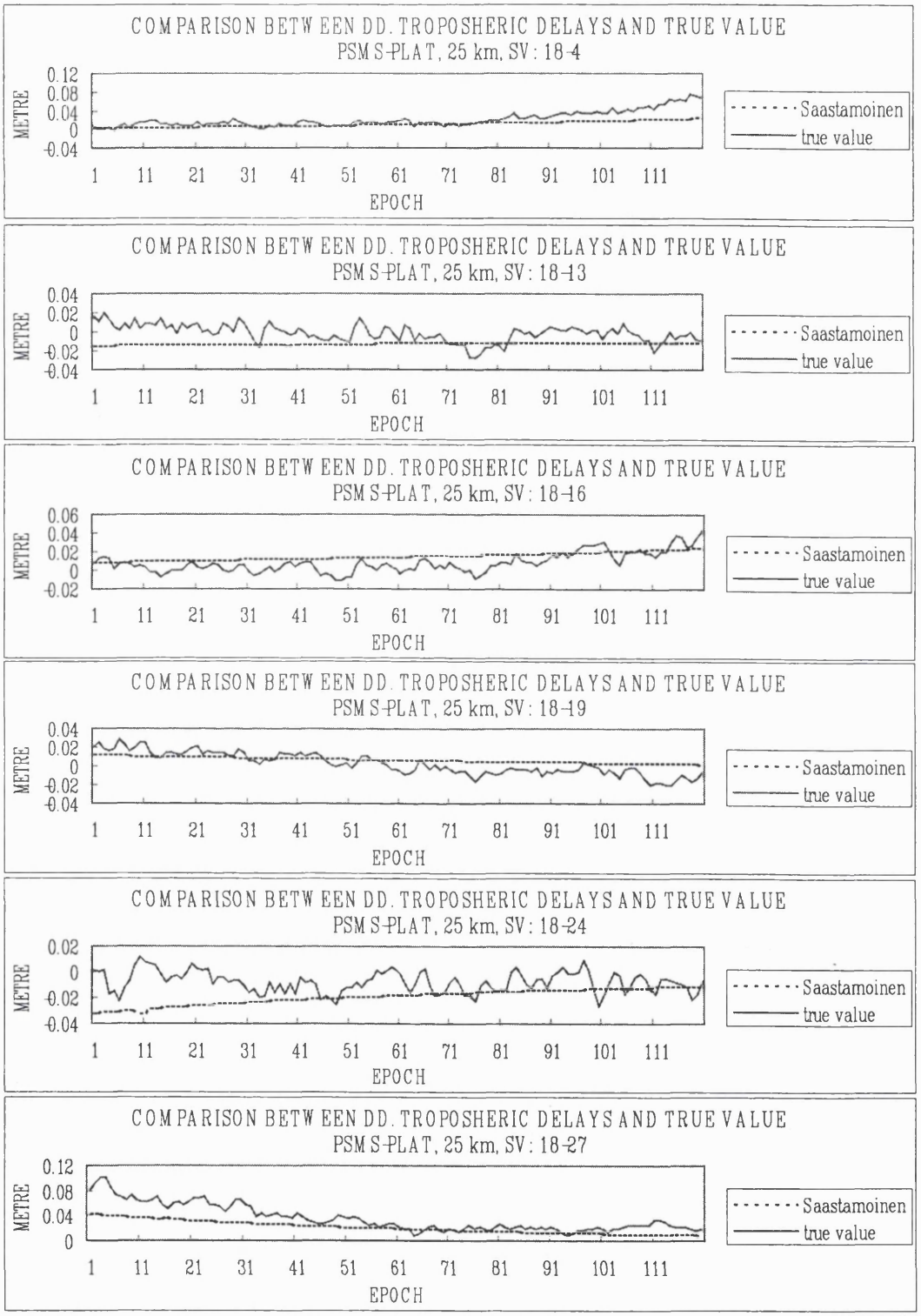

Figure A.37 Comparison between the "true" and the estimation of double differenced tropospheric delays in the trial of baseline PSMS-PLAT

5. Trial of baseline PSMS-SOHO

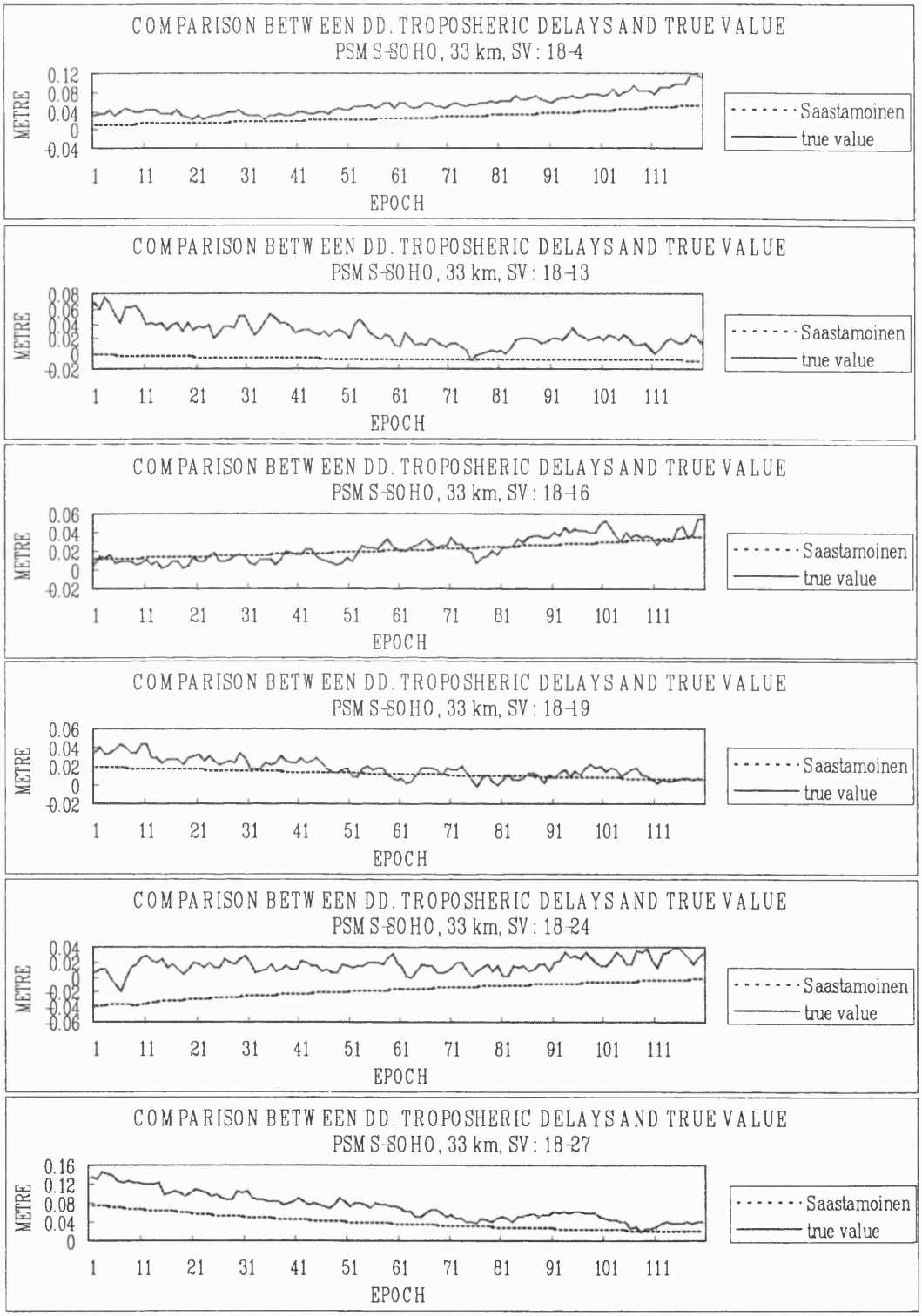

Figure A.38 Comparison between the "true" and the estimation of double differenced tropospheric delays in the trial of baseline PSMS-SOHO

APPENDIX B

SUMMARY OF THE RELATED FIGURES OF DOUBLE DIFFERENCED IONOSPHERIC ESTIMATIONS AND COMPARISONS (CHAPTER SEVEN)

In Appendix B, it includes the related figures of double differenced ionospheric estimations and comparisons of Chapter 7 as follows:

- The double differenced ionospheric delays of the trials tested (Figure B.1-B.30),

1. Trial of 12.8km baseline (Figure B.1-B.6)

2. Trial of 15km baseline (Figure B.7-B.12)

3. Trial of 21km baseline (Figure B.13-B.18)

4. Trial of 25km baseline (Figure B.19-B.24)

5. Trial of 33km baseline (Figure B.25-B.30)

1. Trial of 12.8 km baseline

- Comparison of double differenced ionospheric delays based on LIM1 with the true values.

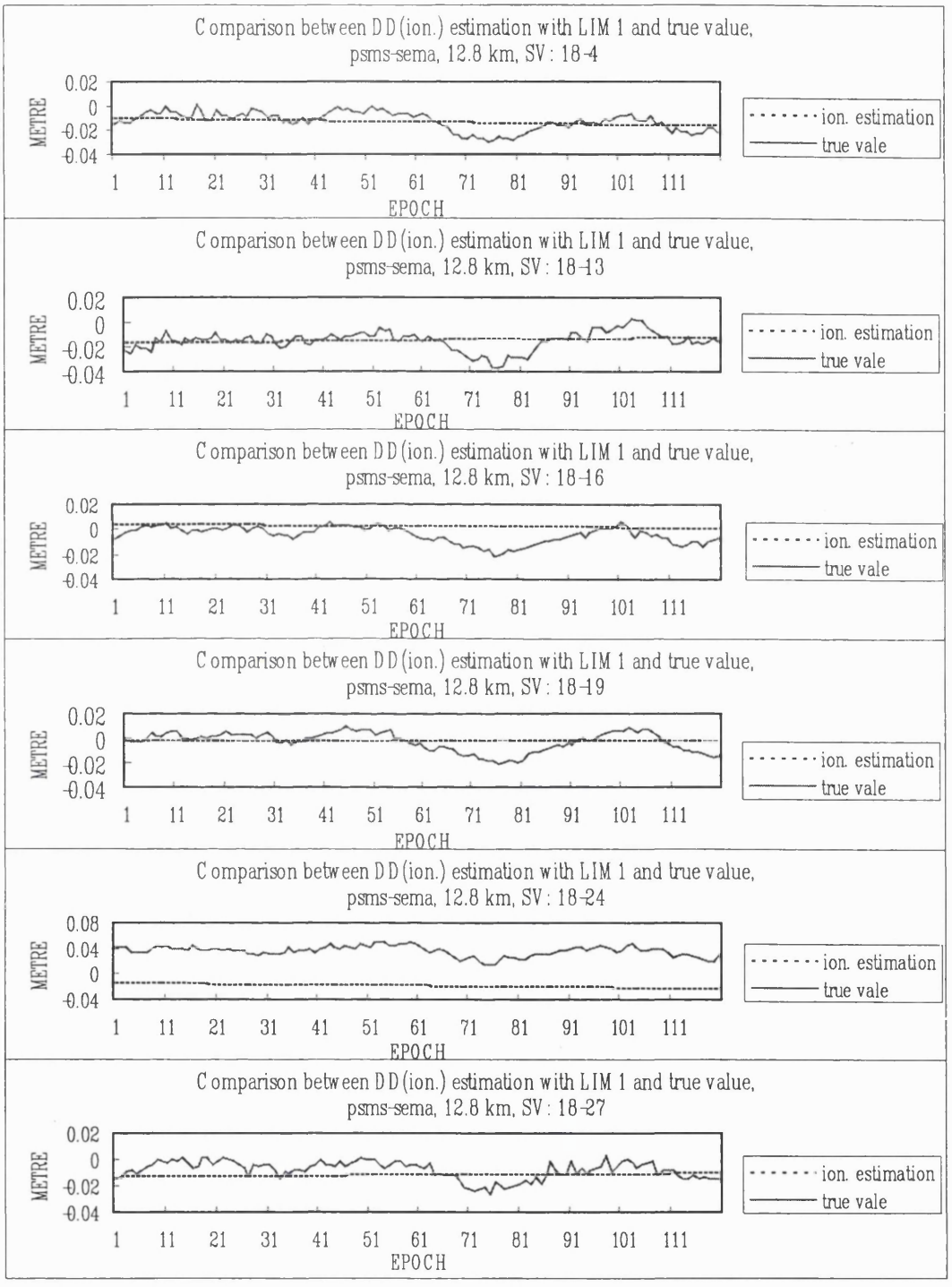

Figure B.1 Comparison of double differenced ionospheric delays based on LIM1 with the true values for the trial of 12.8km baseline

- Comparison of double differenced ionospheric delays based on LIM2 with the true values.

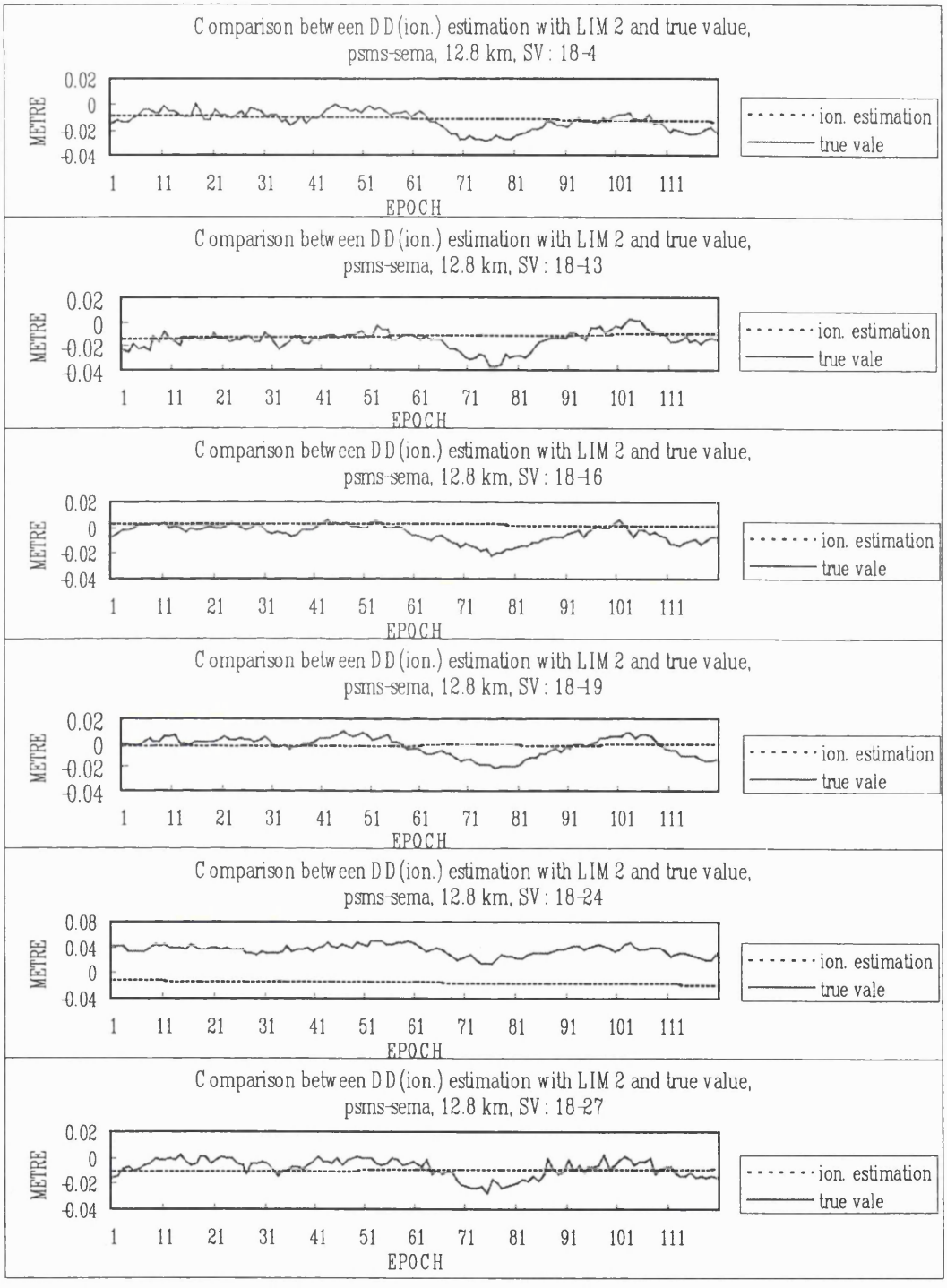

Figure B.2 Comparison of double differenced ionospheric delays based on LIM2 with the true values for the trial of 12.8km baseline

- Comparison of double differenced ionospheric delays based on LIM3 with the true values.

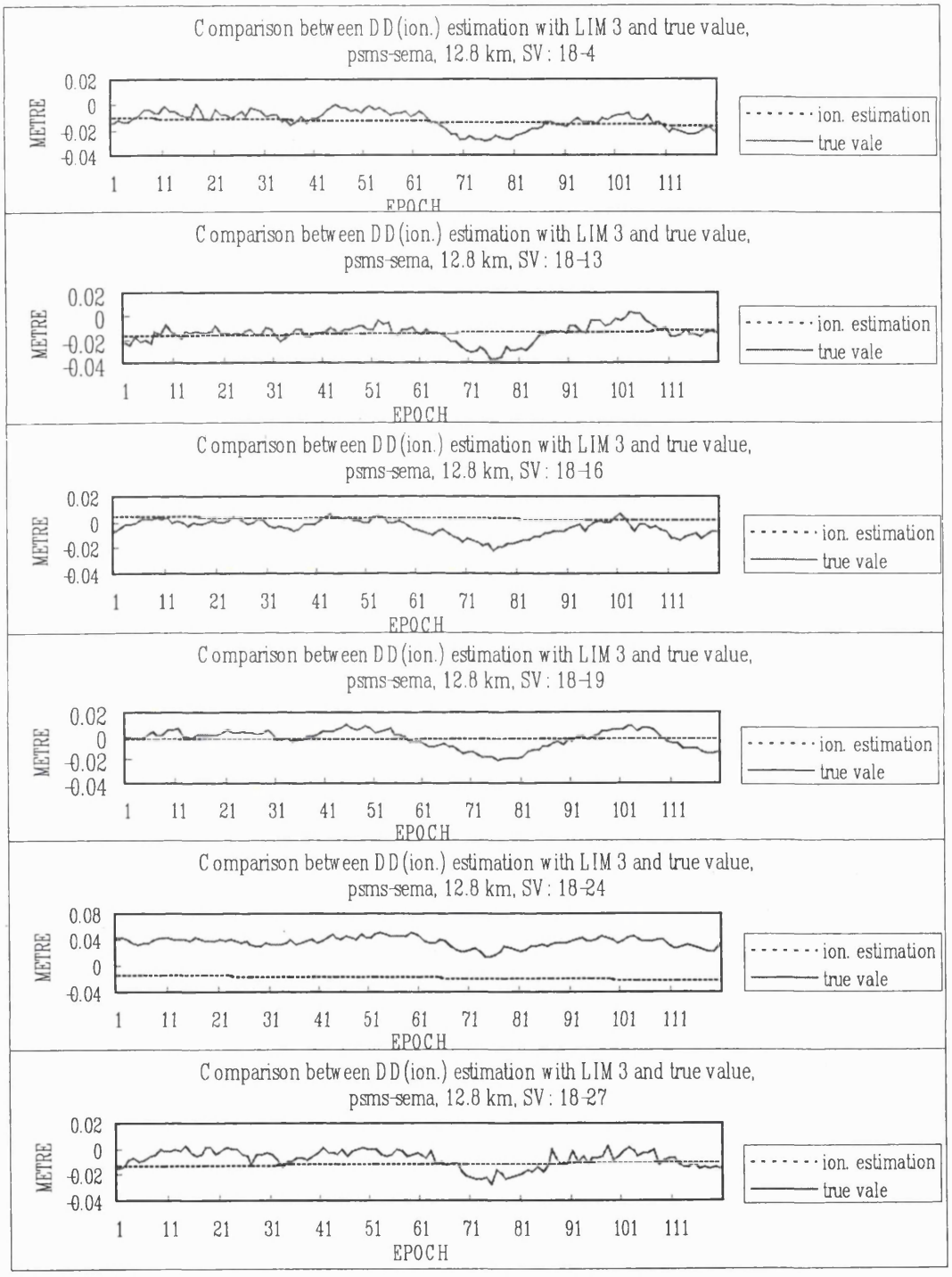

Figure B.3 Comparison of double differenced ionospheric delays based on LIM3 with the true values for the trial of 12.8km baseline

- Comparison of double differenced ionospheric delays based on LIM4 with the true values.

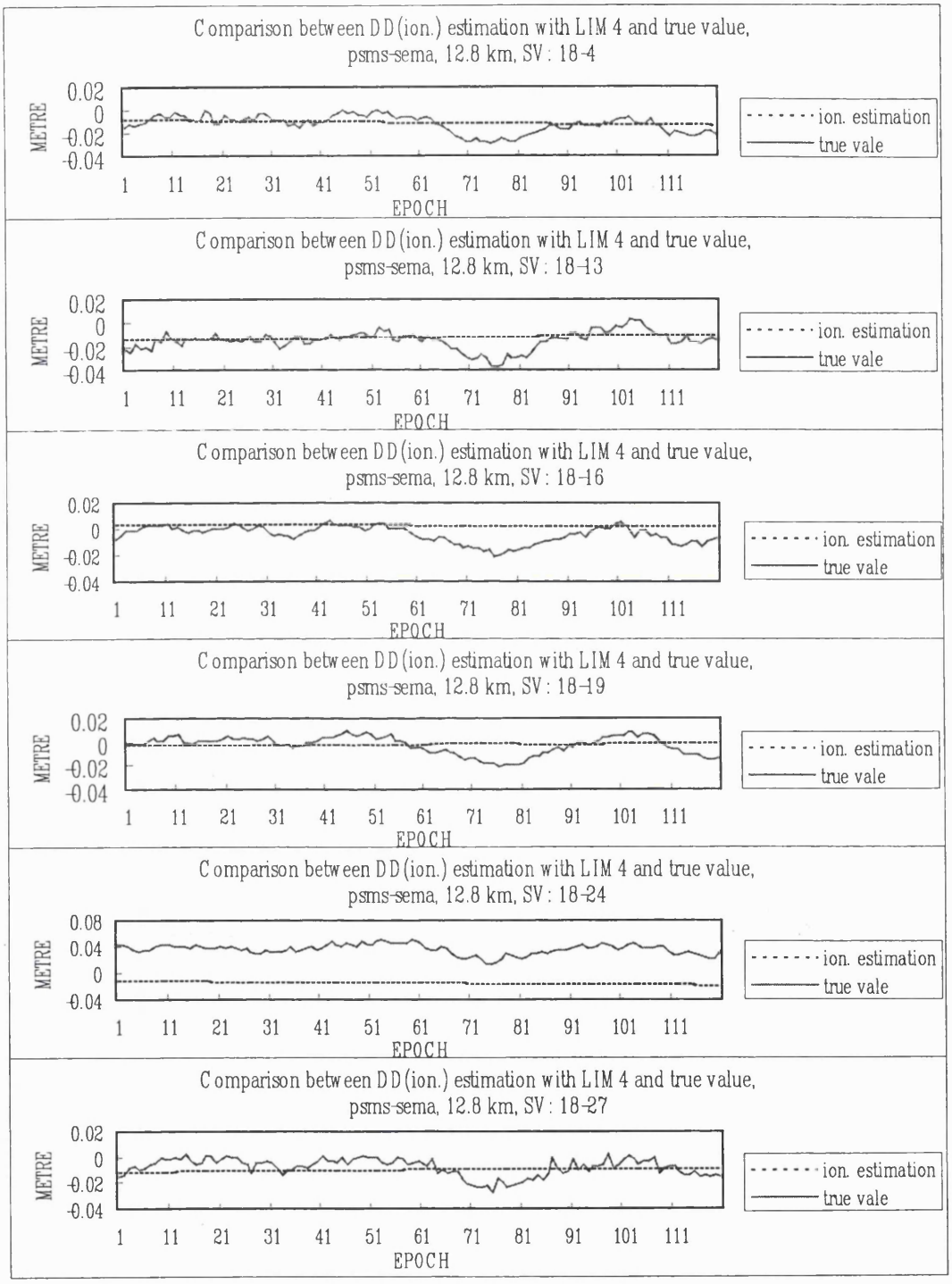

Figure B.4 Comparison of double differenced ionospheric delays based on LIM4 with the true values for the trial of 12.8km baseline

- Comparison of double differenced ionospheric delays based on LIM5 with the true values.

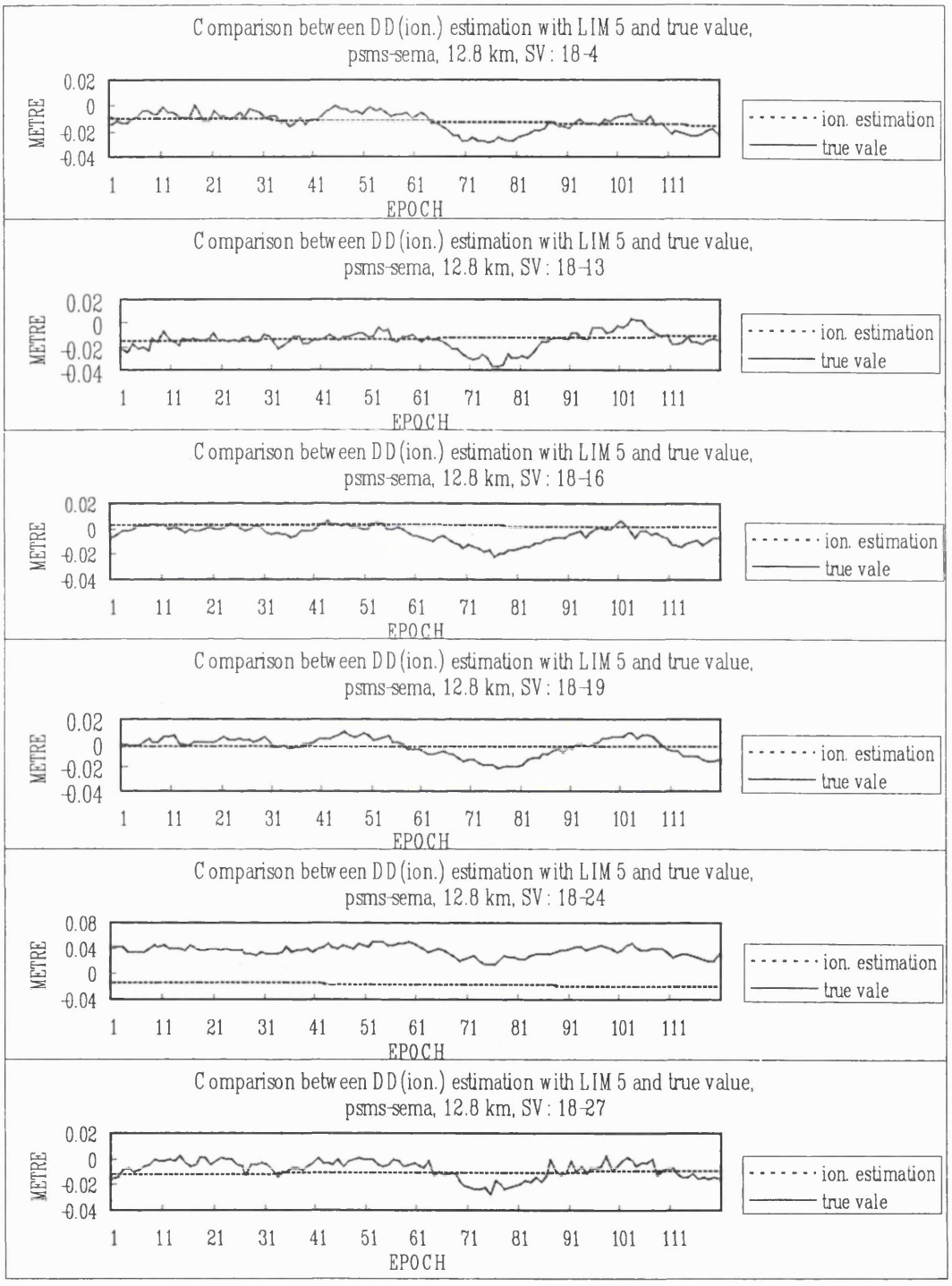

Figure B.5 Comparison of double differenced ionospheric delays based on LIM5 with the true values for the trial of 12.8km baseline

- Comparison of double differenced ionospheric delays based on LIM6 with the true values.

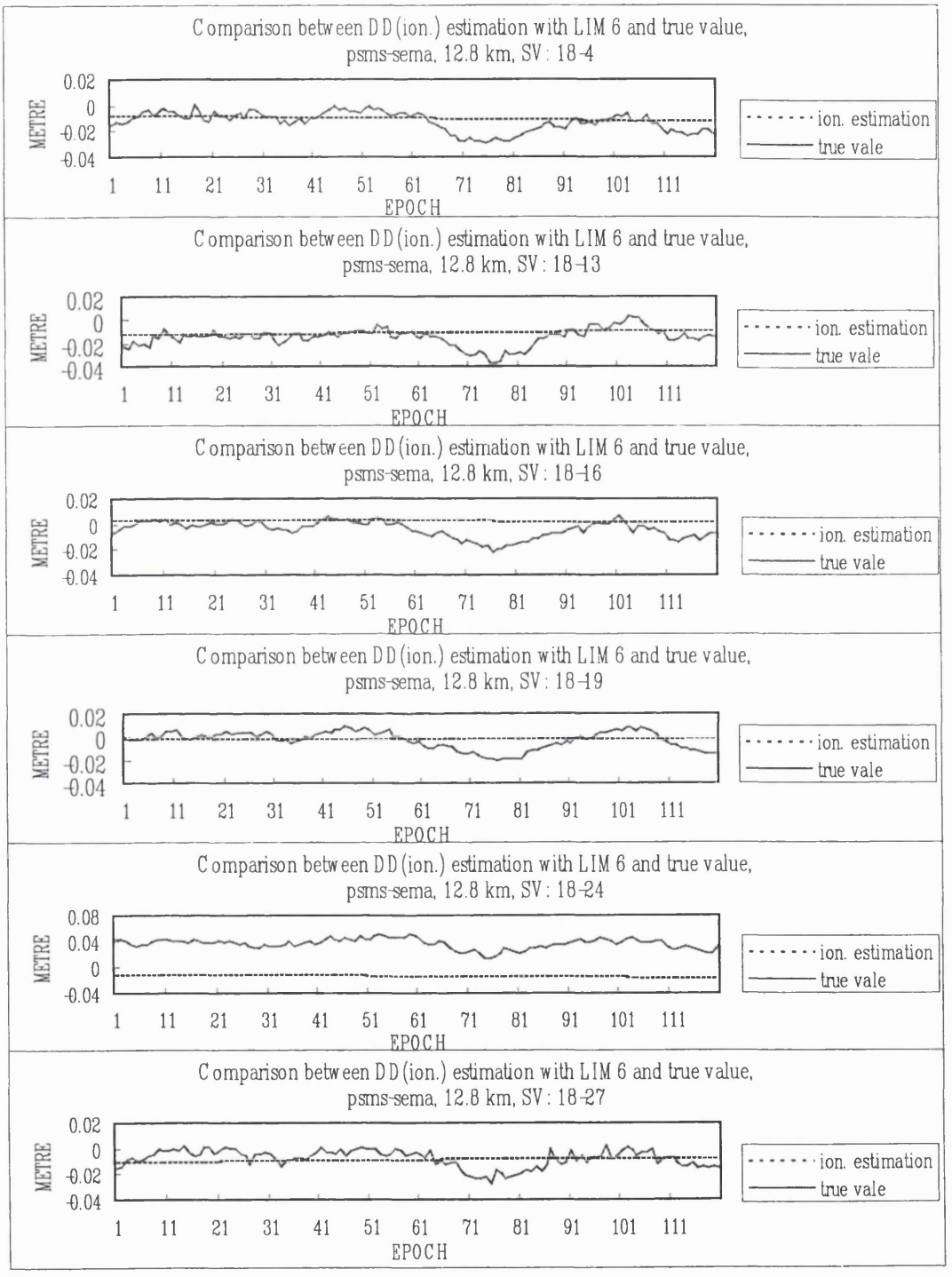

Figure B.6 Comparison of double differenced ionospheric delays based on LIM6 with the true values for the trial of 12.8km baseline

2. Trial of 15km baseline

- Comparison of double differenced ionospheric delays based on LIM1 with the true values.

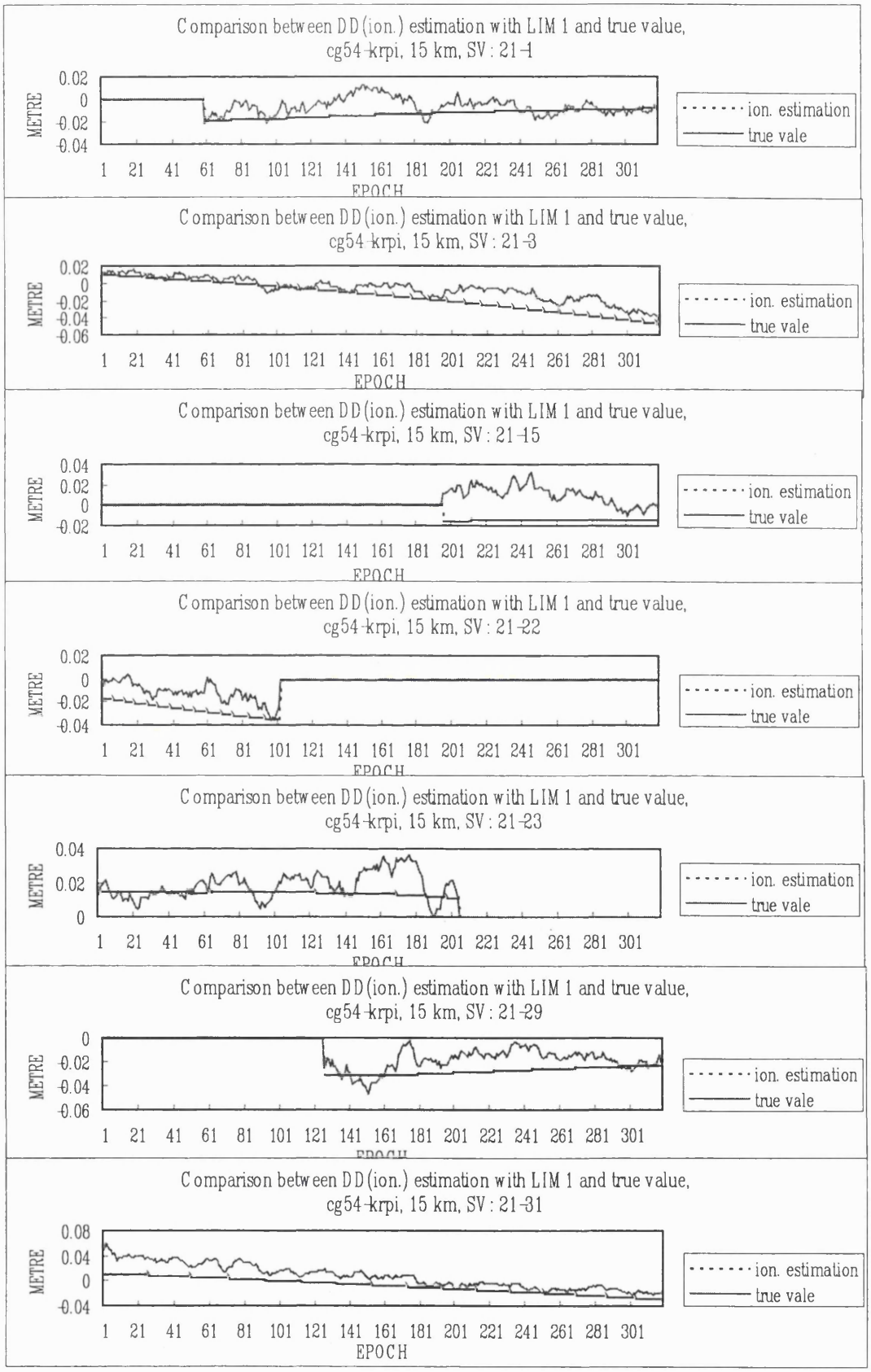

Figure B.7 Comparison of double differenced ionospheric delays based on LIM1 with the true values for the trial of 15km baseline

- Comparison of double differenced ionospheric delays based on LIM2 with the true values.

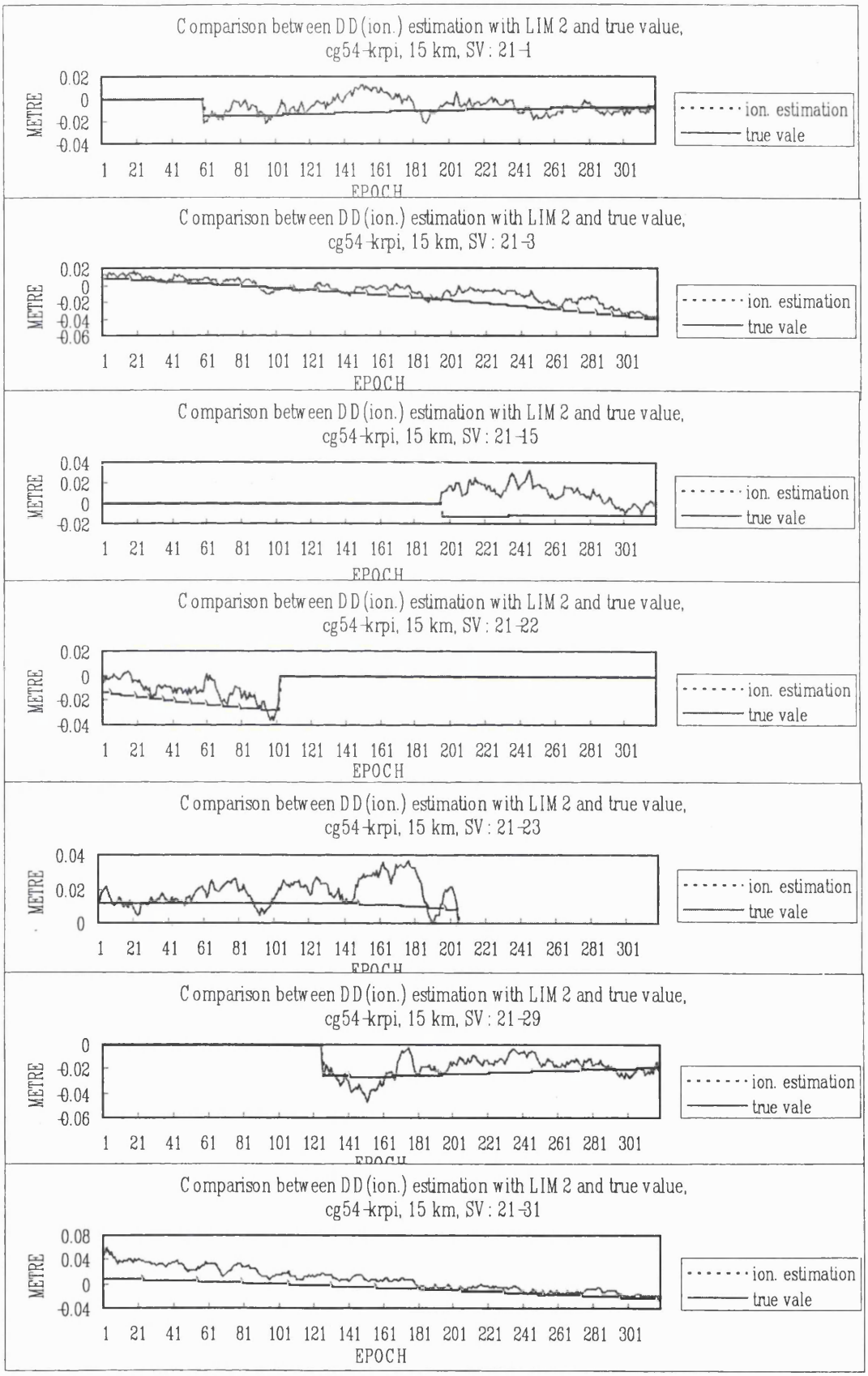

Figure B.8 Comparison of double differenced ionospheric delays based on LIM2 with the true values for the trial of 15km baseline

- Comparison of double differenced ionospheric delays based on LIM3 with the true values.

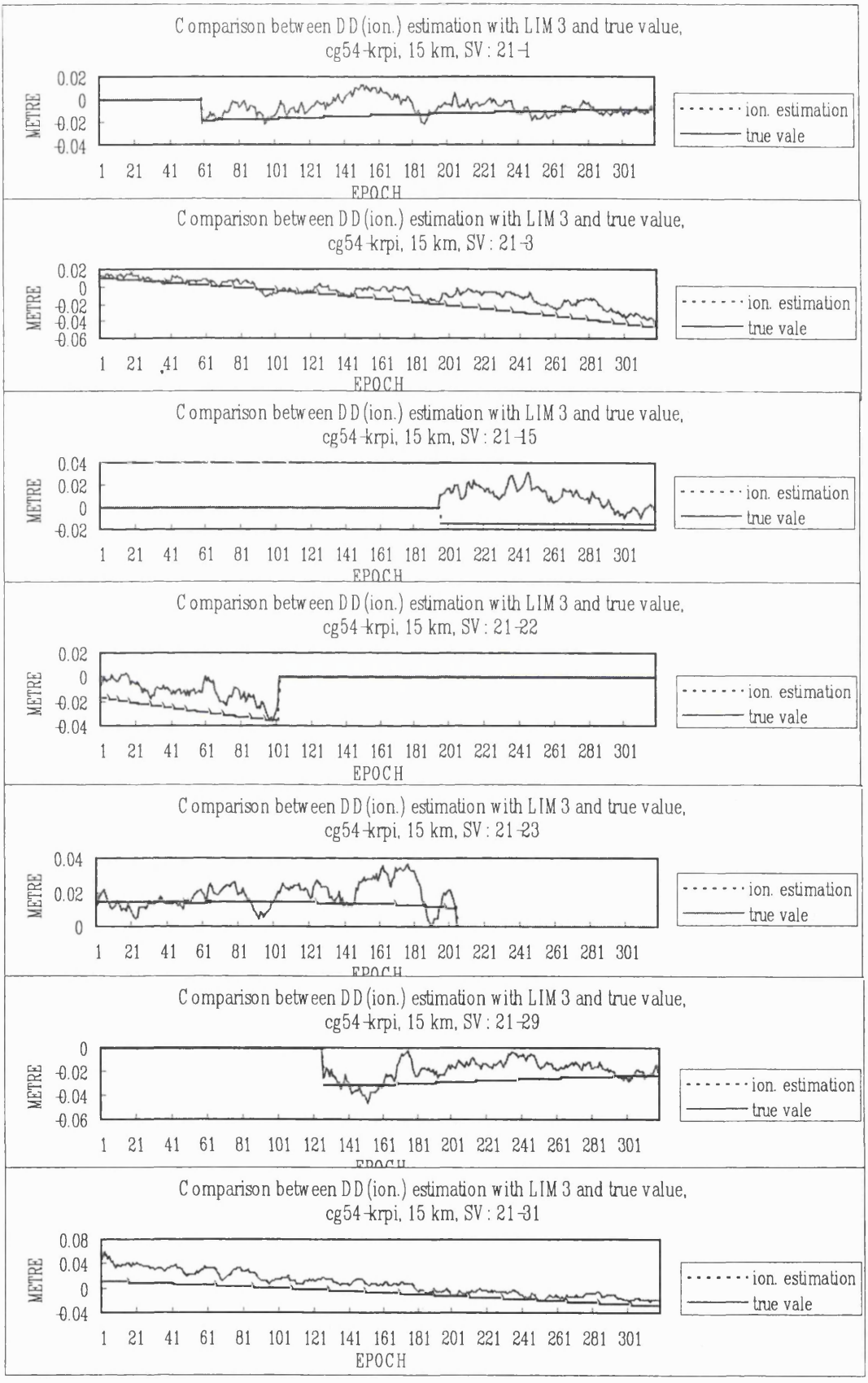

Figure B.9 Comparison of double differenced ionospheric delays based on LIM3 with the true values for the trial of 15km baseline

- Comparison of double differenced ionospheric delays based on LIM4 with the true values.

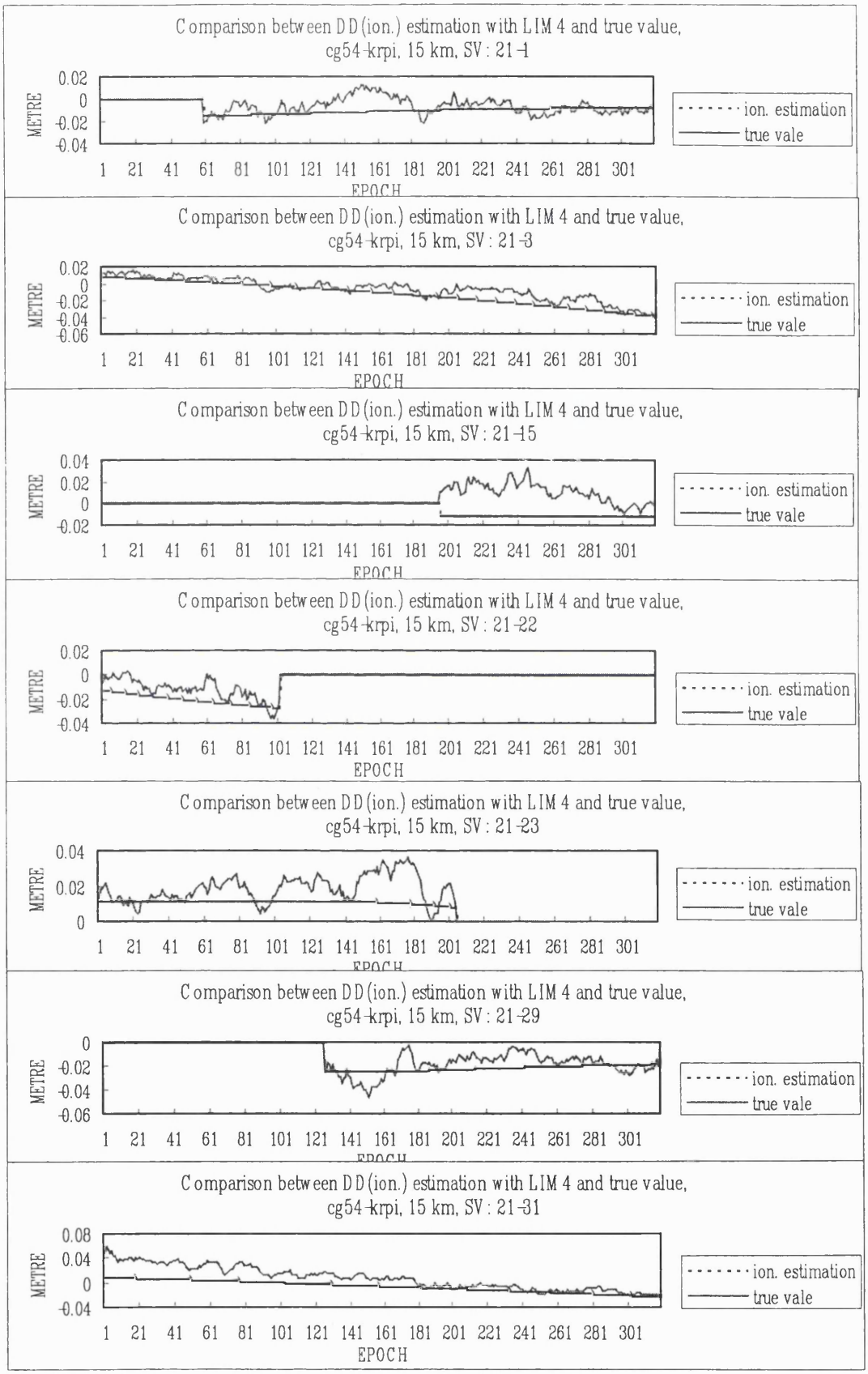

Figure B.10 Comparison of double differenced ionospheric delays based on LIM4 with the true values for the trial of 15km baseline

- Comparison of double differenced ionospheric delays based on LIM5 with the true values.

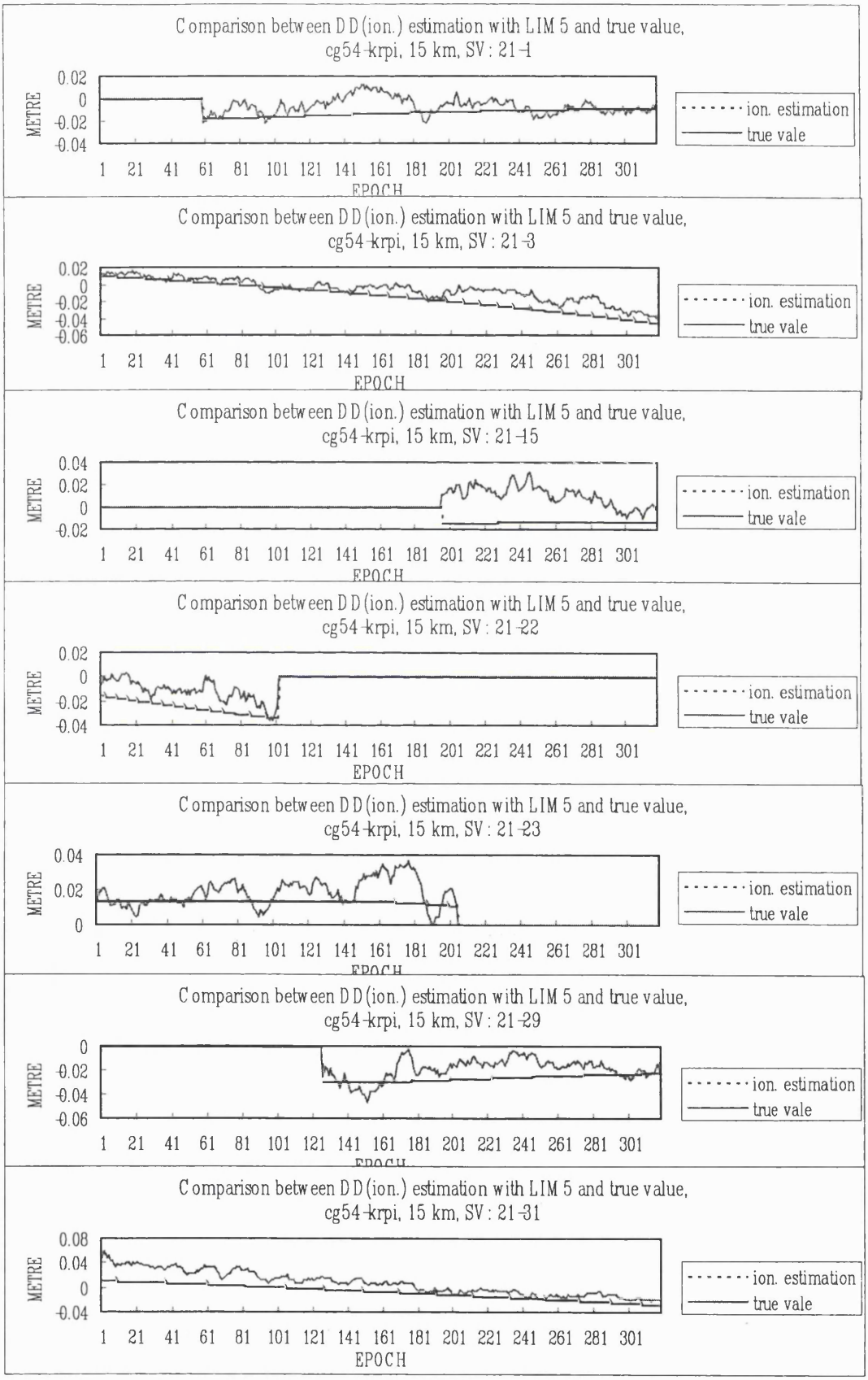

Figure B.11 Comparison of double differenced ionospheric delays based on LIM5 with the true values for the trial of 15km baseline

- Comparison of double differenced ionospheric delays based on LIM6 with the true values.

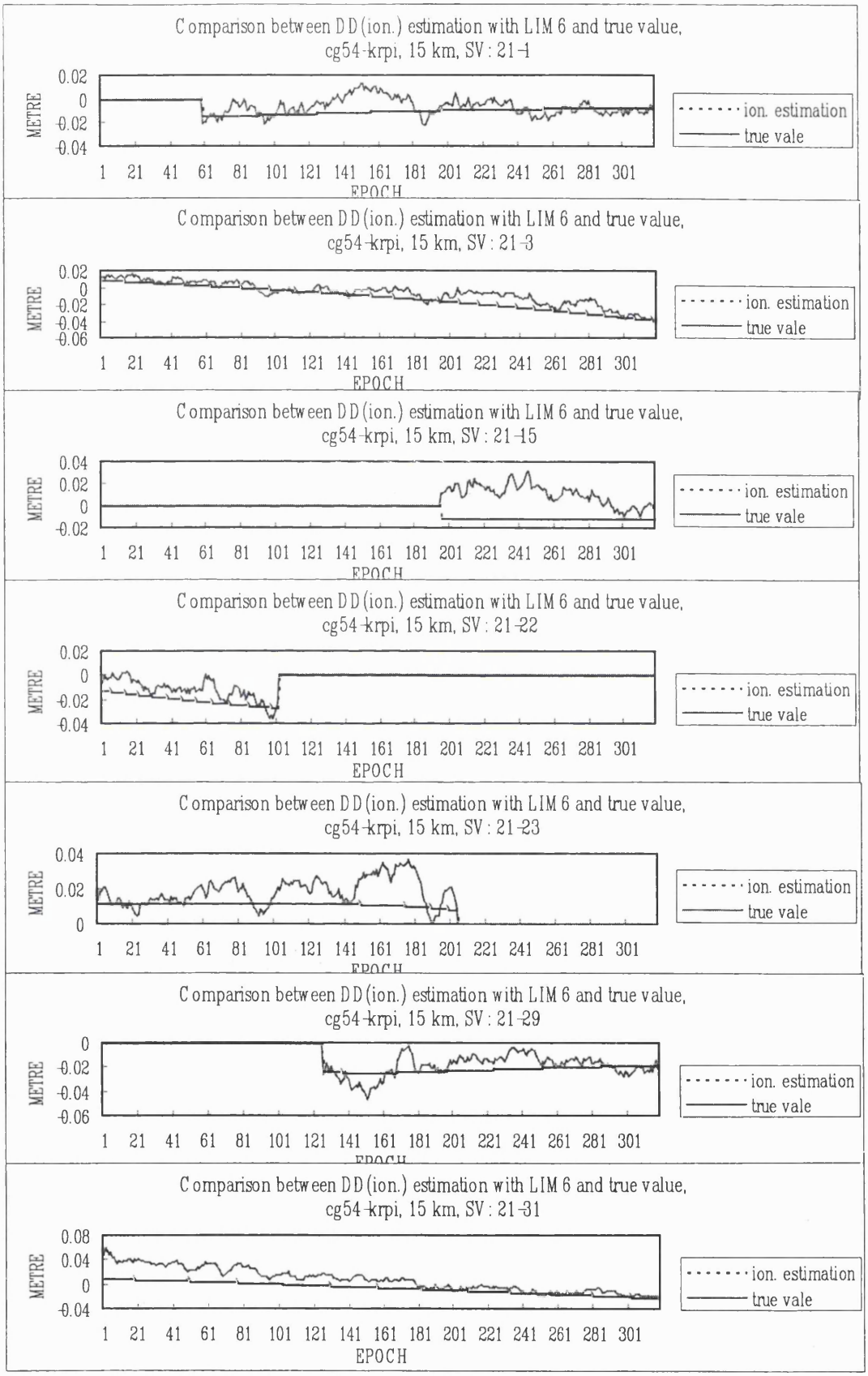

Figure B.12 Comparison of double differenced ionospheric delays based on LIM6 with the true values for the trial of 15km baseline

3. Trial of 21km baseline

- Comparison of double differenced ionospheric delays based on LIM1 with the true values.

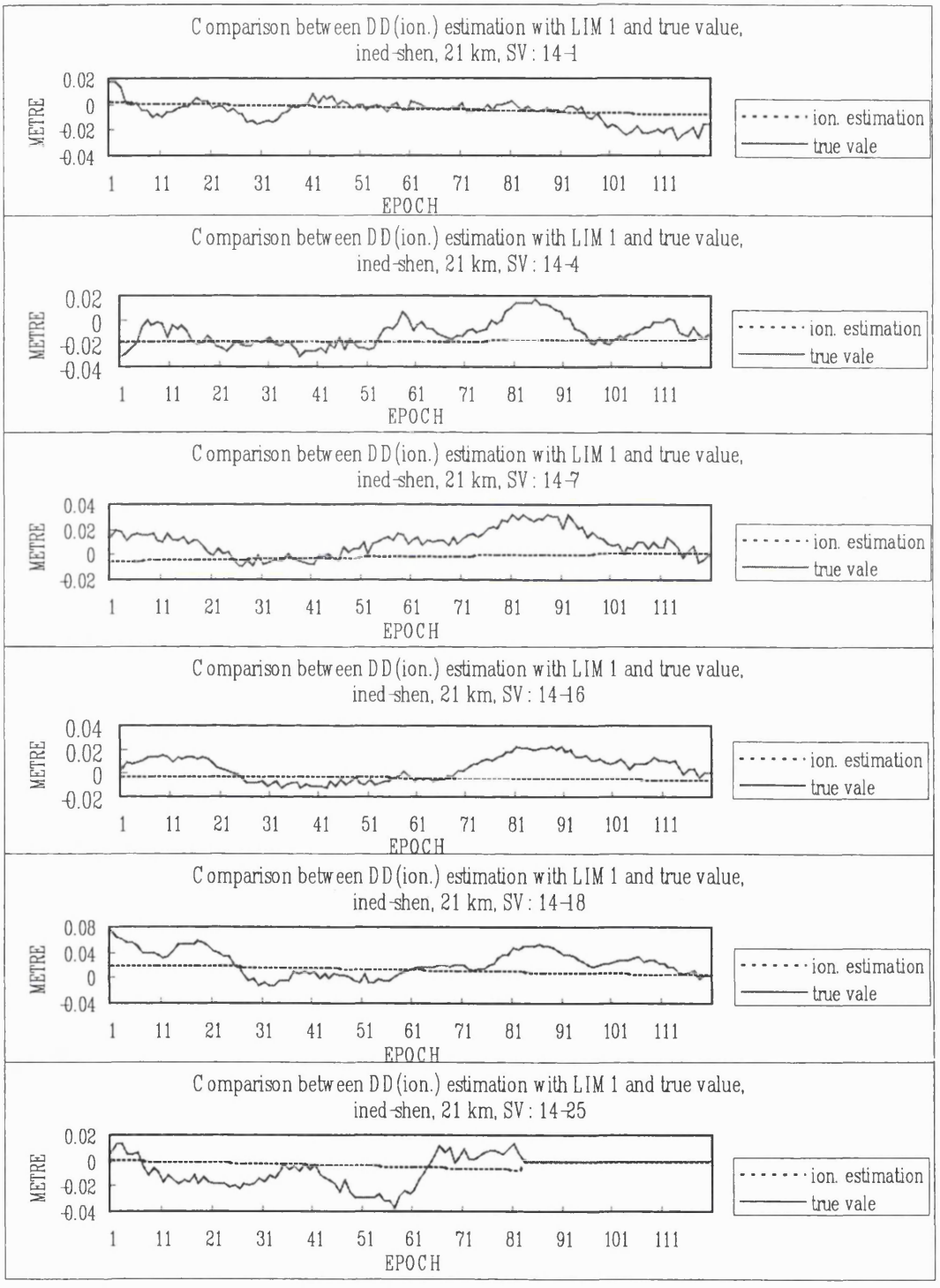

Figure B.13 Comparison of double differenced ionospheric delays based on LIM1 with the true values for the trial of 21km baseline

- Comparison of double differenced ionospheric delays based on LIM2 with the true values.

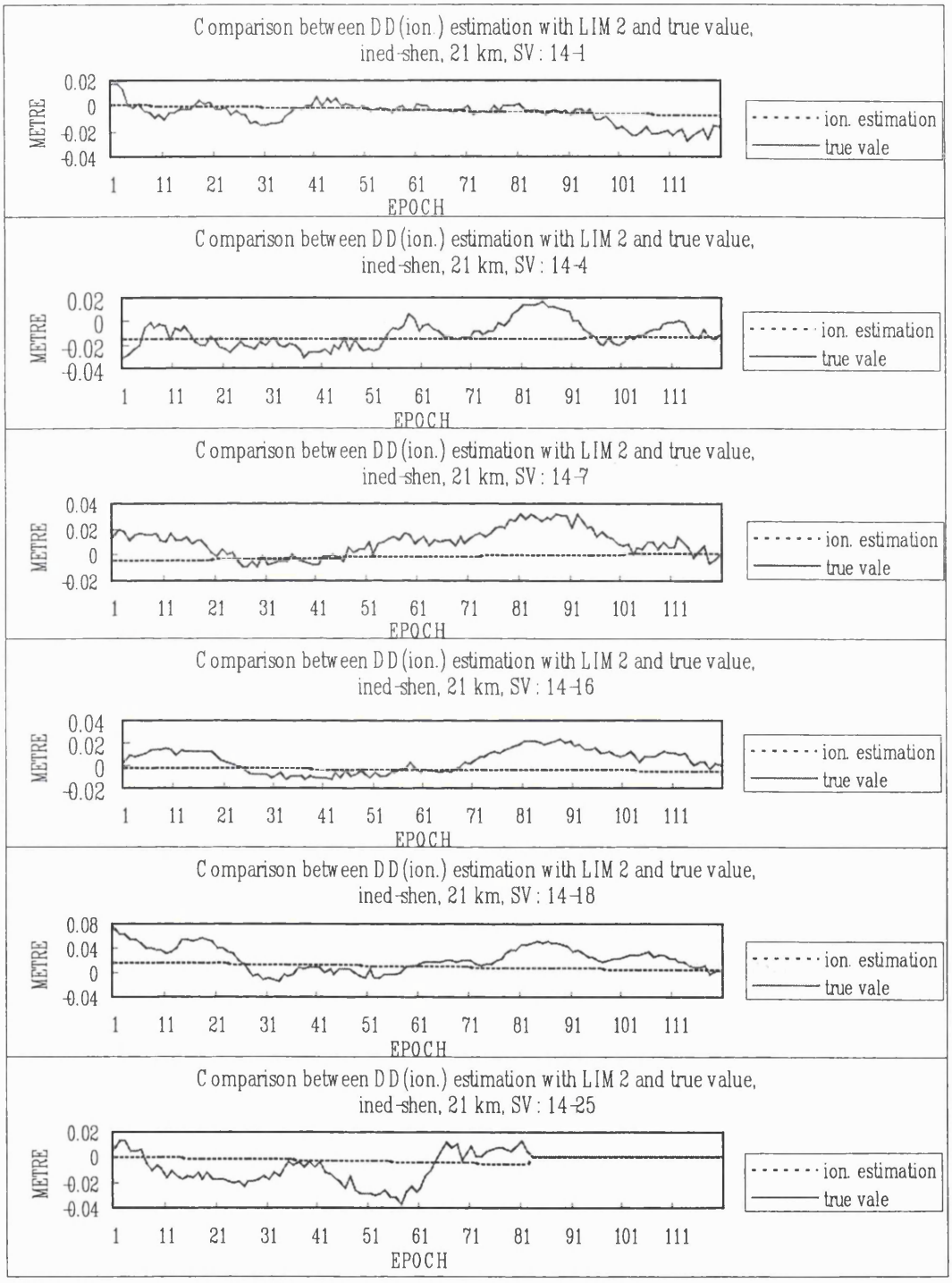

Figure B.14 Comparison of double differenced ionospheric delays based on LIM2 with the true values for the trial of 21km baseline

- Comparison of double differenced ionospheric delays based on LIM3 with the true values.

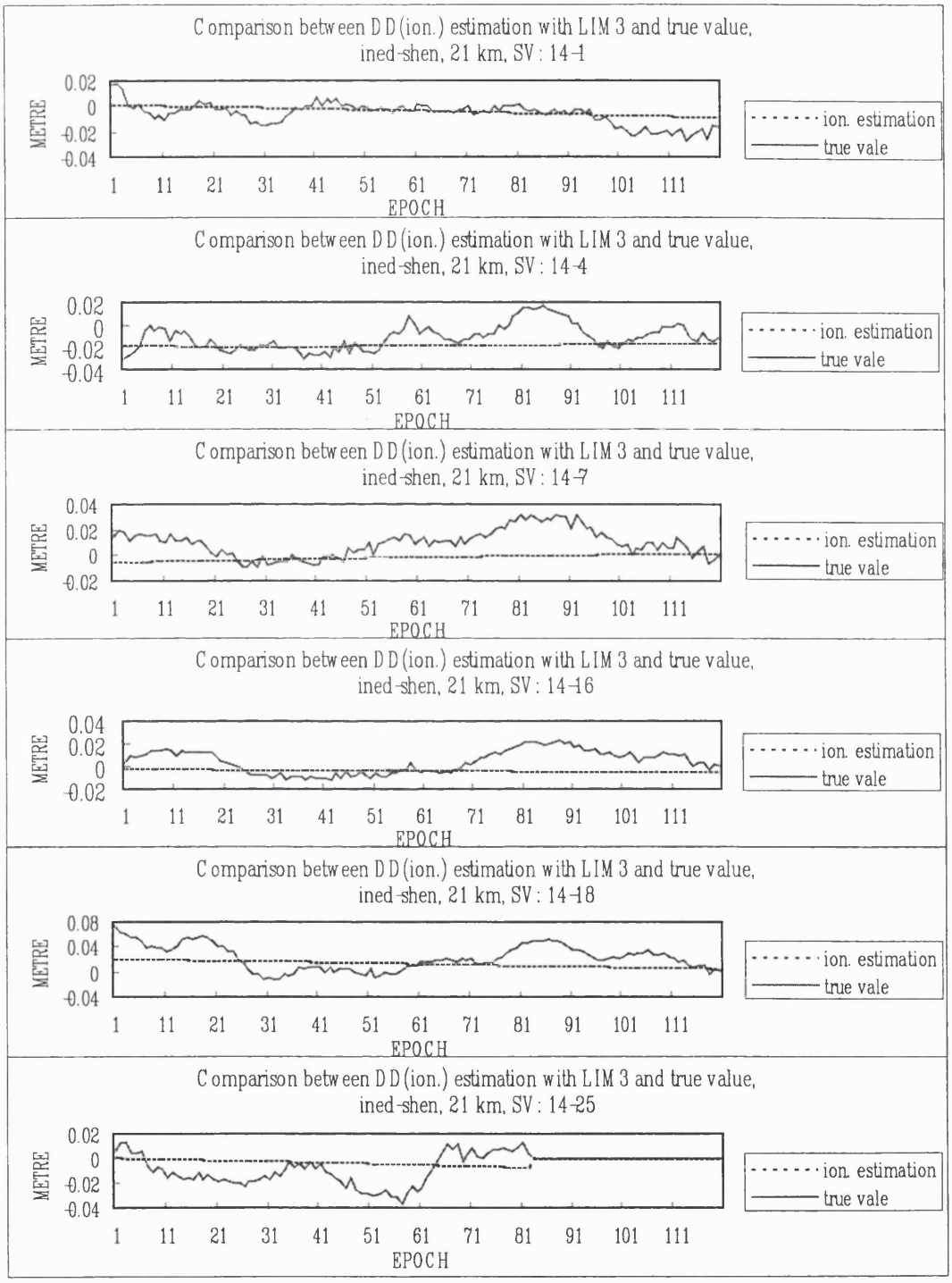

Figure B.15 Comparison of double differenced ionospheric delays based on LIM3 with the true values for the trial of 21km baseline

- Comparison of double differenced ionospheric delays based on LIM4 with the true values.

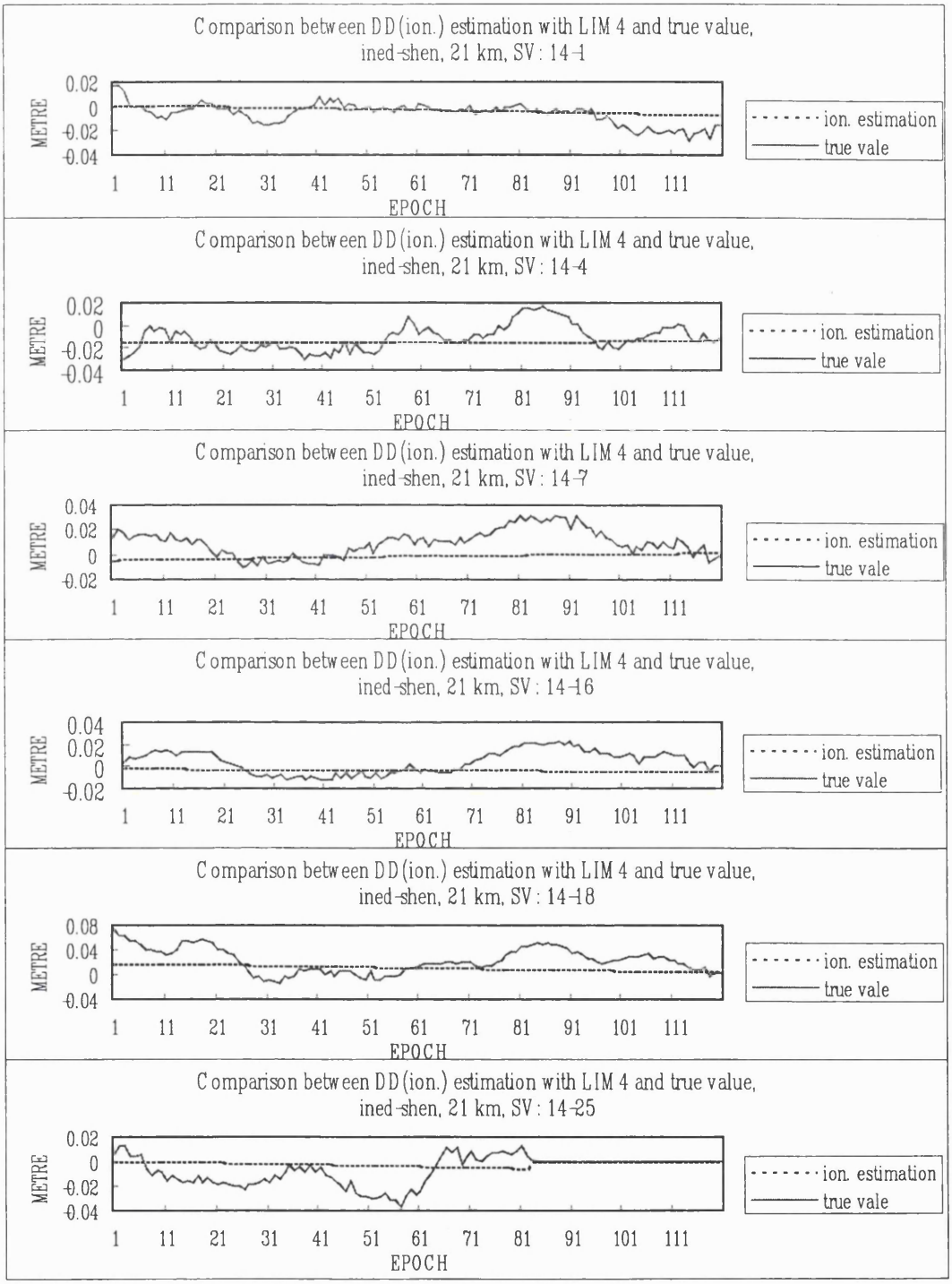

Figure B.16 Comparison of double differenced ionospheric delays based on LIM4 with the true values for the trial of 21km baseline

- Comparison of double differenced ionospheric delays based on LIM5 with the true values.

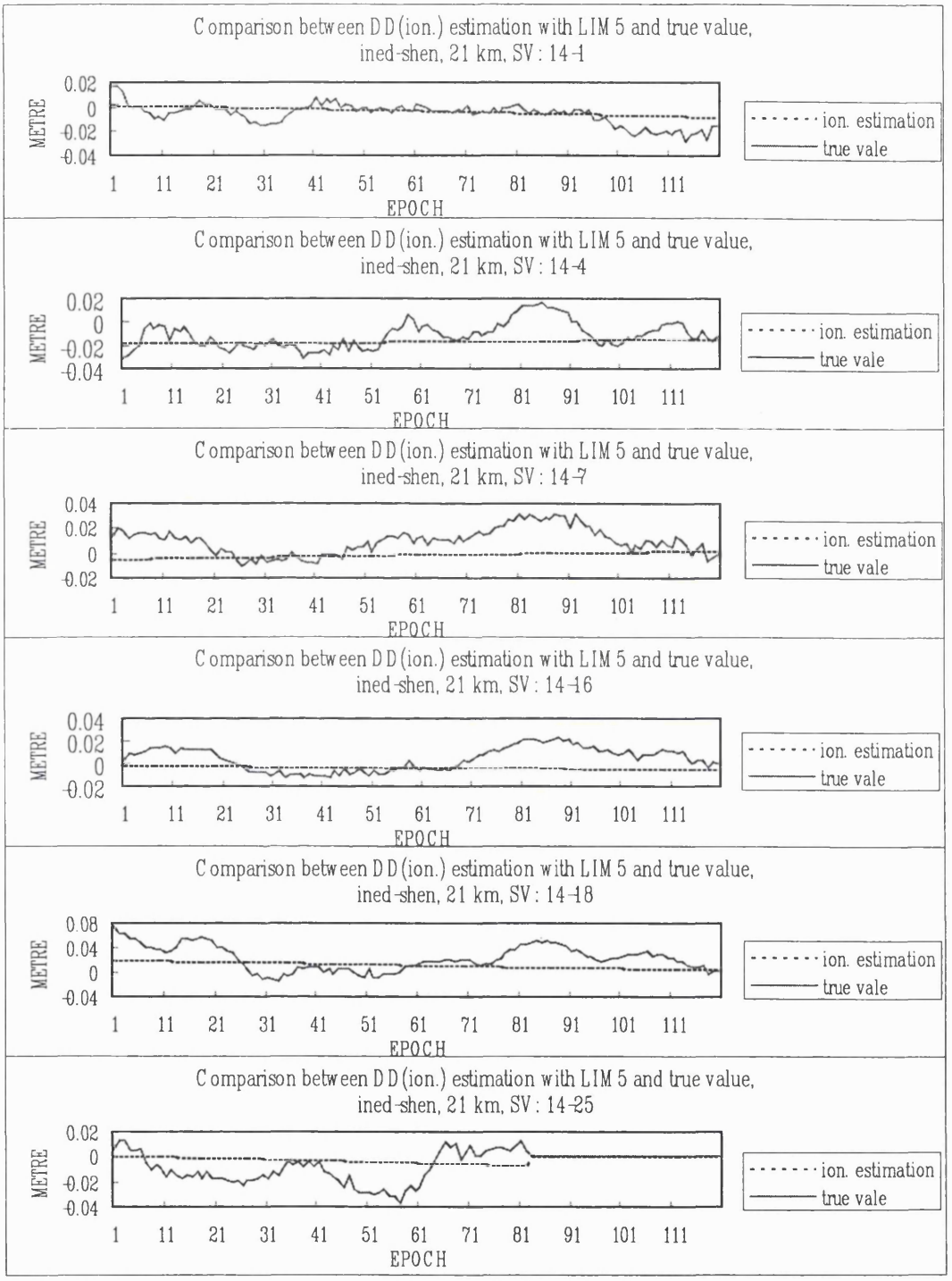

Figure B.17 Comparison of double differenced ionospheric delays based on LIM5 with the true values for the trial of 21km baseline

- Comparison of double differenced ionospheric delays based on LIM6 with the true values.

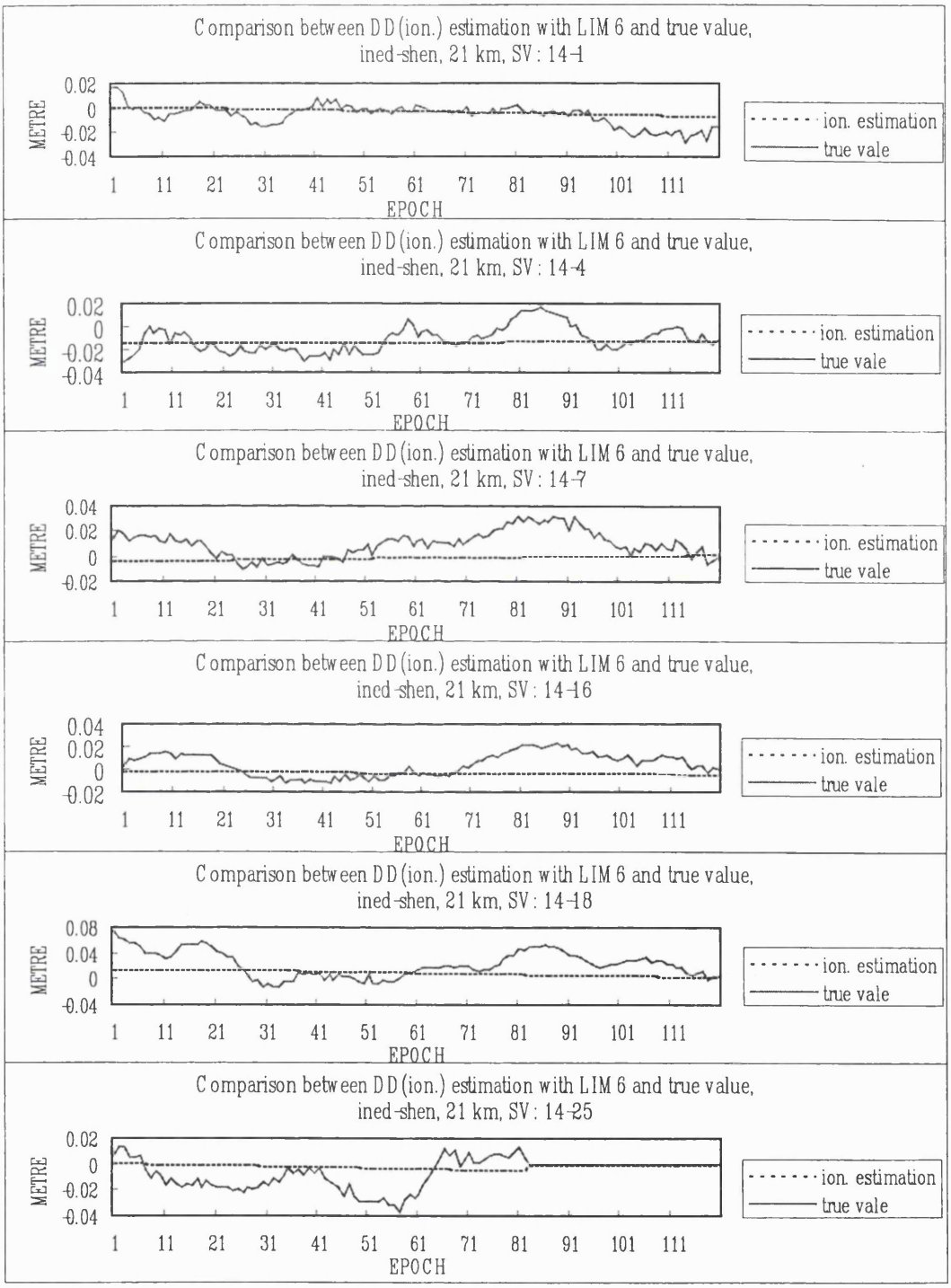

Figure B.18 Comparison of double differenced ionospheric delays based on LIM6 with the true values for the trial of 21km baseline

4. Trial of 25km baseline

- Comparison of double differenced ionospheric delays based on LIM1 with the true values.

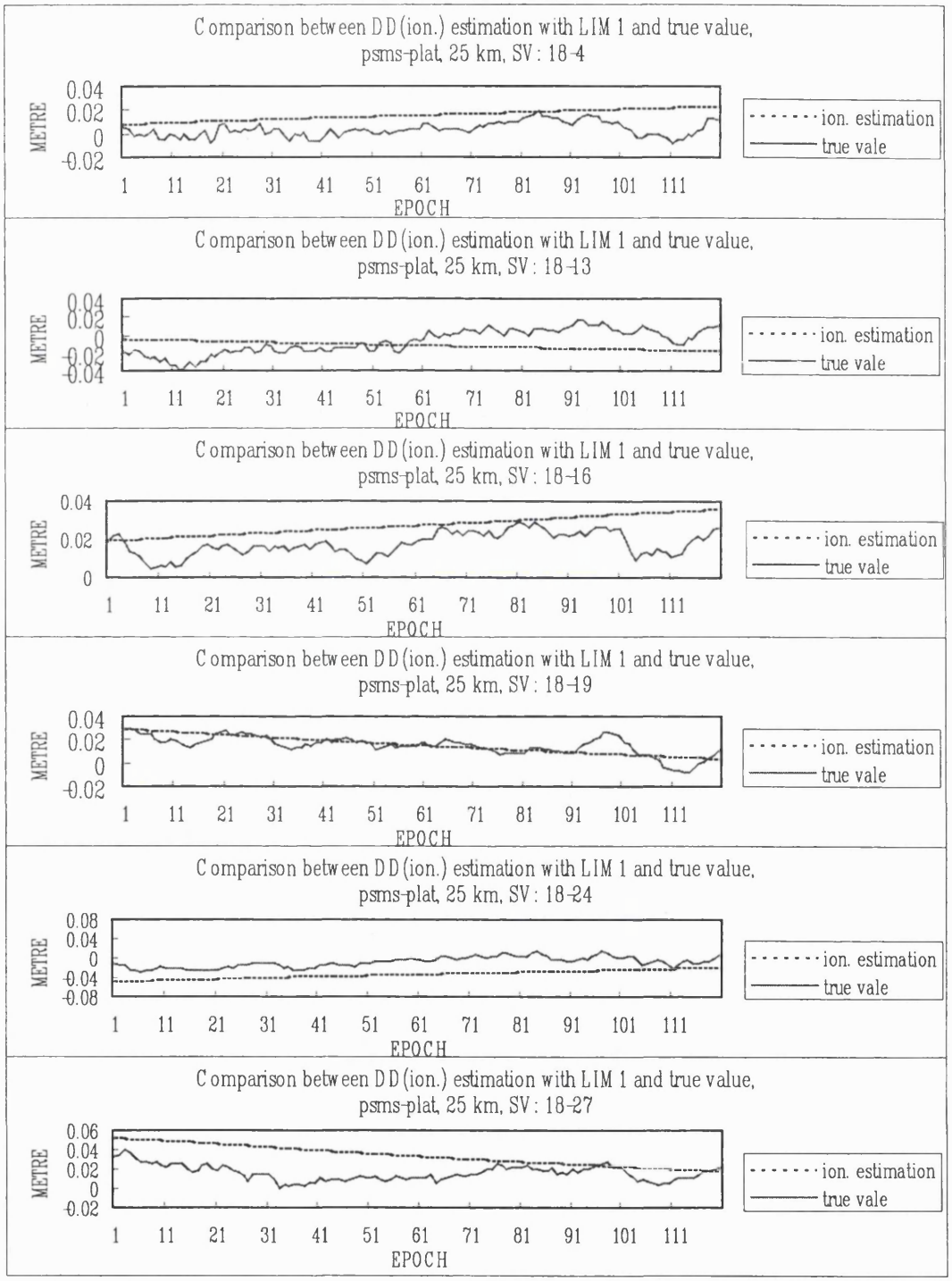

Figure B.19 Comparison of double differenced ionospheric delays based on LIM1 with the true values for the trial of 25km baseline

- Comparison of double differenced ionospheric delays based on LIM2 with the true values.

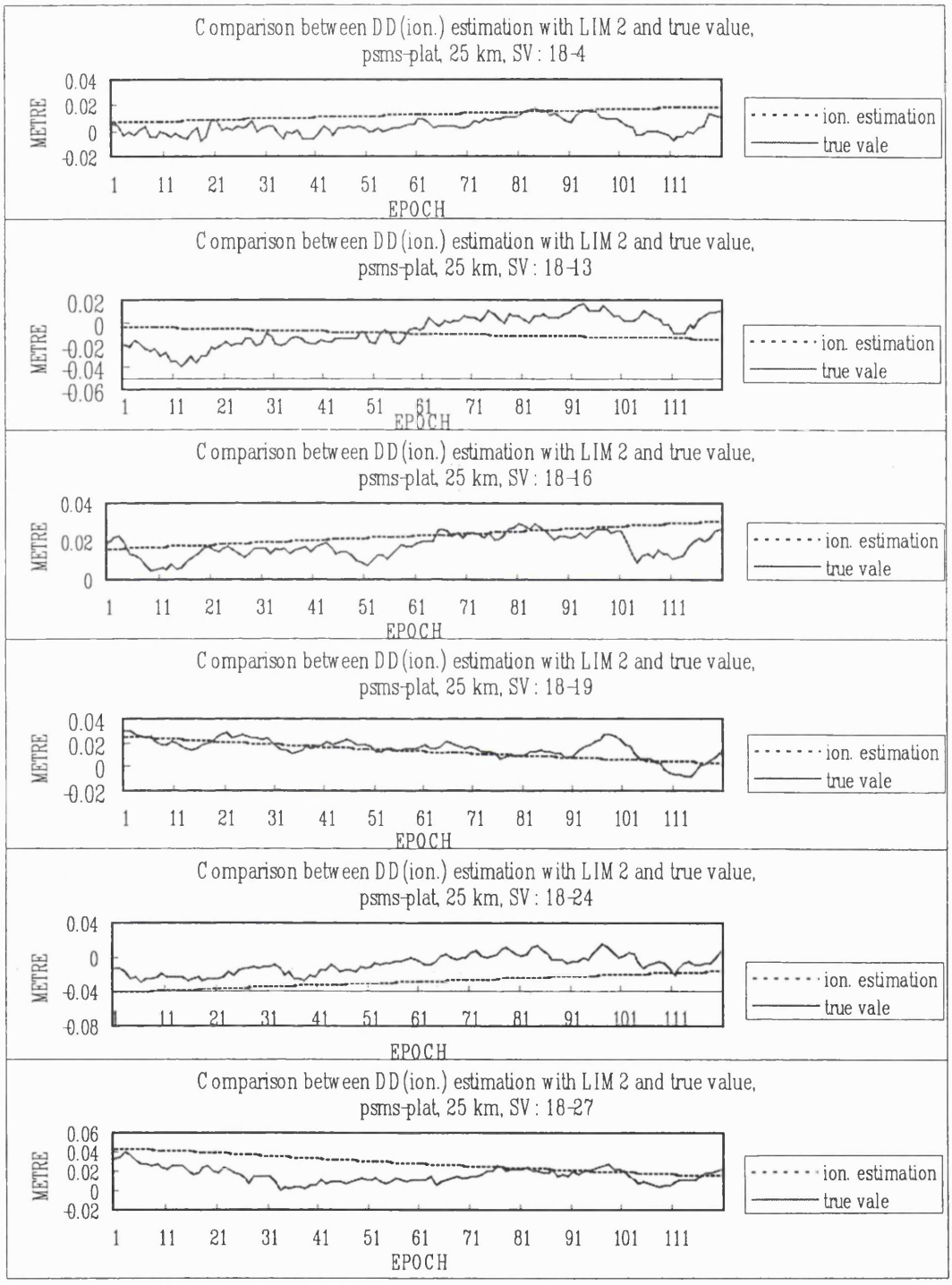

Figure B.20 Comparison of double differenced ionospheric delays based on LIM2 with the true values for the trial of 25km baseline

- Comparison of double differenced ionospheric delays based on LIM3 with the true values.

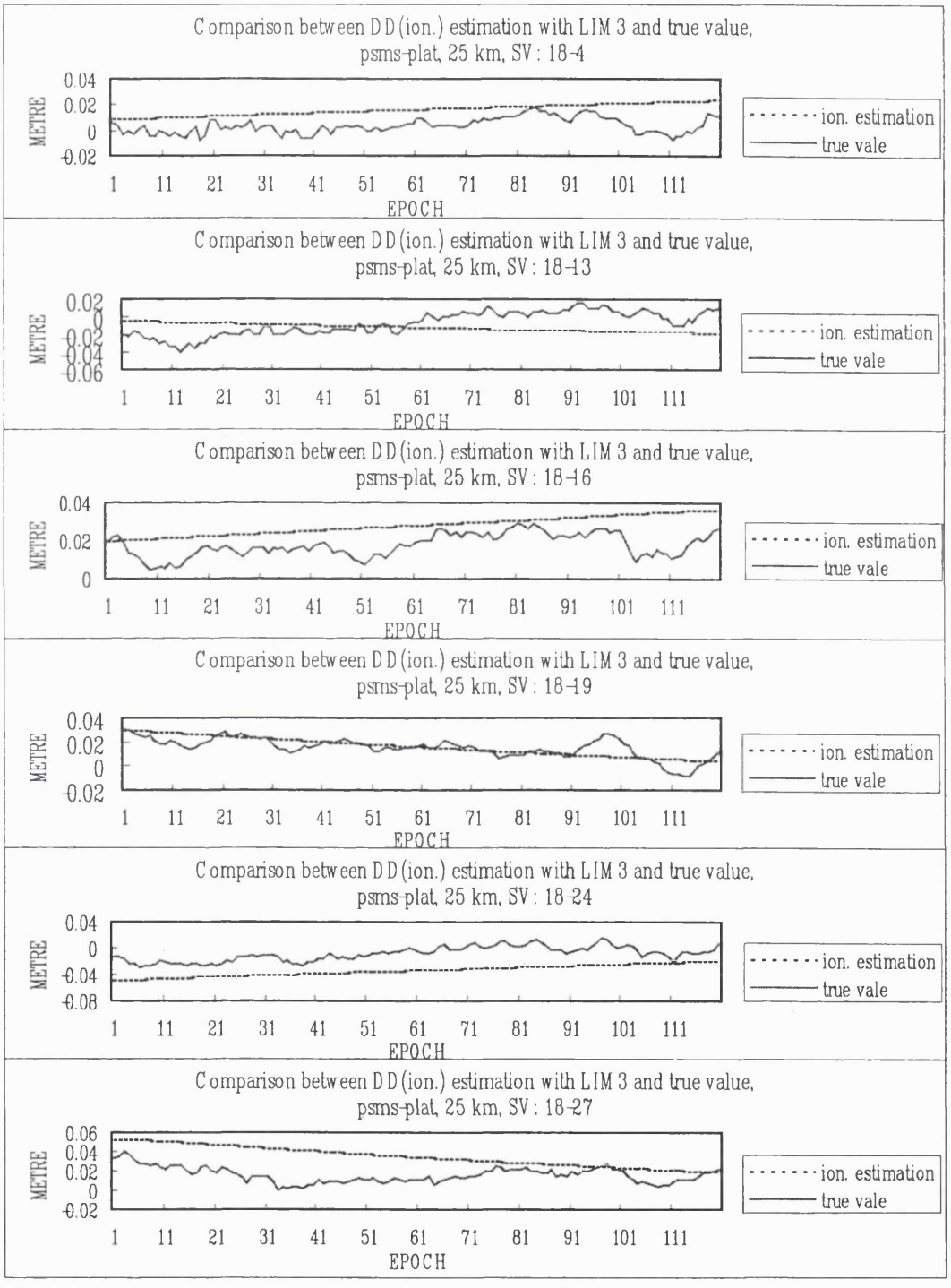

Figure B.21 Comparison of double differenced ionospheric delays based on LIM3 with the true values for the trial of 25km baseline

- Comparison of double differenced ionospheric delays based on LIM4 with the true values.

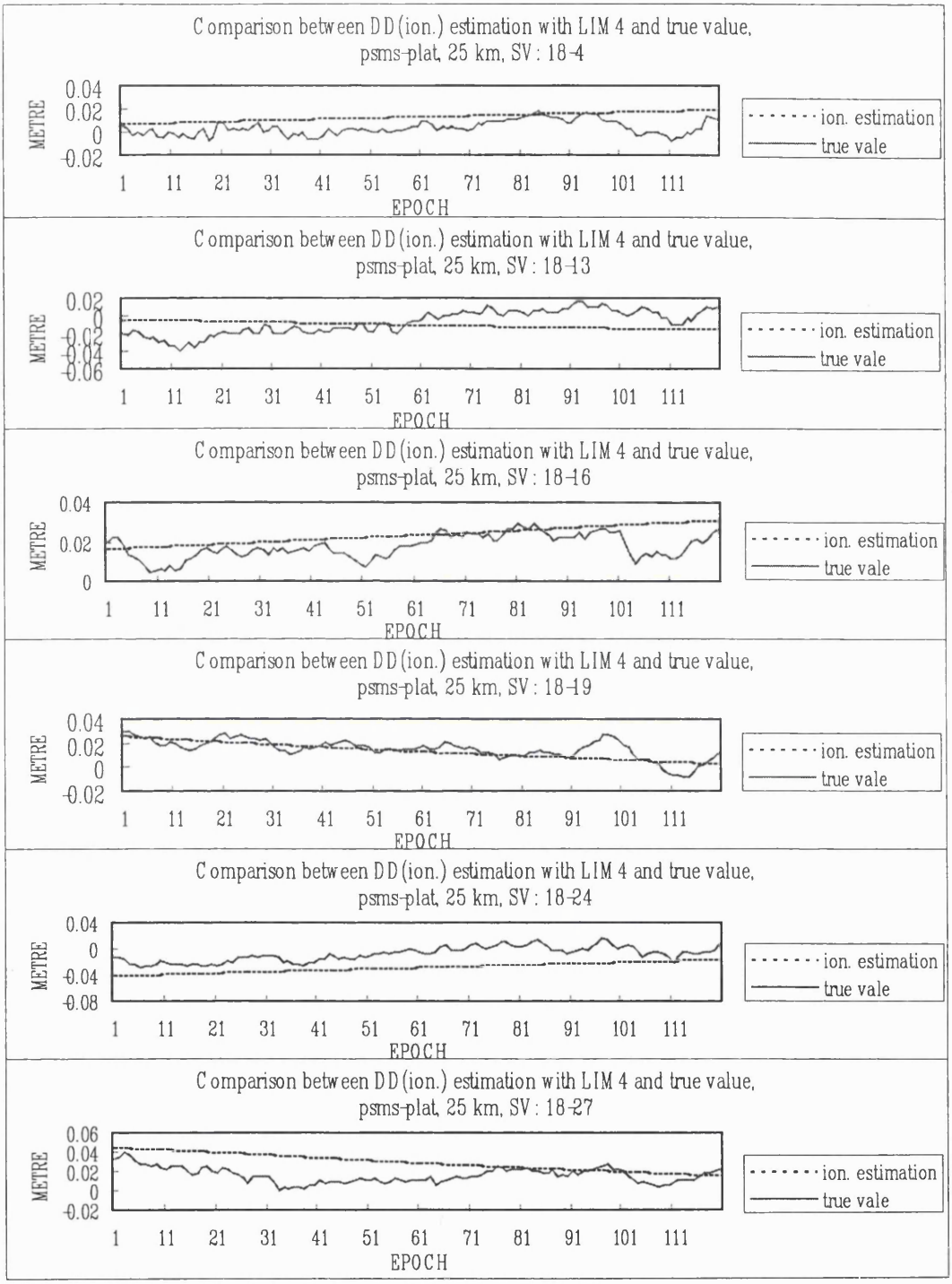

Figure B.22 Comparison of double differenced ionospheric delays based on LIM4 with the true values for the trial of 25km baseline

- Comparison of double differenced ionospheric delays based on LIM5 with the true values.

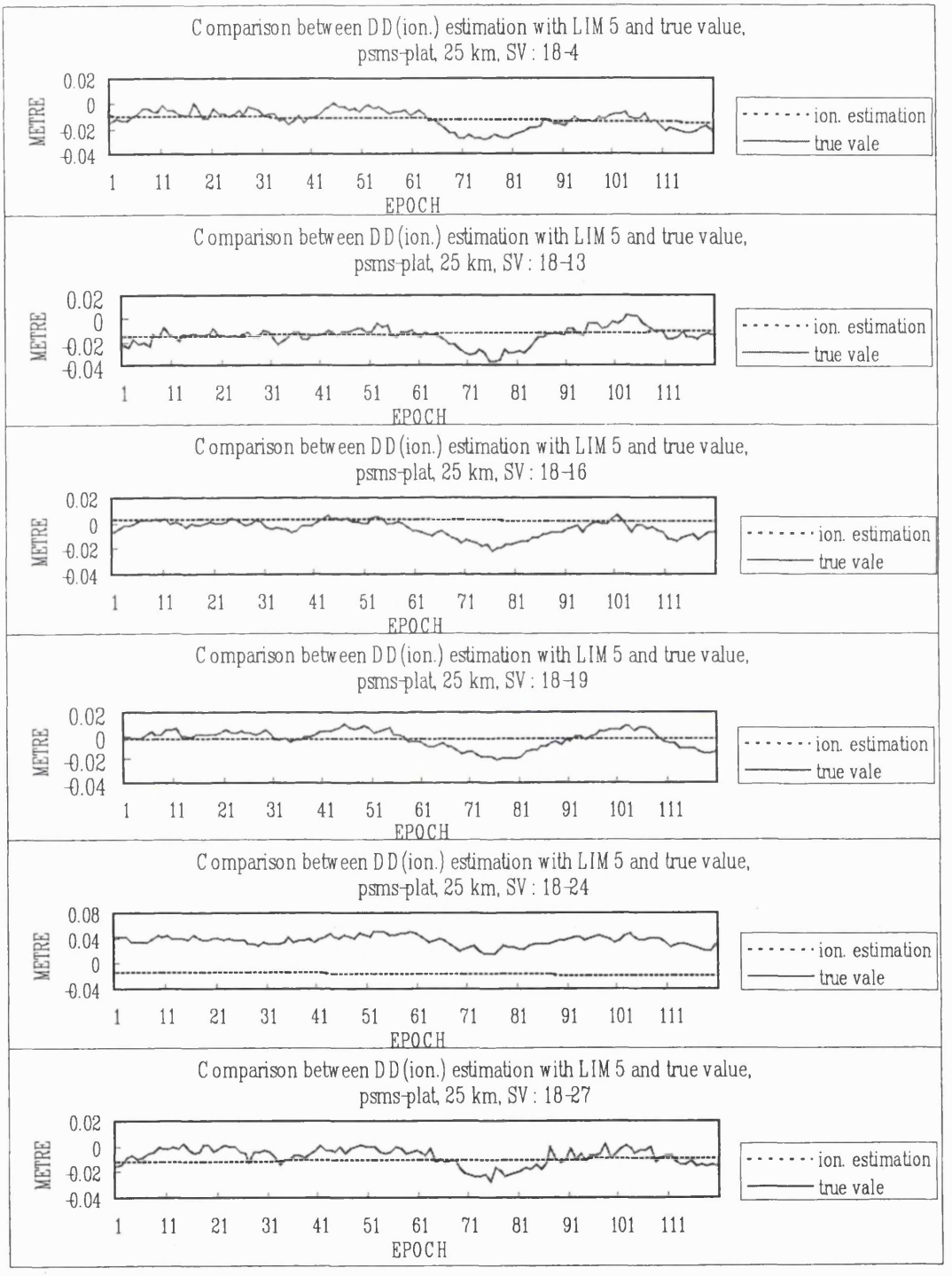

Figure B.23 Comparison of double differenced ionospheric delays based on LIM5 with the true values for the trial of 25km baseline

- Comparison of double differenced ionospheric delays based on LIM6 with the true values.

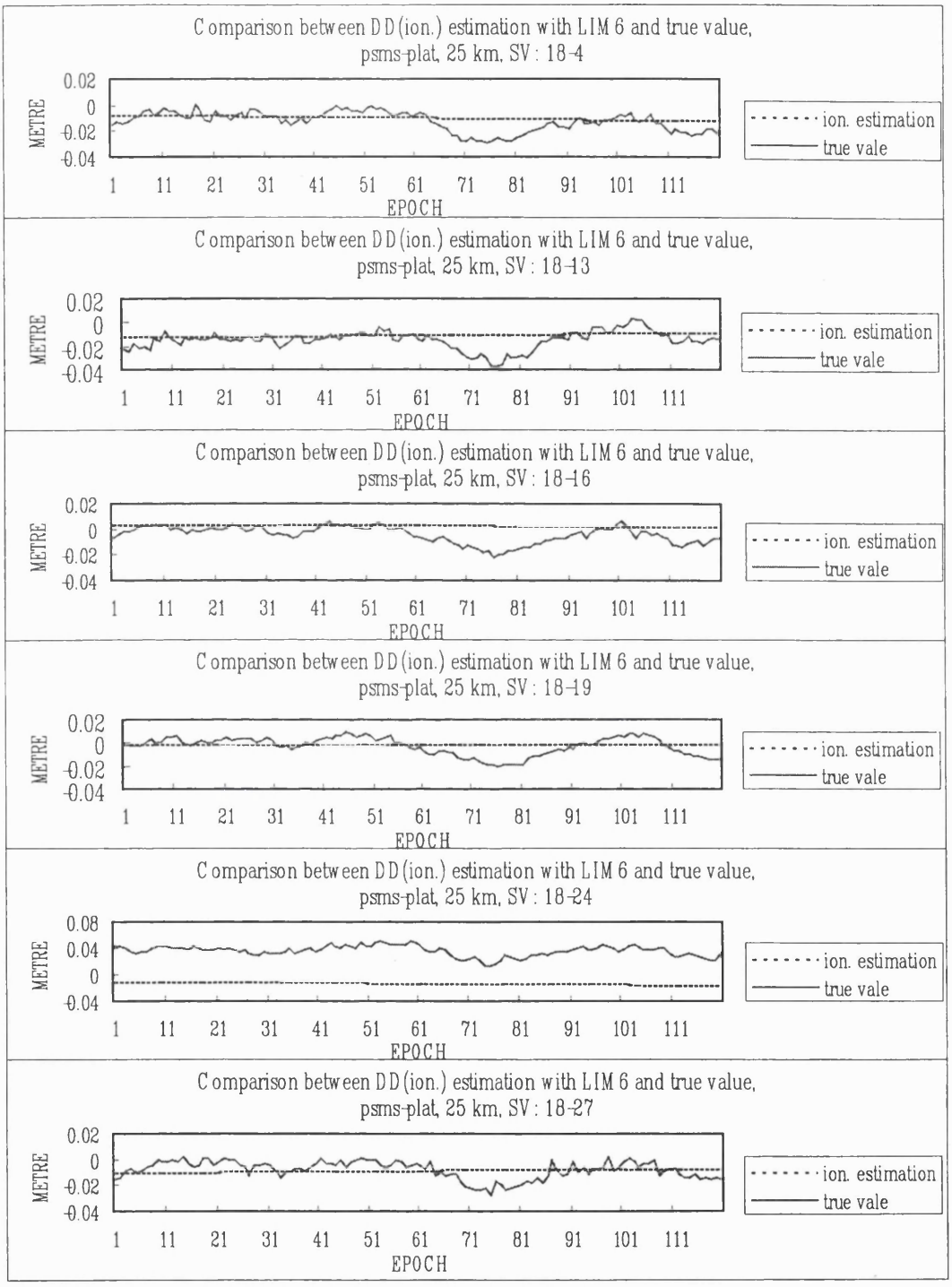

Figure B.24 Comparison of double differenced ionospheric delays based on LIM6 with the true values for the trial of 25km baseline

5. Trial of 33km baseline

- Comparison of double differenced ionospheric delays based on LIM1 with the true values.

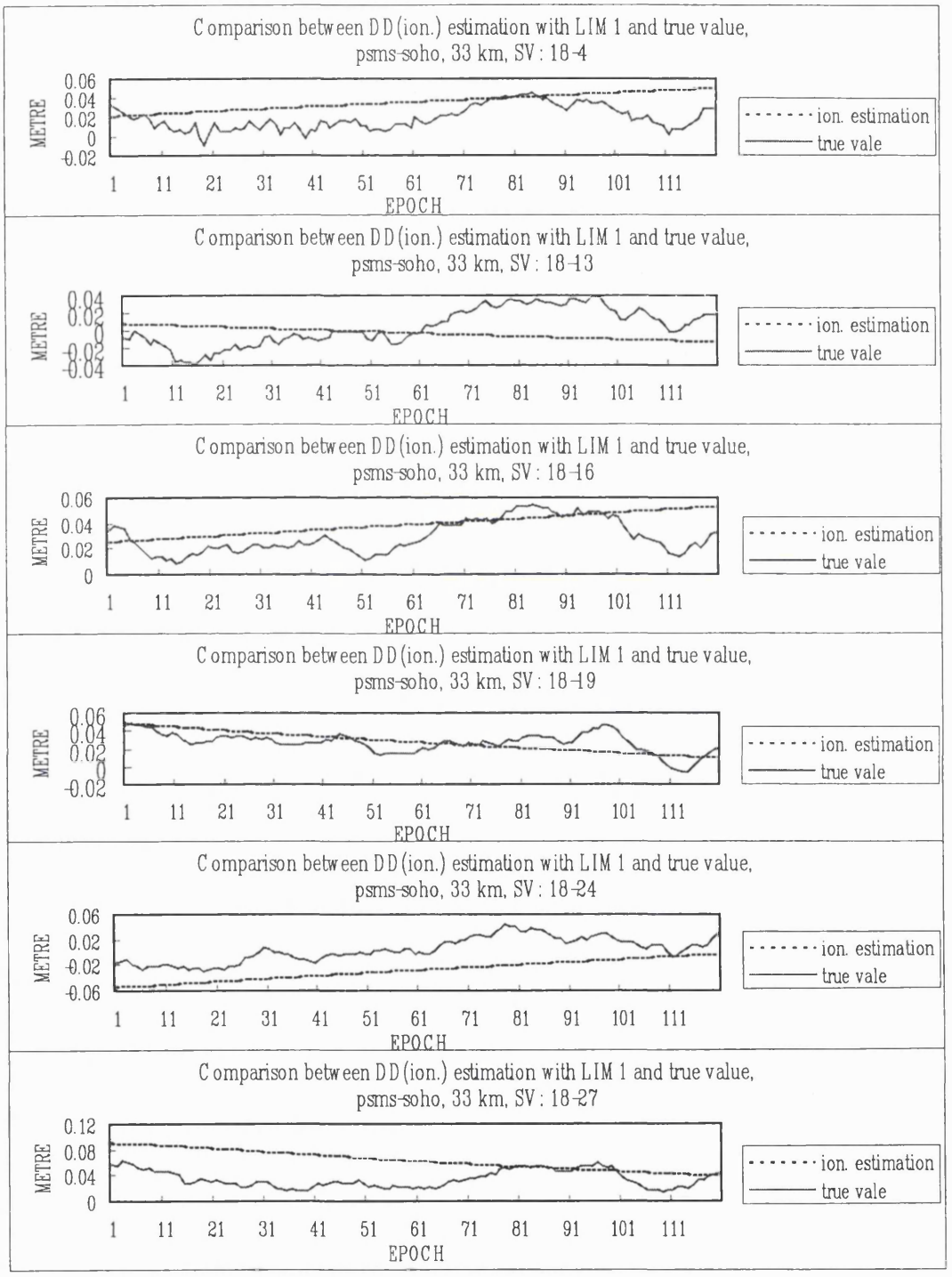

Figure B.25 Comparison of double differenced ionospheric delays based on LIM1 with the true values for the trial of 33km baseline

- Comparison of double differenced ionospheric delays based on LIM2 with the true values.

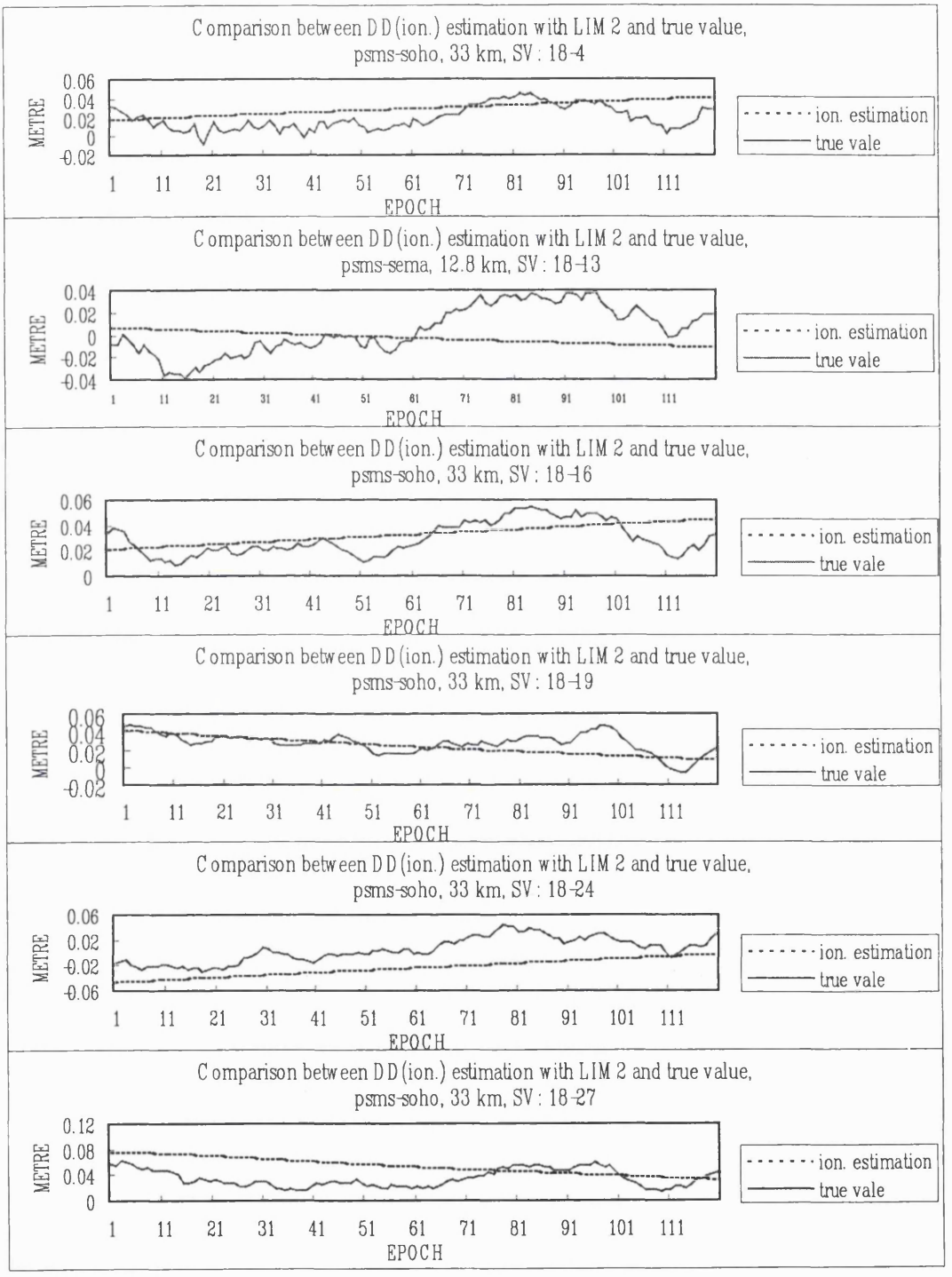

Figure B.26 Comparison of double differenced ionospheric delays based on LIM2 with the true values for the trial of 33km baseline

- Comparison of double differenced ionospheric delays based on LIM3 with the true values.

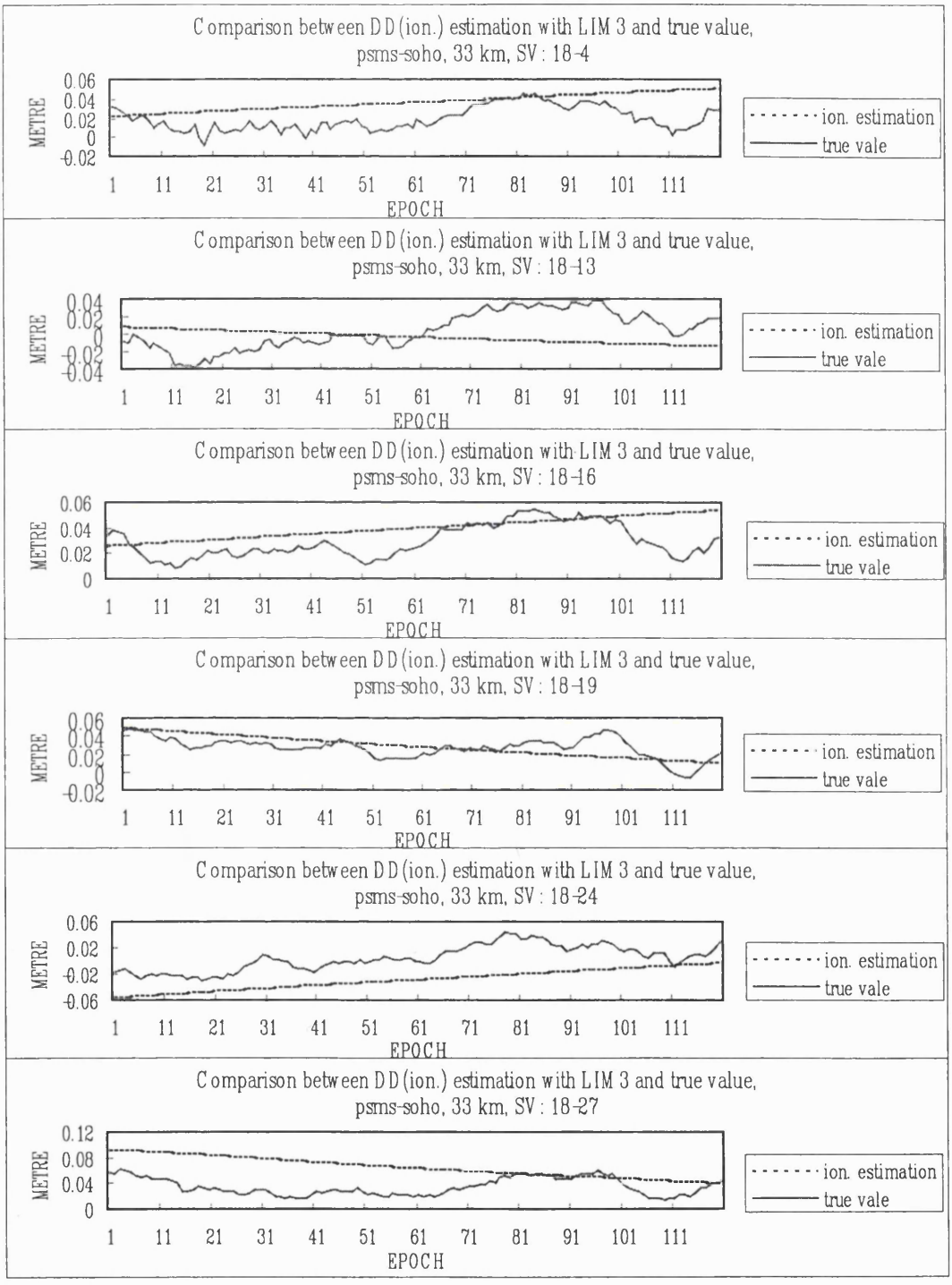

Figure B.27 Comparison of double differenced ionospheric delays based on LIM3 with the true values for the trial of 33km baseline

- Comparison of double differenced ionospheric delays based on LIM4 with the true values.

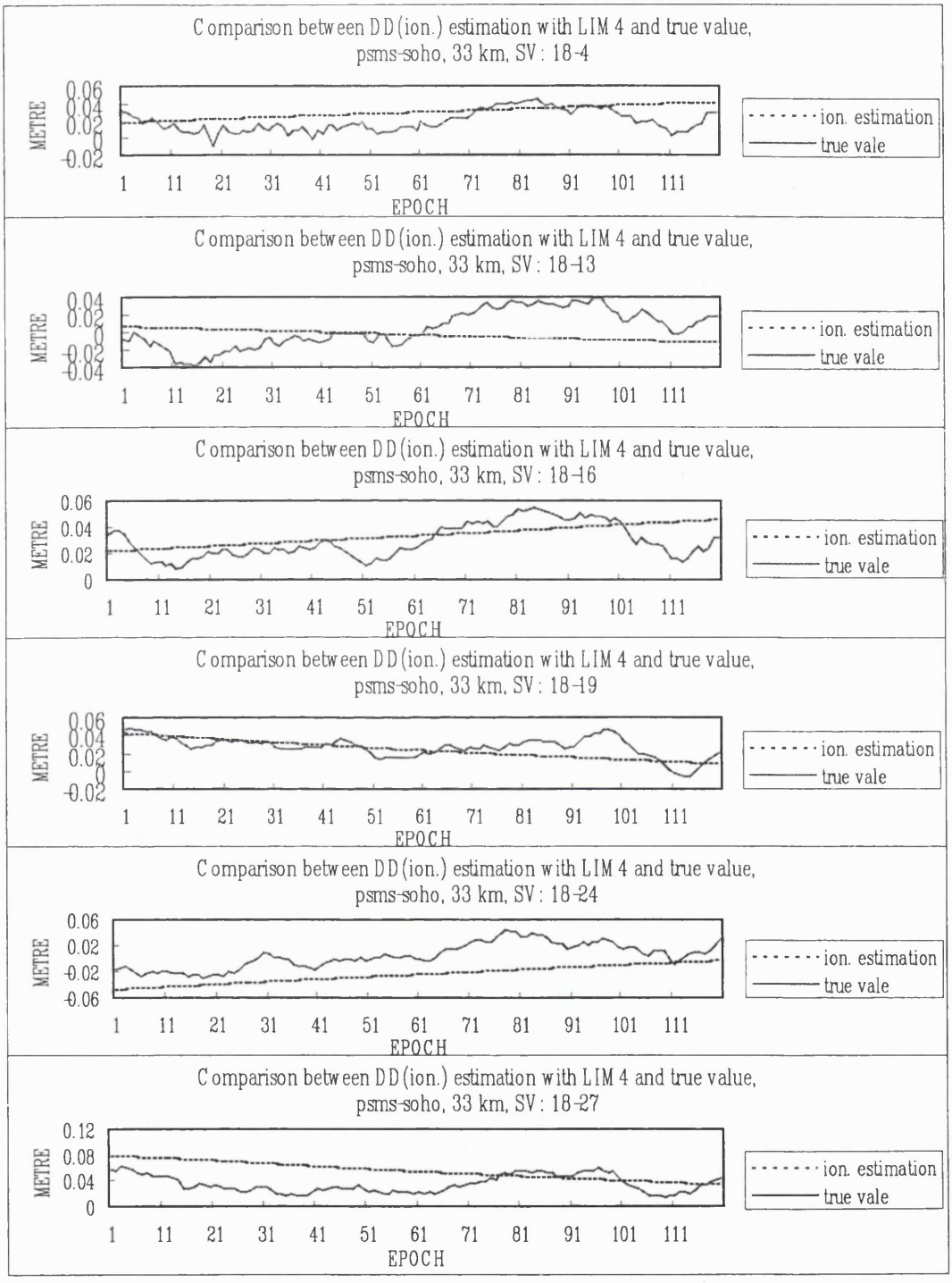

Figure B.28 Comparison of double differenced ionospheric delays based on LIM4 with the true values for the trial of 33km baseline

- Comparison of double differenced ionospheric delays based on LIM5 with the true values.

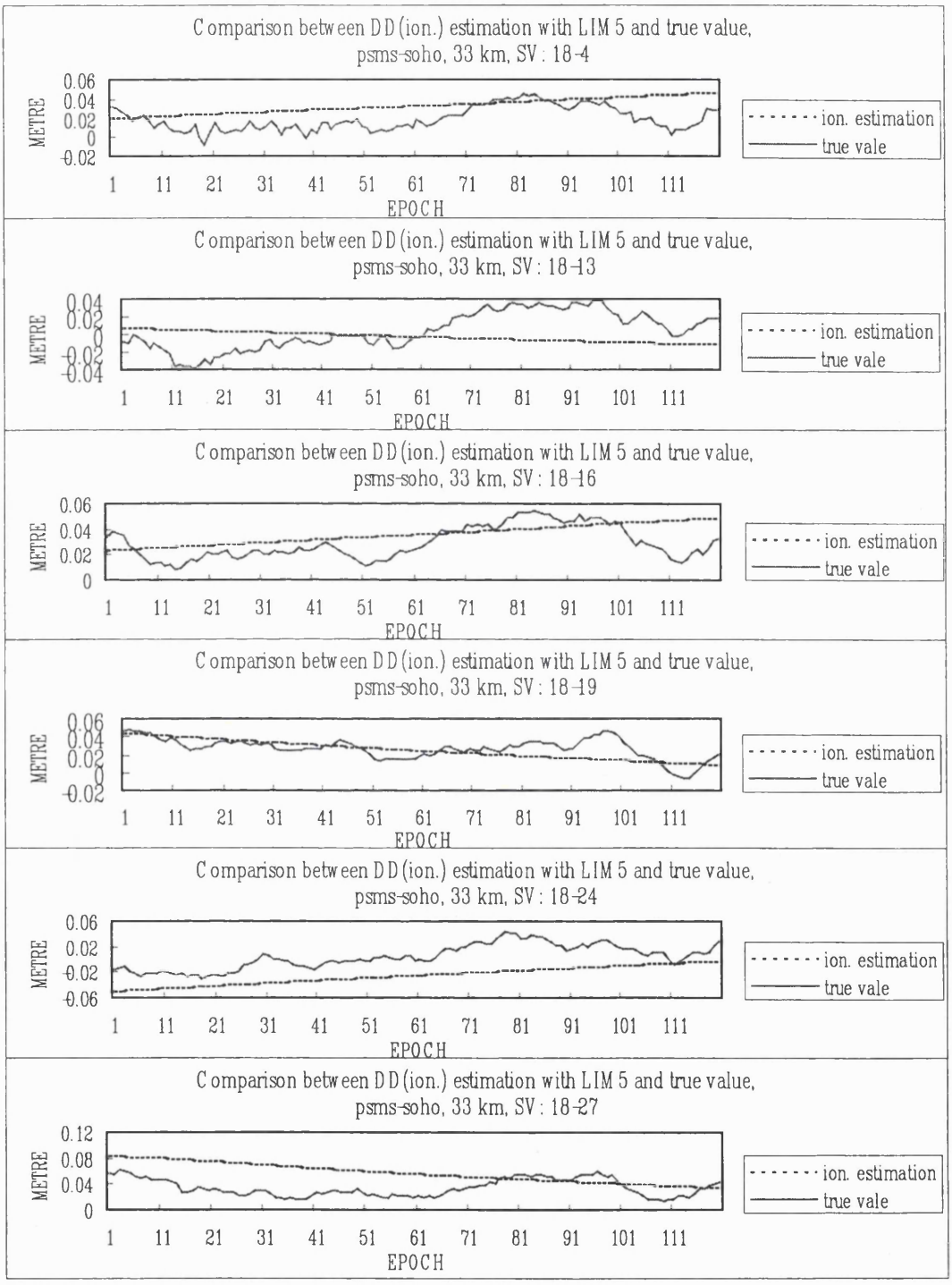

Figure B.29 Comparison of double differenced ionospheric delays based on LIM5 with the true values for the trial of 33km baseline

- Comparison of double differenced ionospheric delays based on LIM6 with the true values.

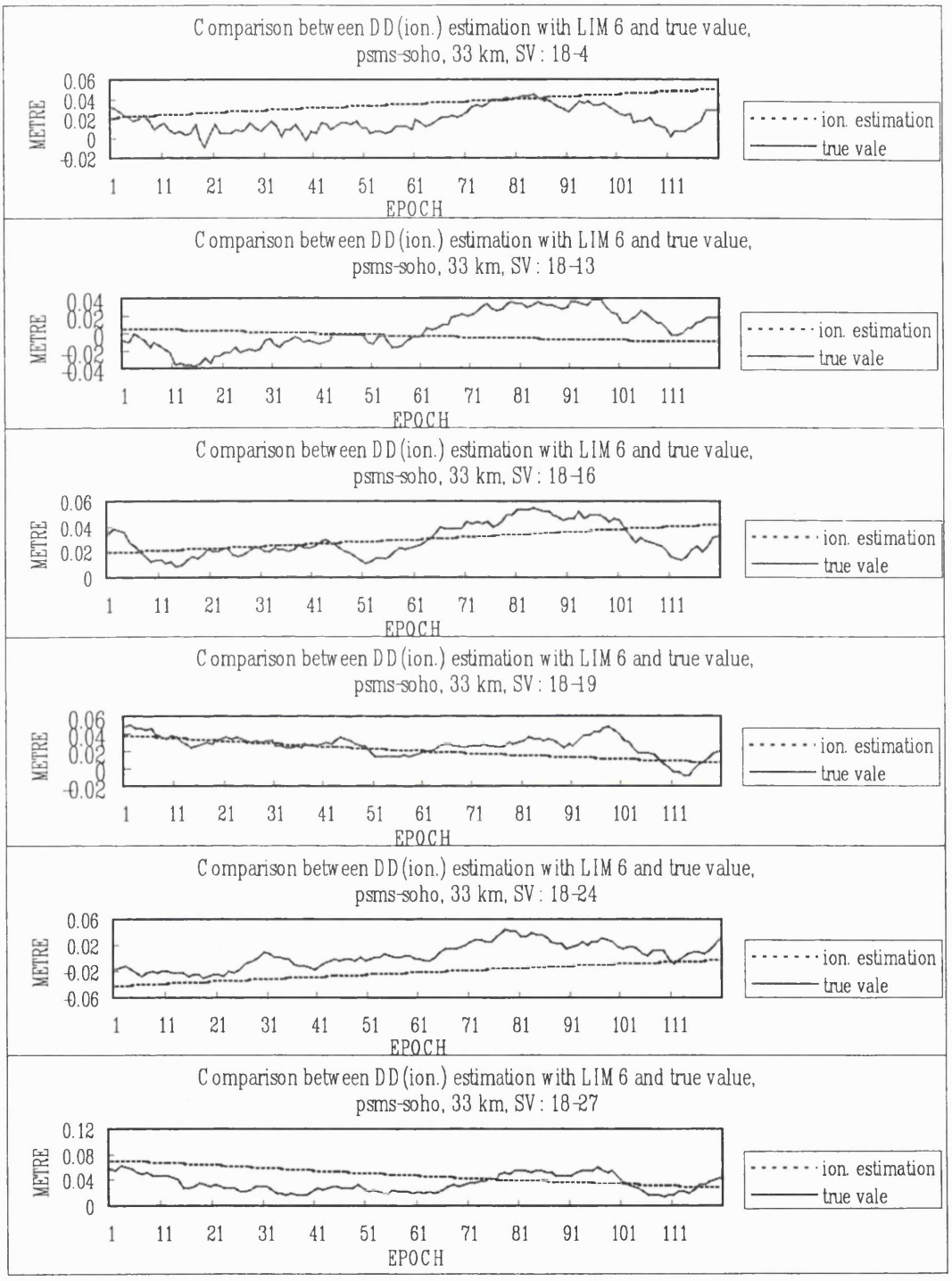

Figure B.30 Comparison of double differenced ionospheric delays based on LIM6 with the true values for the trial of 33km baseline

APPENDIX C

SUMMARY OF THE RELATED FIGURES OF AFT PERFORMANCES (CHAPTER THREE AND SEVEN)

In Appendix C, it includes the related figures of AFT performances with/without ionospheric corrections (Results of Chapter 3 and Chapter 7) as follows:

- Comparisons between the estimation based on GASP without ionospheric corrections and the true value on x, y, z, and baseline length.

1. Trial of 12.8km baseline (Figure C.1)
2. Trial of 15km baseline (Figure C.2)
3. Trial of 21km baseline (Figure C.3)
4. Trial of 25km baseline (Figure C.4)
5. Trial of 33km baseline (Figure C.5)

- Comparisons between the estimation based on GASP with LIM1 ionospheric corrections and the true value on x, y, z, and baseline length.

6. Trial of 12.8km baseline (Figure C.6)
7. Trial of 15km baseline (Figure C.7)
8. Trial of 21km baseline (Figure C.8)
9. Trial of 25km baseline (Figure C.9)
10. Trial of 33km baseline (Figure C.10)

- Comparisons between the estimation based on GASP with LIM2 ionospheric corrections and the true value on x, y, z, and baseline length.

11. Trial of 12.8km baseline (Figure C.11)
12. Trial of 15km baseline (Figure C.12)
13. Trial of 21km baseline (Figure C.13)
14. Trial of 25km baseline (Figure C.14)
15. Trial of 33km baseline (Figure C.15)

- Comparisons between the estimation based on GASP with LIM3 ionospheric corrections and the true value on x, y, z, and baseline length.

16. Trial of 12.8km baseline (Figure C.16)

17. Trial of 15km baseline (Figure C.17)
18. Trial of 21km baseline (Figure C.18)
19. Trial of 25km baseline (Figure C.19)
20. Trial of 33km baseline (Figure C.20)

- Comparisons between the estimation based on GASP with LIM4 ionospheric corrections and the true value on x, y, z, and baseline length.

21. Trial of 12.8km baseline (Figure C.21)
22. Trial of 15km baseline (Figure C.22)
23. Trial of 21km baseline (Figure C.23)
24. Trial of 25km baseline (Figure C.24)
25. Trial of 33km baseline (Figure C.25)

- Comparisons between the estimation based on GASP with LIM5 ionospheric corrections and the true value on x, y, z, and baseline length.

26. Trial of 12.8km baseline (Figure C.26)
27. Trial of 15km baseline (Figure C.27)
28. Trial of 21km baseline (Figure C.28)
29. Trial of 25km baseline (Figure C.29)
30. Trial of 33km baseline (Figure C.30)

- Comparisons between the estimation based on GASP with LIM6 ionospheric corrections and the true value on x, y, z, and baseline length.

31. Trial of 12.8km baseline (Figure C.31)
32. Trial of 15km baseline (Figure C.32)
33. Trial of 21km baseline (Figure C.33)
34. Trial of 25km baseline (Figure C.34)
35. Trial of 33km baseline (Figure C.35)

- Comparisons between the estimation based on GASP without ionospheric corrections and the true value on x, y, z, and baseline length.

1. Trial of 12.8km baseline

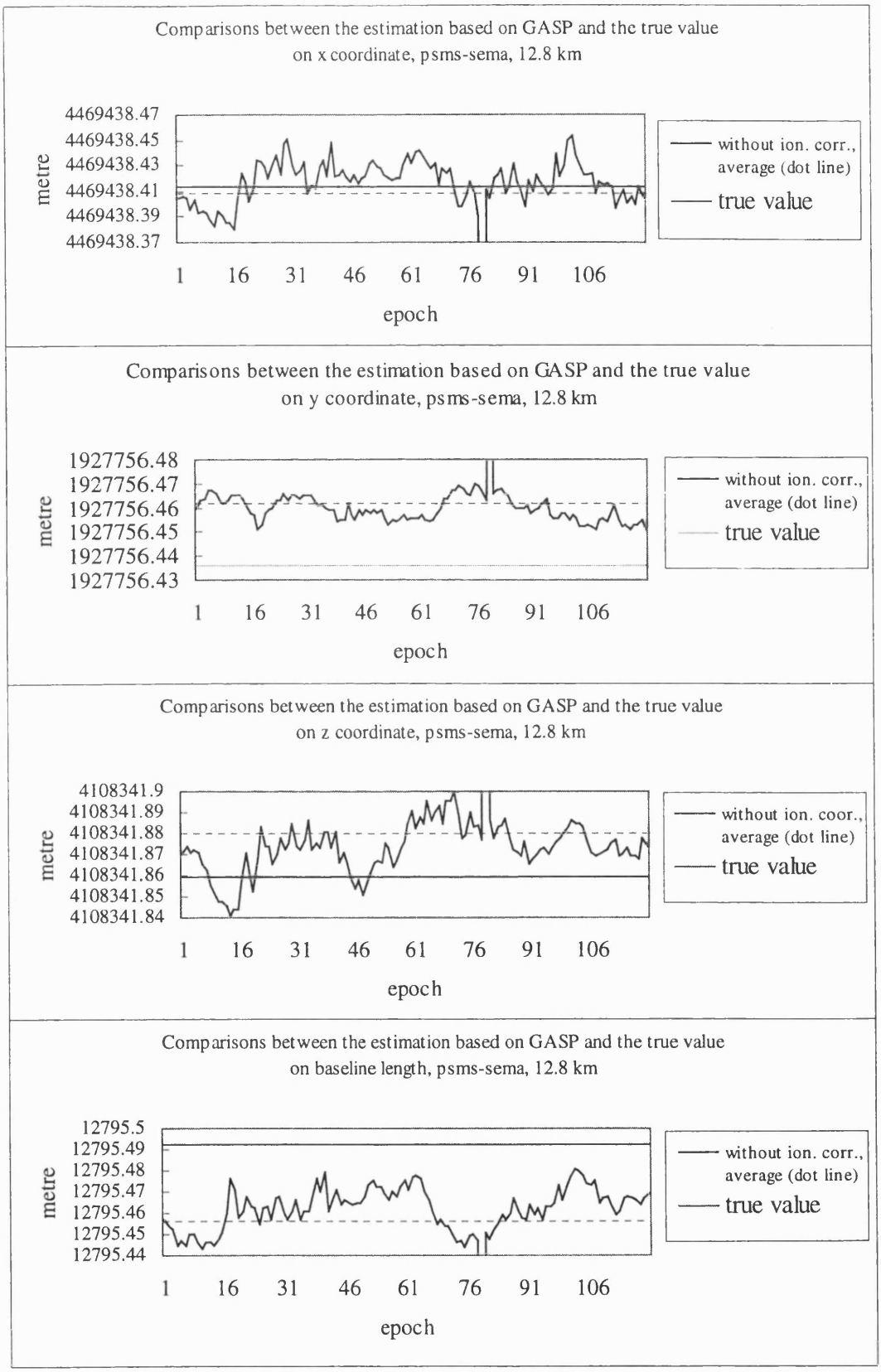

Figure C.1 Comparisons between the estimation based on GASP without ionospheric corrections and the true value on x, y, z, and baseline length (12.8km baseline)

2. Trial of 15km baseline

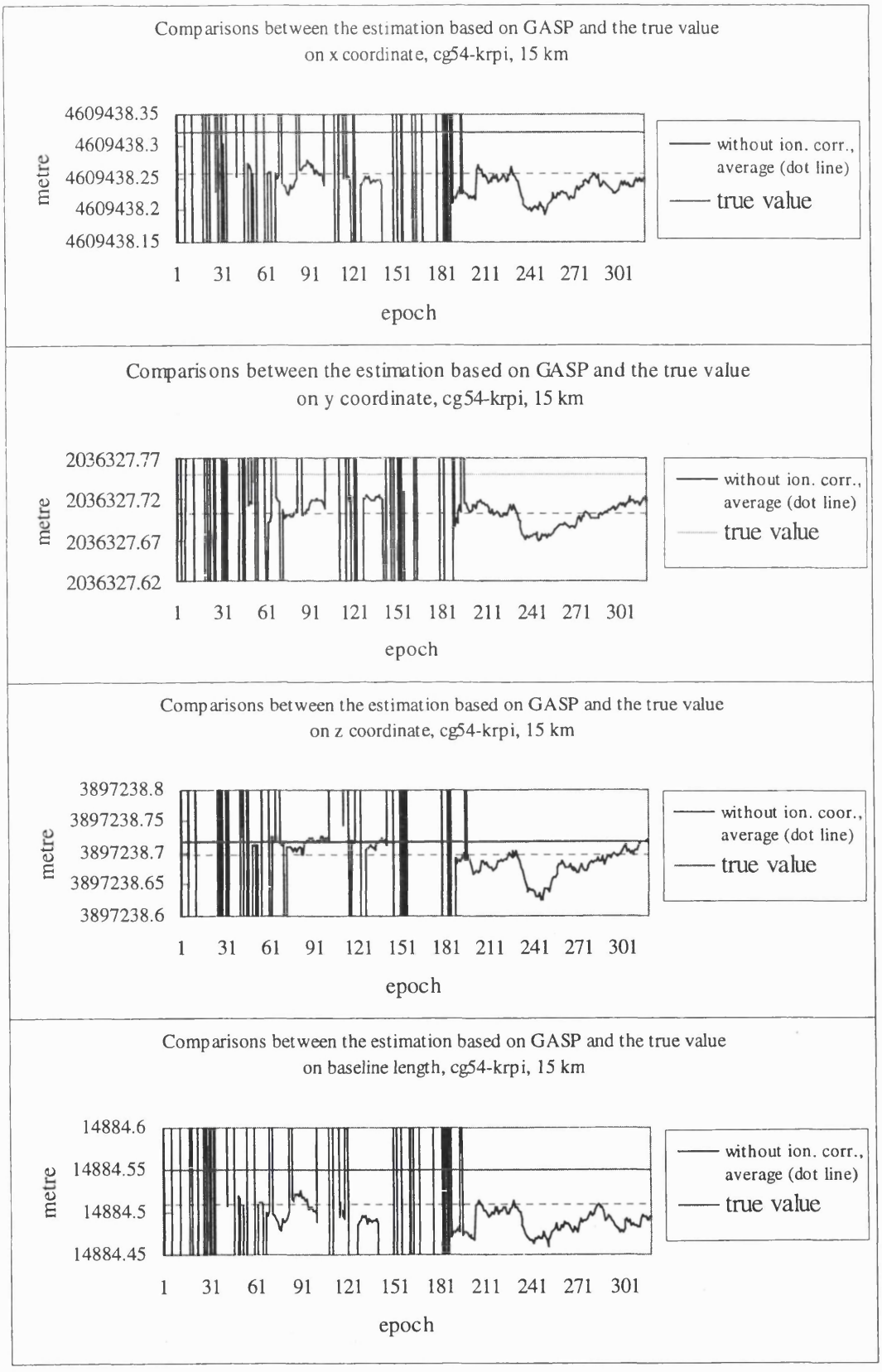

Figure C.2 Comparisons between the estimation based on GASP without ionospheric corrections and the true value on x, y, z, and baseline length (15km baseline)

3. Trial of 21km baseline

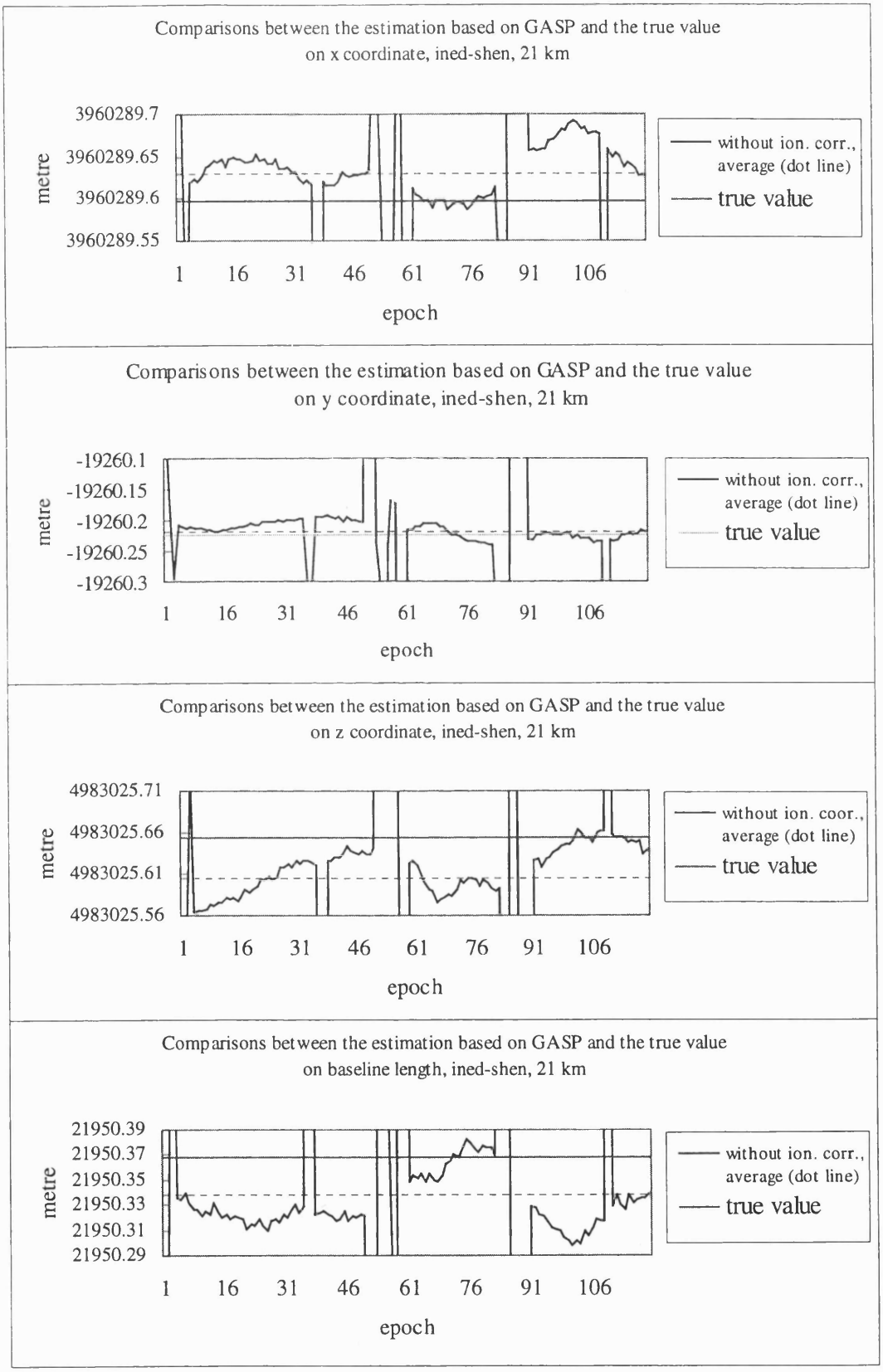

Figure C.3 Comparisons between the estimation based on GASP without ionospheric corrections and the true value on x, y, z, and baseline length (21km baseline)

4. Trial of 25km baseline

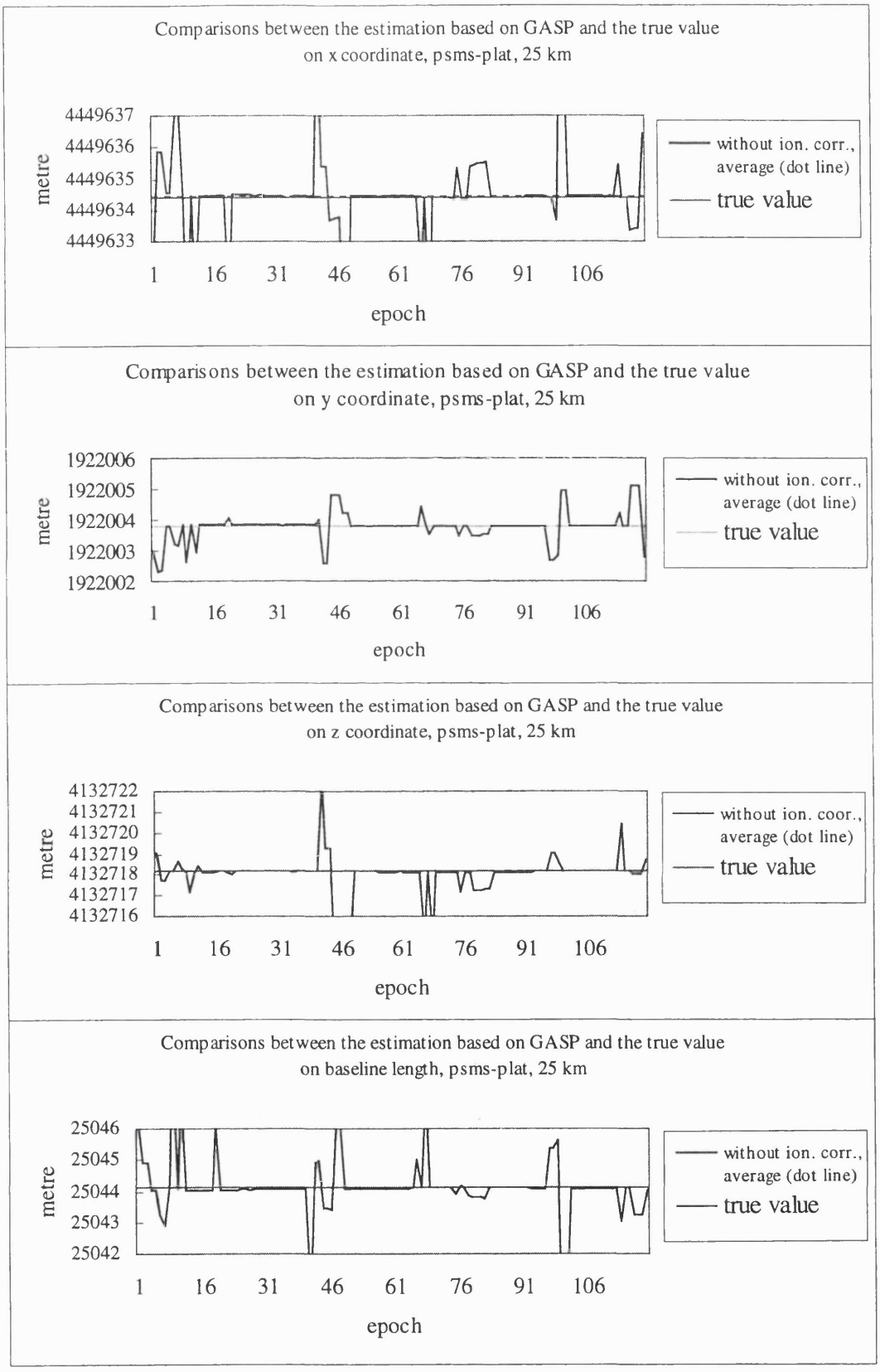

Figure C.4 Comparisons between the estimation based on GASP without ionospheric corrections and the true value on x, y, z, and baseline length (25km baseline)

5. Trial of 33km baseline

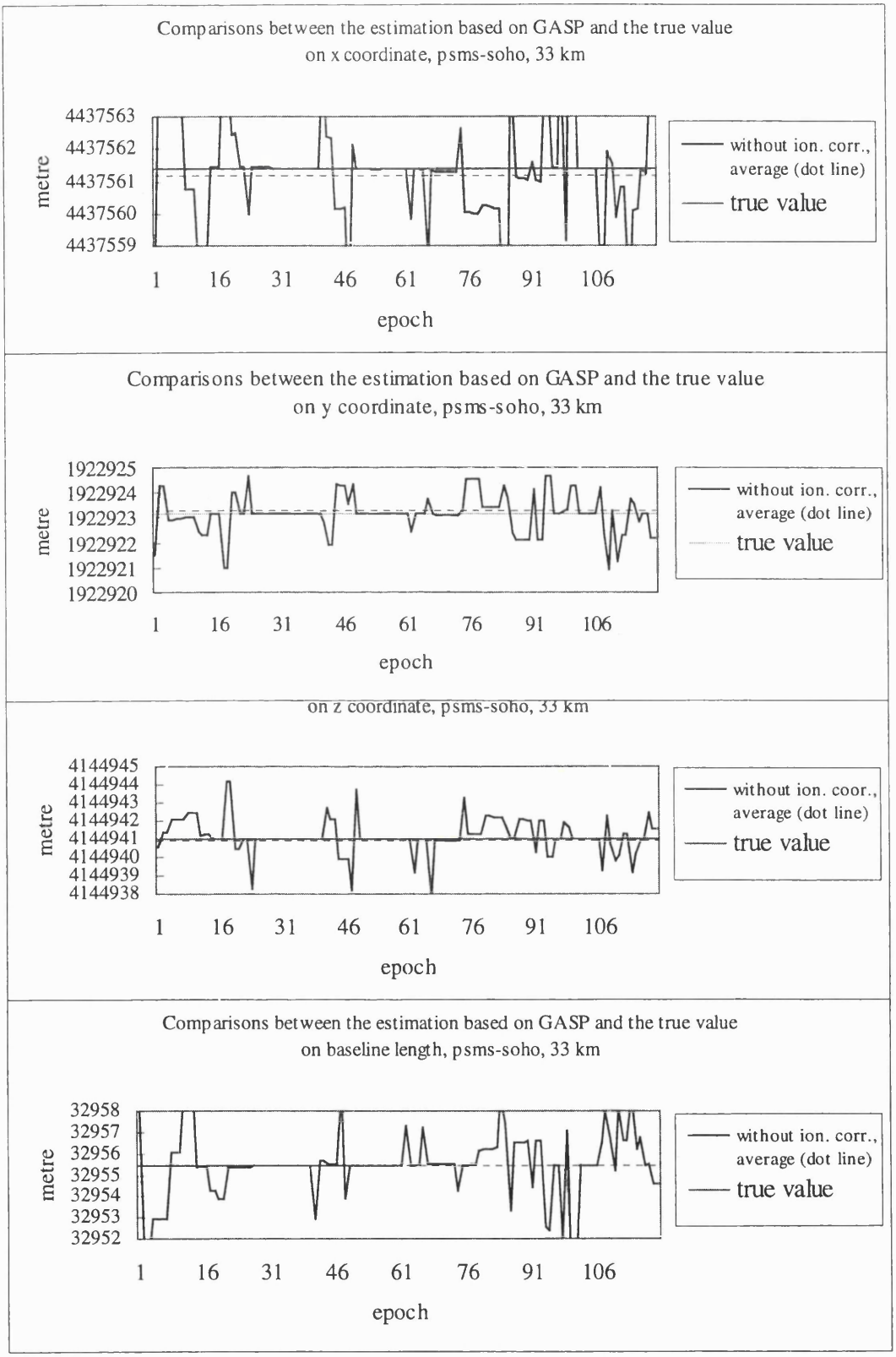

Figure C.5 Comparisons between the estimation based on GASP without ionospheric corrections and the true value on x, y, z, and baseline length (33km baseline)

- Comparisons between the estimation based on GASP with LIM1 ionospheric corrections and the true value on x, y, z, and baseline length.

1. Trial of 12.8km baseline

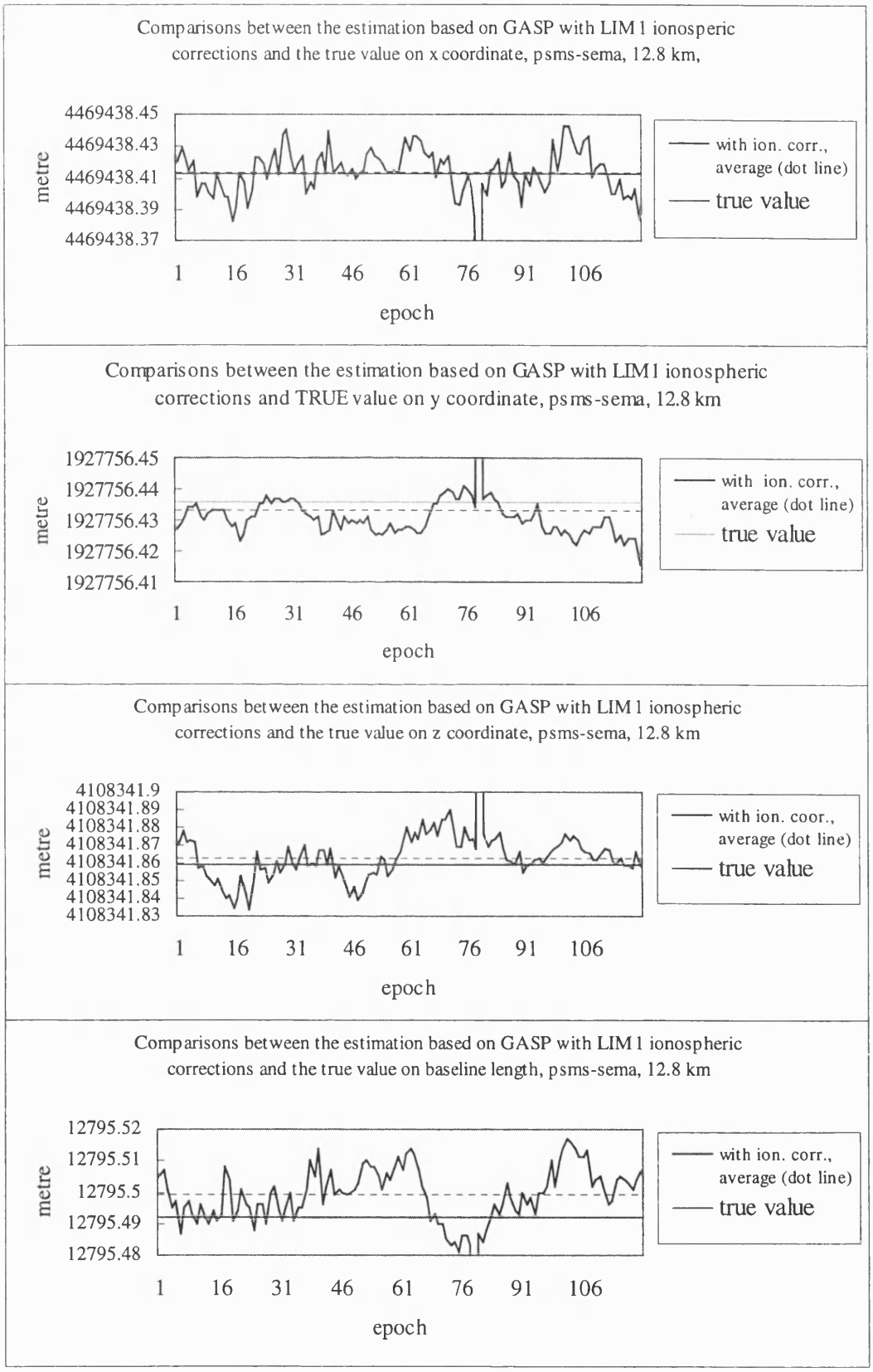

Figure C.6 Comparisons between the estimation based on GASP with LIM1 ionospheric corrections and the true value on x, y, z, and baseline length (12.8km baseline)

2. Trial of 15km baseline

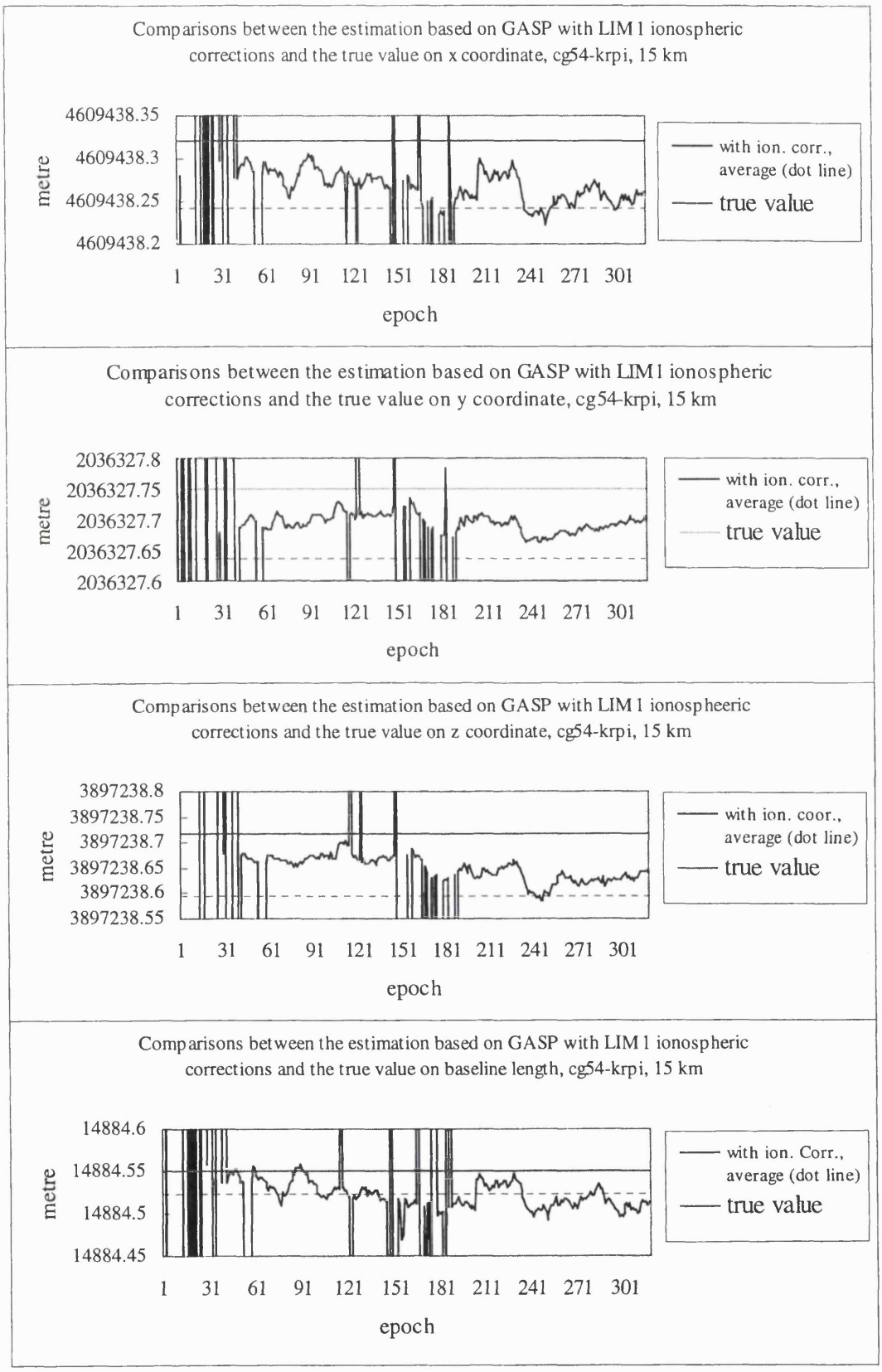

Figure C.7 Comparisons between the estimation based on GASP with LIM1 ionospheric corrections and the true value on x, y, z, and baseline length (15km baseline)

3. Trial of 21km baseline

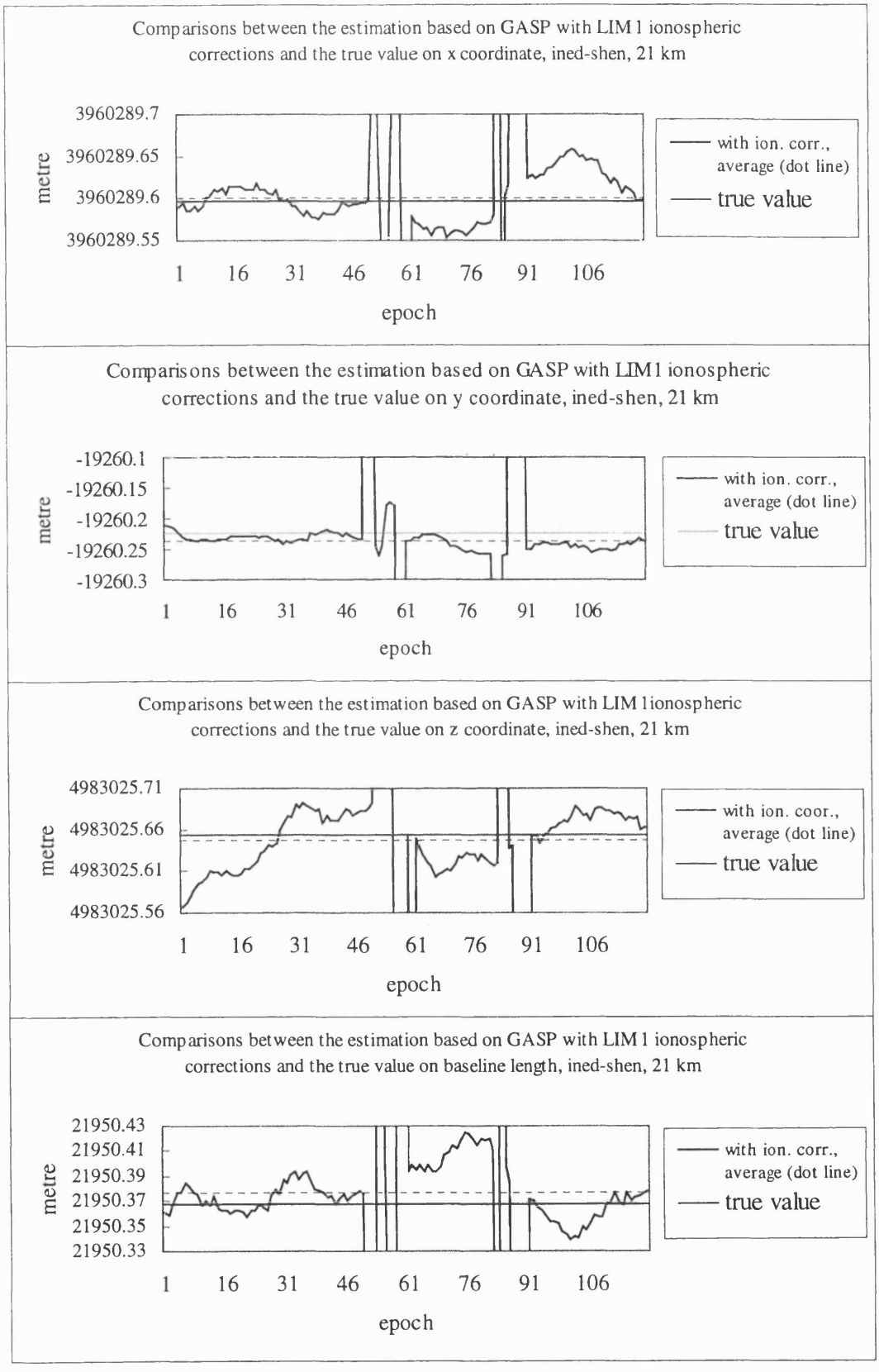

Figure C.8 Comparisons between the estimation based on GASP with LIM1 ionospheric corrections and the true value on x, y, z, and baseline length (21km baseline)

4. Trial of 25km baseline

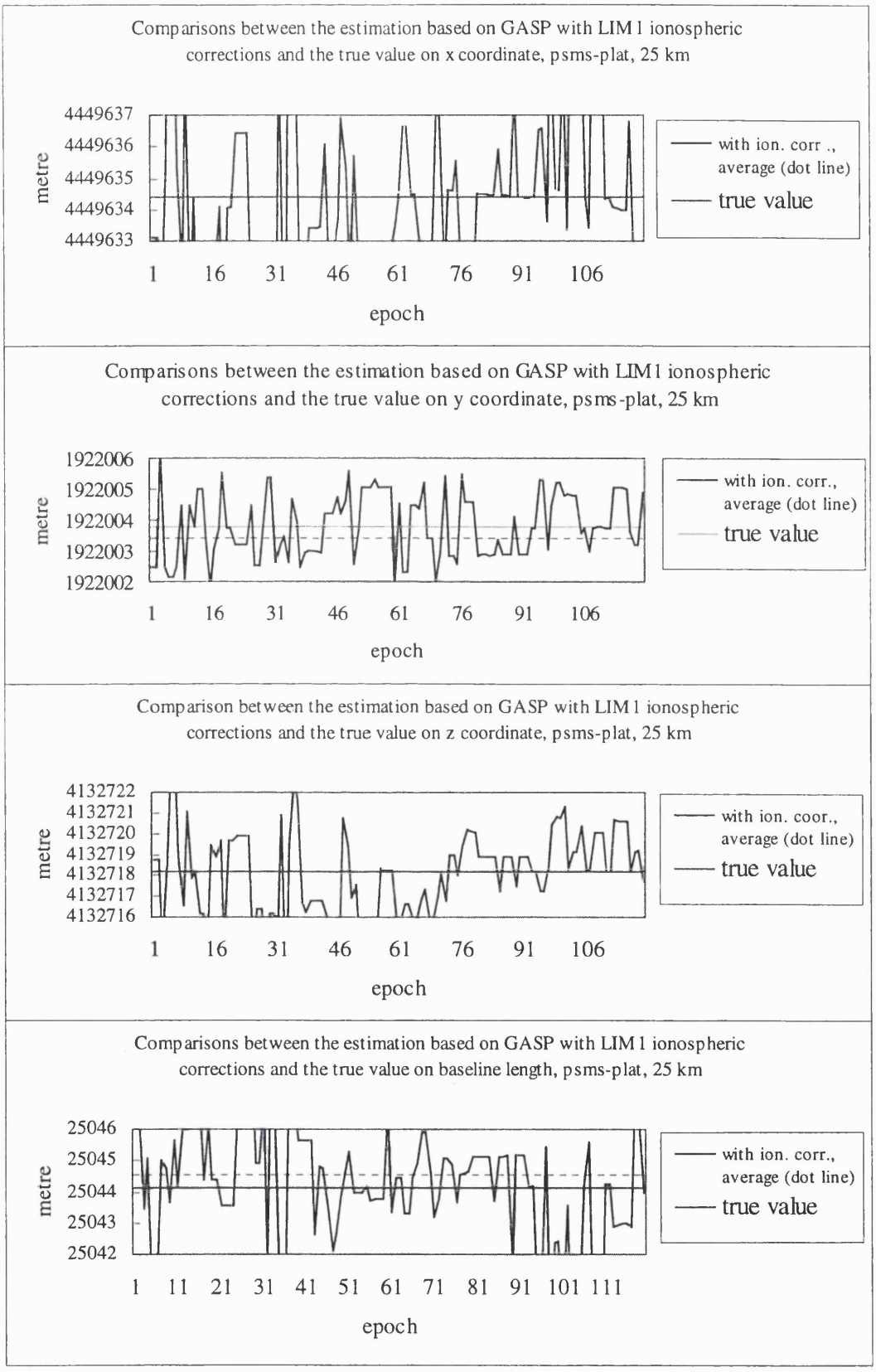

Figure C.9 Comparisons between the estimation based on GASP with LIM1 ionospheric corrections and the true value on x, y, z, and baseline length (25km baseline)

5. Trial of 33km baseline

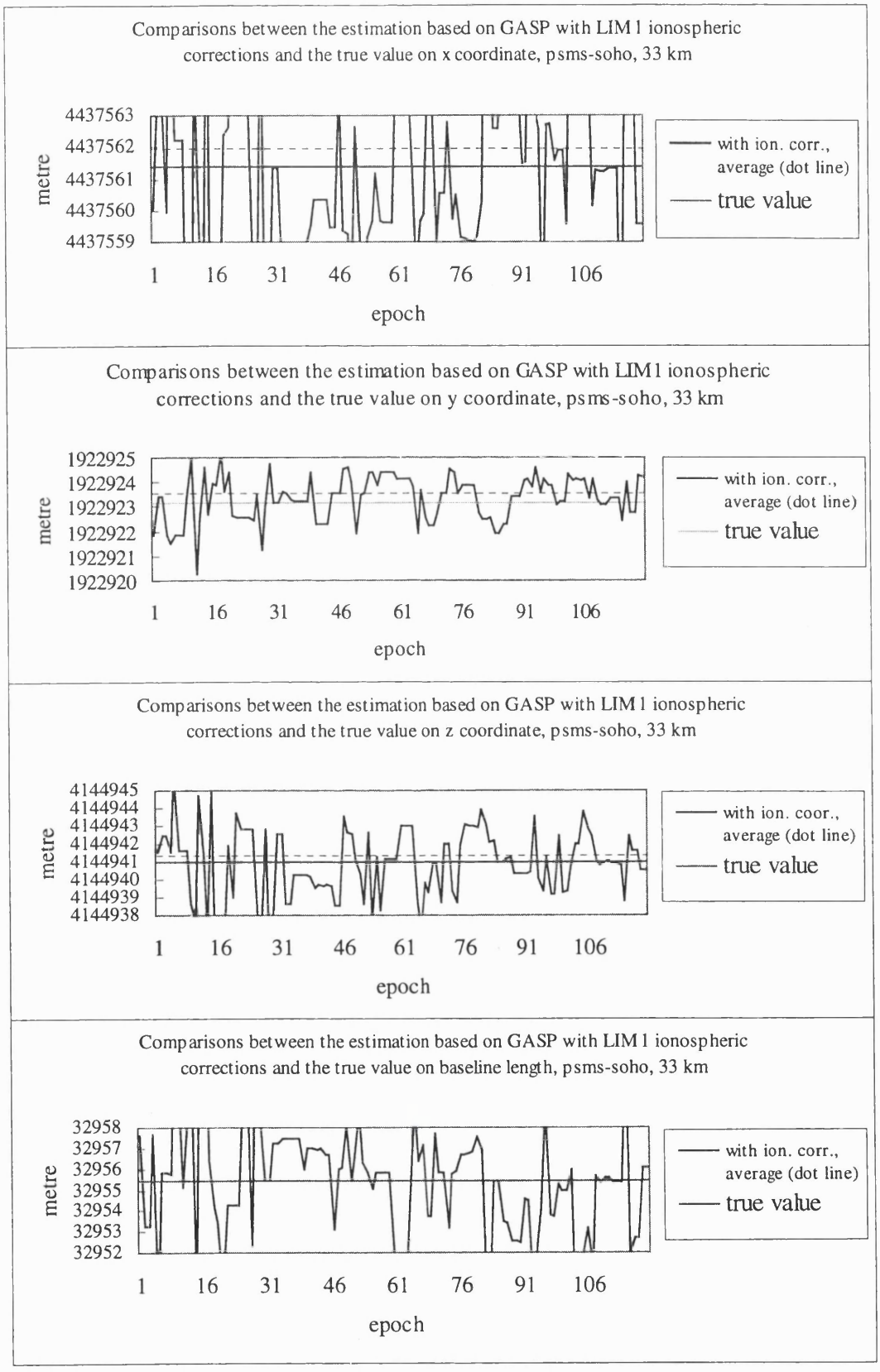

Figure C.10 Comparisons between the estimation based on GASP with LIM1 ionospheric corrections and the true value on x, y, z, and baseline length (33km baseline)

- Comparisons between the estimation based on GASP with LIM2 ionospheric corrections and the true value on x, y, z, and baseline length.

1. Trial of 12.8km baseline

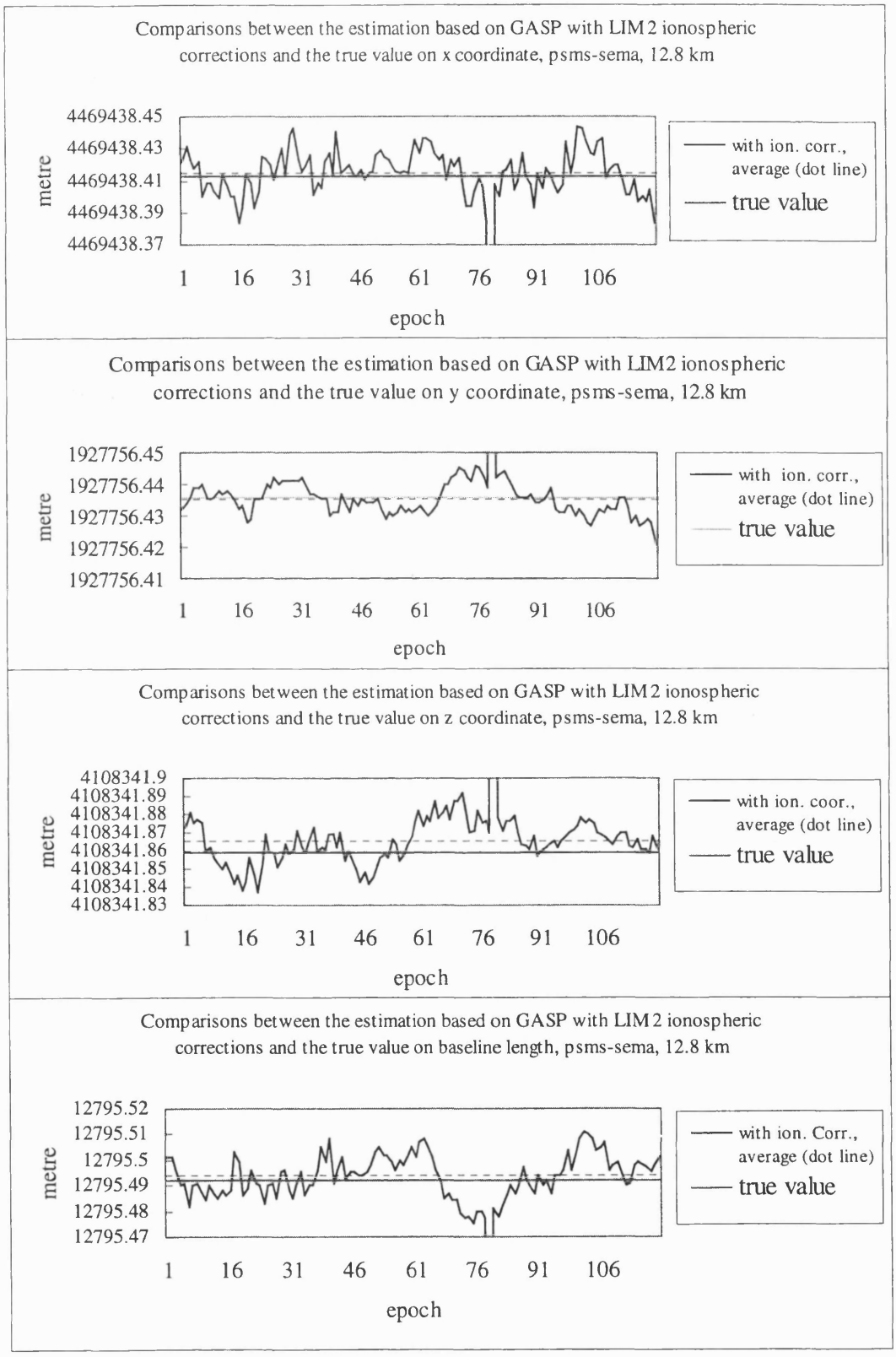

Figure C.11 Comparisons between the estimation based on GASP with LIM2 ionospheric corrections and the true value on x, y, z, and baseline length (12.8km baseline)

2. Trial of 15km baseline

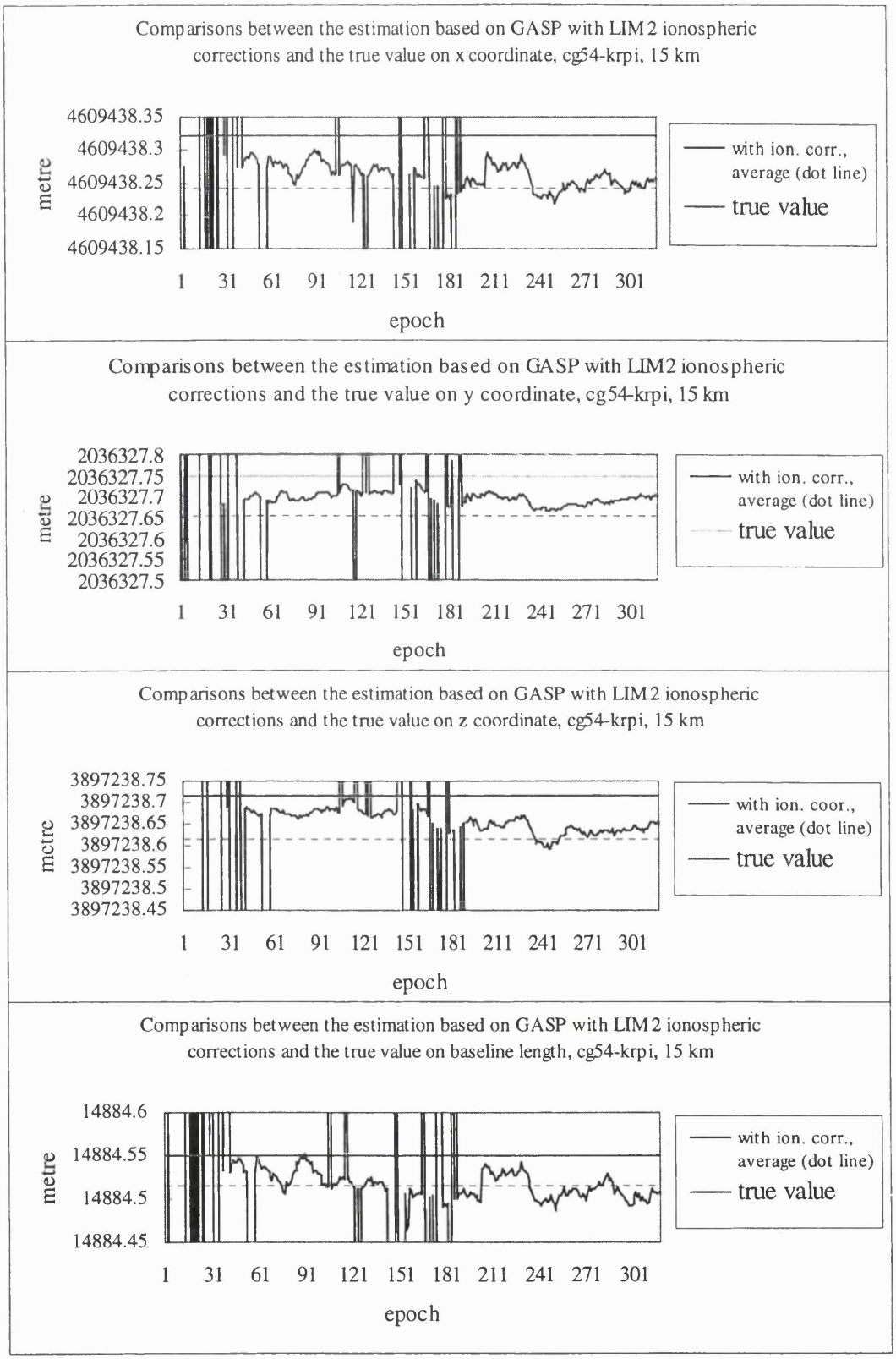

Figure C.12 Comparisons between the estimation based on GASP with LIM2 ionospheric corrections and the true value on x, y, z, and baseline length (15km baseline)

3. Trial of 21km baseline

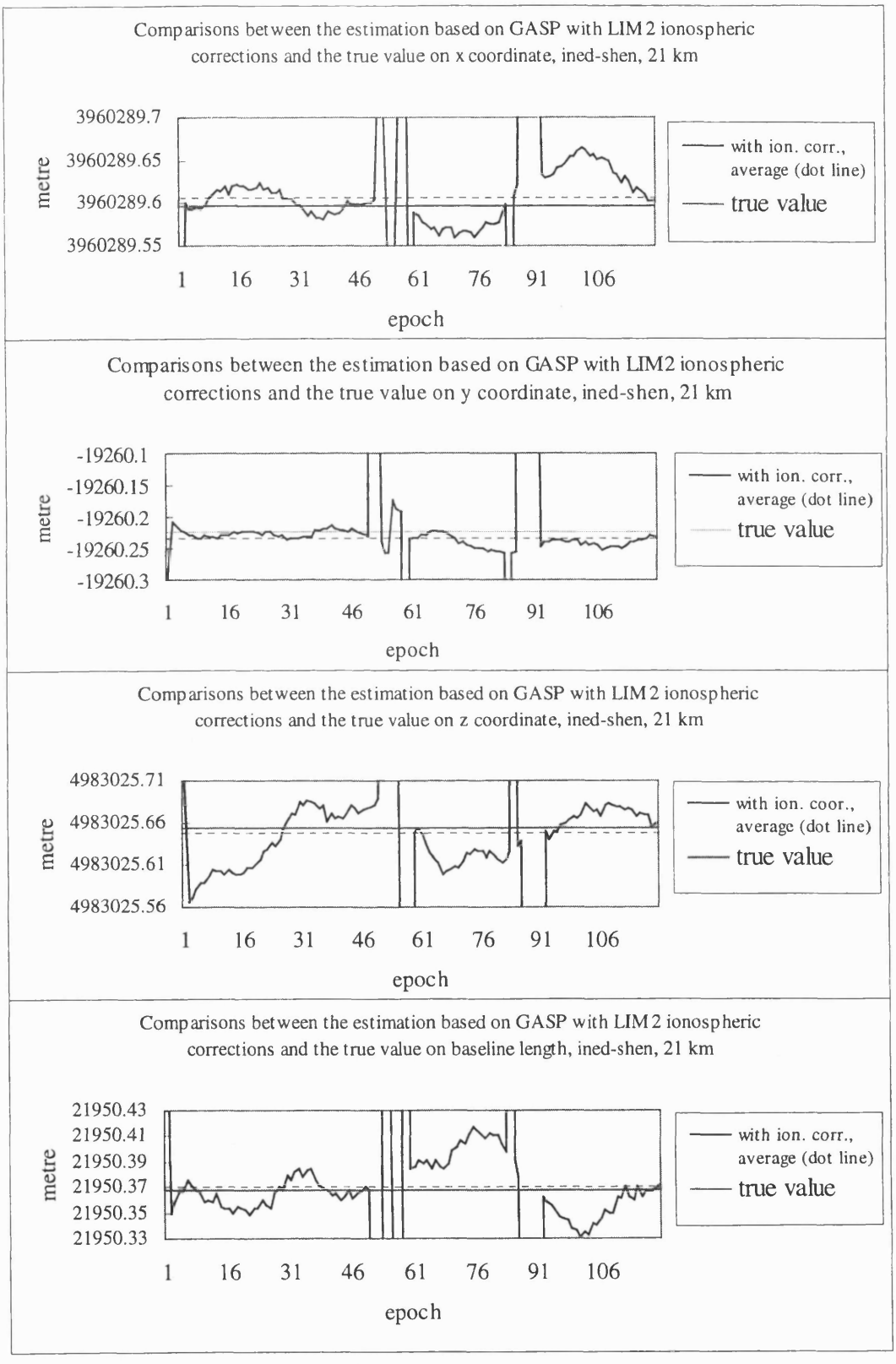

Figure C.13 Comparisons between the estimation based on GASP with LIM2 ionospheric corrections and the true value on x, y, z, and baseline length (21km baseline)

4. Trial of 25km baseline

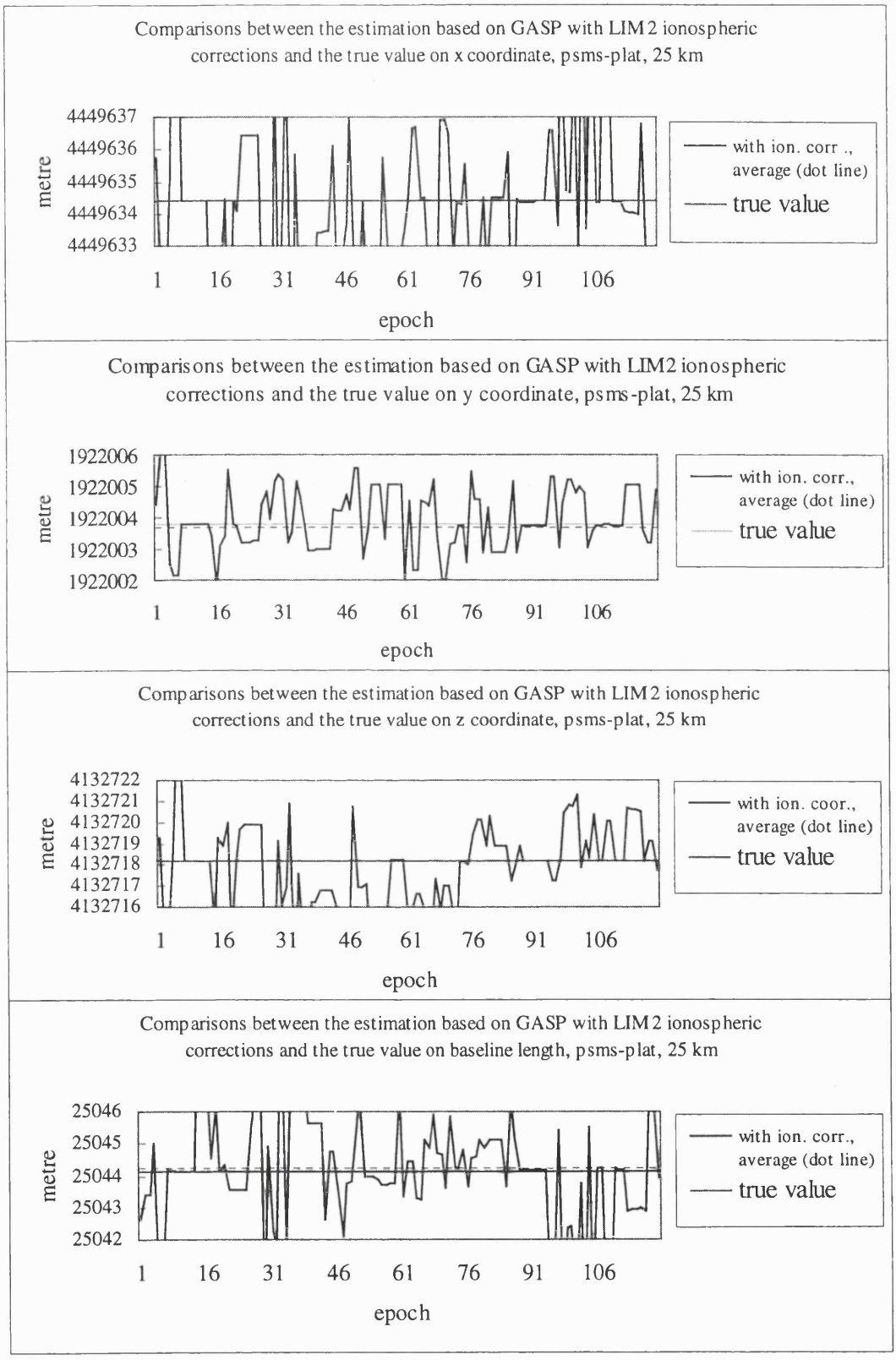

Figure C.14 Comparisons between the estimation based on GASP with LIM2 ionospheric corrections and the true value on x, y, z, and baseline length (25km baseline)

5. Trial of 33km baseline

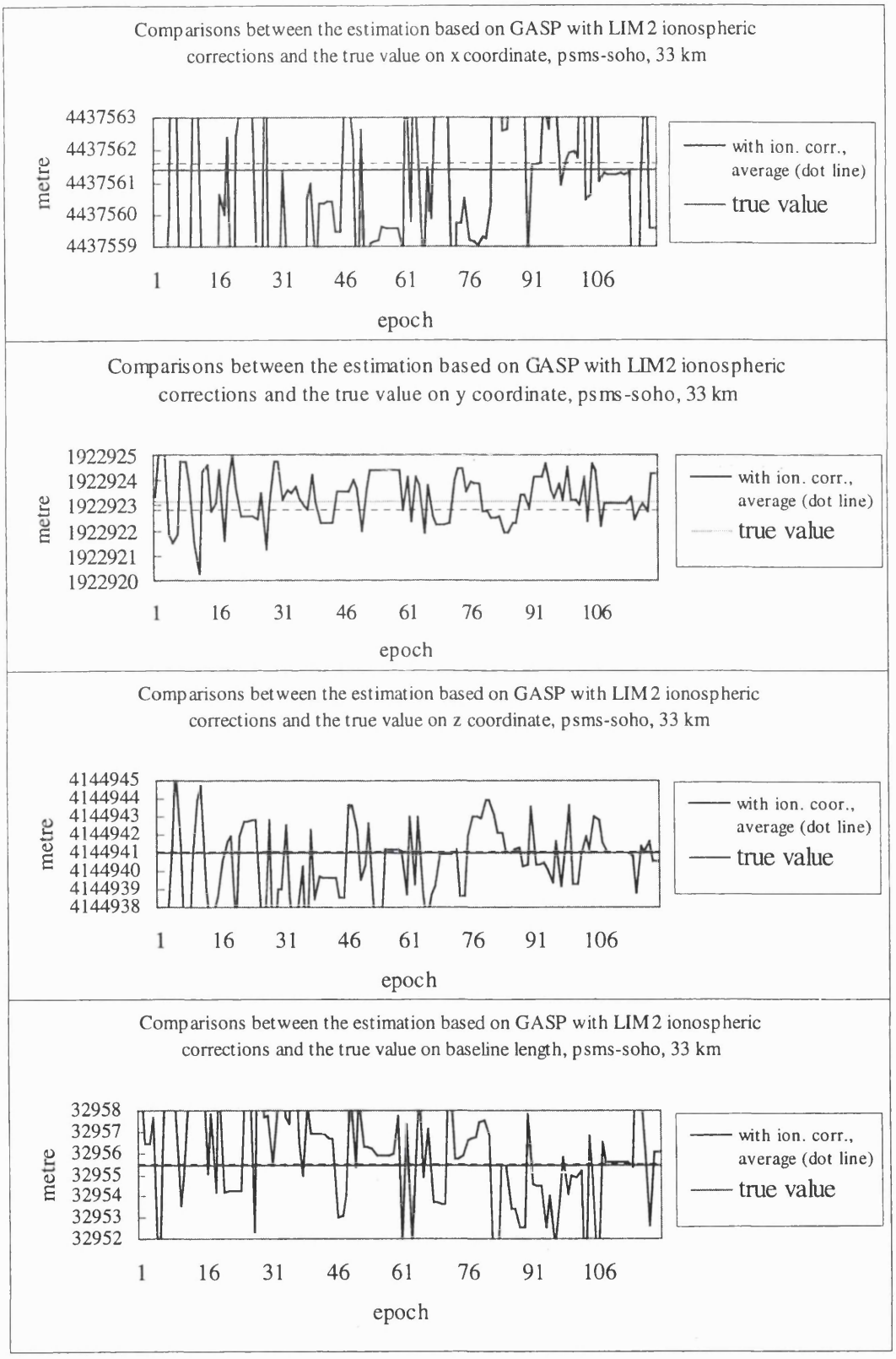

Figure C.15 Comparisons between the estimation based on GASP with LIM2 ionospheric corrections and the true value on x, y, z, and baseline length (33km baseline)

- Comparisons between the estimation based on GASP with LIM3 ionospheric corrections and the true value on x, y, z, and baseline length.

1. Trial of 12.8km baseline

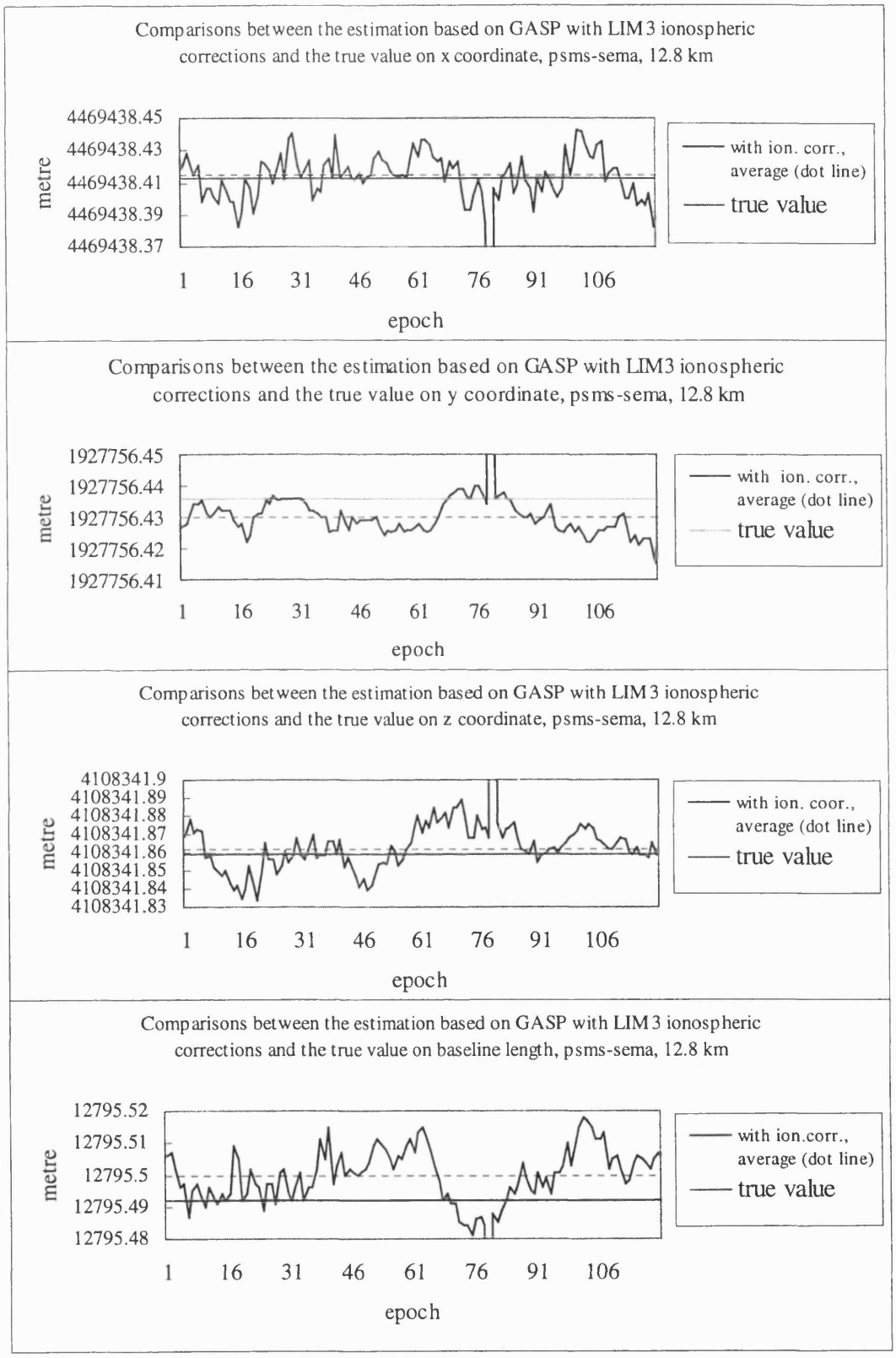

Figure C.16 Comparisons between the estimation based on GASP with LIM3 ionospheric corrections and the true value on x, y, z, and baseline length (12.8km baseline)

2. Trial of 15km baseline

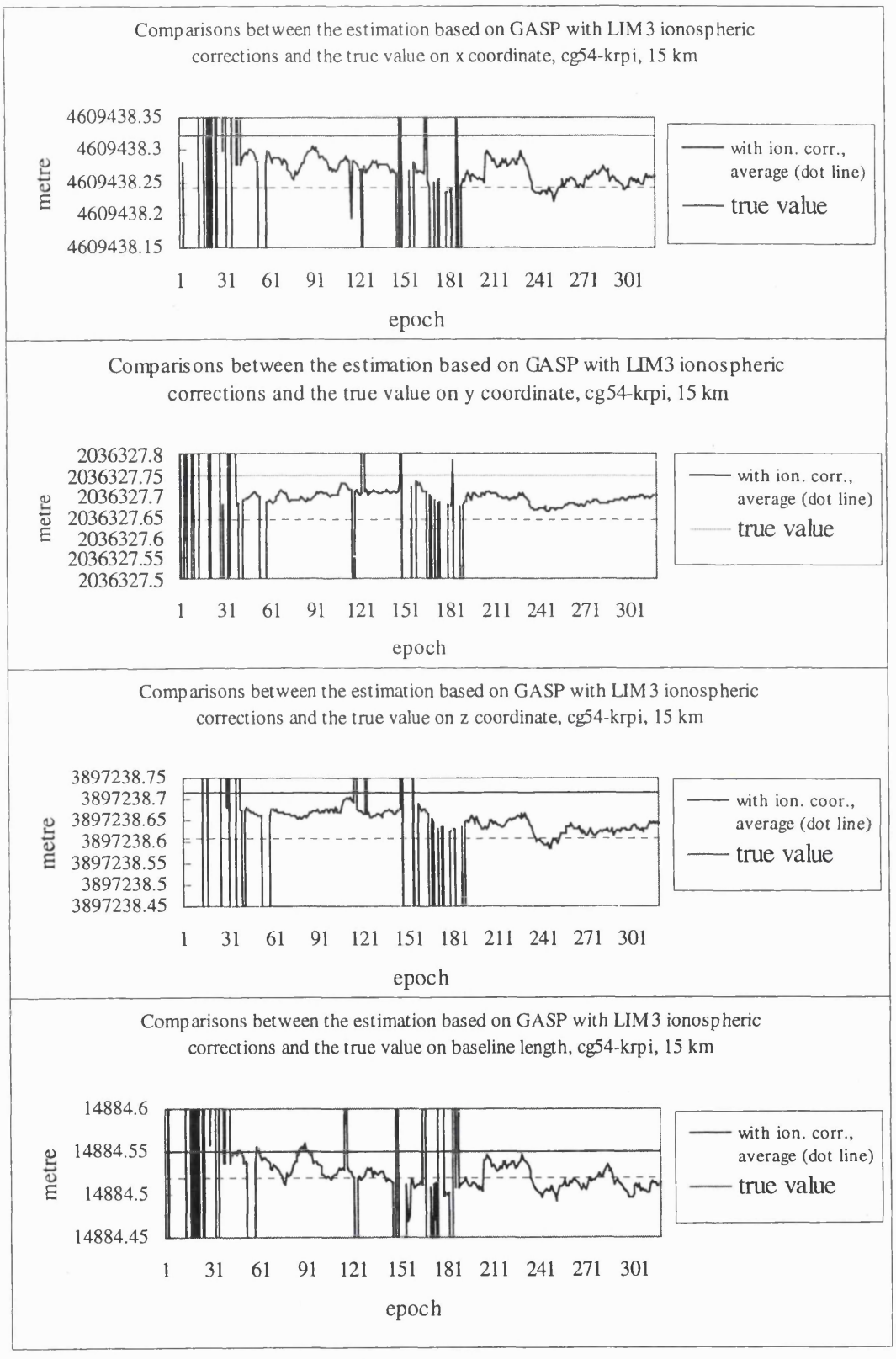

Figure C.17 Comparisons between the estimation based on GASP with LIM3 ionospheric corrections and the true value on x, y, z, and baseline length (15km baseline)

3. Trial of 21km baseline

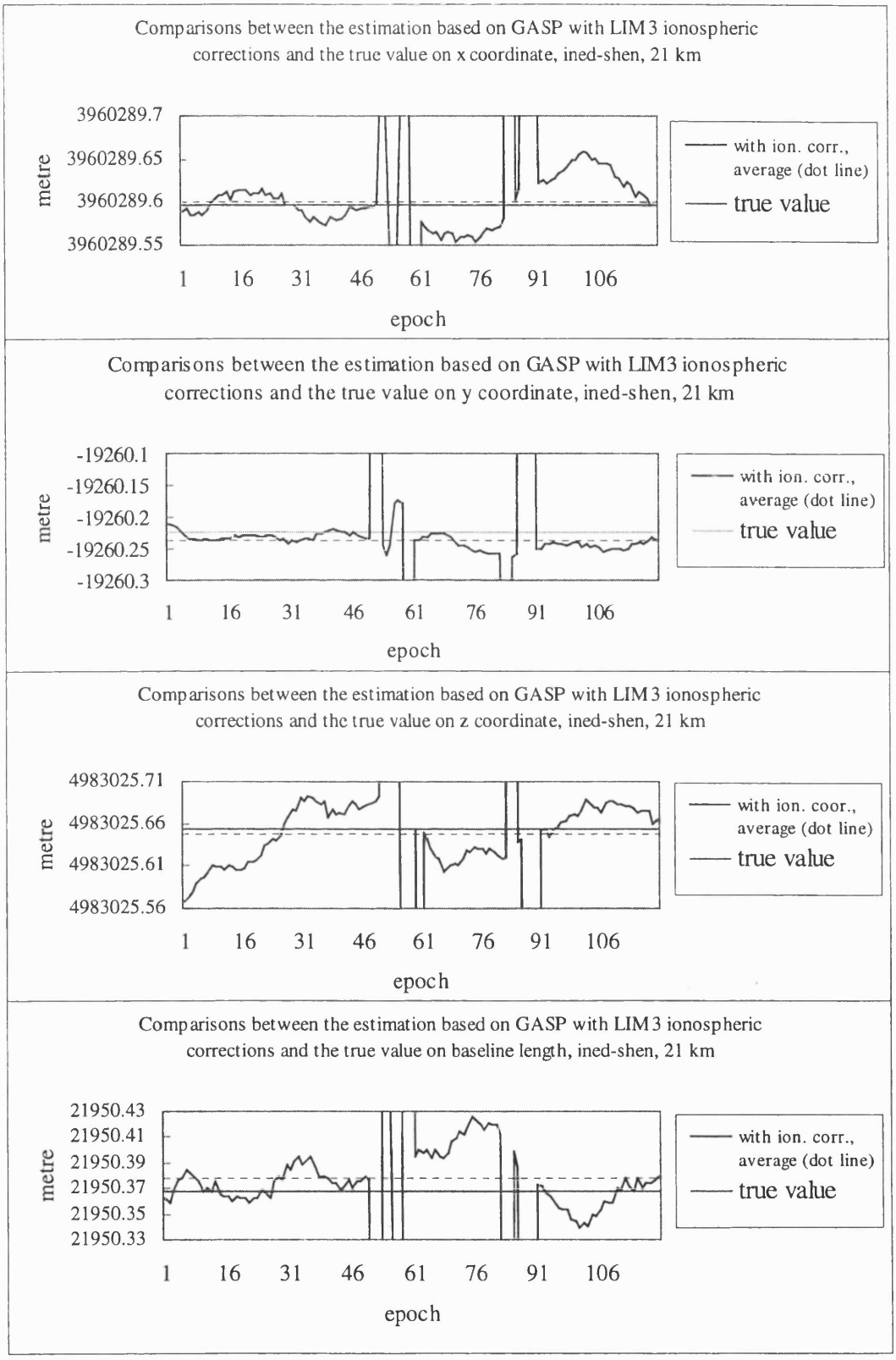

Figure C.18 Comparisons between the estimation based on GASP with LIM3 ionospheric corrections and the true value on x, y, z, and baseline length (21km baseline)

4. Trial of 25km baseline

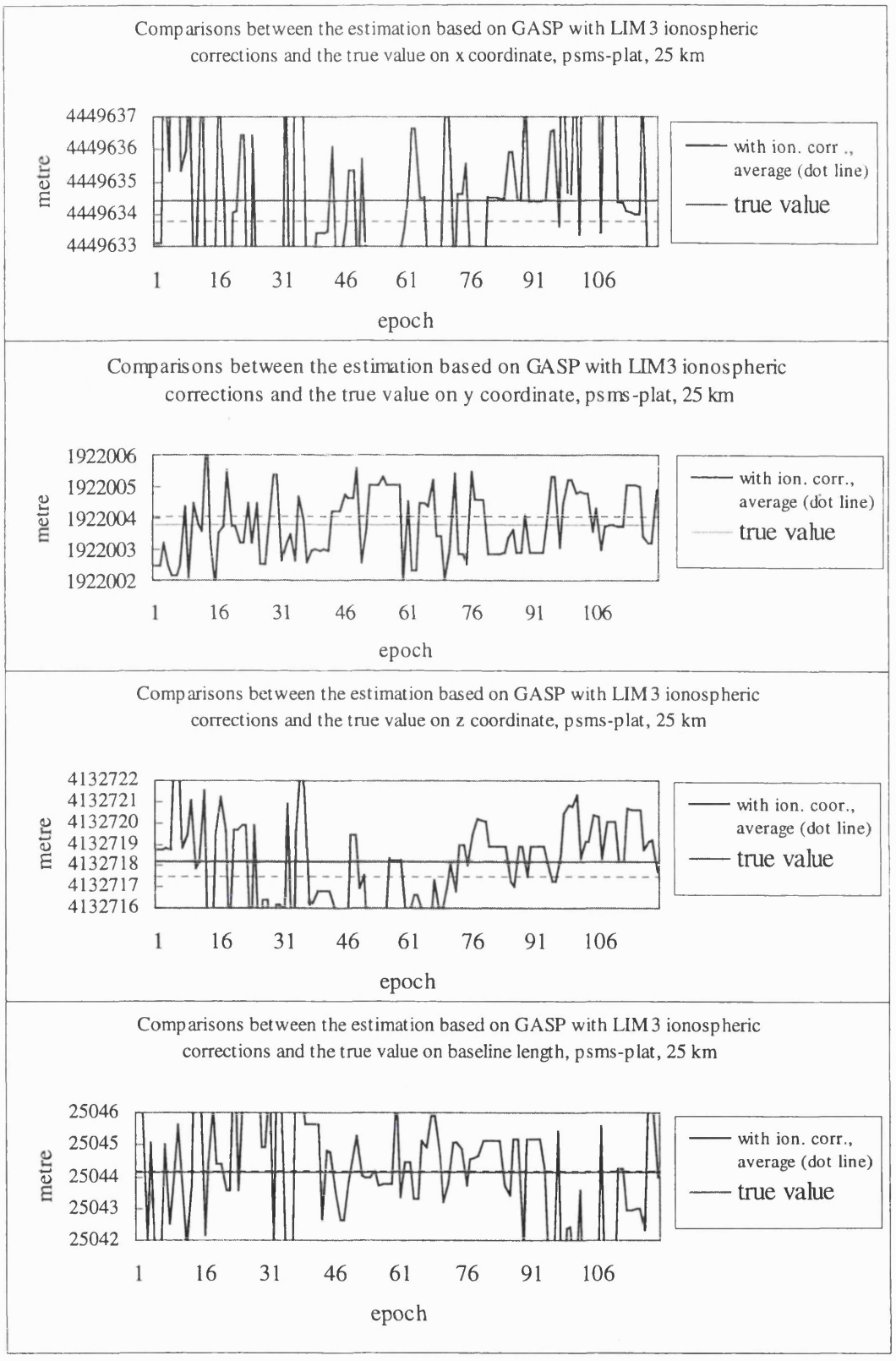

Figure C.19 Comparisons between the estimation based on GASP with LIM3 ionospheric corrections and the true value on x, y, z, and baseline length (25km baseline)

5. Trial of 33km baseline

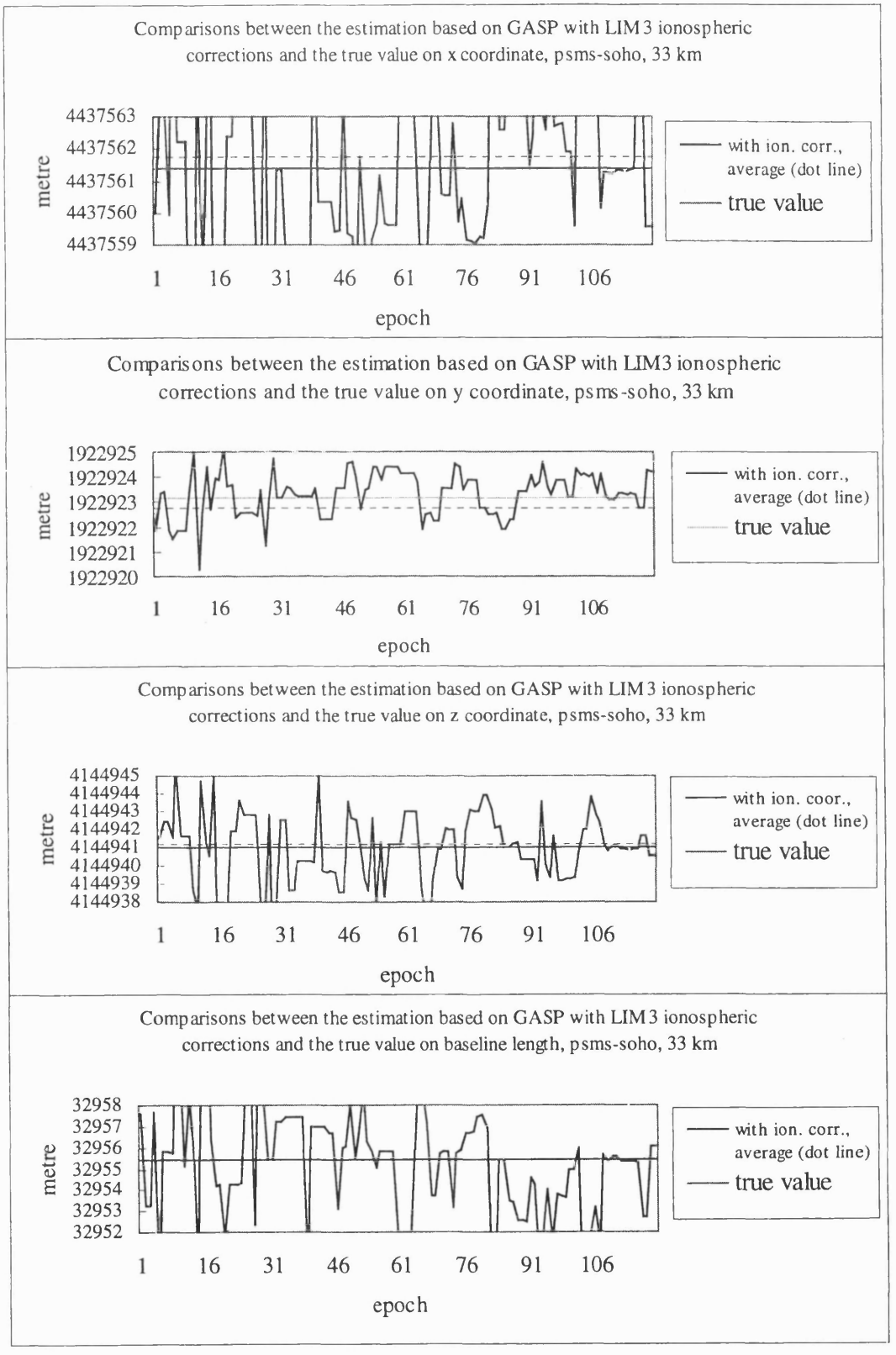

Figure C.20 Comparisons between the estimation based on GASP with LIM3 ionospheric corrections and the true value on x, y, z, and baseline length (33km baseline)

- Comparisons between the estimation based on GASP with LIM4 ionospheric corrections and the true value on x, y, z, and baseline length.

1. Trial of 12.8km baseline

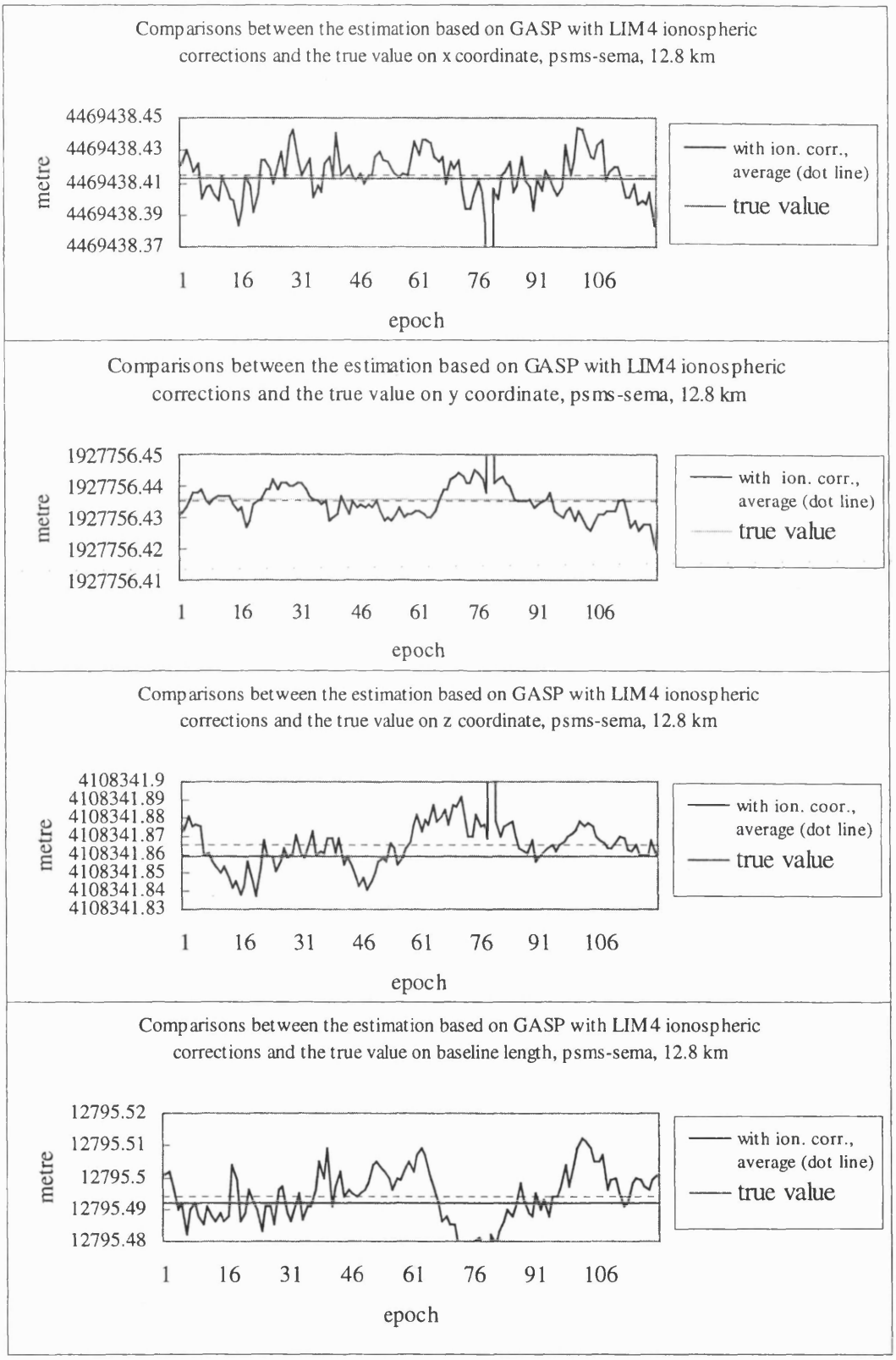

Figure C.21 Comparisons between the estimation based on GASP with LIM4 ionospheric corrections and the true value on x, y, z, and baseline length (12.8km baseline)

2. Trial of 15km baseline

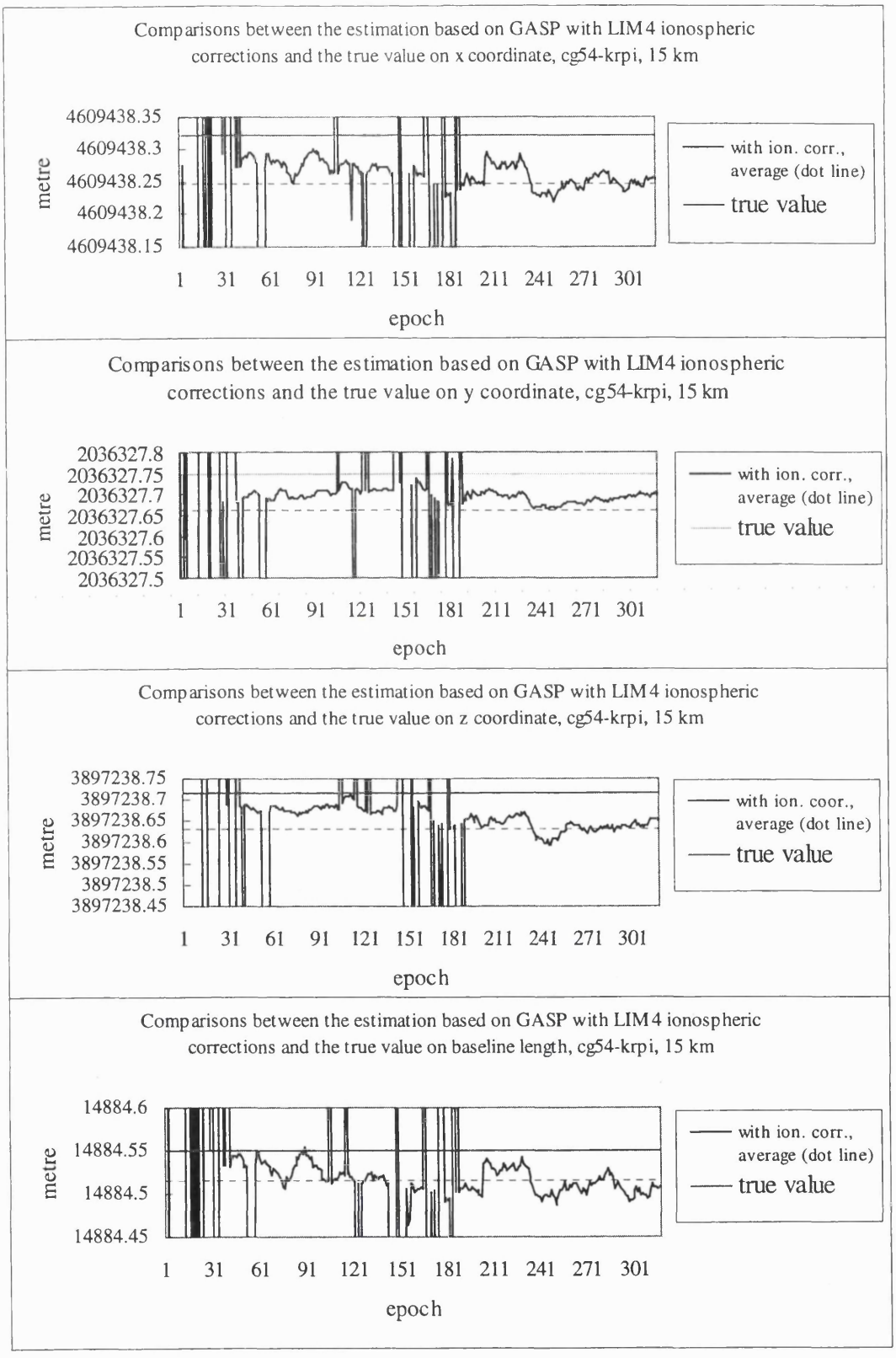

Figure C.22 Comparisons between the estimation based on GASP with LIM4 ionospheric corrections and the true value on x, y, z, and baseline length (15km baseline)

3. Trial of 21km baseline

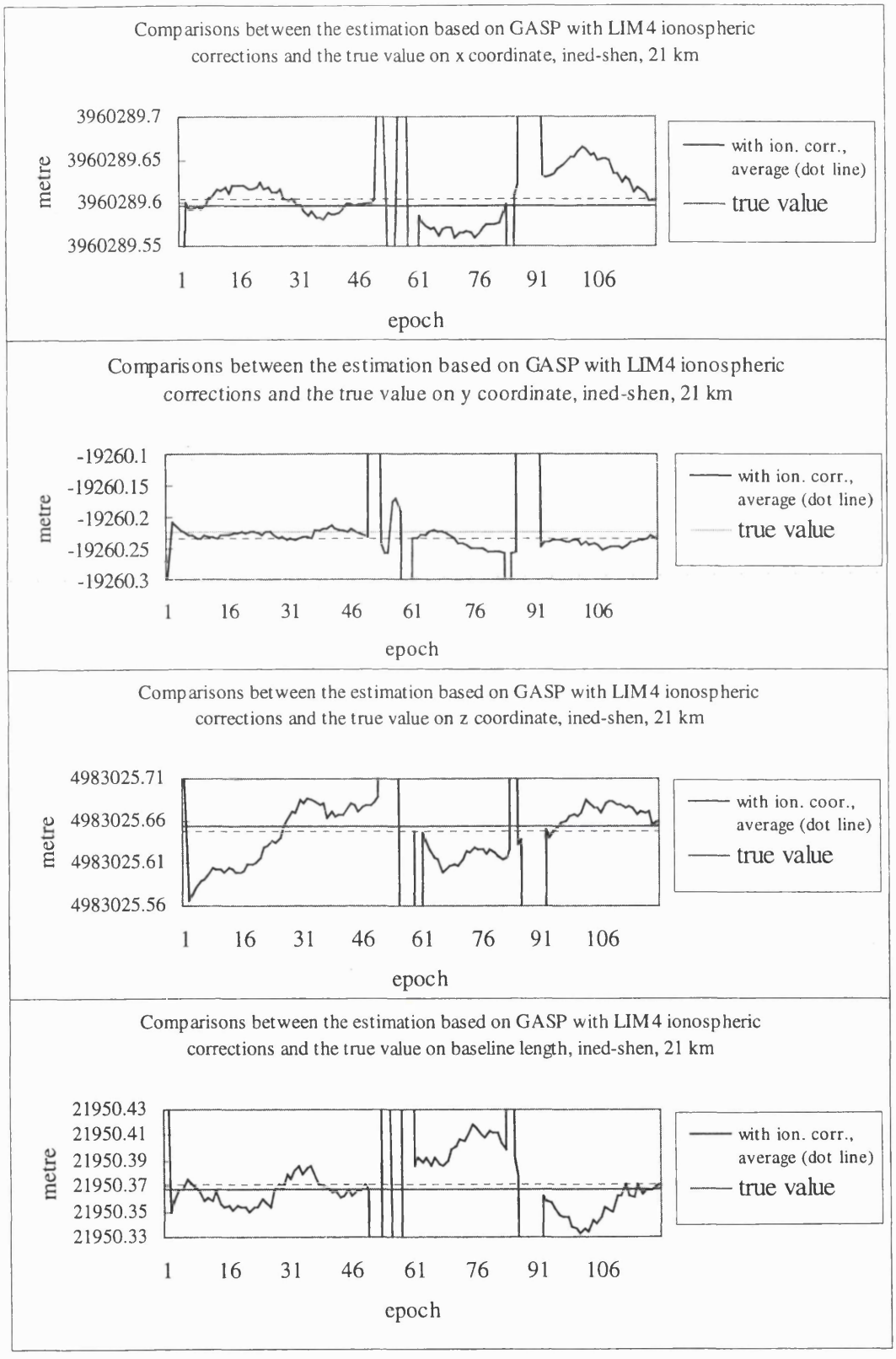

Figure C.23 Comparisons between the estimation based on GASP with LIM4 ionospheric corrections and the true value on x, y, z, and baseline length (21km baseline)

4. Trial of 25km baseline

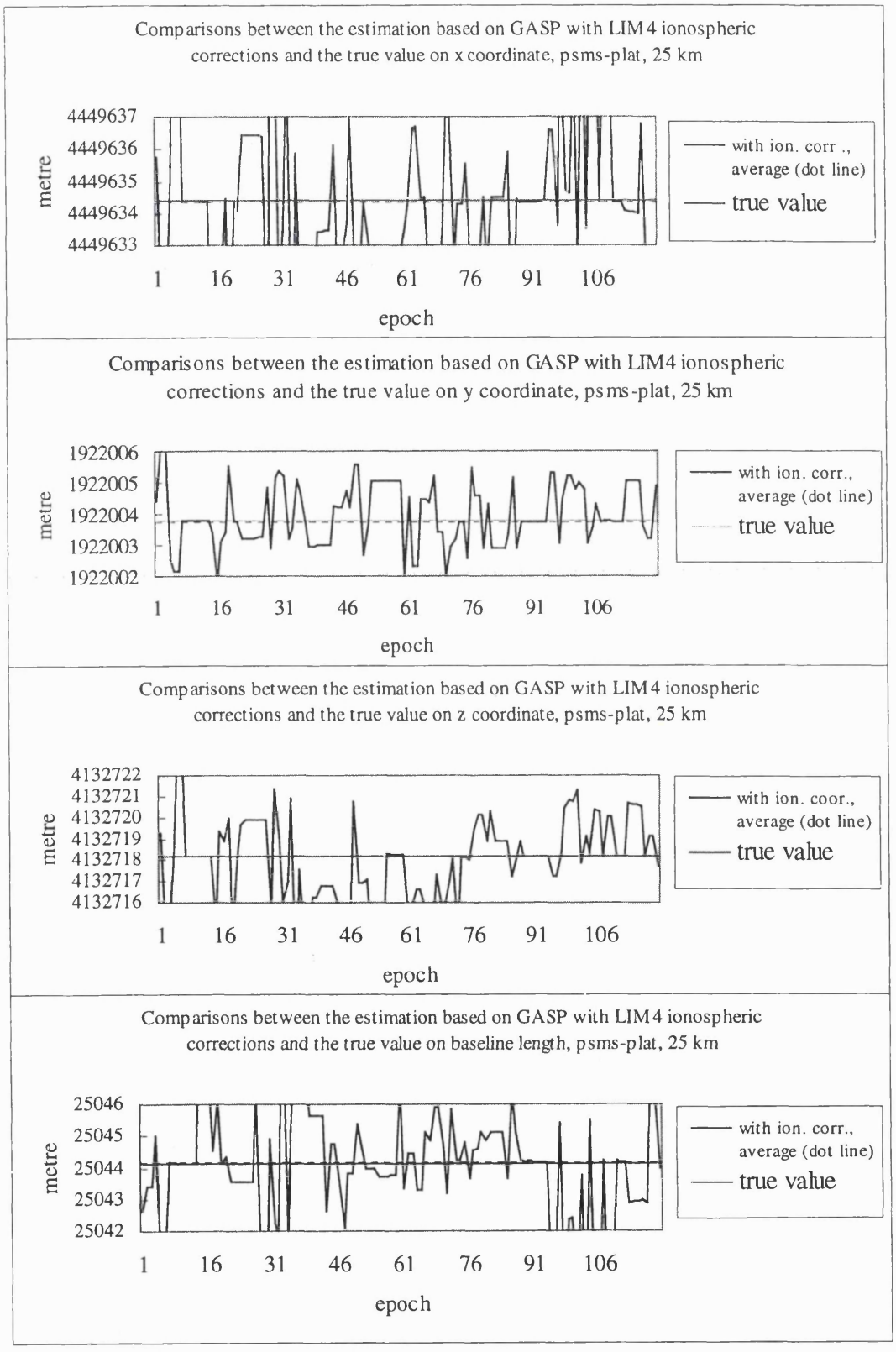

Figure C.24 Comparisons between the estimation based on GASP with LIM4 ionospheric corrections and the true value on x, y, z, and baseline length (25km baseline)

5. Trial of 33km baseline

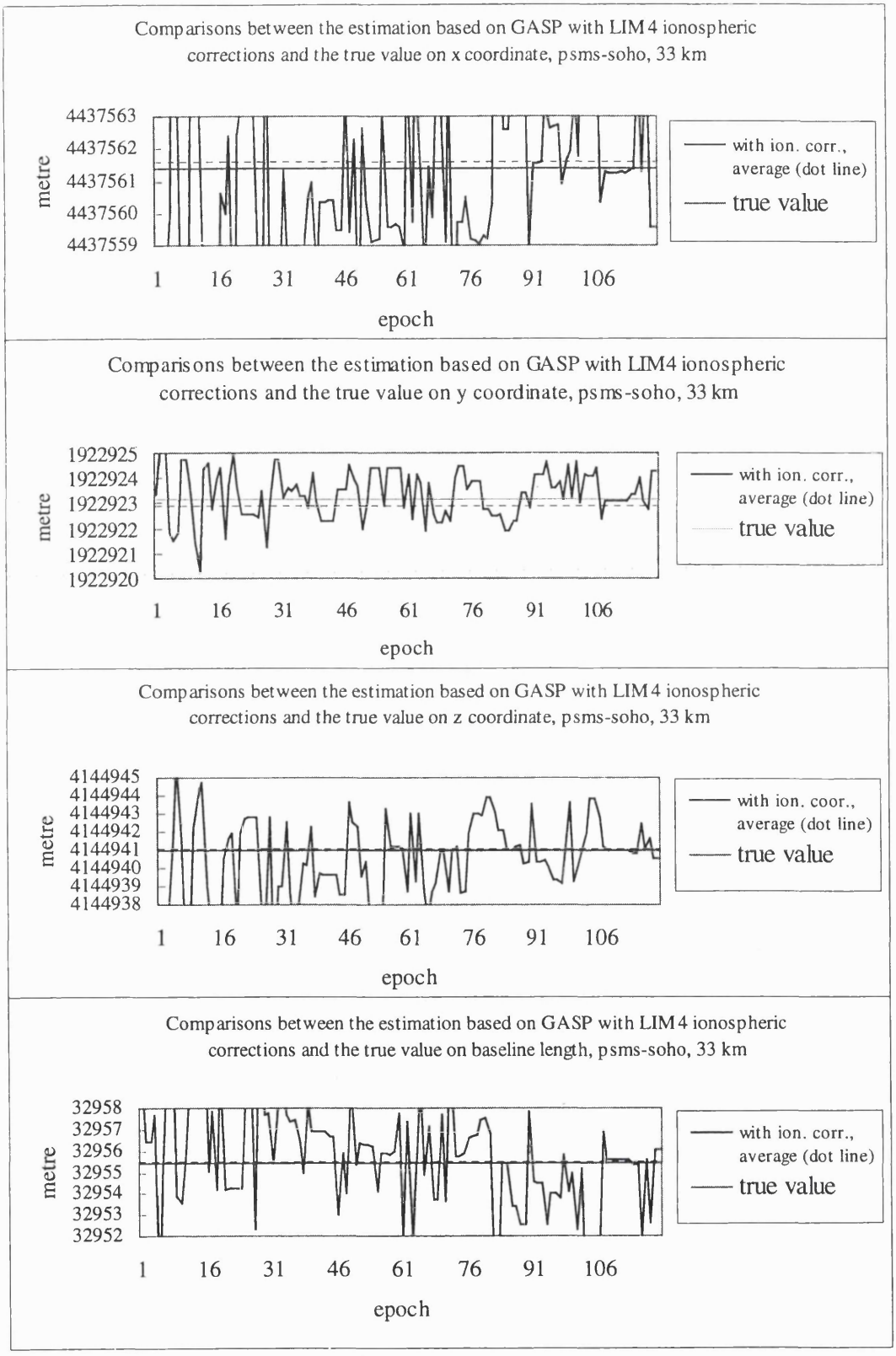

Figure C.25 Comparisons between the estimation based on GASP with LIM4 ionospheric corrections and the true value on x, y, z, and baseline length (33km baseline)

- Comparisons between the estimation based on GASP with LIM5 ionospheric corrections and the true value on x, y, z, and baseline length.

1. Trial of 12.8km baseline

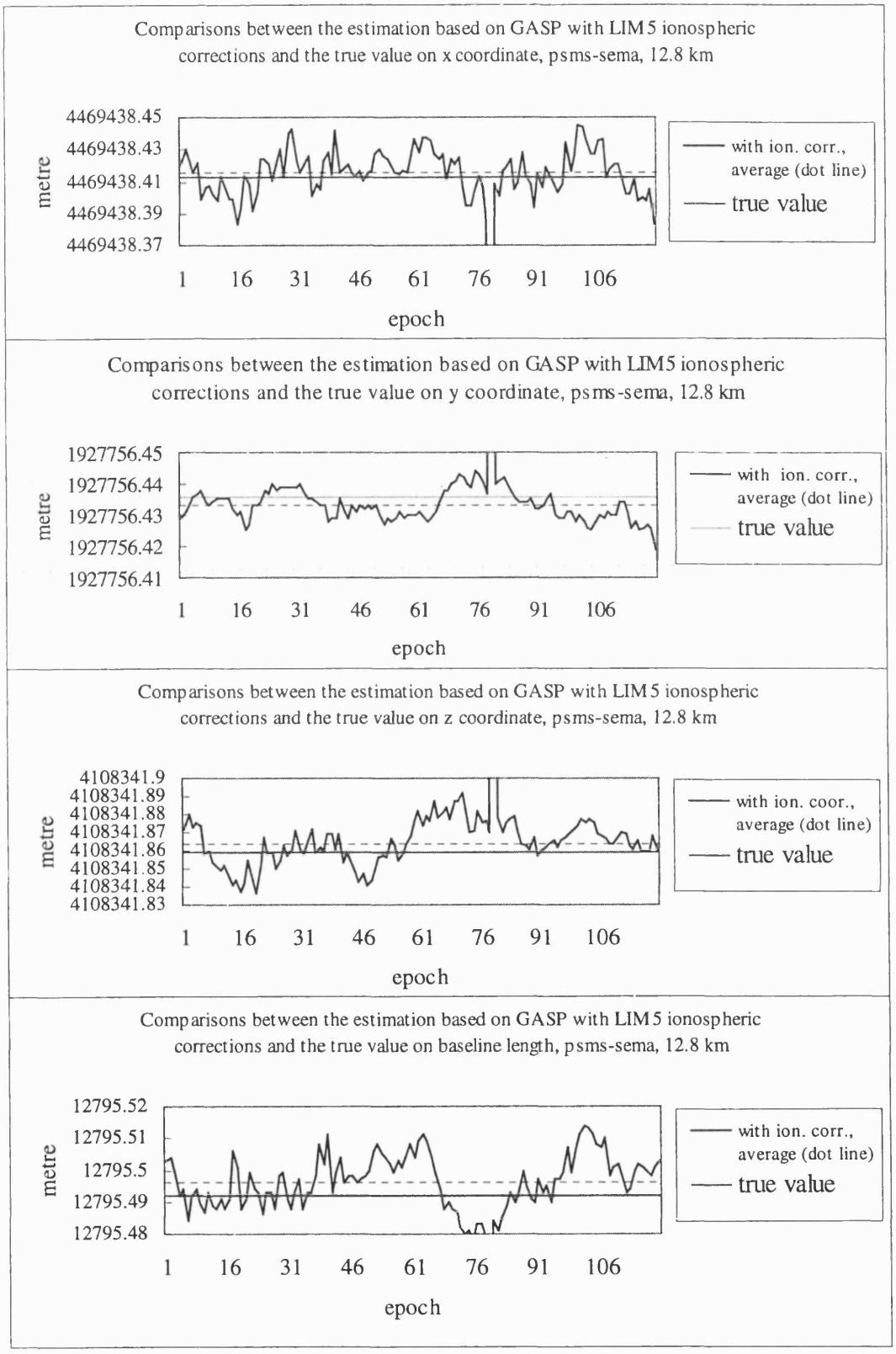

Figure C.26 Comparisons between the estimation based on GASP with LIM5 ionospheric corrections and the true value on x, y, z, and baseline length (12.8km baseline)

2. Trial of 15km baseline

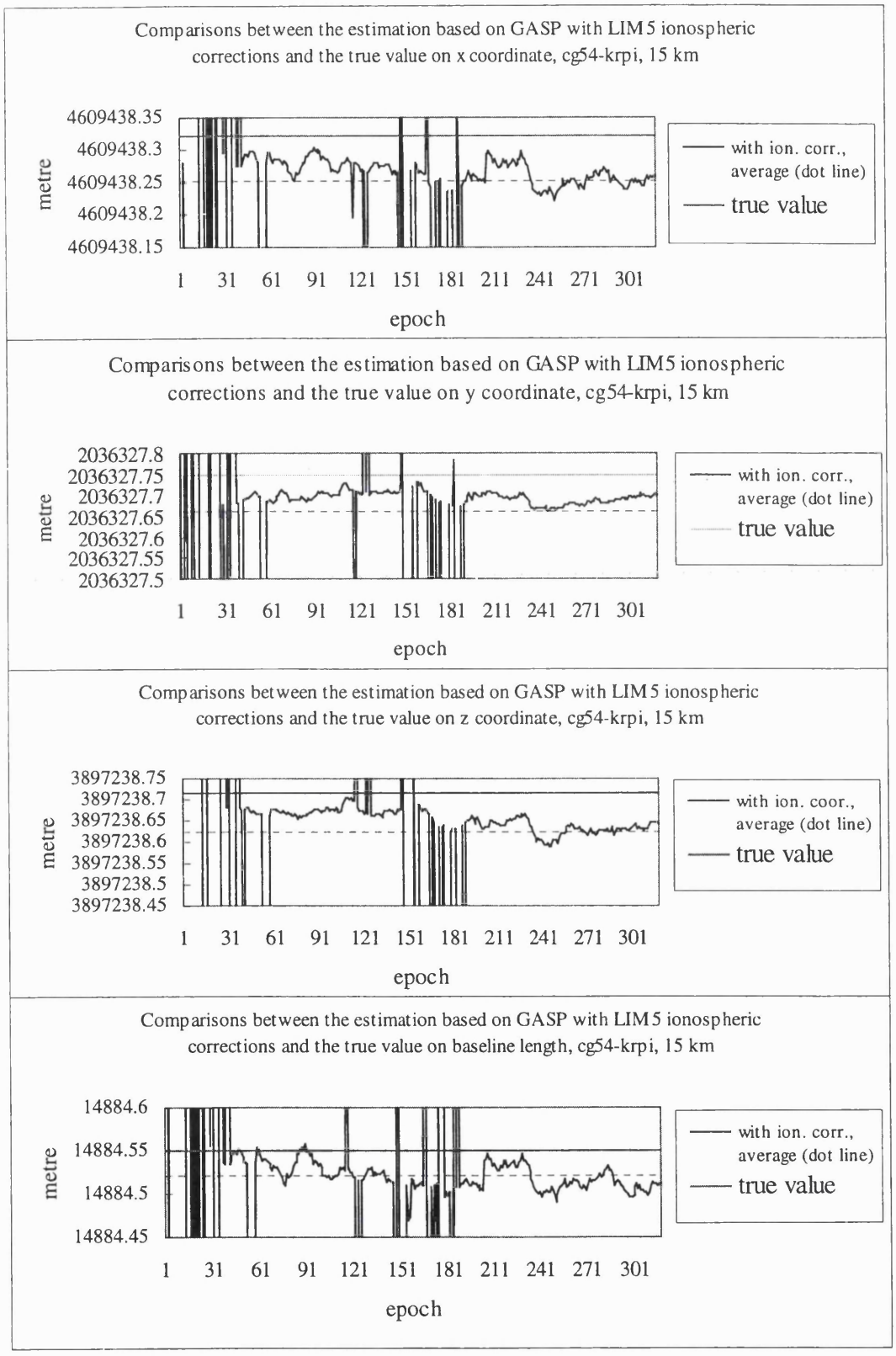

Figure C.27 Comparisons between the estimation based on GASP with LIM5 ionospheric corrections and the true value on x, y, z, and baseline length (15km baseline)

3. Trial of 21km baseline

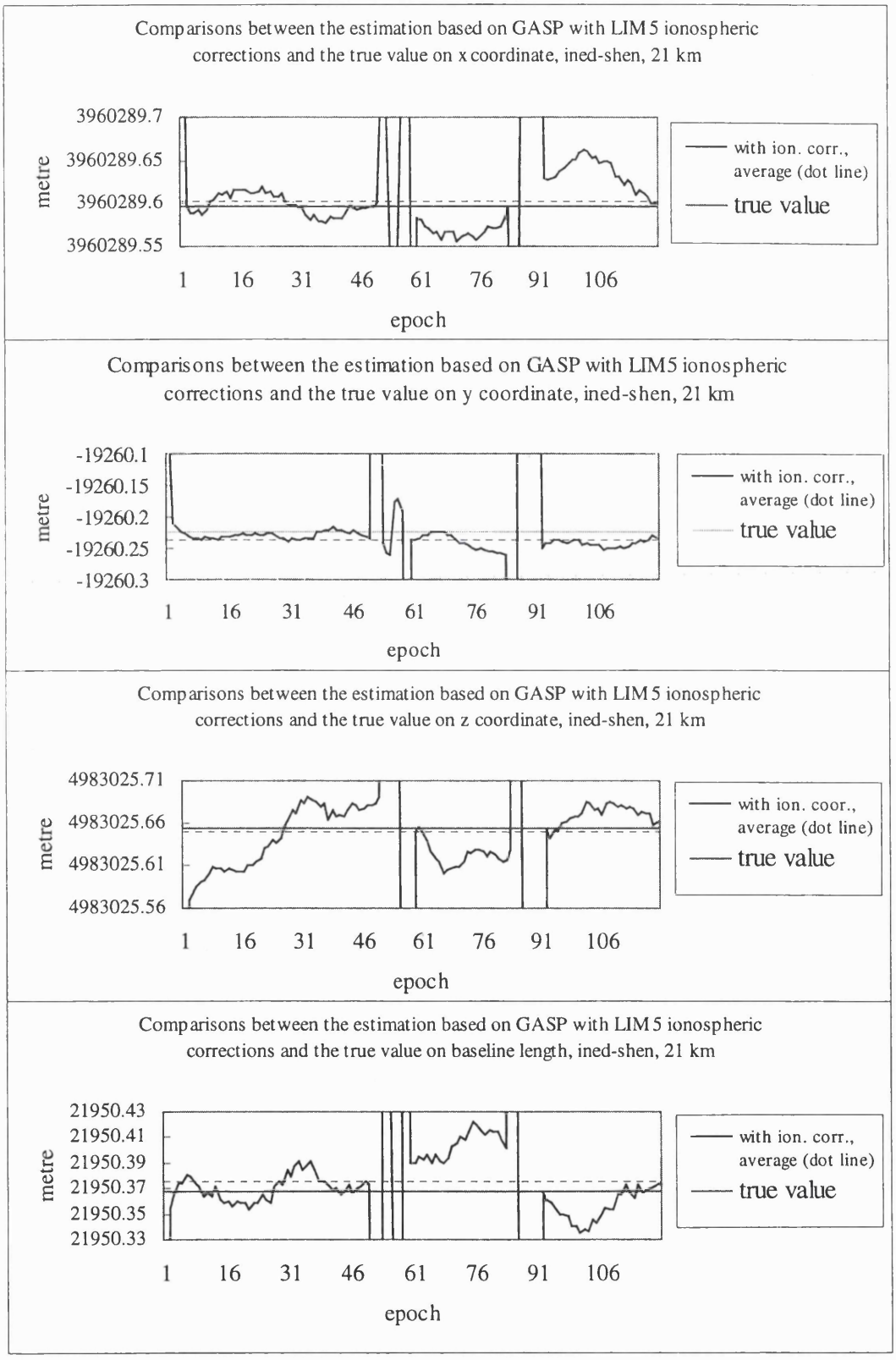

Figure C.28 Comparisons between the estimation based on GASP with LIM5 ionospheric corrections and the true value on x, y, z, and baseline length (21km baseline)

4. Trial of 25km baseline

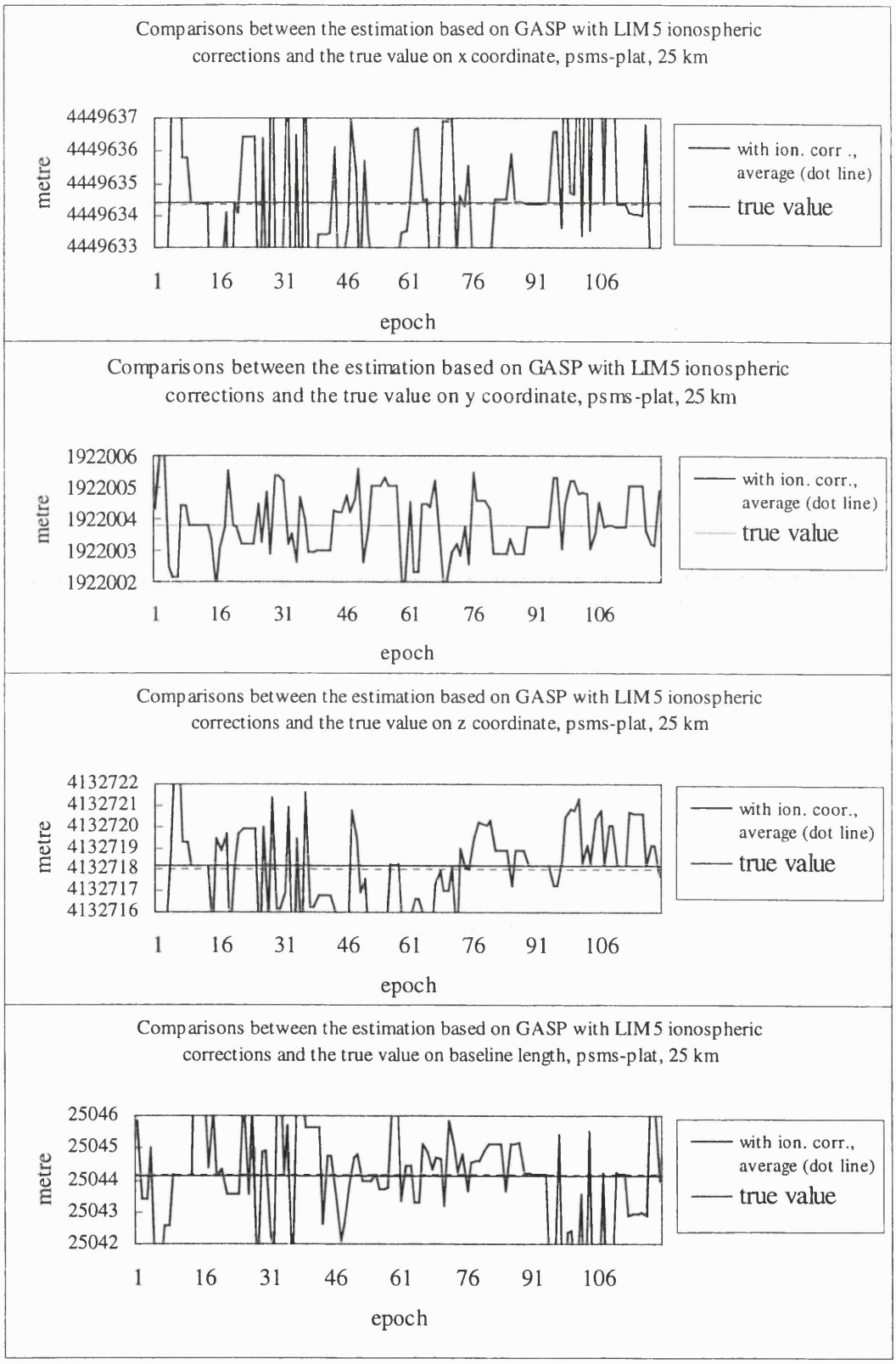

Figure C.29 Comparisons between the estimation based on GASP with LIM5 ionospheric corrections and the true value on x, y, z, and baseline length (25km baseline)

5. Trial of 33km baseline

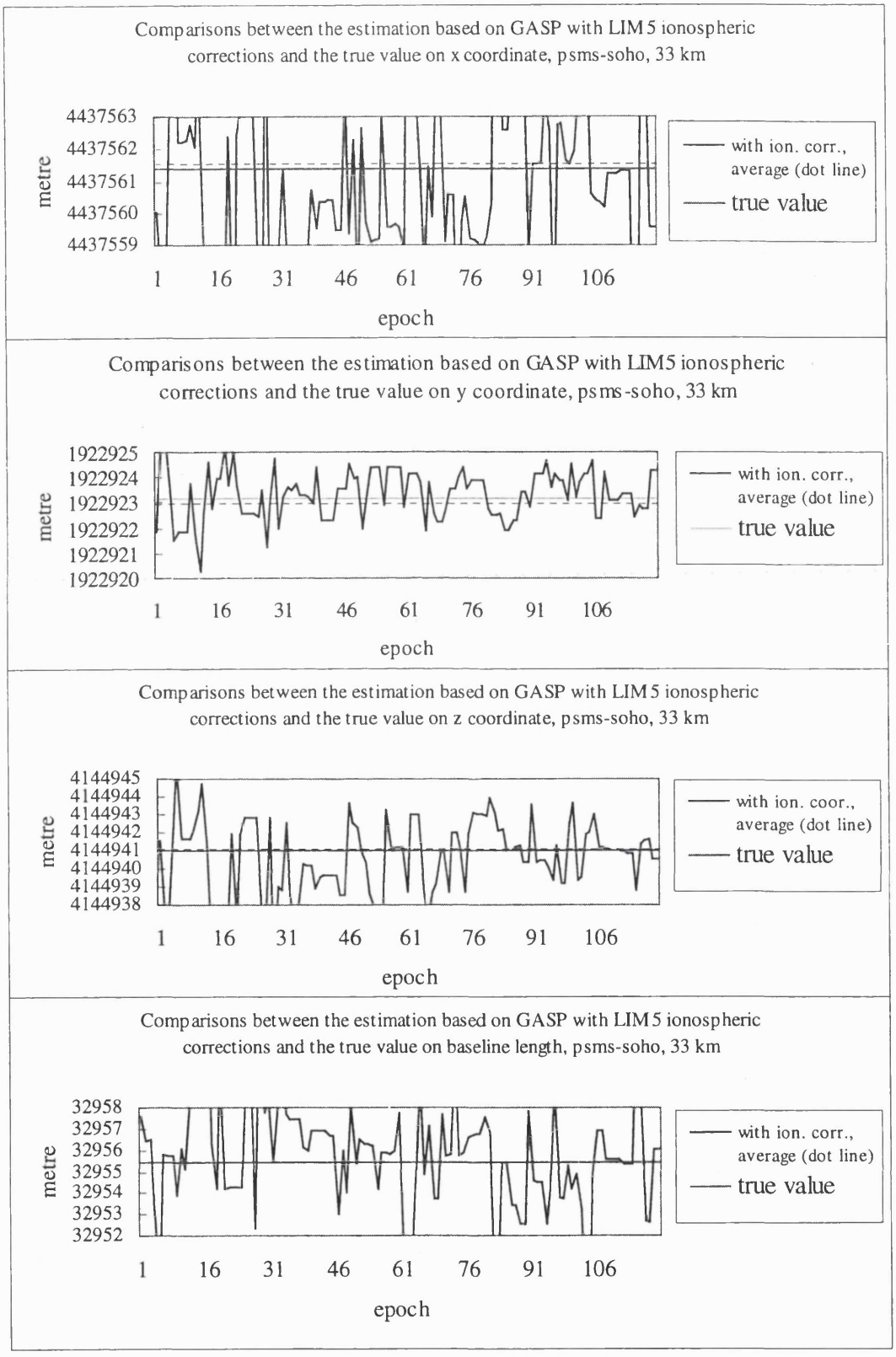

Figure C.30 Comparisons between the estimation based on GASP with LIM5 ionospheric corrections and the true value on x, y, z, and baseline length (33km baseline)

- Comparisons between the estimation based on GASP with LIM6 ionospheric corrections and the true value on x, y, z, and baseline length.

1. Trial of 12.8km baseline

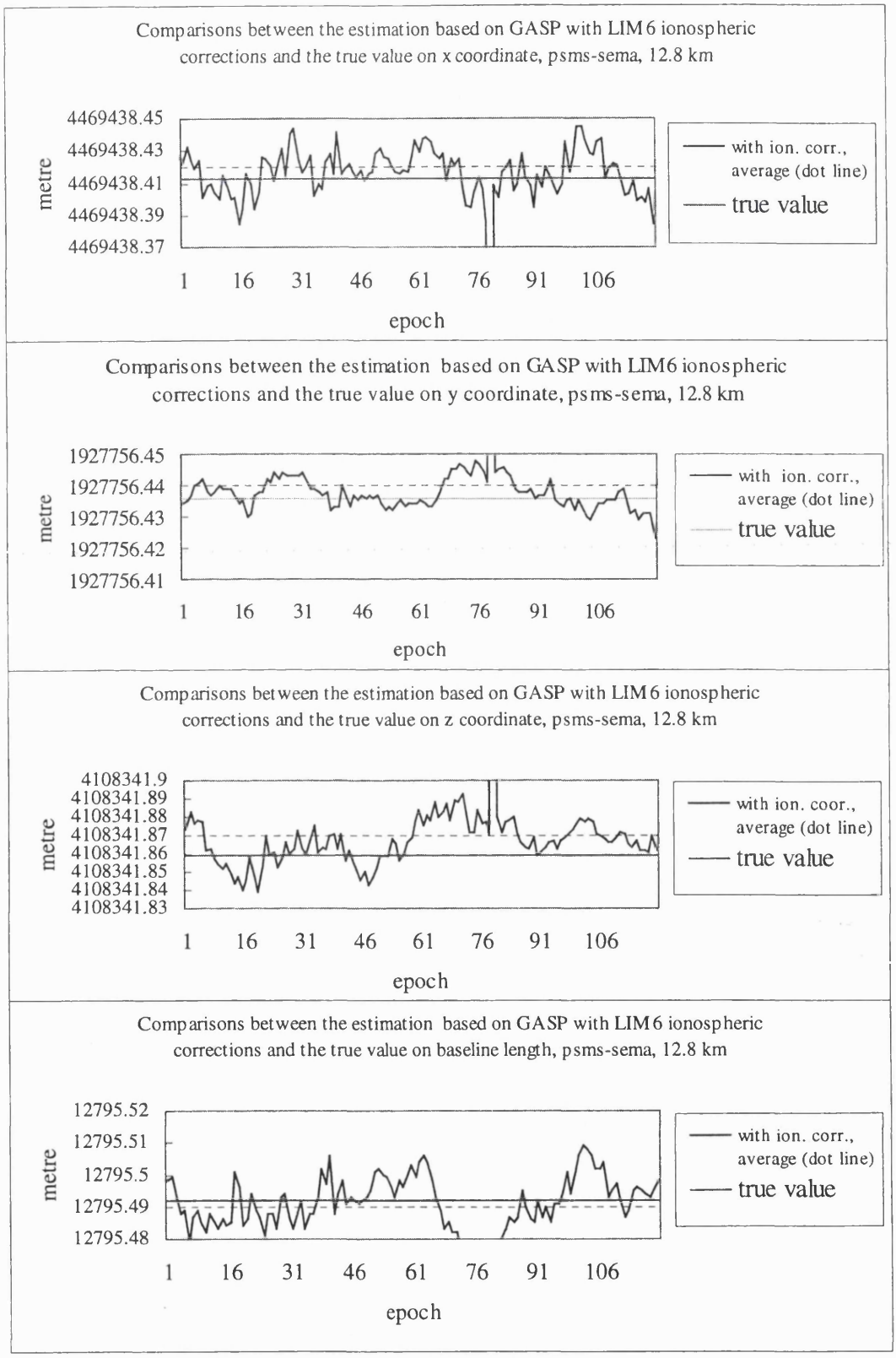

Figure C.31 Comparisons between the estimation based on GASP with LIM6 ionospheric corrections and the true value on x, y, z, and baseline length (12.8km baseline)

2. Trial of 15km baseline

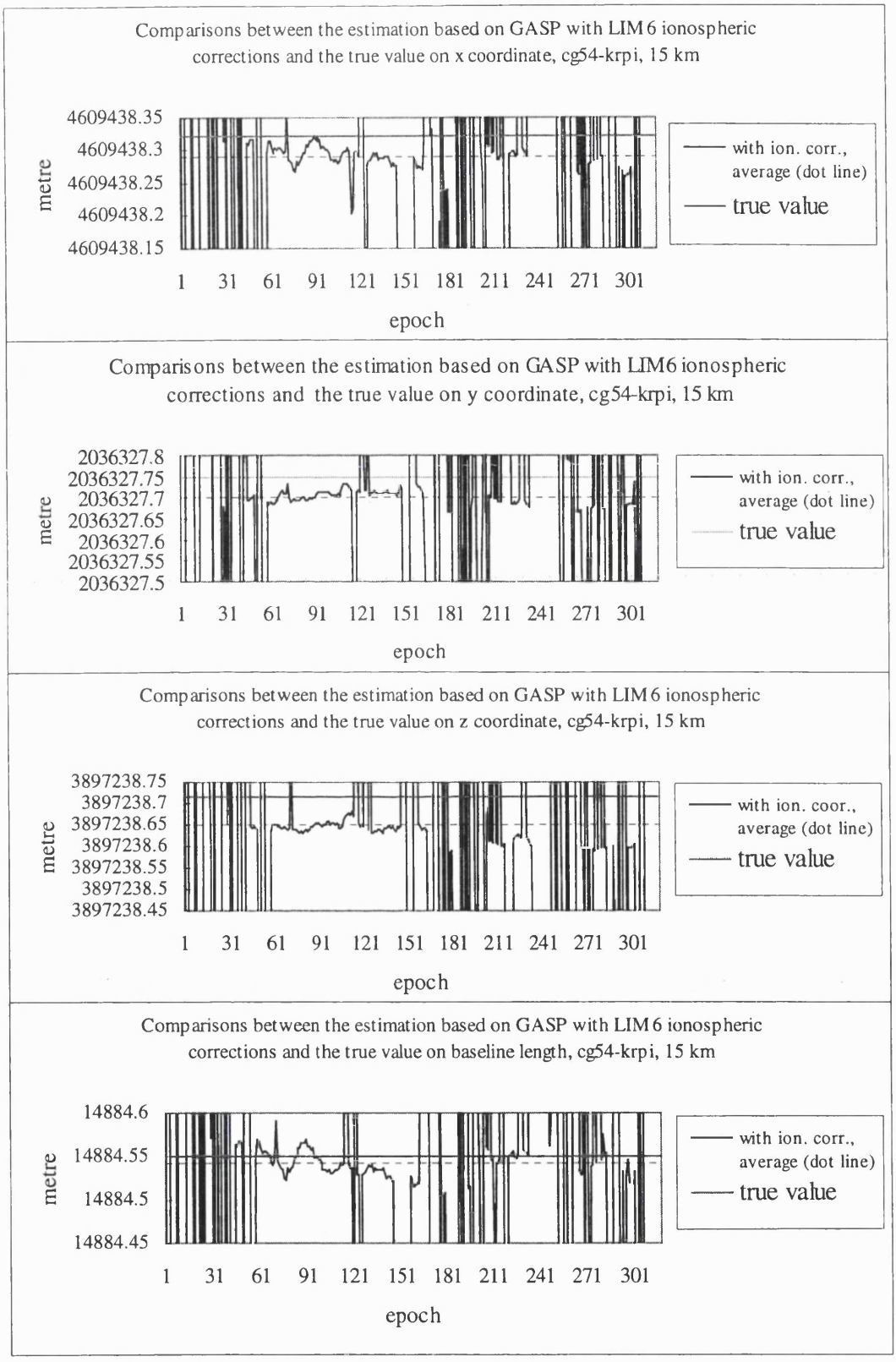

Figure C.32 Comparisons between the estimation based on GASP with LIM6 ionospheric corrections and the true value on x, y, z, and baseline length (15km baseline)

3. Trial of 21km baseline

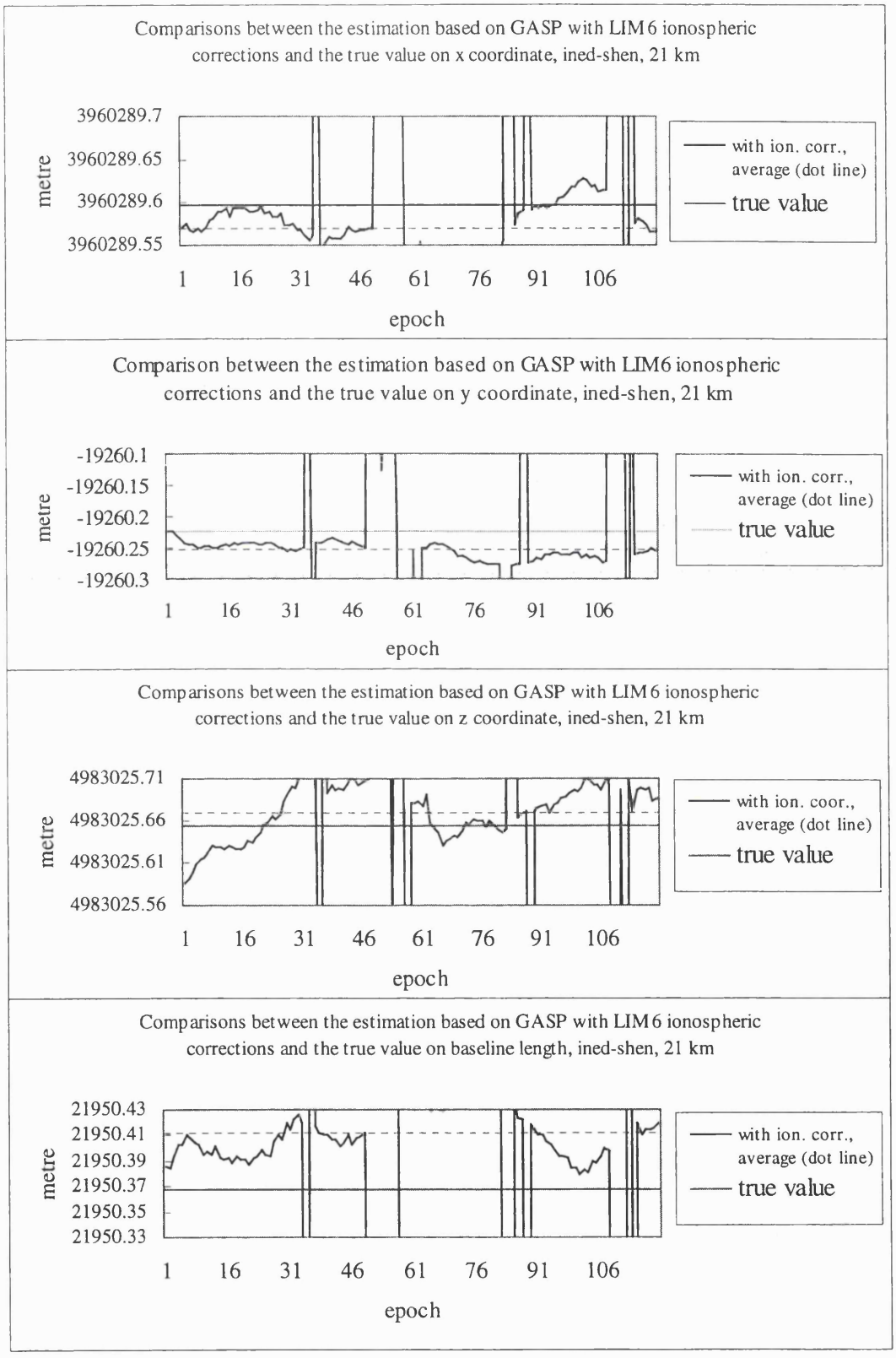

Figure C.33 Comparisons between the estimation based on GASP with LIM6 ionospheric corrections and the true value on x, y, z, and baseline length (21km baseline)

4. Trial of 25km baseline

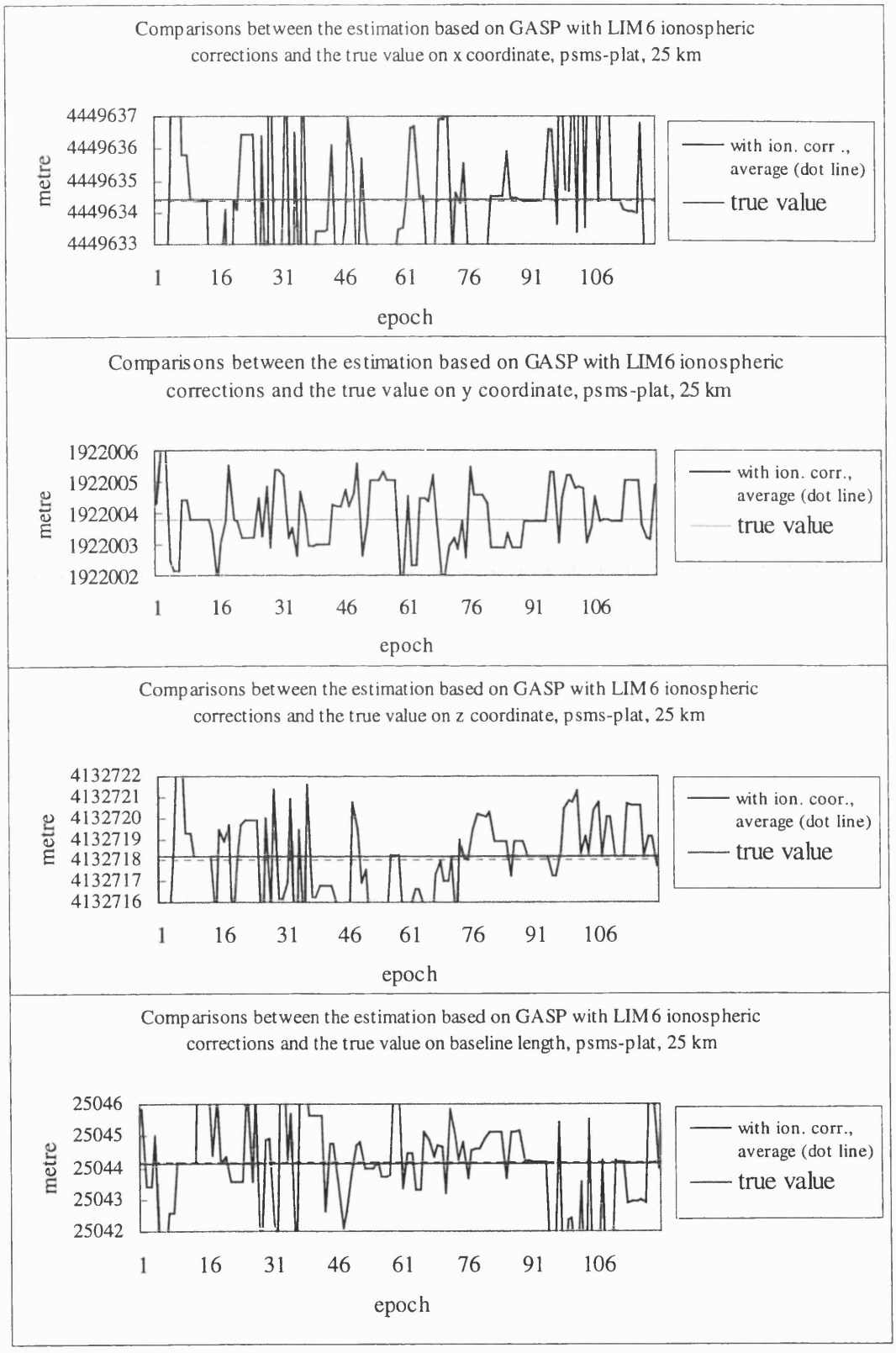

Figure C.34 Comparisons between the estimation based on GASP with LIM6 ionospheric corrections and the true value on x, y, z, and baseline length (25km baseline)

5. Trial of 33km baseline

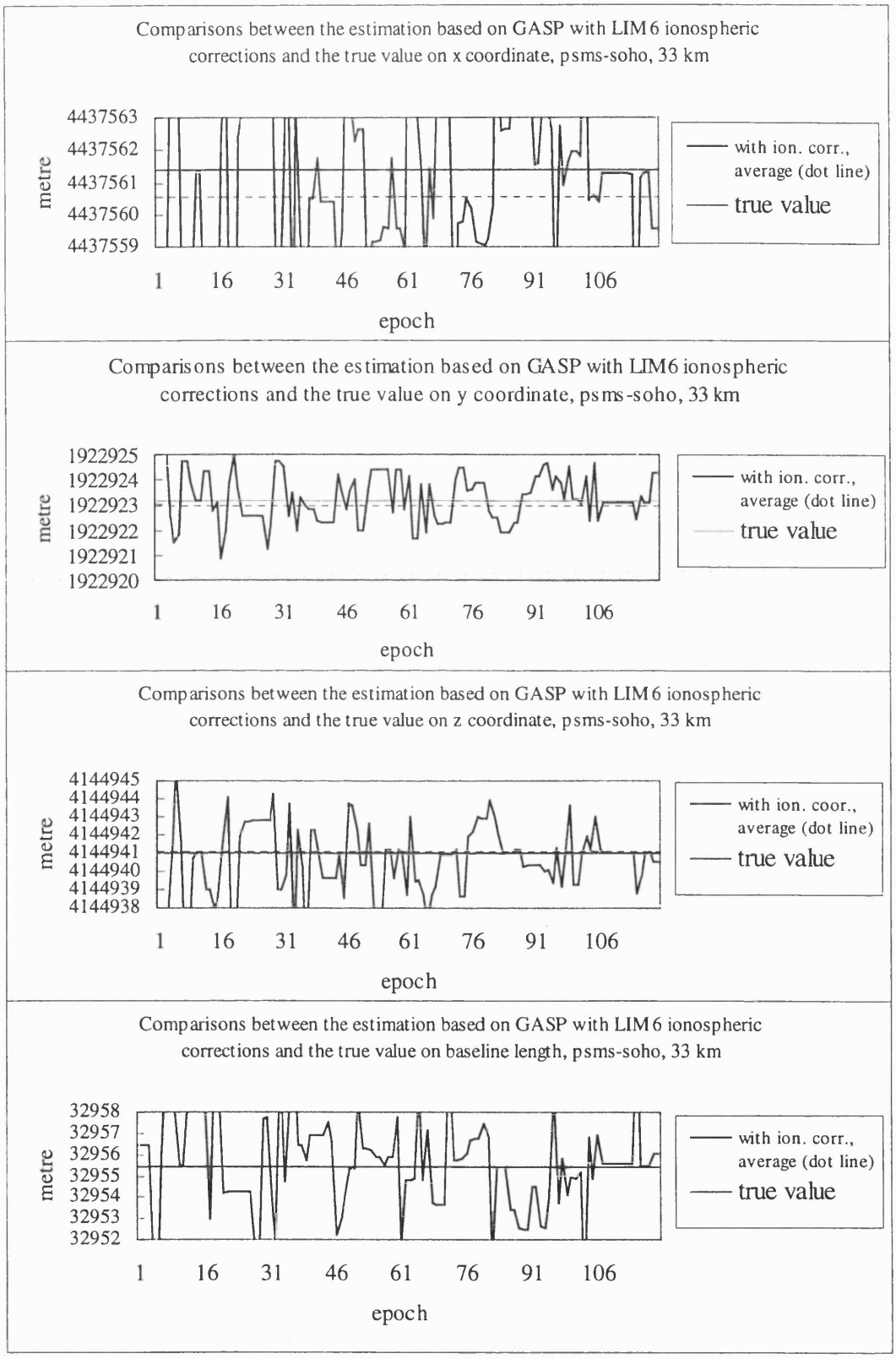

Figure C.35 Comparisons between the estimation based on GASP with LIM6 ionospheric corrections and the true value on x, y, z, and baseline length (33km baseline)